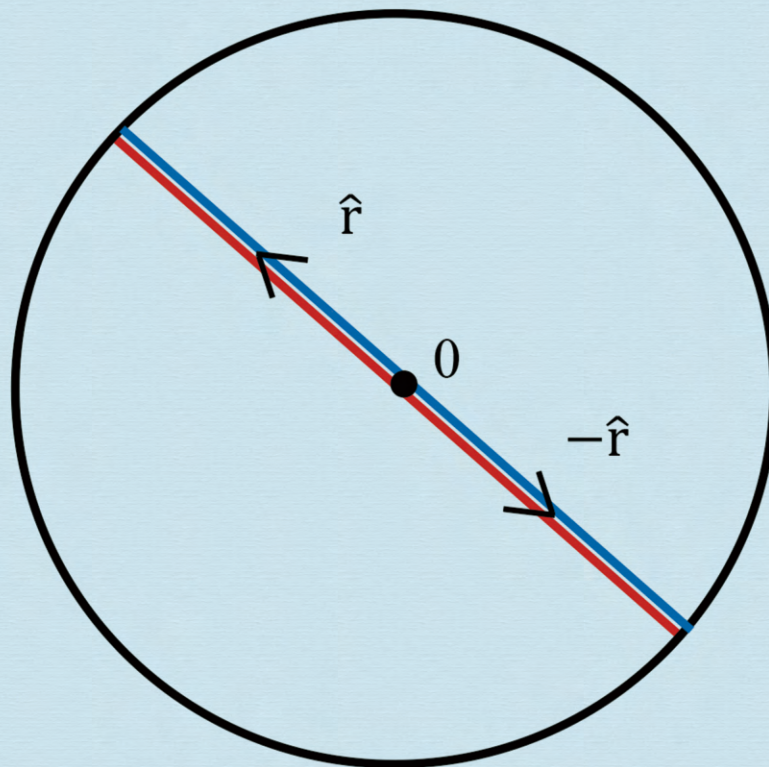


Journal of Modern Physics



Journal Editorial Board

ISSN: 2153-1196 (Print) ISSN: 2153-120X (Online)

<https://www.scirp.org/journal/jmp>

Editor-in-Chief

Prof. Yang-Hui He

City University, UK

Editorial Board

Prof. Nikolai A. Sobolev

Universidade de Aveiro, Portugal

Dr. Mohamed Abu-Shady

Menoufia University, Egypt

Dr. Hamid Alemohammad

Advanced Test and Automation Inc., Canada

Prof. Emad K. Al-Shakarchi

Al-Nahrain University, Iraq

Prof. Antony J. Bourdillon

UHRL, USA

Prof. Tsao Chang

Fudan University, China

Prof. Wan Ki Chow

The Hong Kong Polytechnic University, China

Prof. Jean Cleymans

University of Cape Town, South Africa

Prof. Stephen Robert Cotanch

NC State University, USA

Prof. Claude Daviau

Ministry of National Education, France

Prof. Peter Chin Wan Fung

University of Hong Kong, China

Prof. Ju Gao

The University of Hong Kong, China

Dr. Sachin Goyal

University of California, USA

Dr. Wei Guo

Florida State University, USA

Prof. Karl Hess

University of Illinois, USA

Prof. Peter Otto Hess

Universidad Nacional Autónoma de México, Mexico

Prof. Haikel Jelassi

National Center for Nuclear Science and Technology, Tunisia

Dr. Magd Elias Kahil

October University for Modern Sciences and Arts (MSA), Egypt

Prof. Santosh Kumar Karn

Dr. APJ Abdul Kalam Technical University, India

Dr. Ludi Miao

Cornell University, USA

Prof. Christophe J. Muller

University of Provence, France

Dr. Rada Novakovic

National Research Council, Italy

Dr. Vasilis Oikonomou

Aristotle University of Thessaloniki, Greece

Prof. Tongfei Qi

University of Kentucky, USA

Prof. Mohammad Mehdi Rashidi

University of Birmingham, UK

Prof. Haiduke Sarafian

The Pennsylvania State University, USA

Prof. Kunnat J. Sebastian

University of Massachusetts, USA

Dr. Ramesh C. Sharma

Ministry of Defense, India

Dr. Reinoud Jan Slagter

Astronomisch Fysisch Onderzoek Nederland, Netherlands

Dr. Giorgio SONNINO

Université Libre de Bruxelles, Belgium

Prof. Yogi Srivastava

Northeastern University, USA

Dr. A. L. Roy Vellaisamy

City University of Hong Kong, China

Prof. Anzhong Wang

Baylor University, USA

Prof. Yuan Wang

University of California, Berkeley, USA

Prof. Peter H. Yoon

University of Maryland, USA

Prof. Meishan Zhao

University of Chicago, USA

Prof. Pavel Zhuravlev

University of Maryland at College Park, USA

Table of Contents

Volume 12 Number 3

February 2021

A Summary of the Homogeneous 5D Universe Creation Model: Expressed in the Dirac Second-Order Quantization Representation

K. W. Wong, W. K. Chow.....123

Dark Matter Creation and Anti-Gravity Acceleration of the Expanding Universe

F. C. Hoh.....139

On Dineutron and Deuteron Binding Energies

F. C. Hoh.....161

New Approach to Deep Miniaturization: A Way to Overcoming Moore's Law

M. K. Koleva.....167

Multi-Bubble Universe Model: A Quantum-Relativistic Gravitational Theory of Space-Time

M. Auci.....179

On the Poincaré Algebra in a Complex Space-Time Manifold

N. Debergh, G. D'Agostini, J.-P. Petit.....218

A New Formula of Redshift vs. Space Expansion and Dark Energy

O. Serret.....229

Particle Physics Problems Addressed with Simple Mathematics Related to General Relativity

T. R. Mongan.....254

Theoretical Evidence for Wave Nature of Micro Particle and New Theory of Its Collective Motion in Material

T. Okino.....260

Quantization of the 1-D Forced Harmonic Oscillator in the Space (x, v)

G. V. López, O. J. P. Bravo.....284

Electric Charge, Matter Distribution, and Baryon Asymmetry from Holographic Principle

T. R. Mongan.....295

Time-Neutrality of Natural Laws Challenged: Time Is Not an Illusion but Ongoing Energy-Driven Information Loss

H. Tributsch.....300

Variational Calculations of Energies of the $(2snl)^{1,3}L^\pi$ and $(2pnl)^{1,3}L^\pi$ Doubly Excited States in Two-Electron Systems Applying the Screening Constant per Unit Nuclear Charge

M. T. Gning, I. Sakho, M. Faye, M. Sow, B. Diop, J. K. Badiane, D. Ba, A. Diallo.....328

Possibility of Geometrical Interpretation of Quantum Mechanics and Geometrical Meaning of “Hidden Variables”

O. A. Olkhov.....353

Video-Based Face Recognition with New Classifiers

S. Singhal, M. Hanmandlu, S. Vasikarla.....361

Flavour and Colour of Quarks in Spin Topological Space

S. X. Ren.....380

Journal of Modern Physics (JMP)

Journal Information

SUBSCRIPTIONS

The *Journal of Modern Physics* (Online at Scientific Research Publishing, <https://www.scirp.org/>) is published monthly by Scientific Research Publishing, Inc., USA.

Subscription rates:

Print: \$89 per issue.

To subscribe, please contact Journals Subscriptions Department, E-mail: sub@scirp.org

SERVICES

Advertisements

Advertisement Sales Department, E-mail: service@scirp.org

Reprints (minimum quantity 100 copies)

Reprints Co-ordinator, Scientific Research Publishing, Inc., USA.

E-mail: sub@scirp.org

COPYRIGHT

Copyright and reuse rights for the front matter of the journal:

Copyright © 2021 by Scientific Research Publishing Inc.

This work is licensed under the Creative Commons Attribution International License (CC BY).

<http://creativecommons.org/licenses/by/4.0/>

Copyright for individual papers of the journal:

Copyright © 2021 by author(s) and Scientific Research Publishing Inc.

Reuse rights for individual papers:

Note: At SCIRP authors can choose between CC BY and CC BY-NC. Please consult each paper for its reuse rights.

Disclaimer of liability

Statements and opinions expressed in the articles and communications are those of the individual contributors and not the statements and opinion of Scientific Research Publishing, Inc. We assume no responsibility or liability for any damage or injury to persons or property arising out of the use of any materials, instructions, methods or ideas contained herein. We expressly disclaim any implied warranties of merchantability or fitness for a particular purpose. If expert assistance is required, the services of a competent professional person should be sought.

PRODUCTION INFORMATION

For manuscripts that have been accepted for publication, please contact:

E-mail: jmp@scirp.org

A Summary of the Homogeneous 5D Universe Creation Model: Expressed in the Dirac Second-Order Quantization Representation

Kai Wai Wong¹, Wan Ki Chow²

¹Department of Physics and Astronomy, University of Kansas, Lawrence, USA

²Department of Building Services Engineering, The Hong Kong Polytechnic University, Hong Kong, China

Email: kww88ng@gmail.com

How to cite this paper: Wong, K.W. and Chow, W.K. (2021) A Summary of the Homogeneous 5D Universe Creation Model: Expressed in the Dirac Second-Order Quantization Representation. *Journal of Modern Physics*, 12, 123-138.
<https://doi.org/10.4236/jmp.2021.123012>

Received: December 22, 2020

Accepted: February 5, 2021

Published: February 8, 2021

Copyright © 2021 by author(s) and Scientific Research Publishing Inc.
This work is licensed under the Creative Commons Attribution International License (CC BY 4.0).

<http://creativecommons.org/licenses/by/4.0/>



Open Access

Abstract

A summary of the homogeneous 5D universe model is expressed in the Dirac second-order quantized representation for the magnetic monopoles, identified in terms of the Higgs Bosons, and through systematic ordered excitations of the Higgs vacuum obtained the non-homogeneous 4D Lorentz manifolds filled with masses, corresponding to making space dimension reduction projections, and thus realization of Newtonian gravity, followed by the 3D space symmetry breaking into $2D \times 1D$ that produces the Perelmann-entropy and Ricci-Flow mappings, resulting in the realization of Poincare spheres, represented by nucleus such as Carbon 12, all the way to stars, and matter filled discs, such as stars in galaxies and 2D carbon-based molecular structures like nitrogenous bases. Finally, the forming of RNAs and DNAs, then life forms.

Keywords

Magnetic Monopoles, Higgs Bosons, Space Reduction Projections, Perelmann Mappings, Nitrogenous Bases and Life Forms

1. Introduction

The 4D inhomogeneous Lorentz manifold was obtained by a space dimension projection from a 5D homogeneous space-time manifold [1]. This topological projection is irreversible and is shown to be mathematically equivalent to the Perelmann-entropy Ricci-flow mappings [2] [3] in deriving the donut and the spherical 4D Lorentz mass distributions [4]. It was further shown via the dimension reduction projections, the 5D manifold must become a 4D-Lorentz mani-

fold with direct products to the superposition of the Semi-simple Compact Lie Groups $SU(2) + SU(3)$, as the McGlenn theorem [5] must be obeyed. This topological result is in complete agreement to the Gell-Mann standard model [6]. It was then further shown that by applying Lorentz gauge invariance, in conjunction with deriving the Gluon fields as the tensor products of the 4 Electromagnetic vector potentials, the hadron masses can be very accurately calculated [1]. On top of that achievement, the neutron oscillation was also obtained [7]. As the 4 electromagnetic vector potentials satisfy the 4D homogeneous Klein-Gordon differential equation, the 5D homogeneous 2nd-order differential equation must generate 5 vector potentials instead of just 4. This extra component of the solution was originally proposed by Maxwell [8] and was coined as the magnetic monopole potential. It was relatively recent that we have derived its explicit form [9]. It was then possible to derive the explicit monopole unit as $+2ec$ and $-2ec$. Where they were the product from two oppositely charged, opposite momenta along the 3D spherical radius, and massless spinor solutions to the Dirac linearized 5D equation. Because of the opposite momenta of the spinor pair, this magnetic monopole magnitude must be carried by two Diagonal Long Range Ordered Bosons with opposite magnitudes. Since each charged massless spinor like a neutrino has quantized momentum and energy, these massless charge neutral Bosons also carry energy, despite being in the Bose-Einstein condensed state. It is this mathematical feature that makes them equivalent to the Higgs Bosons [10]. And they must completely fill the homogeneous 5D manifold. Hence on recognizing the universe as a Big Bang, started with absolutely nothing, that is no time and no space, the homogeneous 5D universe must be given by a Higgs vacuum. From which, the creation of mass through space projections or the equivalent Perelmann mappings must be equivalent to the excitation of this Higgs vacuum. In fact, it was discovered by the CERN supercollider experiment that a 125 GeV proton-proton resonance exists [11] and thus verified both the Higgs theory as well as the projection theory [1]. It is through all of these rigorous mathematics and experimental results that we believe it might be helpful to represent these monopole-Higgs Bosons in the Dirac second quantized representation, so that we can further clearly show why there is only energy with no net charge, and net monopoles, actually existed in the homogeneous 5D universe starting at the beginning in complete agreement to the Big Bang model, and the Higgs vacuum. What we have not yet been able to explain after 4D Lorentz manifolds were created, that the dynamics of the masses within would indeed lead to Einstein's General Relativity [12], with the Gravity tensor equation [13], where Einstein postulated the existence of a Cosmic constant. And if it is in some way mathematically related and obtained by excitation giving rise to the symmetry breaking of the Higgs bosons via either the breaking of their Diagonal Long Range Order (DLRO) or the explicit breaking of the charge neutrality, and therefore the Bosons itself, such that a charge density distribution term to the Gravity tensor equation can be realized and the Einstein Cosmic constant ex-

plained. And how the truncation on the bosons energy range together with choice of remaining 3D space symmetry can result in the natural forming of molecules that have natural excitation spectra, that can be divided in turns of coherent and de-coherent [14], a very essential philosophical point raised by Schrodinger [15]. And lastly at the lowest frequencies how it is correlated to the life forms' DNA spectra [1] [16]. It is these loose ends to the 5D grand unified field theory [1] our intension to attempt address in this paper.

2. The Magnetic Monopoles and the Higgs Bosons

According to the 5D homogeneous manifold, there must exist 5 vector potentials, represented by the 4 electromagnetic vector potentials and an orthogonal 5th Maxwell magnetic monopole potential as proposed by Maxwell [8]. The explicit form of this monopole potential was recently derived by us [9], with the magnetic monopole strength given by a DLRO Boson field composed of the product from two opposite momentum massless [1], but with e and $-e$ charges spinor pair, such that the monopole strengths are given by

$$M(+)=2ec; \text{ and } M(-)=-2ec. \quad (1)$$

Let us denote in terms of Dirac second quantization representation.

Let $c_{\vec{p}}$ be that of the destructive operator for the charge “e” e-trino with momentum \vec{p} ; and $d_{-\vec{p}}$ be that of the destructive operator for the charge “-e” anti-e-trino, and with spin indices suppressed. Because e-trino and anti-e-trino are massless spinor, despite their name we gave, they are not the conjugate of each other, massless spinor does not have corresponding anti-spinor, hence $d_{-\vec{p}}$ and $c_{\vec{p}}$ commutes, such that an opposite momentum pair is a Boson with net 0 momentum and forms a Diagonal Long Range order, with a current magnitude of either $2ec$, or $-2ec$, which gives the magnetic monopole strengths. An opposite momentum pair of the same spinor, say e-trino, forms an off-diagonal long range order Boson but carries net 0 monopole strength. All massless fields carry momentum of $h\nu/c$, with energy $h\nu$. A DLRO e-trino and anti-e-trino pair thereby carries net 0 momentum and 0 center of frame energy. It does not mean this DLRO pair has no energy. In fact, it has a total energy E of $2 h\nu$. Thus such an e-trino and anti-e-trino DLRO pair Boson field must be in the Bose-Einstein condensed state. Unlike the photon, as when its momentum is 0, so is its energy. Thus the photon cannot exist in the Higgs vacuum, and therefore cannot exist in the homogeneous 5D manifold. In another word, inside the 5D domain, we cannot have photons. To some this can be viewed as a “black hole” region. Except it does not mean photons are sucked into this 5D domain! And definitely not equivalent to the concept of a black hole, where matters are sucked in and reverted back to pure energy. On the contrary, it verifies Maxwell’s monopole theory, that there exists a 5th magnetic monopole potential orthogonal to the 4 electromagnetic vector potentials, such that it must be a potential along the Fermat’s amplitude, resembling the Coulomb potential of a point charge. Hence, one can conclude that the electromagnetic fields actually serve as a boundary of

the 5D manifold where the monopoles, or the Higgs Bosons exist.

Because the homogeneous 5D manifold does not have time reversal symmetry, the creation of matter through the excitation of the Higgs vacuum constitutes an irreversible entropy mapping, the matter then created must then be in an inhomogeneous 4D Lorentz manifold, as demonstrated by the Perelmann Ricci-flow mapping. Such that no reverse mapping process is allowed. In short matter cannot be reverted back to pure energy and the Higgs vacuum completely restored. Meaning the concept of a “black hole” as such an infinite sink of matter cannot exist in the 5D universe, irrespective of gravity [17] [18].

Therefore the ensemble magnitude of $\langle M(+), M(-) \rangle$ are given in quantum term as

$$\langle M(+)\rangle = 2ec N_E(+); \quad \langle M(-)\rangle = -2ec N_E(-) \tag{2}$$

where $N_E(+)=\langle B_E^*(0)B_E(0)\rangle$; $N_E(-)=\langle D_E^*(0)D_E(0)\rangle$ such that $B_E(0)=c_{\bar{p}}d_{-\bar{p}}$ and $D_E(0)=d_{\bar{p}}c_{-\bar{p}}$, and $\langle \rangle$ represents the canonical ensemble average.

As these boson fields are in the Bose-Einstein condensed state, they must be the Higgs fields and populate the Higgs vacuum.

3. Properties of the Higgs Bosons

To better understand the $B_E(0)$ and $D_E(0)$ topologies, let us illustrate in **Figure 1** with color vectors: $c_{\bar{p}}$ as a red vector along $+\hat{r}$, from the origin of the 5D manifold, and $d_{-\bar{p}}$ then as a blue vector also along $+\hat{r}$. Then $B_E(0)$ would carry a current of $2ec$ along $+\hat{r}$. While $D_E(0)$ carries a current of $-2ec$ also along $+\hat{r}$.

Now let us illustrate in **Figure 2** the operations of \tilde{C} Charge and \tilde{P} Parity acting on $B_E(0)$ and $D_E(0)$.

It is obvious $\tilde{C}B_E(0)$ changes the $+\hat{r}$ current to $-2ec$. In another word $\tilde{C}B_E(0)=D_E(0)$.

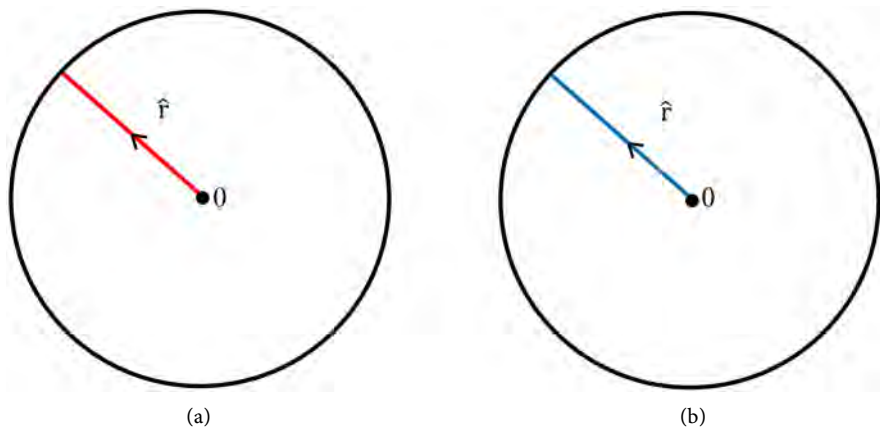


Figure 1. Illustration of $B_E(0)$ and $D_E(0)$. (a) The red line vector from 0, the center represents the Boson $B_E(0)$. (b) The blue line represents the $D_E(0)$.

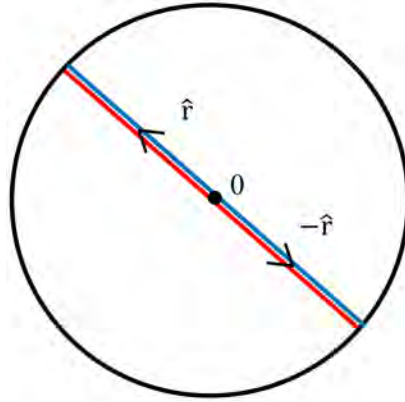


Figure 2. Illustration of Parity operation on $B_E(0)$ and $D_E(0)$. The red and blue parallel lines across the circle diameter represent $B + D$ and its image $B' + D'$ due to $\tilde{C}\tilde{P}\tilde{C}$.

The parity \tilde{P} is a mirror image operation. Hence it changes from $+\hat{r}$, to $-\hat{r}$ from the manifold center. Thus $\tilde{P}B_E(0)$ represents $B'_E(0)$ with $-\hat{r}$ rather than $D_E(0)$. The sum of $B_E(0)$ and $B'_E(0)$ results in 0 magnetic monopole strength.

Now let us consider the operation $\tilde{C}\tilde{P}\tilde{C}$ on $B_E(0)$. We have $\tilde{C}\tilde{P}\tilde{C}B_E(0) = \tilde{C}\tilde{P}D_E(0) = \tilde{C}D'_E(0) = B'_E(0)$. Which looks like $D_E(0)$ but actually is the parity image of $B_E(0)$, a distinct state in the 5D manifold. Hence starting with any DLRO monopole Boson, $\tilde{C}\tilde{P}\tilde{C}$ acting successively on it will produce the remaining 3 independent of the 4 DLRO Bosons. Since the sum of $B_E(0) + B'_E(0)$ is equal to having $M(+)+M(-)=0$. Similarly $D_E(0) + D'_E(0)$ also resulted in no net magnetic monopole strength. It is this result that shows clearly that in the 5D homogeneous manifold we preserve net 0 magnetic monopole strength, as well as net 0 charges. Hence all that remains in the 5D manifold is energy carried by the $B_E(0)$ and $D_E(0)$ fields. Thus together with uncertainty principle, illustrates how the creation of the homogeneous 5D universe, must give rise to the Universe's Big Bang. And all the energies are carried by the $B_E(0)$ and $D_E(0)$ bosons uniformly covering the 5D as it expands with time, thus making up the Higgs vacuum.

It should be noted that matter need not start being created at the same instant as the creation of the homogeneous 5D space-time. In mathematics, only infinity and zero can be divided as many times as we like, and this divided set all remain infinite and zero each. Thus the Perelman-Ricci-flow entropy mappings for the creation of galaxies by exciting the Higgs vacuum can happen later and sequentially, leaving galaxies well separated.

4. Excitation of the Higgs Vacuum and Mass Creation Example

The 5D vacuum is filled with $B_E(0)$ and $D_E(0)$ bosons in the Bose-Einstein condensed state. An excitation requires the breaking of the net 0 momentum of

these boson fields. We can do that as an example by changing the $c_{\bar{p}}d_{-\bar{p}}$ pair for the $B_E(0)$ field to $c_{\bar{p}+\bar{q}}d_{-\bar{p}+\bar{s}}$, where the additional momentum \bar{q} and \bar{s} need not be along \hat{r} . This new pair now has a net center of frame momentum of $\bar{q} + \bar{s}$. Hence it gives rise to a nonzero excitation energy $E' = c|\bar{q} + \bar{s}|$, and hence changes the Bose-Einstein distribution for the B or D field to

$$\frac{1}{e^{E'/kT} - 1}$$

As long as $E' > 0$, the Bose distribution can be expanded in a convergent infinite power series, of e^{-Cj} , where $C = E'/kT$, and $j = 1, 2, 3, \dots$ [19]. Thus for $E' \geq m(e)c^2$, the rest energy of an electron, with high enough T , that of Bethe fusion temperature, matter will be created as suggested by Higgs theory [10]. Topologically it must correspond to destroying the 5D homogeneity. Hence is equivalent to creating a 4D Lorentz manifold boundary on the 5D manifold. As an illustration, let us take $\bar{q} = \bar{s}$ and perpendicular to \hat{r} , we will obtain a net angular momentum $2\bar{q}\bar{x}\bar{r}_o$ around 0. Where \bar{r}_o is the time frozen core radius perpendicular to \bar{q} . Thus this excited angular momentum must be balanced by an equal but opposite angular momentum from the rotating masses outside the 5D domain and in the enclosing 4D Lorentz manifold. While if $\bar{q} = -\bar{s}$, we would result in a creation of a dipole magnetic field, as \bar{q} generates a current loop with radius r_o . It is these excitations that correspond to performing the Perelmann entropy mappings [2] [3]. By separating the results from the Perelmann mappings into preserving the 3D space symmetry, we obtain the Poincare sphere, starting in the microscopic scale for the leptons to the nucleus with a time frozen 5D core, such as Carbon 12, to the astronomical scale stars and planets. Hence for an isolated spherical time frozen core, the remainder $B_E(0)$ and $D_E(0)$ fields within must be standing waves, with frequencies obeying $\nu = nc/4r_o$, where r_o is the core radius, and $n = 1, 2, 3, \dots$. Hence the allowed eigen energy E for $B_E(0)$ and $D_E(0)$ bosons form a discrete set. This implies the smaller the core radius the higher the excitation energy is permitted as long as it is less than $h\nu/4r_o$. Or in a disc like structure, as corresponding to the Ricci-flow mapping, thus breaking 3D into $2D \times 1D$, such as represented by the SU(3) generators in space to space conformal projection, to that astronomical scale the galactic structure. With the standing wave restriction applies to the 2D circle only. In fact, this broken 3D space symmetry is represented by SU(3) in charge separation between $-e$ and $+e$ obeying gauge invariance. Hence producing current source that in turn produces the 4 EM potentials. And for a completely enclosed time frozen 5D void core, it can be elliptical and not solely spherical. It is also very reviewing to investigate the amount of total number of Bose fields N excited due to Perelmann mappings, and the total energy $\langle E' \rangle$ used as a function of Temperature T and the frozen time t_o as measured from each sub-5D manifold by integrating E' from the lower cut-off energy E_o with the 3D spherical symmetry, and the number n of new Bosons those of atoms in the periodic table created. We obtain

$$N = \frac{n4\pi}{3} \frac{(ct_o)^3}{VkT} \sum_{j=1}^{\infty} \frac{e^{-jE_o/kT}}{j} \quad (3)$$

$$E' = \frac{n4\pi}{3V} (ct_o)^3 \sum_{j=1}^{\infty} \left\{ E_o - \frac{kT}{j} \right\} \frac{e^{-jE_o/kT}}{j} \quad (4)$$

where V is the volume of the Lorentz space.

N varies with t_o^3 , n and inversely with T . Thus the lower T value we have more matter including complex matter structures created.

While from $\langle E' \rangle$ always positive, E_o must be greater than $(kT)/j$. Meaning E_o is discretized as T is fixed. It is this result that created the different stages of creation. The lower the Temperature T , the lower would be the allowed excited spectrum of the B, D bosons. For the initial matter creation at Bethe Fusion temperature, $n = 2$, due to only B and D bosons. E_o should be that of the proton pure Quark rest mass, then the highest j value is roughly 64 as the electron rest mass is roughly 1/64 that of the Quark's, with the neutron in between.

As T decreases, t_o increases, and E_o decreases as it represents the gluon binding, and with the atomic Coulomb binding energy, with the number n being those of atoms, from hydrogen to the heaviest element. Thus n becomes quite large. On the other hand, Heavy hydrogen with an extra neutron is not a Boson, and does not satisfy Equation (3). E_o becomes the molecular binding energy cut-off. Leading to the coherent and de-coherent series for molecules studied by Schrodinger, Geesink *et al.* and many other physicists.

As masses within the 4D Lorentz manifold move, we need to express this Lorentz manifold in a covariant form. Hence it gives us naturally the Covariant Riemannian curvatures, which would give us the law of gravity for matter [12], but with a naturally build-in time frozen 5D core, a repulsive worm hole [20] filled with repulsive e-trinos and anti-e-trinos [21].

Following General Relativity [12], we obtain the 4D gravity equation for a mass M within a covariant 4D Lorentz manifold

$$G_{\mu\nu} = 8\pi G \left(T_{\mu\nu} - \rho(E_o/kT, \bar{r}) g_{\mu\nu} \right) \quad (5)$$

where $G_{\mu\nu}$ is the 4×4 gravity tensor, G is the Newtonian constant, $T_{\mu\nu}$ is the

4×4 energy tensor, while $g_{\mu\nu} = \frac{\partial x_\mu}{\partial x_\nu}$ and $\rho(E_o/kT, \bar{r})$ represents the energy

density of the e-trino, anti-e-trino which is geometry and relative phase dependent. For example, if the e-trino and anti-e-trino rotate in phase with a radius r_o , or in opposite phase, these geometrical restrictions lead to self-rotation of stars and planets as well as a dipolar magnetic field [22] [23]. And then there is the totally incoherent separated e-trino, anti-e-trino distribution in a non-regular 4D geometry

$$\rho(E_f/kT, \bar{r}) = \left\langle c |\bar{p}| c_{\bar{p}}^* c_{\bar{p}} e^{i\bar{p}\cdot\bar{r}} \right\rangle_f + \left\langle c |\bar{p}| d_{\bar{p}}^* d_{\bar{p}} e^{i\bar{p}\cdot\bar{r}} \right\rangle_f \quad (6)$$

where $\langle \rangle_f$ represents the Fermi average, and $c_{\bar{p}}$, $d_{\bar{p}}$ are massive electrons

and protons. Only through this would we obtain an electromagnetic component of field energy.

Note because mass is created from the excitation of the Higgs vacuum ρ is not due to the B.E. Bosons B and D.

Should we define Einstein cosmological constant

$$\Lambda = 8\pi G\rho(E_o/kT, \bar{r}) \quad (7)$$

we observed it behaves like the Wheeler wormhole [20]. For the case given by Equation (6) and $E_f/kT \rightarrow 0$, $\rho(\bar{r} \rightarrow 0) \rightarrow 0$. The gravity Equation (5) leads to a singular solution resembling a “black hole”. Except as masses spiral into $\bar{r} \rightarrow 0$, E_o/kT will increase and the singularity will be removed.

It is not necessary to apply the Einstein-Kaluza-Klein compacting of the proper time to unify with electromagnetic theory, as the homogeneous Maxwell 4D is a natural boundary of the homogeneous 5D manifold and thus will coexist with the Lorentz 4D manifold.

Going down in the C cut-off value after protons, neutrons and electrons were created, we would obtain the periodic table elements, so that as the universe expands, creation of galaxies, stars and planets formation follows [22] [23]. Resulting in stars and planets having self-rotations and a dipolar magnetic field. Finally on the climatic surface of a planet allows further breaks of the 3 dimension space symmetry into $2D \times 1D$, as gravity defines the normal axis similar to the Perelman-Ricci Flow mapping, thus favoring formation of 2D type molecules. As represented by the toroidal topology [24] [25], this would then make the z axis of the toroidal an entangled variable between the B, D Bosons and a quantum spectrum with

$$E_n = \sum_{k=1}^M Q_k h\nu_o 2^{n+p} 3^m \quad (8)$$

The factor 2 in Equation (8) comes from the \tilde{P} state while the power n and p correspond to B and D Bosons multiplicity. The factor 3 represents the 3 space variables and the power m is the quantum multiplicity.

And with Carbon-nitrogen molecules creating the nitrogenous bases. It is the thermal averaged excitation energy from that and the allowed quantum tunneling of the B, D DLRO bosons along an RNA or in a closed loop in a DNA. Thus we have the B and D eigenfunctions representing the genome spectra.

To understand Equation (8) let us consider a semi-conductor band, with an empty CB band separated to the filled VB band by a positive band gap. An electron can be excited from the VB into the CB. As this happens, the Coulomb binding will create an exciton, which is obviously a Bose-Einstein condensed Boson, as its center of mass has no translation motion, with quantum energy orbital levels within the band gap. These orbital levels depend on the effective masses of the electron and the hole, a property due to the crystal lattice structure. Suppose, we imposed a toroidal boundary, then it is obvious that both the excited electron and the hole closed orbits must wind around the toroidal. Pictorially we can compare such an orbital to winding a rubber band around a metal

wire, then band the wire into a closed toroidal, which then gives us the expression for Equation (8). Note that each winding around the wire is of only a fraction of a quantum flux. The quantity Q_k then represents the ensemble weight for the fundamental single winding with energy $h\nu_o$, which is a thermal averaged of its environment. The factor 3 thus represents the 3 orthonormal choices of the toroidal normal. The power m is then the stacking number of such toroidal.

5. The Thermal Averaged Excitation Energy

It is interesting to investigate Equation (4). And that all matters are then the result of thermal excitation E' from it.

We can look at the minimization of the thermal averaged excitation energy $\langle E' \rangle$ w.r.t. E_o or w.r.t. T . This optimization procedure is for obtaining the upper limit of j , as the lower limit is fixed at 1.

In the first case, we get

$$\sum_{j=1}^{\infty} \left\{ \frac{2}{j} - \frac{E_o}{kT} \right\} e^{-E_o j/kT} \quad (9)$$

The coefficient depending on j , vanishes at $2kT = jE_o$. And becomes positive as long as

$$2kT > jE_o \quad (10)$$

However that implies E_o/kT must be quite small for $\langle E' \rangle$ to contain a few terms in j .

If E_o is $2m(e)c^2$, the rest energy of two electrons, then with the lowest optimum $j = 2^5 = 32$ gives us the rest energy of the bare Quark. 2^5 represents 2×2^4 , where the power 4 comes from the 4 homogeneous space variables, and the factor 2 comes from the B and D Bosons pair excitation. Fixing these numbers gives us the lowest T value, which would be roughly $10^7 - 10^8$ K, corresponding to the Bethe Fusion temperature.

Should we consider E_o as the hydrogen binding R, which is 13.6 eV. Then we will get T down to the range only of 400 K to 4000 K. With Hydrogen at the lower T end, and j the number of stable elements matches the forming of the chemical elements in the periodic table at averaged temperature in the earth's crust. Note our arguments depend on assuming space homogeneity, or the masses formed from excitation of the Higgs vacuum are Poincare spheres. Thus this argument cannot be applied to the nitrogenous bases and hence life forms, as there the space is $2D \times 1D$. There we must refer back to the toroidal model, leading instead to Equation (8).

Now turning to minimizing $\langle E' \rangle$ w.r.t. T , we get

$$2jE_o > [1 + \sqrt{5}]kT \quad (11)$$

This condition puts E_o as an upper limit for the fundamental molecular coherent and de-coherent members, when T is given at averaged earth surface temperature. This too is interesting because with either too high or too low T values,

these molecules might not be possible. A condition Schrodinger conjectured. Combining Equations (10) and (11) leads to

$$4kT > 2jE_o > [1 + \sqrt{5}]kT \quad (12)$$

Equation (11) puts a limit on E_o/kT

$$4 > 2jE_o/kT > [1 + \sqrt{5}] \quad (13)$$

Since j is an integer starting from 1, for the energy needed to create Quarks, $kT > 64m(e)c^2$. A result consistent with P1 projection for the creation of Quarks, at Bethe Fusion temperatures, so that equal number of protons to electrons can be simultaneously created to maintain the overall charge neutrality of matter as is required from starting with a net 0 charge 5D space-time universe. Therefore for the Higgs vacuum excitation to create matters, kT must be much greater than E_o .

Should T be in the room temperature range, that is around 300 K. which would be of order 10^5 to 10^6 lower than the Fusion temperature, the value of E_o then can be down to 10 - 100 eV, which is in the atomic hydrogen binding range. Thus T plays an important role in the formation of elements and molecules. The width of the E_o range determines the number of stable elements and molecules as well as solid crystals that may exist at T . In fact, it automatically gives us the coherent and de-coherent molecular spectra. Thus T with its varying range plays a most important role in the types of stable matters that can exist. Our argument can be extended to life forms, where j optimum number than corresponds to its genome. Which in turn fixes the life form's body temperature. The more stable the T value as needed for the specific life form, the better would be the DNA spectra to control the reproduction of proteins and cells in the body.

With this simple mathematical estimation, we show the importance of climate change on the survival of all life forms on earth.

As the B, D Bose-Einstein condensed state is excited by introducing $E_o/kT > 0$, it simultaneously created a 4D non-homogeneous Lorentz manifold through a Perelman-Ricci-flow mapping, thereby creating a toroidal structure, thus all energy eigen-solutions due to the kinematic of the masses contain within must satisfy the toroidal boundary. This condition was suggested by Frohlich in 1968 [26]. It is due to such imposed boundary condition, that led Geesink and Meijer [14] to come up with Equation (8).

Based on this formula and for a non-charged molecule, such as water, Geesink and Meijer [14] normalized its weight of 18 atomic mass unit as 1, and considered its spinning energy spectrum which must be proportional to its weight, satisfying Equation (8), they found that there exists two other atoms/molecules that will also be coherent. They were Carbon and Hydrogen molecule. The weight ratio of Carbon to water is $2/3$, while Hydrogen molecule to Water is $[1/3]^2$. Irrespective of charge and gauge invariance, the 5D to Lorentz 4D conformal mapping will result in a set of SU(3) generators, namely: $2/3$, $2/3$ and $-1/3$. Carbon being a covalent atom, therefore represents the two $2/3$ Lie group

generators. For atomic weight there are no negative values. Thus for the $-1/3$, we can only have $[-1/3]^2$. It is therefore clearly verified that the fundamental set of coherent molecules obtained via the Perelmann-Ricci-flow mapping is water, carbon, and hydrogen. This essential result recognition shows the importance of these 3 elements as the key building blocks for more complex importance bio molecules, such as sugar, proteins and fats, and must be the building blocks in all life forms. Other coherent molecules consisted of other elements obviously can exist, but are less essential as they all satisfy higher products of the Lie group generators. A detailed list was provided in ref. [14]. Should we replace hydrogen in water by heavy hydrogen. That is changing the single proton to a proton and a neutron. This heavy water no longer satisfies the mass unit normalization, hence its spinning eigen-energy does not obey Equation (8), and its spectrum becomes Decoherence. The presence of heavy water is then detrimental to life forms. Of course heavy water is radioactive, and one might think this example is a not conclusive proof of Decoherence effect. Because some gases such as chlorine and fluorine dissolve in water, their presence would essentially also change the non-pure water spinning eigen-energies into Decoherence, and hence detrimental to life forms. We use this result for disinfection of our swimming pool water, or in killing germs.

The coherent biomolecular spectra span from roughly 10 Hz to 500 Hz. Because of the low energies, it contains more resolvable information than the higher frequencies, and actually coincide with our modern 5G telecommunication. In fact, this same spectra covers all the life forms DNA spectra and is used in the growth mechanism. Hence constant exposure to such external radiation source would be harmful to the proper growth of our body. Unless there is a technological way to prevent our body exposure to the 5G telecommunication sources it should not be used. On the other hand, realizing this coherence spectra can also be applied beneficially to induce our body to counter cancerous growth. One method is targeting the cancerous growth by applying a corrective radiation through the nerve system via the technique of acupuncture. Both of these topics certainly deserve further research. It was well-known that soothing music in this audible range helps our body and mind, while exposure to decoherent noise is harmful.

6. Life Forms

Although the coherent molecules such as water, hydrogen and carbon are essential building blocks for hydrocarbon bio matters, such as proteins, fats, muscles, bio-cells, etc., we still need a mechanism over and on top of energy to make them happen and grow so that we can get life forms. It was postulated by us [16] that this came about because of the matching of the DNA frequency spectra which are of DLRO as they are eigen-solutions of the B, D bosons to those of the coherent molecules, such that via formation of ODLRO in the bio-systems can such ordered matching occur. In another word, it is via a superconducting tran-

sition that the coherent molecules were assembled to form the bio cells, proteins, fats, etc. and eventually the entire life form.

The superconductivity phase transition can occur if the environmental temperature T is below the superconducting critical Temperature T_c . As such the life form's body temperature T must remain below the T_c 's for each and every bio cell, and bio-structures within its body. But since the coherent molecules building blocks are charge neutral, all bio-structures, its electronic structure can only be semi-conductor like, with a partially filled valence band and an empty conduction band separated from the valence band with a positive band gap G . Such a band structure resembles that of the known High Temperature Cuprate Superconductors [27] [28] [29]. Hence, the bio-growth mechanism is the same as that in the ceramic HTC. The DNA of a life form is composed by the stacking of two linear chain of side by side nitrogenous bases. Within each nitrogenous base, there are three side by side carbons, and then separated with a nitrogen on both ends, before attaching to a backbone carbon twisting chain. There are in fact 3 such distinct bases that permit the B, D bosons that might exist in the side by side carbon nuclear time frozen 5D cores to quantum tunnel to the adjacent level base, while there is one end cap nitrogenous base, that only allows for reflection. Hence, a closed loop of the B, D DLRO can be formed. Because the B, D are DLRO bosons, that are in fact the magnetic monopoles, their quantum flux unit is governed by a π rotation [2] instead of 2π , the 3 adjacent carbons within each nitrogenous base then exactly satisfy this gauge requirement. It is this topological confinement and the 3D space dimension projection into $2D \times 1D$ that must happen according to the 5D symmetry breaking we are led to the formation of these 4 nitrogenous base structures. Because of such features of the 4 nitrogenous bases, there are different stacking orders possible in the formation of the DNA of a life form. It is such distinct stacking orders that give the genome. Since each specific order stacking within the DNA contains a unique DLRO spectrum, it would induce a similarly order the choice of coherent molecules via a ODLRO phase transition of the VB holes to form the specific bio cell and its Point Group structures. Hence, we postulate that life forms are also a natural result from the 5D homogeneous symmetry breaking. Starting with simple viruses, such as COVID-19 [30] [31], to the most complex known for us human [16]. But because its existence is subjected not only to the Bose distribution excitation of the B, D bosons, but also the two key temperature requirements. First that from the liquid phase of water, and second the bio body temperature $T < T_c$'s of all the bio-cells and bio-materials within the body of the life form. Any changes to the temperature would lead to sickness or death of the life. In short, starting with the 5D universe, each successive step of creation appears to follow a determined sequence, all the way to the creation of us human.

7. Conclusions

Since the publication of the book "The Five Dimension Space-Time Universe. A

creation and grand unified field theory model”, we had published several detailed articles covering numerical hadron mass calculations, to astronomical data of stars and planets, as well as the explicit Maxwell’s magnetic monopoles, based on several mathematical theorems, starting with Fermat’s Last Theorem [32] to Perelman’s Ricci-Flow and entropy mappings, and the resolving of the SU(2) and SU(3) Lie Groups as a direct product to the Poincare Group as required by the McGlenn’s Theorem. Thus verifying the Lee-Yang theory [33] on the Parity violation in Beta Decays [34], and the Gell-Mann Standard Model for hadrons. From these, we had also extended to the fully relativistic 2D hydrogen model with the exact 2D Chern-Simons gauge [35]. Less rigorous extensions were also proposed by us for the formation of the nitrogenous bases in RNAs and DNAs, thus leading to our modeling for life forms, from human to COVID. Then starting with the explicit monopoles, we show its mathematical equivalence to the Higgs Bosons. Through that established a Higgs vacuum in the time irreversible ever expanding 5D Universe. Each step of our investigation led to other branches of scientific researches. Including the ideas of Schrodinger that Life is a fully quantum phenomena [26]. It is to all these efforts that this current paper also aims. In particular in this current paper, we try and connect the Florhlich’s idea of the coherence quantum vibration sequence in biomolecules, thus justifying the Geesink-Meijer formula for the coherence biomolecules. Perhaps of most interest is it did lead to the identification of water, carbon and hydrogen as the essential building blocks of all bio-materials [36]. Last but not least, we were able to connect the Einstein’s Cosmo Constant in the Gravity tensor equation to that of the energy density derived from the thermal excitation of the Higgs vacuum, a result due to entropy as postulated in the Perelman’s mappings. In this current paper, the Dirac second quantization representation, only serves as a more pictorial explanation of the physics we have previously found, itself does not give us new knowledge. Yet, indeed there remain many more detailed questions for us to investigate. Including details to each bio cell’s relationship to the DNA and the body’s functions, and methods of RNA, DNA modifications, and its potential in treatment of inherited deceases. [see for example the viro-vector approach in modifying the RNA thus leading to a non-defective DNA for certain rare childhood cancer therapy of Rocket Pharma, RCKT].

So far, we, human have achieved all these because we are the only life form on earth born with a brain capable of sophisticated intelligence, and able to accumulate knowledge through learning and logical analysis. Today we even can modify our own DNAs as we mentioned by RNAi methods. Recently through mRNA method, Pfizer developed a vaccine for the COVID-19 pandemic. As well as biotechnology firms similar to Rocket, through RNAi developed cure for some cancers. However, human is still like all other life forms, he possesses a natural selfish preservation instinct. It is this self-preservation instinct that different races and nations foster racism, and occupation of weaker nations through wars. Today, human technologies have created self-destructive weapons that can

easily lead to its own extinction, just like other animal species in history. For human to survive, it must change its behavior, and promote LOVE, love of all nature's creations, race equality, and global cooperation among nations, if we, human are to be able to succeed to understand fully all of Creation, and the Creator's purpose. Despite the title of this section being called "Conclusions", I would suggest that it should be more appropriately named as an introduction to the effort for understanding the Creator's true purpose and for our own existence.

Acknowledgements

We thank Ms. Winnie So for her help in the manuscript, and Professors G. Dreschhoff, H. Jungner and P.C.W. Fung for their contributions in much of the cited previous publications in particular the Five Dimension Space-Time Universe Book, published by Scientific Research Publishing, USA in 2014, without which this summary note with second quantized Dirac Representation cannot be written.

Conflicts of Interest

The authors declare no conflicts of interest regarding the publication of this paper.

References

- [1] Wong, K.W., Dreschhoff, G.A.M. and Jungner, H. (2014) The Five Dimension Space-Time Universe. A Creation and Grand Unified Field Theory Model. Scientific Research Publishing, USA.
- [2] Perelman, G. (2002) The Entropy Formula for the Ricci Flow and Its Geometric Applications.
- [3] Perelman, G. (2003) Ricci Flow with Surgery on Three-Manifolds.
- [4] Kaluza, T. (1921) Zum Einheitsproblem der Physik, Sitzungsbericht der K. Preussischen Akademie der Wissenschaften. Mathematische Physik, Berlin, 966.
- [5] McGlinn, W.D. (1964) *Physical Review Letters*, **12**, 467. <https://doi.org/10.1103/PhysRevLett.12.467>
- [6] Gell-Mann, M. (1964) *Physical Review Letters*, **12**, 155. <https://doi.org/10.1103/PhysRevLett.12.155>
- [7] Wong, K.W., Dreschhoff, G. and Jungner, H. (2012) *Journal of Modern Physics*, **3**, 1450-1457. <https://doi.org/10.4236/jmp.2012.310179>
- [8] Maxwell, J.C. (1864) *Philosophical Transactions of the Royal Society*, **155**, 459-512.
- [9] Wong, K.W., Dreschhoff, G., Jungner, H., Fung, P.C.W. and Chow, W.K. (2018) *Physics Essays*, **31**, 493-495. <https://doi.org/10.4006/0836-1398-31.4.493>
- [10] Higgs, P.W. (1964) *Physical Review Letters*, **13**, 508-510. <https://doi.org/10.1103/PhysRevLett.13.508>
- [11] The CMS Collaboration (2012) *Science*, **338**, 1569-1575. <https://doi.org/10.1126/science.1230816>
- [12] Einstein, A. (1916) *Annalen der Physik*, **49**, 769-822.

- <https://doi.org/10.1002/andp.19163540702>
- [13] Toms, D.J. (1984) An Introduction to Kaluza-Klein Theories. In: *Workshop on Kaluza-Klein Theories, Chalk River/Deep River*, World Scientific Publication, Singapore, 185.
- [14] Geesink, H.J.H. and Meijer, D.K.F. (2018) *Journal of Modern Physics*, **9**, 898-924. <https://doi.org/10.4236/jmp.2018.95056>
- [15] Streltsov, A., Adesso, G. and Plenio, M.B. (2017) *Review of Modern Physics*, **89**, Article ID: 041003. <https://doi.org/10.1103/RevModPhys.89.041003>
- [16] Wong, K.W., Fung, P.C.W. and Chow, W.K. (2019) *Journal of Modern Physics*, **10**, 1548-1565. <https://doi.org/10.4236/jmp.2019.1013103>
- [17] Liu, J., Zhang, H., Howard, A.W., *et al.* (2019) *Nature*, **575**, 618-621. <https://doi.org/10.1038/s41586-019-1766-2>
- [18] Abdul-Masih, M., Banyard, G., Bodensteiner, J., *et al.* (2020) *Nature*, **580**, E11-E15. <https://doi.org/10.1038/s41586-020-2216-x>
- [19] Wong, K.W., Fung, P.C.W. and Chow, W.K. (2019) *Journal of Modern Physics*, **10**, 557-575. <https://doi.org/10.4236/jmp.2019.105039>
- [20] Wheeler, J.A. (1955) *Physical Review*, **97**, 511-536. <https://doi.org/10.1103/PhysRev.97.511>
- [21] Wong, K.W. and Chow, W.K. (2020) *Journal of Modern Physics*, **11**, 1911-1917. <https://doi.org/10.4236/jmp.2020.1112119>
- [22] Fung, P.C.W. and Wong, K.W. (2015) *Journal of Modern Physics*, **6**, 2303-2341. <https://doi.org/10.4236/jmp.2015.615235>
- [23] Fung, P.C.W. and Wong, K.W. (2017) *Journal of Modern Physics*, **8**, 668-746. <https://doi.org/10.4236/jmp.2017.84045>
- [24] Lu, L., Xia, L., Chen, Z., *et al.* (2020) *NPJ Quantum Information*, **6**, 30. <https://doi.org/10.1038/s41534-020-0260-x>
- [25] Geesink, H.J. (2020) Energy States of Entangled Semiconductors Described by a Toroidal Code and a “Balanced Signal Technology”.
- [26] Frohlich, H. (1968) *International Journal of Quantum Chemistry*, **2**, 641-649. <https://doi.org/10.1002/qua.560020505>
- [27] Ching, W.Y., Xu, Y.N., Zhao, G.L., Wong, K.W. and Zandiehnam, F. (1987) *Physical Review Letters*, **59**, 1333. <https://doi.org/10.1103/PhysRevLett.59.1333>
- [28] Wong, K.W. and Ching, W.Y. (2004) *Physica C*, **416**, 47. <https://doi.org/10.1016/j.physc.2004.09.003>
- [29] Wong, K.W. and Curatolo, S. (2008) EEM: The Exciton Enhancement Mechanism Theory and Experimental Evidence of Optically Enhanced Tc in High Tc Superconductors. In: Chang, O.A., Ed., *Progress in Superconductivity Research*, Nova Science Publishers, Inc., Hauppauge, 55-78.
- [30] Wong, K.W., Fung, P.C.W. and Chow, W.K. (2020) *Open Journal of Biophysics*, **10**, 88-95. <https://doi.org/10.4236/ojbiphys.2020.102008>
- [31] Matsuyama, E. (2020) *Journal of Biomedical Science and Engineering*, **13**, 140-152. <https://doi.org/10.4236/jbise.2020.137014>
- [32] Aczel, A.D. (1997) Fermat’s Last Theorem: Unlocking the Secret of an Ancient Mathematical Problem. Penguin Press, London.
- [33] Lee, T.D. and Yang, C.N. (1956) *Physical Review*, **104**, 254. <https://doi.org/10.1103/PhysRev.104.254>

- [34] Wu, C.S., Ambler, E., Hayward, R.W., Hoppes, D.D. and Hudson, R.P. (1957) *Physical Review*, **105**, 1413-1415. <https://doi.org/10.1103/PhysRev.105.1413>
- [35] Gou, S.H., Yang, X.L., Chan, F.T., Wong, K.W. and Ching, W.Y. (1991) *Physical Reviews A*, **43**, 1197-1205. <https://doi.org/10.1103/PhysRevA.43.1197>
- [36] Geesink, H.J. (2020) Proposed Informational Code of Bio Molecules and Its Building Blocks: Quantum Coherence versus Decoherence.

Dark Matter Creation and Anti-Gravity Acceleration of the Expanding Universe

F. C. Hoh

Retired, Dragarbrunnsg, Uppsala, Sweden

Email: hoh@telia.com

How to cite this paper: Hoh, F.C. (2021)
Dark Matter Creation and Anti-Gravity
Acceleration of the Expanding Universe.
Journal of Modern Physics, 12, 139-160.
<https://doi.org/10.4236/jmp.2021.123013>

Received: December 17, 2020

Accepted: February 6, 2021

Published: February 9, 2021

Copyright © 2021 by author(s) and
Scientific Research Publishing Inc.

This work is licensed under the Creative
Commons Attribution International
License (CC BY 4.0).

<http://creativecommons.org/licenses/by/4.0/>



Open Access

Abstract

Dark matter is identified as negative relative energy between quarks in proton and is generated in cold hydrogen gas with pressure gradient in gravitational field. Positive relative energy PRE can be generated between quarks in protons in cold hydrogen gas in outskirts of the universe. The mechanisms for such creation of dark matter and PRE are reviewed and updated in greater detail and clearer manner. The so-generated dark matter in a galaxy can account for the galaxy's rotation curve. Star formation in this galaxy uses up the hydrogen atoms and thereby reduces its dark matter content. Dark matter created in intergalactic hydrogen gas can form filaments. In a hypothetical model of the universe, a hydrogen atom with a small amount of negative relative energy or dark matter at the outskirts of this universe can via collisions with other atoms turn into one with a small positive relative energy PRE. Once such a sign change takes place, gravitational attraction switches to anti-gravity repulsion unopposed by any pressure gradient. This leads to a "run away" hydrogen atom moving away from the mass center of the universe and provides a basic mechanism for the accelerating expansion of the universe. This theoretical expansion and the measured redshift data are both compatible with the conception of an acceleratingly expanding universe and complement each other. But they cannot verify each other directly because the present model has been constructed for purposes different from those of the measurements. But it can be shown that both approaches do support each other qualitatively under certain circumstances for small velocities. Dark matter and PRE in the present model are not foreign objects like WIMPs and dark energy-cosmological constant but can only be created in cold hydrogen gas in gravitational field. To achieve this, infrequent collisions among the hydrogen atoms must take place. Dark matter was created first and can eventually later evolve into PRE in the outskirts of the universe and in the intergalactic void. Dark matter and PRE will disappear if the hydrogen atom carrying them becomes ionized as in stars.

Keywords

Relative Energy between Quarks, Scalar Strong Interaction Hadron Theory SSI, Negative Relative Energy, Dark Matter, Positive Relative Energy PRE, Anti-Gravity Repulsion, Universe Expansion, Proton Orbit, Hubble's Law

1. Introduction

1.1. Λ CDM and General Relativity

The present standard model of big bang cosmology Λ CDM [1] (Lambda CDM) is based upon general relativity, a first principles' theory, augmented by additional concepts including Friedmann's scale factor and Cold Dark Matter. In the development of this subject, it is desirable to reduce the number such postulates introduced by hand and incorporate some of the aimed effects as natural outcomes of a new such theory.

Further, general relativity is a classical theory in which mass, length and hence also mass density are continuous quantities that can be 0 and ∞ . However, the smallest mass unit contributing to baryonic matter in the universe is the proton mass, a discrete quantity $\neq 0$. In addition, the proton comprises of 3 point-like quarks which do not occupy the same spatial position and do have extension in space so that its mass density cannot be ∞ . Therefore, general relativity breaks down at small distances and high mass densities when applied to the real universe and has to be "cut off" at suitable values from such 0 and ∞ where quark structure of matter enters.

1.2. Standard Model

In the parameter regions cut off from general relativity, an appropriate elementary particle theory is supposed to fill in. The obvious first choice is the current mainstream particle theory, the standard model SM [2]. This half century old theory is based upon a hypothetical Higgs boson. The Higgs-like boson found in 2012 [3] was assigned to it. Subsequently, however, it has not been possible to establish that this boson is the SM Higgs boson (re isospin, assigned to $W^+ W^-$ bound state below). This model, including quantum-chromodynamics QCD, has turned out to be not useful; it cannot account for even the most basic meson spectra and does not describe the behavior of quarks in proton. Further, it cannot explain the existence of dark matter and dark energy.

Cosmologists have been attracted to SM by its Higgs mechanism which converts the energy created in the big bang to electron and quark masses. Such fermions obey Dirac's equation and hence are observable, as does the electron. But the so-generated quarks cannot be observed and this contradicts the Higgs hypothesis. The situation reminds me of Einstein's citation of a Bertrand Russell formulation: "Naive realism, if true, is false. Therefore, it is false".

1.3. SSI and PRE-Positive Relative Energy

In its place, the scalar strong interaction hadron theory SSI has been proposed [4] [5]. This theory has been relatively successful in treating basic aspects of meson spectra, some meson decays, kaon CP violation, quark structure of nucleon, neutron decay, baryon magnetic moment, and transition to QCD. The 125 GeV Higgs-like boson [3] was assigned to the estimated 117 GeV $W^+ W^-$ bound state [5] (p. 158). Of particular interest here are the interquark wave functions in proton needed in (2.1) below. In SSI, a hadron consists of quarks interacting via scalar force. The unknown relative energy between these quarks has been put to 0. Gravitation is absent and only nonrelativistic hadrons have been treated.

Recently, it has been pointed out that such relative energy of a nucleon interacts with gravitational fields on equal footing as does the nucleon itself [6]. In cosmic situations, therefore, such relative energy needs to be restored in SSI. Negative and positive relative energies have been assigned to the inferred dark matter and dark energy, respectively [6] [7] [8].

Negative relative energy or dark matter generated in a neutron on the Schwarzschild sphere of a neutron star falling towards its center can exactly cancel the gravitational energy gained in this fall. This neutron becomes weightless and the fall is halted. This mechanism can prevent the creation of gravitational singularity [7] (Section 6 - 7). Dark matter is also generated in cold hydrogen gas in an expanding galaxy. It provides additional attractive force to keep fast moving stars from escaping this galaxy [7] (Section 8).

Positive relative energy can be generated in outskirts of the observable universe but not where dark matter is created. Conventionally, dark energy is assumed to permeate throughout the universe and has been associated with the cosmological constant, as in the Λ CDM model. Therefore, the earlier assignment of positive relative energy to dark energy in [6] [7] [8] leads to confusion and has to be retracted. Here, the following definitions

$$-\omega = \text{relative energy between } uu \text{ diquark and } d \text{ quark in proton} \quad (1.1)$$

with mass E_0

$$\text{dark matter} = \text{negative relative energy between } uu \text{ diquark and } d \text{ quark in proton, } -\omega < 0 \quad (1.2)$$

$$\text{PRE} = \text{Positive Relative Energy between } uu \text{ diquark and } d \text{ quark} \quad (1.3)$$

in a proton, $-\omega > 0$

are adopted. The conventional meaning of dark energy remains unaltered. Like dark energy, PRE is also not observable but for different reasons.

1.4. Purpose

The above results have been obtained using simple models to illustrate the mechanisms. The purpose of this paper is to review and update these mechanisms in greater detail and clearer manner. A simple model of a galaxy and a hypothetical model of the universe have been constructed for this purpose. Further, ex-

pansion of the universe via anti-gravity repulsion caused by PRE is treated semi-quantitatively.

In Section 2, the basic mechanism of the generation of dark matter in a galaxy model is reviewed and clarified in greater detail. The so-created dark matter phenomenologically accounts for the galaxy rotation curve and filaments. This also paves the way for the mechanism of creation of PRE in Section 3. By means of a hypothetical model of the universe, such PRE leads to anti-gravity repulsion which expands the universe in Section 4. The so-obtained nonlinear equations of motion for a test hydrogen atom participating in such expansion is solved on computer in Section 5. Relations between the so-obtained results and Hubble's law and a partial comparison to the Λ CDM model are given in Section 6. The **Appendix** reproduces some earlier results for reference.

2. Dark Matter Generation and Applications

2.1. Basic Mechanism for Dark Matter Creation

The mechanism of dark matter generation [7] (Section 8), [8] (Section 4) will be explained in greater detail.

The coordinates of the diquark uu at x_I and the quark d at x_{II} in a proton cannot be observed. In SSI, they have been transformed into an observable laboratory coordinate X for the proton and an unobservable, "hidden" relative coordinate x (A2) between uu and d . The transformation constant a_m can in principle be any real number. In the plane wave expansion of the proton wave function (A3), the relative energy $-\omega$ is however connected to a_m via (A4), which insures that the proton mass and behaviour are unaffected by such a variable transformation [7] (5.1, 2), [5] (3.1.10a). The third of (A2) and (A4) then yield the ratio R_D between the relative energy generated to the proton mass E_0 ,

$$R_D = \frac{-\omega}{E_0} = -a_m + \frac{1}{2} = -\frac{|X - x_I|}{|x_{II} - x_I|} + \frac{1}{2} = -\frac{X_p - x_I}{r_a} + \frac{1}{2} \quad (2.1)$$

where X_p is the proton coordinate. The time components have been left out. The distance between uu and d , $|x_{II} - x_I|$, has been approximated by its average value $r_a = 3.23$ fm [8] (2.5) which depends upon the strong uu - d potential $\Phi_b(r)$ (A6) and wave functions (A7) in relative space. This situation is illustrated in **Figure 1** for a "test" proton at X_p in a "test" hydrogen atom in an expanding "test" galaxy.

This test hydrogen atom is acted upon by the ambient gravitational force and eventual centrifugal force due to its motion. These forces accelerate the proton and the electron in this atom equally and move the test atom as a single entity.

Phenomenologically, an average test atom is being pushed towards the right in **Figure 1** by the gas pressure gradient present due to the higher gas density and temperature in the inner part of the galaxy. This pushing force comes from collisions between this test atom and other atoms in the gas, acts on the electron of the test atom only and is a Coulomb force. In cold hydrogen gas in interstellar space, such

collisions are elastic. The proton inside this atom is largely shielded from this force by the charge of its orbiting electron. It will however be dragged along via just this electrostatic coupling to the electron. This force tends to move the electron and proton clouds to the right in **Figure 1** and increase the value of X_p in (2.1).

On the other hand, the gravitational pull from the galaxy center also acts directly on the quarks of the proton [8] (A1-2). This pull tends to move the uu - d aggregate in the opposite direction, towards the left, as is shown on the left half of **Figure 1**. This leads to a decrease of x_l in (2.1).

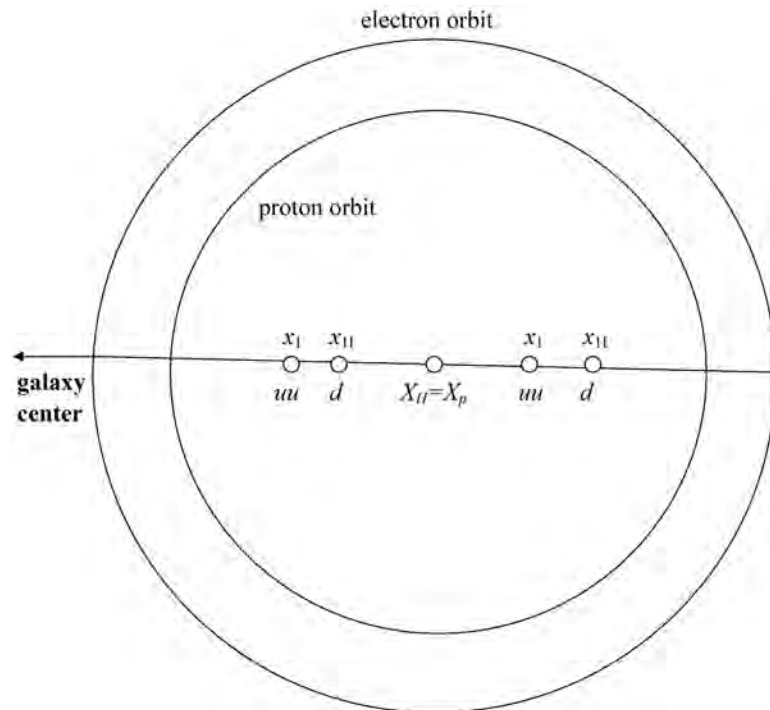


Figure 1. Schematic structure of a “test” hydrogen atom in an expanding “test” galaxy. The large electron orbit has been scaled down to fit inside this figure for illustration. Inside the proton orbit lies the center of the hydrogen atom X_H which is also the center X_p of the proton charge cloud having a radius of 28.8 fm (proton Bohr radius $a_{0,p}$, inner circle) as well as the center X_c (not shown) of the electron charge cloud having a radius of 0.53\AA (Bohr radius a_0 , outer circle). The aggregate of diquark uu at x_l and quark d at x_{ll} , normally also centered at X_p , has been pulled to its left by gravitational pull from the galaxy center while the electron tends to move away from the center due to higher gas pressure closer to this center (left half of figure). These deviations from the normal, centered position generate negative relative energy between uu and d which behaves like dark matter and enhances the gravitational pull. Near the outskirts of the galaxy, this uu - d aggregate may eventually end up on the right half of the figure after an elastic collision with another atom. Positive relative energy PRE, also invisible or dark, between uu and d is then generated instead of the dark matter above. This sign change of the relative energy causes this test atom to experience an anti-gravity repulsion pushing the quarks further away from the galactic center. The heavier uu diquark experiences a stronger gravitational pull from this center and therefore lies to the left of the lighter d quark. The average of the uu to d distance $|\underline{x}_{ll} - \underline{x}_l|$ is $r_d = 3.23$ fm. Dark matter and PRE can be created in cold, tenuous hydrogen gas. When this gas turns into fully ionized plasma in stars, the above mechanism no longer works and no such dark constituents can be generated.

It is this left shift of the position of the $uu-d$ aggregate relative to the position of the center of the proton and electron clouds corresponding to greater $X_p - x_l$ values in (2.1) that generates the negative relative energy or dark matter between uu and d ; $-\omega < 0$. If this $uu-d$ aggregate were shifted to the right, as is depicted on the right half of **Figure 1**, positive relative energy $PRE - \omega > 0$ would be generated. This case will be treated in Section 3.

The gravitational force exerts a greater pull on the heavier diquark uu than it does on the lighter quark d so that uu lies to the left of d and is closer to the galactic center in **Figure 1**. In SSI, the mass of these 3 quarks is about 50% greater than the nucleon mass [5] (Table 5.2); the difference is taken up by the strong, interquark potential Φ_b (A6).

2.2. Upper Limits of Dark Matter Generation

The above dark matter generation mechanism is phenomenological. A formal treatment would require an integration of SSI and gravitation. This is out of the scope of this paper. The mechanism in Section 2.1 holds for a single test hydrogen atom for some time before this test atom experiences a new collision and ends up in a new state in which the dark matter generated in Section 2.1 is altered or lost. Therefore, the gas containing this test hydrogen atom needs to be cold and tenuous so that collisions, necessary for such generation, are infrequent.

Under such circumstances, the direction of the pressure gradient in Section 2.1 will cause an average test proton to generate dark matter that, together with other similar hydrogen atoms, can lead to observable phenomena such as the galaxy rotation curve.

The amount of dark matter so-generated depends upon the value of the transformation constant a_m which can so far assume any real value. The interquark separation r_a in (2.1) depends upon the interquark strong potential (A6) in the relative space, decoupled from the laboratory space X , and is hence largely unaffected by an atomic collision. Thus, large a_m implies large $X_p - x_l$ which in its turn depends upon the unknown collision parameters. However, $X_p - x_l$ can be constrained in this test atom's environment.

For example, consider a collision that kicks the electron to the right which in its turn drags the proton at X_p along in **Figure 1**; $X_p - x_l$ assumes some positive value and dark matter $-\omega < 0$ is created according to (2.1). A harder collision leads to a greater $X_p - x_l$ and yields a larger amount of dark matter. But if the collision is too hard, the electron can be knocked off its orbit around the proton so that the test atom becomes ionized. In this case, the mechanism in Section 2.1 no longer works; the generated dark matter vanishes. In this case, $X_p - x_l$ is restricted by an unspecified *nonionization* limit. This restriction is practically satisfied because a temperature of $> 50,000$ °K is needed for ionization which far exceeds the temperature of the cold hydrogen gas environment of the test atom.

A milder form of restriction on $X_p - x_l$ is the *heuristic* limit which requires that the $uu-d$ aggregate belonging to a proton has to lie inside the proton cloud. How this can eventually be verified formally would require a formalism beyond

the scope of this paper. This heuristic restriction limits $X_p - x_l$ in **Figure 1** to the proton Bohr radius $a_{0p} = 28.8$ fm so that (2.1) becomes [8] (4.2)

$$R_{DM} = \frac{-\omega}{E_0} = -a_m + \frac{1}{2} \geq -\frac{a_{0p}}{r_a} + \frac{1}{2} = -8.4 \quad (2.2)$$

This magnitude is much smaller than that due to the above-mentioned non-ionization limit.

The observed average over the entire visible universe is $R_{DM} \rightarrow R_{DMEXP} = -5.6$ [1] which is not directly comparable to the heuristic R_{DM} (2.2) or to the unspecified nonionization R_{DM} . This is due to that these two R_{DM} values refer to a test atom in cold, tenuous hydrogen gas. Warm, rarified hydrogen gas and hydrogen molecule gas may eventually contribute to a less degree. On the other hand, R_{DMEXP} refers to all forms of ordinary matter in the observable universe including in addition ionized media, dust, stars, planets, etc in which no dark matter can be created by the mechanism of Section 2.1. Thus, R_{DMEXP} is created from the hydrogen gas part of the universe only. This part has therefore to produce $|R_{DM}| > |R_{DMEXP}|$. The actual $|R_{DM}|$ may perhaps lie around 8.4 of the heuristic (2.2) but well below the much higher, unspecified nonionization value.

This situation appears to be qualitatively compatible with Milky Way data. Milky Way has 1% - 5% cold hydrogen gas in volume and hence also a small % in mass. Therefore, it is expected to have a fairly small $|R_{DM}|$ value. The Milky Way dark matter density at the sun's position is $\sim 6 \times 10^4$ times smaller than average mass density of the universe.

The heuristic limit $|R_{DM}|$ is essentially the number of $uu-d$ aggregates with size $r_a = 3.23$ fm that can be fitted into one side of the proton cloud with radius 28.8 fm in **Figure 1**. For every shift of the $uu-d$ aggregate away from X_p by its own size 3.23 fm, a new dark proton is created, up to 8.4 such in (2.2). The energy needed to move X_p 28.8 fm, negligible on atomic scale, is very small and is estimated to be well covered in the momentum exchange of the collision.

The so-produced negative relative energy or dark matter in a proton is on equal footing with the proton mass itself [6], as will be shown in (4.2) below. It will therefore exert extra gravitational pull on fast moving stars farther away from the galactic center and prevent them from escaping the galaxy (**Figure 1** caption); it can account for the galaxy rotation curve [7] (Section 8). Similarly, it can also give rise to gravitational lensing.

Such an effect is also expected to be prevalent in the early phases of the expansions of galaxies and the universe. Near the centers, the temperature and pressure and their gradients were high and the gravitational pull was strong. The former leads to greater X_p and the latter to smaller x_l in **Figure 1**. Large $X_p - x_l$ values yield greater amount of dark matter $-\omega < 0$ via (2.1). No dark "energy" is created at this stage. These results are in agreement with our current conception.

2.3. Model for Filament Formation

Consider the following prototype scenario. A cold hydrogen gas cloud exists

between two galaxy clusters. Consider a cylinder of this cloud between these clusters. The gas near the cylinder surface will fall towards the cylinder axis. This gas will according to the mechanism on the left side of **Figure 1**, where the galaxy center is replaced by the cylinder axis, produce dark matter which tends to increase the fall speed. The gas along the cylinder axis will not produce any dark matter due to symmetry but will be compressed by the falling matter and dark matter and produce a radial pressure gradient. This cylinder then shrinks into a thin cylinder or a tube consisting mostly of dark matter except for its core which now contains hydrogen gas with high density. Galaxies may be formed along this matter and dark matter tube, resembling a filament [9]. The observed ratio of dark matter/visible matter of about 5 in such filaments is compatible to the upper limit of $|R_{DM}| < 8.4$ in (2.2).

2.4. Star Production and Decrease of Dark Matter

According to Section 2.1, dark matter can only be created in cold hydrogen gas in gravitational field. An exception can be some neutrons in neutron stars (see Section 1.3). However, stars are also being formed from the same gas. When a hydrogen atom in this gas is used to build a new star, it gets ionized and becomes part of the hot plasma in this star. The dark matter generated by this atom is lost and the so-produced free proton can, contrary to the proton in a hydrogen atom, not generate any dark matter via the mechanism of Section 2.1. Conversion of a hydrogen atom to a proton and an electron in a star implies a loss of dark matter in the gas.

Therefore, star formation in a galaxy reduces its dark matter content. The amount of dark matter that contributes to the galaxy rotation curve is diminished by star formation. This galaxy will appear to expand faster.

Similarly, if the universe runs out of hydrogen gas, all dark matter and PRE will also vanish, except possibly in neutron stars and some other exotic objects.

In helium, the simple two-body, uu and d , problem here turns into a many-body problem involving many quarks and relative spaces. This problem has not been investigated.

3. Mechanism of Generation of Positive Relative Energy PRE

The mechanism of positive relative energy PRE generation described in [7] (Section 9), [8] (Section 5) will be updated in greater detail.

As the test hydrogen atom in Section 2 moves outwards and eventually reaches the outskirts of the test galaxy, where the gas pressure gradient, eventual centrifugal force and gravitational pull acting on it become very small and nearly balance off each other so that the expansion of this galaxy nearly comes to a halt. In the absence of force acting on this hydrogen atom, its $uu-d$ aggregate will move back to its normal positions centered at X_p (see **Figure 1** caption) [7] (Figure 4, position e).

Although the net outward movement of this test hydrogen atom and its like

may nearly vanish, they will still have some small random velocities corresponding at least to the cosmic microwave background average temperature in the universe $\sim 2.8 \text{ }^\circ\text{K}$. Over time, this test hydrogen atom will experience a collision with another hydrogen atom that happens to be moving inward towards the galaxy center in **Figure 1**. The electron orbit of the test atom will then be slightly pushed to the left. This motion drags the proton at $X_H = X_p$ also to the left via Coulomb force. This atomic force is small compared to strong interaction forces in the relative space x . The $uu-d$ aggregate centered in **Figure 1** is $\sim 50\%$ heavier than the proton mass (see end of Section 2.1), is thus at least phenomenologically less affected by the collision and now lies to the right of X_p . This situation is equivalent to the right half in **Figure 1** (see also “lag” in Section 5.1 above 1)-3) below).

In this switched configuration, from the left half of **Figure 1** in Section 2 to the right half here, the positive $X_p - x_l$ values in (2.1) in Section 2 turns negative so that the negative relative energy generated in Section 2 changes its sign in (2.1) and turns into positive relative energy. This energy has been assigned to dark energy earlier [6] (Section 6), [7] (Section 9) but is here defined as PRE in (1.3). The gravitational attraction or pull on the dark matter in the test atom in Section 2 turns now into anti-gravity repulsion or push on the PRE produced, trying to push this test atom outwards, towards the right of **Figure 1**. Contrary to the gravitational attraction in Section 2, which is countered by gas pressure gradient, this anti-gravitational repulsion is unopposed, even supported by the very small pressure gradient present. For sufficiently large PRE created (see (4.5) below), this test hydrogen atom will “run away” [7] (Section 9) into the intergalactic void outside the test galaxy.

Applying the assumption in Section 2 that led to (2.2), (2.1) yields the heuristic upper limit of the ratio between the so-generated PRE to proton mass [8] (5.1),

$$R_{PRE} = \frac{-\omega}{E_0} = -a_m + \frac{1}{2} \leq \frac{a_{op}}{r_a} - \frac{1}{2} = 8.4 \quad (3.1)$$

which has the same magnitude as that in (2.2) due to the left-right symmetry of the proton orbit in **Figure 1**. There is also an analogous nonionization limit corresponding to that mentioned below (2.2). This limit will similarly not be reached due to the even lower gas temperatures here.

Again, such R_{PRE} limits refer to the by now cold hydrogen test atom in the outskirts of the test galaxy. Such R_{PRE} values can also not be directly compared to the measured ratio of dark energy to ordinary matter averaged over the universe $R_{DEEXP} = 13.6$ [1] for analogous reasons as those given for $|R_{DM}|$ given below (2.2). R_{DEEXP} refers to dark energies caused by entirely different mechanisms, *i.e.*, cosmological constant throughout the universe in the Λ CDM model.

The above developments show that dark matter and PRE are not foreign objects in SSI, like those in the Λ CDM model, but are generated in hydrogen gas in gravitational field and can vary and transform into each other dependent upon the positions of the $uu-d$ aggregates relative to the centers of the proton clouds.

The present scenario is compatible with a current view that dark matter appears first and dark energy later, about 6×10^9 years ago.

4. Expansion of a Model Universe

The mechanism in Section 3 can be applied to the expansion of the universe. Anticipating greater velocities for the accelerated test hydrogen atom, a Lorentz boost is performed on the rest frame proton whereby the heuristic limit (3.1) is approximately modified to

$$R_{PRE} = \frac{-\omega}{\gamma E_0} \leq \frac{a_{op}}{\gamma r_a} - \frac{1}{2}, \gamma = 1/\sqrt{1-v^2/c^2} \tag{4.1}$$

for slow protons, where v is the proton velocity and c the light speed.

4.1. SSI Model of Universe

The following SSI model of the universe shown in **Figure 2** is constructed to illustrate the expansion of the outer parts of the observable universe via the anti-gravity repulsion on the generated PRE.

Note that this model is not realistic because there is no known center of the observable universe. It is employed mainly for a semi-quantitative treatment of the anti-gravity expansion mechanism.

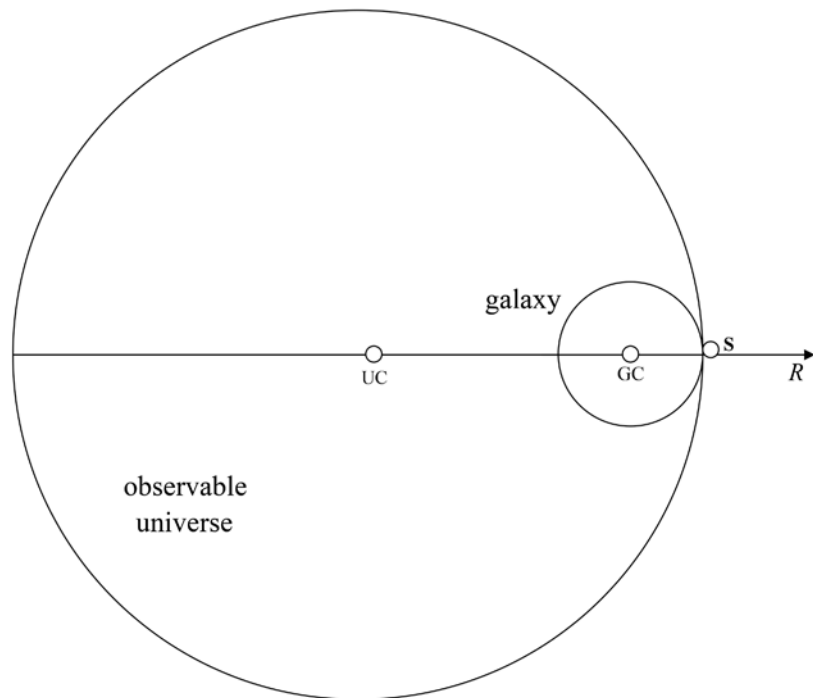


Figure 2. A hypothetical SSI model of the observable universe for illustration of the expansion of the outer parts of this universe. The large circle represents the observable universe as a sphere surrounded by vacuum. The actual boundary of this universe is not as sharp as is depicted but is somewhat diffuse. This universe is populated by galaxies with homogeneous distribution. The earth’s position is unknown. The small circle represents the “test” galaxy in **Figure 1** and is also a sphere lying in an outskirts of this universe. *UC* denotes the center of this universe and may eventually be associated with the big bang itself. *GC* is the center of the test galaxy. *S* denotes the point where the outer edges of both circles coincide. *R* is the distance of the test hydrogen atom from *S*.

From [1], the radius of the observable universe is $R_{US} = 4.4 \times 10^{26}$ m. The mass of this universe is estimated from the average density 9.9×10^{-30} g/cm³ of the universe and its volume and is $M_U = 3.53 \times 10^{54}$ kg. The test galaxy is taken to be a copy of the Milky Way in spherical shape. The radius is $R_{GS} = 100$ kly = 9.46×10^{20} m and the mass $M_G = 2.4 \times 10^{42}$ kg. This is about 3 times the mass of the Milky Way and reflects the modification of its disc form to sphere form here.

4.2. Equation of Motion and Applications

Let the position of the test hydrogen atom after the collision in Section 3 be $R(t)$ from S in **Figure 2**; t denotes the laboratory frame time X^0 and $R(0) = 0$. This test hydrogen atom will in time experience another collision. Before this happens, the proton in this atom obeys the equation of motion

$$\frac{d}{dt} E_0 \gamma(t) v(t) = G \left[\frac{M_G}{(R_{GS} + R(t))^2} + \frac{M_U}{(R_{US} + R(t))^2} \right] (-\omega - E_0 \gamma(t)), \quad (4.2)$$

$$v(t) = \frac{dR(t)}{dt}$$

where G is the gravitational constant.

Inclusion of the relative energy $-\omega$ next to the proton energy $E_0 \gamma$ in (4.2) has been demonstrated in [6] (Section 5). This can also be seen from (A3) where $-\omega X^0$ and $E_0 X^0$ are on equal footing. Since the proton mass E_0 is known to interact with gravitational field, the associated relative energy $-\omega$ has to do so also in view that x and X are both linear combinations of the quark coordinates x_i and x_{ij} in (A2). Equation (4.2) is general and holds for all free hydrogen atoms.

Initially, t is small, $R(t)$ can be neglected in (4.2) and $\gamma \cong 1$. Using the values given below **Figure 2**, (4.2) becomes

$$dv(t)/dt = -a_{c0} (1 + \omega/E_0), \quad a_{c0} = 1.396 \times 10^{-9} \text{ m/s}^2 \quad (4.3)$$

$$v(t) = v(0) - a_{c0} (1 + \omega/E_0) t, \quad R(t) = v(0)t - a_{c0} (1 + \omega/E_0) t^2 / 2 \quad (4.4)$$

where $v(0)$ is the initial velocity of this test hydrogen atom. About 13% of the initial acceleration a_{c0} comes from the galaxy mass M_G and 87% from the mass M_U of the universe.

If (4.3 - 4) were applied to the test hydrogen atom in Section 2.1, a_{c0} needs to be reduced by 87%. In the absence of relative energy, $-\omega = 0$, (4.3) simply describes the “free fall” of this test atom towards the galaxy center. If dark matter is generated, $-\omega < 0$, and this atom will fall faster. This inward movement is on the average largely balanced off by outward movement produced by the pressure gradient in the hydrogen gas in Section 2.1.

Picking up the “run away” test hydrogen atom mentioned above (3.1), which now lies at S in **Figure 2**. It has a small initial velocity and a PRE. The collision mentioned in the beginning of Section 3 was assumed to be strong enough to overcome the gravitational pull on the proton and produce a sufficiently large PRE $-\omega > E_0$. Then the right side of (4.3) becomes positive and accelerates this

test atom outwards; the above gravitational “free fall” now turns into *anti-gravity* “free rise”. A formal way to include such a collision in (4.2) is to put

$$-\omega = (1 + \Delta)u(t)E_0 < \left(8.9 - \frac{\gamma(t)}{2}\right)E_0 \quad (4.5)$$

Here, $u(t)$ is a step function; $u(t < 0) = 0$ and $u(t > 0) = 1$ representing the effect of the collision which takes place at time $t = 0$. $1 + \Delta$ is the amplitude of this step function and has to be > 1 to overcome the gravitational pull on the test hydrogen atom; $\Delta > 0$. Following the considerations on R_{PRE} below (3.1), the limit (4.1) is tentatively adopted on the right of (4.5). Inserting (4.5) into (4.2) yields

$$\frac{d}{dt}v(t) = G \left[\frac{M_G}{(R_{GS} + R(t))^2} + \frac{M_U}{(R_{US} + R(t))^2} \right] \left[\frac{(1 + \Delta)}{\gamma(t)} - 1 \right], \quad (4.6)$$

$$\Delta + 1 < 8.9 - \frac{\gamma(t)}{2}$$

For small $-\omega$ or negative relative energy $-\omega < 0$, the right side of (4.2) is negative. The accompanying attraction force increases with time as $R(t) < 0$ increases the magnitude of this side. Acceleration of the gravitational “fall” increases with time. On the other hand, for PRE satisfying (4.5) with $\Delta > 0$, the right side of (4.6) is positive but decreases with time because $R(t) > 0$ increases with time. This causes the acceleration of anti-gravity “rise” to slow down with time.

5. Computer Solutions and Anti-Gravity Expansion of the Model Universe

5.1. Computer Solutions and Accelerating Expansion

Here, the initial velocity $v(0)$ of the test atom will be taken to be the mean thermal speed of hydrogen atoms corresponding to the average temperature of the universe of $\sim 2.8 \text{ }^\circ\text{K}$ mentioned in Section 3,

$$v(0) = 263 \text{ m/s} \quad (5.1)$$

It is unknown how Δ in §4 can be evaluated. It will be regarded as a free parameter here tentatively limited by the heuristic $0 < \Delta < 7.4$ due to (3.1) and (4.5); the associated higher nonionization limit is ignored here.

The nonlinear (4.6) with the initial conditions $R(t = 0) = 0$, $v(t = 0) = v(0)$ has been solved on computers at Uppsala University. Some results are given in **Table 1**.

This table shows that the position $R(t)$ of the test atom and its velocity $v(t)$ increase with time compatible with an acceleratingly expanding universe [10]. For small t , these values follow the anti-gravity repulsion (4.4 - 5) closely. As $R(t)$ approaches first R_{GS} and then R_{US} (4.6) shows that the acceleration a_c slows down, mentioned at the end of Section 4.2. This is also reflected in **Table 1**. As $v(t)$ approaches the light speed, the present mainly nonrelativistic treatment of the motion of the proton in [5] breaks down and the results, marked by * in this table, are unreliable.

Table 1. Some results from numerical integration of the equation of motion of the test hydrogen atom (4.6). Δ is defined in (4.5) and characterizes the surplus of the positive relative energy PRE generated in the test hydrogen atom after a sufficiently strong collision with another atom near S in the model of **Figure 2**. It is a free parameter here satisfying $0 < \Delta < 7.4$. R is the distance of this test hydrogen atom from S and v its speed at time t after the collision. a_c/a_{c0} is the acceleration $a_c = d^2r/dt^2$ of this test atom in (4.6) normalized to its initial value a_{c0} in (4.3) just after the collision. H_0 is the Hubble constant given in (6.1) and H the Hubble parameter calculated from (6.5) below. The * specifies that this entry is relativistic with $\gamma > 1.2$ and hence is not reliable.

$t(\text{yr})$	0	10^4	10^5	10^6	10^7	10^8	10^9	10^{10}
$\Delta = 1.0$								
$R(\text{ly})$	0	1.61×10^{-2}	0.821	74.2	7.32×10^3	6.82×10^5	6.43×10^7	4.97×10^9
$v(\text{m/s})$	263.3	703	4.66×10^3	4.43×10^4	4.38×10^5	4×10^6	3.83×10^7	2.38×10^8
a_c/a_{c0}	1.0	1.0	1.0	1.0	0.983	0.874	0.855	0.156*
H/H_0	1.0	2.67	17.7	167	1040	267	27.6	2.22*
$\Delta = 4.6$								
$R(\text{ly})$	0	4.25×10^{-2}	3.46	338	3.33×10^4	3.05×10^6	2.85×10^8	8.85×10^9
$v(\text{m/s})$	263.3	2290	2.05×10^4	2.03×10^5	1.98×10^6	1.8×10^7	1.64×10^8	2.95×10^8
a_c/a_{c0}	1.0	1.0	1.0	0.999	0.944	0.87	0.69	1.5×10^{-11} *
H/H_0	1.0	8.69	77.9	740	2020	273	26.7	1.55*
$\Delta = 7.4$								
$R(\text{ly})$	0	6.31×10^{-2}	5.52	544	5.33×10^4	4.87×10^6	4.35×10^8	9.32×10^9
$v(\text{m/s})$	263.3	3250	3.28×10^4	3.06×10^5	3.16×10^6	2.88×10^7	2.38×10^8	2.98×10^8
a_c/a_{c0}	1.0	1.0	1.0	0.999	0.926	0.867	0.474*	7.5×10^{-12} *
H/H_0	1.0	13.4	125	1180	2030	274	25.4*	1.48*

For $v(0) = 0$, (4.3 - 5) show that R , v and a_c are all proportional to Δ . With (4.1), (4.6) is seen to behave similarly for small v . These three sets of values in **Table 1** then largely reduce to one multiplied by 3 different Δ values. Since $v(0)$ in (5.1) is small relative to $v(t)$ in general, results in **Table 1** are not sensitive to $v(0)$ and are nearly independent of it for large Δ values. For a collision that led to $\Delta = 4.6$, which corresponds to the measured average ratio $|R_{DM}| = 5.6$ for dark matter below (2.2), the test hydrogen atom will reach a distance of 3×10^6 ly with a velocity of 1.8×10^7 m/s 10^8 years after its collision at S in **Figure 2** provided that it did not collide with another atom.

As was shown beneath (4.5), $\Delta > 0$. Computer runs with $\Delta < 0$ leads to negative $v(t)$ and blueshift. The bulk of the random collisions will yield $\Delta < 0$ and these do not contribute to expansion. But sooner or later, a subsequent collision will produce $\Delta > 0$. Once this occurs, one of the colliding atoms will become of the “run away” type obeying (4.6) and starts to move outwards and leave the S region in **Figure 2** and cannot back off. An analogy may be to push a “test ball” onto a road with a downward slope $\propto \Delta$; it will “roll away” and cannot back up.

Δ is driven by (5.1). At the outskirts of a galaxy on an outskirts of the universe, the electron and proton clouds and the center of the $uu-d$ pair all lie at the center in **Figure 1**, as was mentioned in the beginning of Section 3 and in the caption

of **Figure 1**. Under such circumstances, a “run away” $\Delta > 0$ collision needs to move the electron and proton clouds only a few fm to the left of the $uu-d$ pair to produce $\Delta \sim 1$. Equivalently, with the electron and proton clouds remain centered in **Figure 1**, the right half of **Figure 1** depicts this case. The heavier diquark-quark pair $uu-d$ there “lag” behind relative to the charged clouds’ motion towards left.

It is this “lag” that produces PRE, positive relative energy, which is repulsed by the anti-gravity turned gravitational force from the mass inside the large circle in **Figure 2**. The atom containing this $uu-d$ pair, instead of “falling” towards the mass centers, will “rise” from them and moves away from them.

Analogous to the considerations above Section 2.3, the momentum exchange in such a collision is sufficiently energetic to move the charged clouds up to $a_{0p} = 28.8$ fm (2.2) away from the $uu-d$ pair in some of such collisions so as to produce all allowed Δ values up to 7.4.

If the above treatment for a single test hydrogen atom is to be applied to real expansion of the universe, the following ad-hoc assumptions need made:

- 1) All hydrogen atoms arriving at the outskirts of the observable universe indicated by the large circle in **Figure 2** will become of the “run away” test atom type near S there. They obey (4.6) between collisions but are slowed down on the average by collisions with other atoms.
- 2) All these atoms form hydrogen gas clouds in regions outside the large circle in **Figure 2** and condense to galaxies in which some stars are created. Complications with respect to different generations of stars are disregarded.
- 3) The protons in these stars cannot be accelerated according to (4.6) (see Section 2.4, end of **Figure 1**’s caption). These stars are assumed to be dragged along by the moving galaxies containing them via gravitational interaction and acquire the same speeds.

5.2. Scenarios of Expanding Model Universe

1) With the assumptions 1)-3) above, the velocity $v(t)$ increases with time t and with the distance $R(t)$ in **Table 1** compatible with the observed accelerating expansion of the universe in time [10] as well as with the distance from the observer (see Hubble’s law in Section 6.1 below). These results arise from the generated PRE. There are only dark matter and PRE but no dark energy in the model.

In this SSI model universe, hydrogen gas “leaks” out at its boundary (large circle in **Figure 2**) via PRE generated there whereby the hydrogen gas pressure also diminishes. This will maintain the gas pressure gradient there and the leak can continue. A semi-steady state scenario of the expansion of the universe at the present time is reached.

2) The scenario in 1) is derived from (4.6) and holds only for $R(t) \ll R_{US}$ because the newly created energy in the shell with thickness $R(t)$ outside the original universe (large circle in **Figure 2**) has not been taken into account. In time, this shell will be filled with the “run away” hydrogen atoms with PRE and part of them will collide with each other. As was mentioned above **Table 1**, the bulk of

such random collisions will yield $\Delta < 0$ so that the PRE carried by the participating atoms are lost. These atoms now return on the average to their normal state of a hydrogen atom. Only a small portion of collisions will produce new $\Delta > 0$ “run away” hydrogen atoms with PRE.

In this qualitative manner, the hydrogen atoms “leaked” out from the universe inside the large circle in **Figure 2** are largely recovered in the shell. The universe with radius R_{US} in **Figure 2** has now expanded into one with larger radius $R_{US} + R(t)$. This process is repeated as this model universe expands. As was mentioned at the end of Section 4.2, this anti-gravity accelerating expansion itself slows down with increasing t and $R(t)$ according to (4.6).

3) Another scenario concerns the assumed form of (4.5). The collision of the test hydrogen atom with another atom mentioned above (3.1) causes the relative energy $-\omega$ to change its sign. This implies that $-\omega$, a constant in the relative space x , can depend upon the laboratory time coordinate $X^0 = t$. There is no conflict here as such gravitationally induced time dependence is negligibly weak relative to those normally associated with strong inter-quark forces. Such a time dependence was included in (4.5) in form of the step function $u(t)$ with a constant amplitude $1 + \Delta$. This may be regarded to be a first order t dependence. To second order, a linear dependence in form of βt , where β is another unknown constant, may be added to the above step function and modify (4.5) to

$$-\omega = (1 + \Delta)u(t)E_0 + \beta t \quad (5.2)$$

Inserting this into (4.2) renders the acceleration in (4.6) to increase with time instead and enhances the rate of acceleration. The heuristic limit in (4.5 - 6) may then need be modified. Furthermore, as the expansion velocities approach the light speed, relativistic effects become important so that (4.2) as well as the treatment in the **Appendix** no longer holds.

5.3. Application to Dark Energy in Intergalactic Void

The mechanism of Section 5.2 1) for the expansion at the outskirts of the model universe can be taken over to apply to the outer edges of a galaxy, as was indicated above (3.1). The hypothetical center UC of the universe in **Figure 2** is replaced by the actual galaxy center. The analogously generated PRE in the gas near the outer boundary of this galaxy will “leak” into the space outside it. Such PRE loaded hydrogen gas can play the role of the “dark energy” observed in the intergalactic void.

6. Comparison of SSI to Hubble and Λ CDM Scenarios

6.1. Estimate of Hubble’s Parameter

Evidence of the expansion of the universe comes from Hubble’s law

$$v_H(t) = H(t)D(t), \quad H(0) = H_0 = 2.28 \times 10^{-18} / \text{s} \quad (6.1)$$

where v_H denotes redshift velocities of stars in distant galaxies measured from

the earth, D the earth to stars distances, $H(t)$ the Hubble parameter, and H_0 the measured Hubble constant. Differentiation of (6.1) yields

$$\begin{aligned} \frac{dv_H(t)}{dt} &= H(t)v_H(t) + \frac{dH(t)}{dt}D(t), \quad v_H(t) = \frac{dD(t)}{dt} \\ \frac{dH(t)}{dt} &= -H^2(t) + H(t)\frac{1}{v_H(t)}\frac{dv_H(t)}{dt} \end{aligned} \tag{6.2}$$

Let the earth be on a radius in **Figure 2**, closer to the boundary of the universe (large circle) than to its center UC. There is no loss of generality to choose this radius to be that ending at S in **Figure 2**. Let the distance from the earth to S be $R_{ES}(t)$ and the light emitting stars be located near $R(t)$, the position of the test hydrogen atom governed by (4.6). Then,

$$D(t) = R(t) + R_{ES}(t) \tag{6.3}$$

The Hubble constant H_0 in (6.1) cannot be derived from the present model because $R_{ES}(t)$ is unknown. Now $R_{ES}(t)$ lies inside the observable universe and changes with t slowly compared to $R(t)$ for a “run away” test atom accelerated via PRE near S in **Figure 2**. With the assumptions 1)-3) given above Section 5.2, differentiation of (6.3) together with the second of (6.2) and (4.2) leads approximately to

$$v(t) = v_H(t) \tag{6.4}$$

where the unknown $R_{ES}(t)$ drops out upon differentiation. Equations (6.4), (4.6) and the last of (6.2) leads to

$$\frac{dH(t)}{dt} = -H^2(t) + H(t)\frac{G}{v(t)}\left[\frac{M_G}{(R_{GS} + R(t))^2} + \frac{M_U}{(R_{US} + R(t))^2}\right]\left[\frac{1+\Delta}{\gamma(t)} - 1\right] \tag{6.5}$$

For small t , (4.6) can be replaced by (4.3 - 5) and (6.5) becomes

$$\frac{dH(t)}{dt} = -H^2(t) + H(t)\frac{\Delta a_{c0}}{v(0) + a_{c0}\Delta t} \tag{6.6}$$

For small Δ , the last term can be dropped and the solution is

$$H(t) = \frac{H_0}{1 + H_0 t} \tag{6.7}$$

which reduces to the second of (6.1) at $t = 0$. This deceleration is extremely weak. A 1% reduction of $H(t)$ will take 1.4×10^8 years.

A linearized approximation, valid for small t , is achieved via $H^2(t) \rightarrow H_0 H(t)$ in (6.6) which now yields

$$H(t) = H_0 \left(1 + \frac{\Delta a_{c0} t}{v(0)}\right) \exp\left(-\frac{H_0}{\Delta} t\right) \tag{6.8}$$

For Δ values in **Table 1**, $H_0/\Delta \ll \Delta a_{c0}/v(0)$ and the exponential factor in (6.8) can be dropped. This is equivalent to putting the small decelerating term $-H^2(t)$ in (6.6) to 0. Equation (6.8) then becomes the same as the first of (4.4) using (4.5) if $H(t)$ and H_0 were replaced by $v(t)$ and $v(0)$, respectively. Thus, the

Hubble parameter $H(t)$ increases with time at the same rate as does the accelerating expansion $v(t)$ in (4.4) for small t . As was mentioned above **Table 1**, this acceleration is qualitatively compatible with data [10].

This increase is due to that the last term in (6.6) arising from PRE acceleration is positive and large compared to the decelerating $-H^2(t)$. This last term becomes large as $H(t)$ become greater at larger times; (6.8) then no longer holds and the nonlinear (6.5) has to be solved on computer.

The computer results in **Table 1** show that $H(t)$ increases initially as in (6.8). At some intermediate time, the decelerating $-H^2(t)$ term becomes large enough to cancel out the last, accelerating term in (6.5) so that $H(t)$ reaches very large maxima there and then starts to decrease to smaller values at larger times, of the order of magnitude of 10^{8-9} years. At such large times, the test atom may have collided with other atoms so that the PRE gained via (6.5) was lost and the results in **Table 1** no longer hold.

These results are based upon the identification (6.4) which in its turn depends upon the gross, ad-hoc assumptions 1)-3) above Section 5.2. Therefore, the $H(t)$ predictions in **Table 1** can only be taken to be qualitative estimates that indicate the mechanism involved.

6.2. Relations to Hubble's Law

The Hubble law (6.1) is empirical and valid in the part of the observable universe containing the earth and the galaxies visible from it. This scenario is more realistic in this respect but does not include dark matter. This law cannot be derived from any first principles' theory without introducing additional concepts. The expansion mechanism is not clear; the mainstream candidate is the unidentified dark energy.

On the other hand, in the present SSI model in **Figure 2**, there is a center of the universe but no specified position of the earth. This model however includes dark matter and can be connected to the first principles' theory SSI [5] partially verified by hadron data. The accelerating expansion mechanism is delineated. But the expansions predicted in this model cannot be connected to any observable data; the positions and velocities of atoms in neutral hydrogen gas cannot be measured as such.

Results from both of these approaches are compatible with the general conception of an acceleratingly expanding universe and complement each other. In the Hubble case, measurements can be made but no theory exists to account for them. In the SSI model, theory exists to explain the accelerating expansion but no measurement can be made to verify it. The theoretical results can thus not confirm data directly because they refer to different environments.

Nevertheless, with the aid of the assumptions 1)-3) above Section 5.2, the connection (6.4) could be set in a heuristic manner. This connection leads to qualitative compatibility between data and present theory under such circumstances for small velocities.

Table 2. Comparison of the Λ CDM model of the universe with the present SSI model.

Model	Λ CDM	SSI
Foundation	General relativity and additional basic postulates	First principles' theory supported by hadron data. No additional basic postulate
Dark Matter	Assumed CDM, cold dark matter, WIMPs not found	As negative relative energy generated among quarks in inhomogeneous, cold hydrogen gas in gravitational field
Dark Energy	Difficulty with the cosmological constant problem	No dark energy. Only positive relative energy generated in hydrogen gas in outskirts of observable universe yielding anti-gravity expansion
Distribution	Universe has no center, no boundary, supported by Hubble's law	Universe has an unobserved center and is bounded by surrounding vacuum. into which it expands

Another approximately mutually compatible scenario may be that evolution according to the SSI model took place long, perhaps $10^9 - 10^{10}$ years, ago. Evolution of such a universe may eventually have ended up in the present state of the observable universe in which Hubble's law (6.1) can be established.

6.3. Λ CDM vs SSI Model

As was mentioned in the caption of **Figure 2**, the present SSI scenario was originally constructed for illustration of the mechanisms for the generation of dark matter and the anti-gravity expansion of the universe via PRE and was not aimed at a model for the universe per se. It turned out however that this scenario covers several areas also considered in the current mainstream Λ CDM model. Therefore, a comparison of these two models in these areas listed in **Table 2** may illuminate the pros and cons for both.

7. Summary

Negative relative energy between the diquark uu and the quark d in a proton plays the role of dark matter. Positive relative energy PRE between these quarks can lead to anti-gravity expansion of the universe.

Inside the universe, the amount of negative relative energies or dark matter produced depends upon the gravitational force acting on the quarks in hydrogen gas opposed by the pressure gradients acting on the electrons in this gas. In a galaxy, such amount can prevent fast moving stars from escaping the galaxy and cause gravitational lensing. Star formation in this gas uses up the hydrogen atoms that create such dark matter and hence reduces the dark matter content in this galaxy and increases the galaxy's apparent expansion rate. In intergalactic space, such dark matter can contribute to formation of filaments.

To account for the expansion of the universe, a hypothetical model of the un-

iverse is proposed. Near the outskirts of the observable universe, both the gas pressure gradient and gravitational force become very weak and the amount of dark matter generated nearly vanishes. Random collisions between hydrogen atoms in this region can flip such a small amount of negative relative energy or dark matter into a small positive relative energy or PRE in a hydrogen atom. Once such a sign change takes place, gravitational attraction switches into anti-gravity repulsion now unopposed by any pressure gradient. This leads to a “run away” hydrogen atom and provides the mechanism for an acceleratingly expanding universe.

This theoretical expansion and the measured Hubble data are both compatible with the conception of an expanding universe and complement each other. But they cannot verify each other directly because the present model has been constructed for purposes different from those of the measurements. On the other hand, the present accelerating expansion mechanism of the universe is based upon a first principles’ theory while Hubble’s law cannot be derived from any such theory. However, both approaches can under certain circumstances be shown to support each other qualitatively at small velocities.

Dark matter and PRE are not foreign objects like WIMPs and dark energy-cosmological constant but can only be created in cold hydrogen gas in gravitational field. To achieve this, collisions among the hydrogen atoms must take place. Dark matter was created first and can eventually later evolve into PRE in the outskirts of the universe. Dark matter and PRE will disappear if the hydrogen atom creating them becomes ionized as in stars.

Conflicts of Interest

The author declares no conflicts of interest regarding the publication of this paper.

References

- [1] Wikipedia (2020) https://en.wikipedia.org/wiki/Main_Page
- [2] Burgess, C. and Moore, G. (2007) *The Standard Model, A Primer*. Cambridge University Press, Cambridge
- [3] ATLAS, CMS Collaboration (2012) *Phys Lett*, **B716**, 30.
- [4] Hoh, F.C. (1993) *International Journal of Theoretical Physics*, **32**, 1111-1133. <https://doi.org/10.1007/BF00671793>
- [5] Hoh, F.C. (2019) *Scalar Strong Interaction Hadron Theory II*. Nova Science Publishers, New York.
- [6] Hoh, F.C. (2019) *Journal of Modern Physics*, **10**, 635-640. <https://doi.org/10.4236/jmp.2019.106045>
- [7] Hoh, F.C. (2019) *Journal of Modern Physics*, **10**, 1645-1658. <https://doi.org/10.4236/jmp.2019.1014108>
- [8] Hoh, F.C. (2020) *Journal of Modern Physics*, **11**, 967-975. <https://doi.org/10.4236/jmp.2020.117060>
- [9] Riordan, M. and Schramm, D.N. (1991) *Shadows of Creation: Dark Matter and the*

Structure of the Universe, W H Freeman & Co.

- [10] Peebles, P.J.E. and Ratra, B. (2003) *Reviews of Modern Physics*, **75**, 559.
<https://doi.org/10.1103/RevModPhys.75.559>

Appendix. Equations of Motion for Baryons and Nucleon Wave Functions

The equations of motion for baryons in SSI are [7] (2.2), [8] (A9 - A10) or [5] (9.3.16, 19), (9.2.13b), Š

$$\partial_I^{ab} \partial_I^{gh} \partial_{II\,ef} \chi_{\{bh\}}^f(x_I, x_{II}) = -i(M_b^3 + \Phi_b(x_I, x_{II})) \psi_e^{\{ag\}}(x_I, x_{II}) \tag{A1a}$$

$$\partial_{Ibc} \partial_{Ihk} \partial_{II}^{de} \psi_e^{\{ck\}}(x_I, x_{II}) = -i(M_b^3 + \Phi_b(x_I, x_{II}))_{\{bh\}}^d(x_I, x_{II}) \tag{A1b}$$

$$M_b = (2m_A + m_B)/2 \tag{A1c}$$

$$\overline{\square}_I \overline{\square}_I \overline{\square}_{II} \Phi_b(x_I, x_{II}) = \frac{1}{4} g_s^6 \left\{ \chi_{\{bh\}}^f(x_I, x_{II}) \psi_f^{\{bh\}}(x_I, x_{II}) + c.c. \right\} \tag{A1d}$$

where the spinor indices run from 1 to 2, x_I is the coordinate of the diquark, x_{II} that of the quark, $\partial_I = \partial/\partial x_I$, $\partial_{II} = \partial/\partial x_{II}$, the m 's quark masses [5] (Table 5.2), χ and ψ the ground state baryon wave functions, Φ_b the interquark potential dependent only upon the interquark distance $|\underline{x}_{II} - \underline{x}_I|$ for free baryons [5] (Sec. 10.1), and g_s^2 the strong quark-quark coupling constant. Introduce the observable laboratory frame X and the "hidden", unobservable relative coordinates x and separate χ and ψ according to [8] (2.1 - 3) or [5] (3.1.3a), (3.1.10a) (10.1.1),

$$x^\mu = x_{II}^\mu - x_I^\mu, X^\mu = (1 - a_m)x_I^\mu + a_m x_{II}^\mu, a_m = (X^\mu - x_I^\mu)/(x_{II}^\mu - x_I^\mu) \tag{A2}$$

$$\begin{aligned} \chi_{\{a\hat{c}\}}^e(x_I, x_{II}) &= \chi_{\{a\hat{c}\}}^e(\underline{x}) \exp(i\omega x^0) \times \exp(-iK_\mu X^\mu) \\ \psi_e^{\{ac\}}(x_I, x_{II}) &= \psi_e^{\{ac\}}(\underline{x}) \exp(i\omega x^0) \times \exp(-iK_\mu X^\mu), \\ K_\mu &= (E_K, -\underline{K}) \end{aligned} \tag{A3}$$

Here, E_K is the baryon energy, \underline{K} its momentum and ω the relative energy between the diquark and the quark, and a_m a real constant. The baryon wave functions χ and ψ have 6 components each comprising of a spin 1/2 doublet part $\chi_{0\hat{a}}, \psi_0^a$ [5] (9.2.2) and a spin 3/2 quartet part $\chi_{\pm 3/2}, \chi_{\pm 1/2}, \psi^{\pm 3/2}, \psi^{\pm 1/2}$ [5] (9.2.8).

Consider the rest frame $\underline{K} = 0$ doublet baryons and put [5] (3.1.10a), (Sec. 10.1) or [8] (2.4)

$$a_m = 1/2 + \omega/E_0 \tag{A4}$$

Substituting (A2-A4) into (A1) and put $\underline{K} = 0$, (A1) can be decomposed into a quartet part for the spin 3/2 baryons [5] (10.5.1) and a doublet part for the spin 1/2 baryons [5] (10.2.1a),

$$\begin{aligned} (i\delta^{ab} E_0/2 + \underline{\sigma}^{ab} \hat{\partial}) (E_0^2/4 + \Delta) \chi_{0\hat{b}}(\underline{x}) &= i(M_b^3 + \Phi_b(\underline{x})) \psi_0^a(\underline{x}) \\ (i\delta_{bc} E_0/2 - \underline{\sigma}_{bc} \hat{\partial}) (E_0^2/4 + \Delta) \psi_0^c(\underline{x}) &= i(M_b^3 + \Phi_b(\underline{x})) \chi_{0\hat{b}}(\underline{x}), \\ \Delta &= \partial^2/\partial \underline{x}^2 \end{aligned} \tag{A5}$$

For the plane wave solution in (A3), the normalized amplitude of the wave functions in (A3) with $\underline{K} = 0$ vanishes so that the right side of (A1d) also drops out to yield [7] (4.2) or [5] (10.2.2a),

$$\Phi_b(\underline{x}) = \frac{d_b}{r} + d_{b0} + d_{b1}r + d_{b2}r^2 + d_{b4}r^4, \quad r = |\underline{x}| \quad (\text{A6})$$

where the d_b 's are constants. The ansatz [5] (10.3.8a) reads

$$\begin{aligned} \psi_0^1(\underline{x}) &= \frac{1}{\sqrt{4\pi}}(g_0(r) + if_0(r)\cos\theta), \quad \chi_{0i}(\underline{x}) = (\psi_0^1(\underline{x}))^* \\ \psi_0^2(\underline{x}) &= \frac{1}{\sqrt{4\pi}}if_0(r)\sin\theta\exp(i\phi), \quad \chi_{0\dot{2}}(\underline{x}) = -\psi_0^2(\underline{x}) \end{aligned} \quad (\text{A7})$$

where θ, ϕ are angles in the "hidden" relative space \underline{x} . Equations (A-6-7) have been inserted into (A5) which has been converted into a first order system [5] (10.4.5) which in its turn has been solved on a computer for the neutron, Σ^0 and Ξ^0 baryons. The associated d_b values needed to obtain confinement, $g_0(r \rightarrow \infty) \rightarrow 0$ and $f_0(r \rightarrow \infty) \rightarrow 0$, as well as $g_0(r)$ and $f_0(r)$ themselves are given in [5] (Section 11.1.2). In particular [5] (Figure 11.1b), also reproduced in [7] (Figure 1), gives $g_0(r)$ and $f_0(r)$ for the neutron that led to correct prediction of its life [5] (Table 12.1).

Due to the small differences in the mass E_0 and quark masses (A1c) between the neutron and proton, the above neutron results can be taken over for proton here.

On Dineutron and Deuteron Binding Energies

F. C. Hoh

Retired, Dragarbrunnsg, Uppsala, Sweden

Email: hoh@telia.com

How to cite this paper: Hoh, F.C. (2021) On Dineutron and Deuteron Binding Energies. *Journal of Modern Physics*, 12, 161-166.

<https://doi.org/10.4236/jmp.2021.123014>

Received: January 8, 2021

Accepted: February 6, 2021

Published: February 9, 2021

Copyright © 2021 by author(s) and Scientific Research Publishing Inc.

This work is licensed under the Creative Commons Attribution International License (CC BY 4.0).

<http://creativecommons.org/licenses/by/4.0/>



Open Access

Abstract

The binding energy of the deuteron is estimated from the scalar strong interaction hadron theory SSI. The predicted value is 7.7% lower than the measured value. Existence of a spin 1 dineutron with a binding energy 4/5 that of the deuteron or 1.78 MeV is predicted. This is verified by the dineutron, first observed in 2012, in ^{16}Be decay. No free dineutrons are expected to exist in nature as they can decay into deuterons. These binding energies are limited by short range strong interaction internucleon forces but consist of long range electrostatic energies from quark charges.

Keywords

Scalar Strong Interaction Hadron Theory SSI, Deuteron Structure, Dineutron Structure, Electromagnetic Energy, Deuteron Binding Energy, Dineutron Binding Energy, Dineutron Decay

1. Introduction

The current mainstream particle theory, the standard model SM [1], can say nothing about binding energies of two nucleon nuclei. In its place, the scalar strong interaction hadron theory SSI has been proposed [2] [3]. The purpose of this paper is to provide estimates of the binding energies in the two nucleon system based upon SSI.

In Section 2, the triplet deuteron binding energy is estimated and compared to data. Section 3 shows that the singlet deuteron is not a bound state. The same conclusion is reached for the singlet dineutron in Section 4. In Section 5, the triplet dineutron binding energy is estimated and its decay mode is shown. This dineutron is assigned to the observed one in ^{16}Be decay. Some related considerations are given in Section 6.

2. Triplet Deuteron Binding Energy

In SSI [3] (Ch 9), the ground state of a proton consists of a diquark uu and a

quark d .

Consider such a free proton and change its u quarks into d quarks and vice versa. The result is a neutron with the same spin configuration. Put these two nucleons next to each other to form a deuteron, as is depicted in **Figure 1**.

The configuration in **Figure 1** is fixed by the: following two conditions: 1) the total spin in a two nucleon system can only be 1 with the nucleon spins parallel or 0 with the spins antiparallel and 2) both nucleons are on equal footing and the configuration remains symmetric with respect to them after an interchange or a space inversion.

In SSI, R_a is in the “hidden” relative space x between the diquark and the quark [4] (A1) and is determined by strong interquark forces. It is hence not observable. On the other hand, the internucleon distance R_{nn} in the laboratory space is observable.

When the two nucleons in **Figure 1** are far apart or R_{nn} is large, they do not interact with each other. When they are sufficiently close to each other, they form a triplet deuteron 2H_1 . Let q denote quark charge, then

$$q_u = 2e/3, q_{uu} = 4e/3, q_d = -e/3, q_{dd} = -2e/3 \tag{1}$$

Consider the total electrostatic energy E_{em2H_1} of the triplet deuteron in **Figure 1**. There are four contributions, between uu and dd , uu and u, d and dd , and d and u so that

$$E_{em2H_1} = \frac{q_{uu}q_{dd} + q_dq_u}{R_{nn}} + \frac{q_{uu}q_u + q_dq_{dd}}{\sqrt{R_{nn}^2 + R_a^2}} = \frac{10e^2}{9} \frac{1}{R_{nn}} \left[-1 + \frac{1}{\sqrt{1 + R_a^2/R_{nn}^2}} \right] \leq 0 \tag{2}$$

For large neutron-proton separation R_{nn} , $E_{em2H_1} \approx 0$ but < 0 . Let now the neutron move closer to the proton, R_{nn} decreases and E_{em2H_1} becomes more negative. However, R_{nn} cannot be too small because the neutron will then experience the short range strong interaction force from the proton which prevents the merger of these two nucleons.

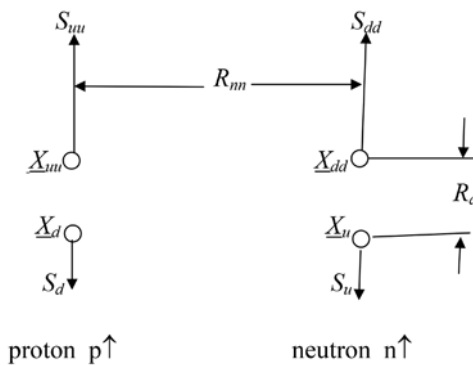


Figure 1. Schematic configuration of the spin $\uparrow\uparrow$ component of a triplet deuteron 2H_1 . X denotes the coordinate and S the spin of the diquarks and quarks. The subscripts refer to the quark content. $S_{uu} = S_{dd} = 1$ and $S_u = S_d = -1/2$ with signs given by the arrow \uparrow for + and \downarrow for -. $X_{uu} = X_d$ and $X_d = X_u$ in [3] (10.1.1) or [4] (A2). $R_a \approx 3.23$ fm [5] (2.5) is the mean value of the diquark-quark distance. The neutron configuration is obtained from the proton configuration via the interchange $u \leftrightarrow d$. R_{nn} is distance between the both nucleons.

Let the diquark uu be fixed at \underline{X}_{uu} in **Figure 1**. Then the d quark can lie anywhere on the surface of a sphere with radius R_a centered at \underline{X}_{uu} to form the same proton. This scenario can be taken over by the neutron in **Figure 1** via the interchange $u \leftrightarrow d$. The same neutron is obtained when the u quark is R_a away from \underline{X}_{dd} . Since the proton and the neutron cannot occupy the same space,

$$R_{nn} \geq 2R_a, \frac{R_a}{R_{nn}} \leq 0.5 \tag{3}$$

With $R_a \approx 3.23$ fm from the caption of **Figure 1**, $e^2 = 4\pi/137$, (2) and (3) yield the estimate

$$E_{em2H1} \geq -2.0653 \text{ MeV} \tag{4}$$

The lower limit of $R_{nn} = 2R_a$ in (3) leads to the triplet deuteron binding energy $E_{B2H1} = -E_{em2H1} = 2.0653$ MeV which is 7.7% smaller than the measured 2.2245 MeV.

The present treatment is phenomenological and $R_{nn} = 2R_a$ used above is not an exact criterion. If $R_{nn} = 1.846R_a$ were used instead, the predicted binding energy E_{B2H1} will agree with the measured one. Similarly, the diquark-quark distance is a continuous variable represented by an average value R_a here. If $R_a \approx 3.23$ fm \rightarrow 3 fm, then prediction and data will likewise agree.

The above R_a/R_{nn} ratios are also in qualitative agreement with the ratio

$$\frac{\text{proton charge radius}}{\text{deuteron charge radius}} = \frac{0.843 \text{ fm}}{2.128 \text{ fm}} = 0.395 < 0.5 \tag{5}$$

Note here that the charge radius arises from long range electromagnetic interactions and is an observable in the laboratory space. It is not to be confused with the unobservable short range strong interaction interquark radius $R_a \approx 3.23$ fm in the “hidden” relative space x between quarks.

3. Singlet Deuteron Binding Energy

The neutron spin in **Figure 1** has been chosen to be parallel to that of the proton spin. But it can also be chosen to be antiparallel to the proton spin. This can be achieved by inverting the neutron configuration in **Figure 1** upside down or, equivalently, by rotating this configuration 180° . This is carried out in **Figure 2**.

Analogous to (2), there are also four contributions, now between uu and u , d and dd , uu and dd , and d and u so that the total electrostatic energy E_{em2H1} in (2) is changed to E_{em2H0} ,

$$\begin{aligned} E_{em2H0} &= \frac{q_{uu}q_u + q_dq_{dd}}{R_{nn}} + \frac{q_{uu}q_{dd} + q_dq_u}{\sqrt{R_{nn}^2 + R_a^2}} = \frac{10e^2}{9} \frac{1}{R_{nn}} \left[1 - \frac{1}{\sqrt{1 + R_a^2/R_{nn}^2}} \right] \\ &= -E_{em2H1} \geq 0 \end{aligned} \tag{6}$$

For large neutron-proton separation R_{pn} , $E_{em2H0} \approx 0$ but now > 0 . Let now the neutron move closer to the proton, R_{nn} decreases and E_{em2H0} becomes more positive. Using the lower limit in (3), the singlet deuteron binding energy $E_{B2H0} = -E_{em2H0} = -2.0653$ MeV is negative so that there is no stable spin 0 deuteron, in

agreement with observation.

4. Singlet Dineutron Binding Energy

Perform the interchange $u \leftrightarrow d$ for the proton $p \uparrow$ in **Figure 1**. This turns $p \uparrow$ into $n \uparrow$ which is the same as the $n \uparrow$ on the right half of **Figure 1**. By Pauli's principle, these two neutrons $n \uparrow$ and $n \uparrow$ cannot coexist. However, if the spin of this left neutron is switched to \downarrow , then the aggregate $n \downarrow$ and $n \uparrow$, assigned to the singlet dineutron 2n_0 , can exist. The configuration is depicted in **Figure 3**.

Analogous to (6), the total electrostatic energy E_{em2n0} for 2n_0 reads

$$E_{em2n0} = \frac{q_u q_u + q_{dd} q_{dd}}{R_m} + \frac{q_u q_{dd} + q_{dd} q_u}{\sqrt{R_m^2 + R_a^2}} = \frac{8e^2}{9} \frac{1}{R_m} \left[1 - \frac{1}{\sqrt{1 + R_a^2/R_m^2}} \right] \geq 0 \quad (7)$$

which is simply $0.8 \times E_{em2H0} = -1.652$ MeV for the lower limit of (3). Analogous to the singlet deuteron 2H_0 case in Section 3, the singlet dineutron 2n_0 binding energy $E_{B2n0} = -E_{em2n0} = -1.652$ MeV is similarly negative so there is no stable spin 0 dineutron.

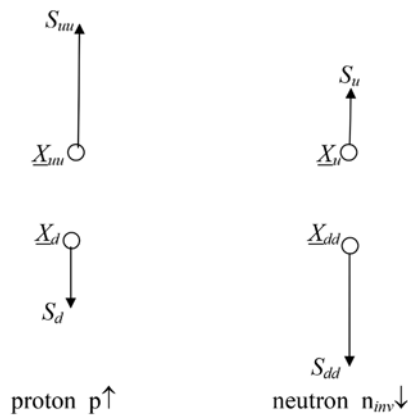


Figure 2. Schematic configuration of a singlet deuteron 2H_0 with spin 0. The proton configuration is the same as that in **Figure 1**. The neutron configuration has been inverted upside down relative to that in **Figure 1**, indicated by the subscript *inv*.

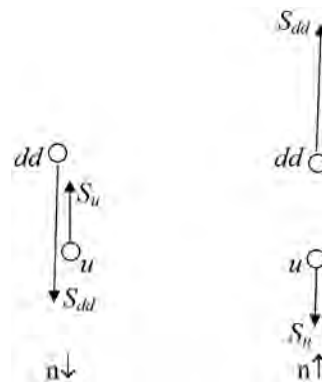


Figure 3. Schematic configuration of a singlet dineutron 2n_0 . The right neutron configuration is the same as that in **Figure 1**. Switching the spin directions in $n \uparrow$ on the right leads to the $n \downarrow$ configuration on the left.

5. Triplet Dineutron Binding Energy and Decay

In Section 3, the right neutron configuration in **Figure 1** has been inverted to become the right configuration in **Figure 2**. Perform the same inversion to the right neutron in **Figure 3** yields **Figure 4**.

Analogous to (2), the total electrostatic energy E_{em2n1} for 2n_1 reads

$$\begin{aligned}
 E_{em2n1} &= \frac{q_u q_{dd} + q_{dd} q_u}{R_{nn}} + \frac{q_u q_u + q_{dd} q_{dd}}{\sqrt{R_{nn}^2 + R_a^2}} \\
 &= \frac{8e^2}{9} \frac{1}{R_{nn}} \left[-1 + \frac{1}{\sqrt{1 + R_a^2/R_{nn}^2}} \right] = -E_{em2n1} \leq 0
 \end{aligned}
 \tag{8}$$

Comparison with (2) together with the lower limit of (4) yields the triplet dineutron 2n_1 binding energy $E_{B2n1} = -E_{em2n1} = 0.8 \times E_{B2H1} = 1.652$ MeV. This value is expected to be 7.7 % smaller than its actual value by analogy to the triplet deuteron case mentioned beneath (4). Correcting for this discrepancy, the binding energy E_{B2n1} becomes $1.077 \times E_{B2n1} = 1.78$ MeV.

2n_1 is thus a stable nucleus, like 2H_1 , but its binding energy 1.78 MeV is weaker than 2.2245 MeV for 2H_1 . Energetically, it can decay into deuteron via neutron beta decay,



where ν_e denotes the electron neutrino. Since each of the neutrons in 2n_1 can decay separately, the decay time is expected to be half of the neutron decay time or 440 sec.

While the deuteron can be the nucleus of an atom, the deuterium, the neutral dineutron cannot form an atom. The decay (9) implies that there are no free dineutrons in nature, just like neutrons.

Dineutron has been first observed some years ago in ${}^{16}\text{Be}$ decay [6]. It is assigned to 2n_1 here but needs not decay according to (9). Instead, it can decay into two neutrons when excess energy is available. The predicted 2n_1 binding energy 1.78 MeV has not been measured.

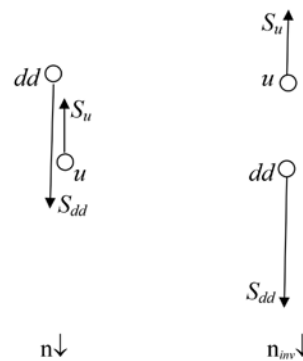


Figure 4. Schematic configuration of the spin $\downarrow\downarrow$ component of a triplet dineutron 2n_1 . The right neutron configuration is the same as that in **Figure 2**. The left neutron configuration is the same as that in **Figure 3**.

6. Related Considerations

The third member in the two nucleon system, the diproton pp , can be treated in an entirely analogous fashion. The results are that the binding energies of a singlet diproton E_{B2p0} as well as that for a triplet diproton E_{B2p1} are the classical value $-\epsilon^2/R_{nn}$ for large R_{nn} . For the lower limit in (3), $R_{nn} = 2R_a$, $E_{B2p1} = -19.26$ MeV and $E_{B2p0} = -14.1$ MeV. Thus, pp is not bound, as expected.

Thus, in the two nucleon system, only the triplet deuteron 2H_1 and the triplet dineutron 2n_1 are bound electromagnetically. The former is 20% stronger than the latter. The remaining four combinations, 2H_0 , 2n_0 and the triplet and singlet diprotons are not electromagnetically bound states. This is reflected in the composition of nuclei which consist mostly of pn pairs, to an less degree nn pairs but no pp pair.

The above results show that the binding energies of the deuteron and dineutron are of long range, electromagnetic nature arising from the quark charges. Short range, strong interaction forces between the nucleons set the limits of these binding energies but do not contribute to them.

For heavier nuclei, the above electrostatic confinement is insufficient and strong interaction forces, akin to those that led to the confinement characterized by R_a in Section 2, need be included. To accommodate the additional quarks, the two dimensional **Figures 1-4** here have to be extended to three dimensions.

Conflicts of Interest

The author declares no conflicts of interest regarding the publication of this paper.

References

- [1] Burgess, C. and Moore, G. (2007) *The Standard Model, A Primer*. Cambridge University Press, Cambridge. <https://doi.org/10.1017/CBO9780511819698>
- [2] Hoh, F.C. (1994) *International Journal of Theoretical Physics*, **33**, 2325-2349. <https://doi.org/10.1007/BF00673960>
- [3] Hoh, F.C. (2019) *Scalar Strong Interaction Hadron Theory II*. Nova Science Publishers, New York.
- [4] Hoh, F.C. (2021) *Journal of Modern Physics*, **12**, 139-160.
- [5] Hoh, F.C. (2020) *Journal of Modern Physics*, **11**, 967-975. <https://doi.org/10.4236/jmp.2020.117060>
- [6] Spyrou, A., Kohley, Z., Baumann, T., Bazin, D., *et al.* (2012) *Physical Review Letters*, **108**, Article ID: 102501.

New Approach to Deep Miniaturization: A Way to Overcoming Moore's Law

Maria K. Koleva

Institute of Catalysis, Bulgarian Academy of Sciences, Sofia, Bulgaria

Email: mkoleva_1113@yahoo.com

How to cite this paper: Koleva, M.K. (2021) New Approach to Deep Miniaturization: A Way to Overcoming Moore's Law. *Journal of Modern Physics*, 12, 167-178. <https://doi.org/10.4236/jmp.2021.123015>

Received: January 4, 2021

Accepted: February 7, 2021

Published: February 10, 2021

Copyright © 2021 by author(s) and Scientific Research Publishing Inc.

This work is licensed under the Creative Commons Attribution International License (CC BY 4.0).

<http://creativecommons.org/licenses/by/4.0/>



Open Access

Abstract

The matter about some far-going consequences commencing from the replacement of one of the basic principles of the traditional physics that is the principle of locality, with the recently put forward principle of boundedness is considered. It is proven that the thermodynamic theory which is explicitly grounded on the principle of locality, suffers inherent contradiction which roots lay down to the principle of locality. The way to overcome it goes via the replacement of the principle of locality with the recently put forward by the author principle of boundedness. In turn, the latter gives rise not only to a fundamentally novel notion for a number of ideas but also it yields replacement of the proportionality between the software and hardware components with a new non-extensive approach to the matter. It is proven that the famous Moore's law stands in new reading both in its support and the way to overcome its limitations. Apart from its role for the technical applications, the present considerations stand also as a methodological example how the role of the basics of any theory affects practical rules such as the Moore's law.

Keywords

Principle of Locality, Principle of Boundedness, Moore's Law, Decomposition Theorem, Chemical Potential, Semantic Intelligence

1. Introduction

One of the greatest challenges to the general theory of artificial intelligence is establishing of general protocols for organization of the match between software and hardware for different types of intelligence. Up-to-now the only studied and developed type of intelligence is the algorithmic intelligence. In the line of the present considerations, one of its major properties is proportionality between the logical steps involved in software and the number of components involved in

the corresponding hardware. This result is justified by the use of Boolean logic for the software components and the “switches” between elementary components for the hardware. The common between the Boolean logic and the switches between components is that they both are executed locally so that the next step (switch) is free not to be physically correlated with either of the previous and/or the next one. Consequently, proportionality between the number of logical steps and the number of components commences.

Then, the meeting of ever-growing demands of the human mankind to devices of all kinds is focused mainly on further downsizing and doubling of components as well as on finding the most efficient algorithms for classes of problems. It is widely accepted that this route has its limits proclaimed by the famous Moore’s law. So far, it is taken for granted that the limits to further downsizing are to be considered as formation of new phenomena such as, e.g., how many atoms are needed to be removed from a metallic system so that the latter to start exhibiting non-metallic properties. Thus, the Moore’s law stands as limit which delineates the boundary between phenomena of different qualities (e.g. transition from a non-metal to a metal). Yet, now I will outline that the Moore’s law is more than that.

Still the dominant view on our human intelligence is that it operates on the grounds of the same Boolean logic for the “software” executed by means of cleverly designed “hardware” consisting of components each and every of which operates locally, *i.e.* on the principle of “switches”. This view commences from principle of locality of physical laws which is the very grounding principle of reductionist type of sciences to which the physics belongs. However, the theory built on that principle suffers fundamental contradictions. One of them, a consequence of the thermodynamic theory, is that there are no limits (both lower and upper) on the number of components of any circuit to operate steadily. Thus, it seems possible to build a circuit out of a single atom. Then, is the human brain so imperfect to need myriads of atoms and molecules for its functioning?

The fundamental flaw of the thermodynamic theory is that it considers only systems which are in general equilibrium and/or in a state that represents small deviations from it. The principle of locality, which assumes that the laws of Nature can be formulated at a single spatio-temporal point, e.g. a material point, and instantaneously acting forces concentrated in the center of mass, is here expressed by the assumption about Markovianity for the small deviations from the general equilibrium regardless to the origin of those deviations, *i.e.* whether they represent fluctuations or they come as a response to environmental impacts. Then, this setting renders the association/dissociation of species to be considered as a process unlimited in its number and as un-affecting the other properties of the corresponding system. Thus, not only the thermodynamic theory is not able to distinguish between a “bunch” of grains and a pile of sand, but it is not able to define a critical size for steady operation. Thus, a question arises, is it possible to

re-define the thermodynamic theory so that to overcome the above conundrum and what are the consequences.

It turns out that such re-definition is possible but at the expense of withdrawal from the principle of locality and its replacement with the principle of boundedness, recently introduced by the author in her book [1]. The far going consequences of that replacement read that there exists a “kinetic” (operational) threshold below which any given circuit cannot operate steadily. The threshold is specific for each and every circuit but its existence is universal. The existence of operational thresholds not only puts the Moore’s law on formal grounds, but it delineates the major strategy for its overcoming: it is the use of new materials for further downsizing. Since the realm of new materials is vast, most promises hold on its exploration.

Yet, the story is not finished: the principle of boundedness renders the matter about doubling of components to develop under another strategy as well. In a nutshell this strategy withdraws from growth of the number of components and applies non-extensive view on the matter. It is considered in section 2.

The non-extensive approach to the matter about the match between software and hardware is an exclusive property of the naturally aroused in the frame of the theory of boundedness [1] semantic intelligence where the logic is not Boolean and is grounded on specific for each task highly non-trivial interplay between long- and short-distant logical correlations executed by a “hardware” which is driven by spontaneously executed specific natural physico-chemical processes. To recall the major property of the semantic intelligence is autonomous comprehension and creation of information [1]. To compare, the algorithmic intelligence is non-autonomous because both the design of software and hardware, and decoding of each and every output are subject to artificial intervention.

Summarizing, the establishing of a new general protocol for the match between software and hardware provides the new general strategy for overcoming the Moore’s law which along with the prescribed use of new materials will be the next milestone on the way to constructing devices for exploration of hazardous events, distant outer space endeavors and study of events where information is incomplete and/or uncertain.

2. Kinetic (Operational) Threshold

The goal of the present section is to prove that the existence of an operational threshold over stable functioning of any device is a generic property of all circuits. In turn, the Moore’s law gains another argument in its favor as well as providing the way of overcoming it. The reason for presenting it in a separate section is that the matter about existing of an operational threshold is highly non-trivial because it requires new setting for the notion of chemical potential.

At first, let me demonstrate why the traditional notion of chemical potential is inherently contradictive. Below I reproduce the derivation in the way it is pre-

sented in Chapter 8 of the book [1].

The traditional thermodynamics is grounded on the principle of locality which, among all, asserts that the basic characteristics of a system, (internal energy, entropy, chemical potential) are functions of the general equilibrium only and they do not depend on the path through which a system arrives at it. The most widespread definition of the chemical potential reads that it is the Gibbs energy necessary for associating/dissociating a species in/out a system in equilibrium. In order to meet the principle of locality, basic characteristics of a system, chemical potential included, are assumed to be intensive variables. Among all, the latter implies that the chemical potential must be independent from the number of species. However, next I will present a proof that the chemical equilibrium is not able to maintain this property of the chemical potential. Thus, it turns out that the traditional thermodynamics experiences a fundamental flaw.

Let us follow the traditional derivation of the necessary condition that a chemical reaction at fixed pressure and temperature should obey in order to reside in chemical equilibrium. It is demonstrated that it produces dependence of the chemical potential on the number of species of all sorts which in turn constitutes an immediate violation of the condition for separation of the variables to intensive and extensive ones.

In chemical equilibrium the amount of each of the reactants and products is constant and corresponds to the stoichiometric relation:

$$\sum_{i=1}^S \nu_i A_i = 0 \quad (1)$$

where ν_i is the stoichiometric coefficient of the i -th sort, A_i is its amount and S is the number of the i -th sort species.

Equation (1) is equivalent to the following relation:

$$\frac{\partial \Phi}{\partial N_1} + \frac{\partial \Phi}{\partial N_2} \frac{\partial N_2}{\partial N_1} + \dots + \frac{\partial \Phi}{\partial N_i} \frac{\partial N_i}{\partial N_1} + \dots + \frac{\partial \Phi}{\partial N_S} \frac{\partial N_S}{\partial N_1} = 0 \quad (2)$$

where Φ is the Gibbs energy, N_i is the number of species of the i -th sort.

Let us now rewrite (2) in slightly different form:

$$\sum_{i=1}^S \frac{\partial \Phi}{\partial N_i} \frac{\nu_i}{\nu} = 0. \quad (3)$$

By definition:

$$\frac{\partial \Phi}{\partial N_i} = \mu_i \quad (4)$$

where μ_i is the chemical potential.

Thus, at equilibrium the following relation holds:

$$\sum_{i=1}^S \nu_i \mu_i = 0 \quad (5)$$

Further, since the Gibbs energy is thermodynamic potential in the linear do-

main around the equilibrium state, the condition for independence of the arrival at equilibrium from the path is provided by its smoothness:

$$\frac{\partial^2 \Phi}{\partial N_i \partial N_j} = \frac{\partial^2 \Phi}{\partial N_j \partial N_i} \quad (6)$$

which immediately leads to the following relation:

$$\frac{\partial \mu_i}{\partial N_j} = \frac{\partial \mu_j}{\partial N_i} \quad (7)$$

where μ_i , μ_j are the chemical potentials of the i -th and j -th sort species correspondingly. Let us now have a closer look on (7)—it turns out that (7) makes the chemical identity dependent on the number of the species! In addition, it is obvious that thereby the chemical potential turns a non-intensive variable so that it depends not only on the number of the species of its sort but on the number of species of all other sorts. However, this is in a sharp controversy with the idea of its meaning presented by Equation (4), that the chemical potential is predetermined by the chemical identity of the species of any given sort alone.

The way out from the above contradiction is to adopt a new definition for the notion of the chemical potential. It is well known that there exists another definition which derives it from the notion of Lagrangian. The inconvenience of that definition in the frame of the traditional thermodynamics, however, lies in the fact that the notion of Lagrangian is associated with extremal properties of a system such as minimum energy, maximum entropy etc.

Luckily, in the theory of boundedness the notion of stationarity of the action is associated with those trajectories where the boundedness of rates and amplitudes of exchanging energy/matter/information with the current environment is permanently maintained. Thus, stationarity of the action is not any longer to be associated with any form of extremization. A crucial test for the new definition of the chemical potential is whether it puts a ban over association/dissociation of arbitrary amount of species. This is very important for delineating a system from its environment in the process of its interaction with not apriori specified environment. Thus, if the exchange of species is not limited, a system could either enlarge to arbitrary size or deplete to extinction. This suggests straightforward relation of the new notion of chemical potential to the notion of stability of a system. The fundamental advantage of the definition of a chemical potential in the setting of boundedness (through non-extremizing Lagrangian) is that it renders the functional properties of the system to play an apparent role in the notion of the chemical potential. Thus it renders the chemical potential to depend on the spatio-temporal order of association/dissociation of species. In turn, the latter renders the option for the chemical potential to turn to zero during those processes which immediately implies collapse of the corresponding system.

That is why I define the chemical potential as follows:

$$\mu_i = -\Omega \frac{\delta L}{\delta n_i} \quad (8)$$

where Ω is the volume of the system; n_i is the number of the species of the i -th sort; L is the Lagrangian of a system. Equation (8) describes a process initiated by small deviations from the general equilibrium condition $\delta S = 0$, where S is the action. It is worth noting that in the frame of the theory of boundedness the condition for stationarity of the action holds for all trajectories where the condition for boundedness of rates and amplitudes holds. Thus, the advantage of this definition is that it automatically delineates only admissible trajectories where the boundedness holds permanently by means of taking into account the functional relations built-in in the state space of a many-body system. Indeed, Equation (8) is an explicit expression for taking into account the intrinsic functional “relations” among the constituting species as well as their modification under the interaction of the system with its environment. By means of the new definition, I will demonstrate that a system stays stable if and only if the amount of energy/matter that it exchanges with the environment is bounded.

Thus, the condition for providing stability of a system stands primary. In the line of the present considerations, it implies that breaking the stability of a system happens when its chemical potential turns to zero. The structure of the state space under boundedness is supposed divided into a “bulk” and a “surface” part. The former one is to be associated with that part of the system that remains stable under a given interaction and as I will demonstrate further it is to be associated with the so called “homeostatic” pattern of a system. On the contrary, the “surface” part is associated with the current boundary of a state space and as it will become clear in the next section, it is to be associated with current interactions with the environment. In turn, the “surface” part of the chemical potential is strongly sensitive to the current curvature which culminates in strong sensitivity on the current number of exchanged species. Since any exchange of a species modifies the shape of state space “surface”, the natural measure of the surface part of the chemical potential is its local curvature:

$$\mu_s = \int_S \alpha k ds \quad (9)$$

where α is the density of the surface energy; S is the area of the state space surface. The permanent variations of the number of species result in permanent modification of the value and sign of the local curvature. So, μ_s permanently varies and eventually turns the total chemical potential μ_{tot} to zero. This immediately yields the system falling apart. The next task is to illustrate that this happens when the number of exchanged species is limited. According to the above considerations, the destruction of the system happens whenever:

$$\mu_{tot} = 0 \quad (10)$$

Since the bulk part of the chemical potential is insensitive to the variations of the state variables, Equation (10) holds whenever the following relation holds:

$$\mu_s = -\mu_b \quad (11)$$

where μ_b is the bulk part of the chemical potential.

An immediate consequence of the above setting is that a collapse happens always at bounded number of associated/dissociated species and so that the way to collapse strongly depends on the spatio-temporal path through which the association/dissociation proceeds. The chemical potential for different species and paths also turns different. This result constitutes the fundamental difference with the traditional thermodynamics where notion of the chemical potential is supposed to be inherent property of the chemical identity of a single sort of species. It is worth noting that the notion of functional relations among species and the notion of stability straightforwardly participate in the notion of the chemical potential in the present setting.

An immediate consequence of the above considerations is that it sets a condition for a system to operate steadily to be a permanent sustaining its chemical potential to be non-zero. It is obvious that the notion of the chemical potential is apparently related to the size, the structural and the functional organization of any system. In turn, the latter justifies the assertion that for each and every system a threshold arises below which the system is not able to operate steadily. The size, structure and functional organization of the threshold are specific to a system, but the existence of the general ban over further miniaturization is a general property. It should be stressed that it appears as an exclusive property for the theory of boundedness. Thereby, the way to further miniaturization lays in the use of new materials and is grounded on the specificity of any concrete ban.

One of the major goals of tailoring any device is providing its stable functioning in any environment. So far the major approach for accomplishing this task is to put the device at stationary stable conditions by means of, e.g., plugging to an artificially designed electric grid. Then, the principle of locality provides a one-to-one correspondence between any software and any hardware. The latter correspondence culminates in the properties of the so-called Turing machine. Consequently, any hardware (those constituting by a single component included) can execute any software (a probabilistic one included). At first glance this matter becomes extremely difficult since the path dependence of the chemical potential opens the door to functional inequality of otherwise structurally identical species. Then, it seems that any such system is doomed to unstable and unreproducible functioning because different inputs would create different path dependences and thus different functional structure. This issue is resolved by means of the central for the entire theory of boundedness result, the so called by the author decomposition theorem and proven by her in [1].

The decomposition theorem states that for each and every bounded irregular sequence (BIS) a presentation basis exists which is power spectrum, where the latter is additively decomposed to two parts: a specific to a system discrete pattern, called, homeostasis, and a universal continuous component whose shape is $1/f^{\alpha(f)}$ where $\alpha(f)=1$ at $f=1/T$ where T is the current length of any given

BIS. Both the structure of the discrete pattern and the shape of the continuous band are robust to the details of the statistics of the variations in any given BIS. The crucial property of that decomposition is that it holds even when a system operates in a non-specified ever-changing environment under the mild condition of keeping rates and amplitudes of exchanging matter/information/energy with the environment permanently bounded within specific margins alone.

An immediate consequence of the decomposition theorem is that any homeostatic pattern appears as stable functional pattern robust to small environmental variations. It is worth noting that the latter property justifies the intuitive notion about the “bulk” part of the state space involved in the considerations of the previous section about constituting a new notion for the chemical potential. Alongside, the continuous part is to be associated with the current interaction of a system with its environment and hence with the “surface” part.

Let me now briefly discuss the withdrawal from the principle of locality. Indeed, in the traditional setting, it is strongly involved through the idea of separation of the thermodynamic variables to intensive and extensive ones. Then, chemical potential turns provided by chemical identity alone and turns robust to the functional relations among the constituting a system species which yields to the opportunity for association/dissociation of arbitrary amount of species regardless to whether a system remains stable or not. On the contrary, the replacing of the principle of locality with the principle of boundedness renders the notion of the chemical potential to be apparently related to the notion of stability and renders strong sensitivity on the path through which the association/dissociation proceeds.

In turn, this justifies Moore’s law by means of providing another strong argument in its favor. Yet, it also opens the door to its overcoming: by means of the use of new materials, new structural and functional organizations. In turn, this makes the relation structure/functionality to be more diverse than mere proportionality alone. In the next section, it is demonstrated that this yields to its diversity through non-extensivity.

3. Non-Extensivity and Diversity of the Relation Structure-Functionality

The roots of non-extensivity of the relation “software-hardware” lay deeply into the decomposition theorem. It is worth reminding one of its most non-trivial immediate consequences, that is that the notion of homeostatic pattern represents steady causal correlations for any functionality [2] [3] so that the logical and quantal error are kept bounded in a long run [4]. These properties give rise to the question about whether a general rule for their match to the relation “structure-functionality”, *i.e.* “software-hardware”, exists. It is worth noting that since the semantic intelligence is spontaneously executed by natural physico-chemical processes, the role of “software” is played by the functionality, the role of “hardware” is played by the structure and their relation is provided by the

existence of a general protocol for their match governed by an equation of the following general type:

$$\frac{\partial X}{\partial t} = (\alpha(\mathbf{r}, t)X - \beta(\mathbf{r}, t)X + \mu(\mathbf{r}, t)X) - \nabla \cdot (\hat{D}(\mathbf{r}, t, X) \cdot \nabla X) \quad (12)$$

where $\alpha(\mathbf{r}, t)$ and $\beta(\mathbf{r}, t)$ are the “stoichiometric” coefficients of the corresponding local adsorption and reaction terms; $\mu(\mathbf{r}, t)X$ is the current bounded noise. The basic equation is a single scalar equation for the entire network because it represents a system without stirring thus allowing formation of utilizable long-range physico-chemical correlations. To remind, the stirring destroys long-range correlations thus making different species (hence different types of species) independent and in turn it makes the governing equation local.

This type of governing equation was derived in [1] and its solution comprises both a real and imaginary part. The solutions of both real and imaginary part of the above equation are trajectories which are confined in tubes restrained by the specific thresholds which commence from the thresholds of the noise component but not proportional to them. Since each part of a solution is a BIS, both real and imaginary part comprises a stable discrete pattern which contributes to the corresponding homeostatic pattern.

The imaginary part of the solution has a generic solution which consists of emitting specific travel waves so that to deliver specific reaction outputs to specific distant spatio-temporal points where they serve as inputs for other specific reactions.

It should be stressed on the exclusive generic property of the adsorption and reaction terms in the governing Equation (12) to be linear with respect to the total concentration. This is because different species, in non-reactive conformations, maintain the same relative velocity [5] which property provides laminarity without stirring of a flow consisting of different sorts of species. Thus all different species participate linearly in the flow yet with different “weights” (adsorption and reaction rates correspondingly). Put in other words, the stoichiometry is executed in fundamentally different way. Note that the “stoichiometry” for the same reaction could be different in different spatio-temporal points which assertion is in sharp contrast with the case of stirring where the stoichiometry is local and thus is the same throughout the entire system. This contrast arises because the reactants are brought together not by means of stirring but by means of a sequence of specific passages from one spatio-temporal point to another. Note that stirring destroys any correlations among species thus rendering reactions only local.

In turn, the linearity of the adsorption and reaction terms with respect to concentration, viewed as their generic property, provides not only the emitting of travel waves as a generic type of solution of the imaginary part of Equation (12) but it also immediately constitutes a generic property of those matter waves to be the confinement of any matter wave into a specific to it “tube” of bounded section. The proof of this confinement can be traced back to the Chapter 7 of

[1]. This confinement could be considered figuratively speaking as a process of auto-collimation. The value of the latter property lies in its ability to provide exact repetition of distant spatio-temporal homeostatic relations in an ever-changing environment. It is worth noting that the auto-collimation turns out to play also the role of implement for providing and self-controlling the robustness of any homeostatic pattern in an ever-changing environment. The role of self-control is that when a travel wave deviates from the target, the corresponding reaction do not happen which in turn signals out a local damage.

Thus, the solution of any basic governing equation is a result of highly non-trivial interplay between short- and long-range correlations. The goal of that interplay is to maintain a stable long-run functioning of any current homeostatic pattern. It is worth noting on the non-separability of spatial and time coordinates for distinguishing the causal correlations encapsulated in a homeostatic pattern from the provisional ones and from the correlations associated with the individual peculiarities. That non-separability is best illustrated by the fact that the separation of the causal correlations from the other types occurs only in the power spectrum of any time series which represents the behavior of a complex system. These considerations are one argument more in favor of the assertion sustained by the author why the semantic intelligence is irreducible to the Boolean logic.

It is worth noting that one of the most general properties of any solution of the governing Equation (12), that is that its state space is partitioned into basins of attractions each of which is characterizing by a specific to it homeostatic pattern, lays the fundament for diversity of the relation “hardware-software” for the semantic intelligence.

Moreover, the governing Equation (12) provides not only a stable diversification of the relation structure-functionality but the highly non-trivial interplay among short- and long-distant correlations renders the match between structure and functionality non-extensive as well. It is worth comparing to the algorithmic intelligence where the principle of locality renders all physical correlations only local thereby making the recognition of any long-range correlations subject to artificial, *i.e.* that of a human mind, intervention. To remind, our human mind is subject to our current beliefs, views and abilities and so any thus obtained long-range correlations would be subjective and indiscriminating from the provisional ones and from those that come from the individuality of any complex system.

Yet, there is a decisive step ahead to further diversification of the match structure-functionality. This step is grounded on the exclusive properties of semantic intelligence that read: 1) the meaning of each and every semantic unit is executed as a non-mechanical engine built on the different basins-of-attractions to which the state space of Equation (12) is divided. Thus, the semantic meaning turns irreducible to that sequence of “letters” which constitute it and thus it is irreducible to the Boolean logic encapsulated in that sequence; 2) the semantic

units are organized in a bi-directional hierarchy so that governing equation on each and every hierarchical level is equation of the type represented by Equation (12). From the computation point of view its greatest advantage lies in the fact that the computation at all hierarchical levels is not always necessary: sometimes it is enough to complete computation only on higher hierarchical levels. This result is an immediate consequence of the rule for synchronization of homeostatic patterns that comes from different hierarchical levels [6].

Thus, further diversification of the relation structure-functionality goes in two ways: 1) changing the number of hierarchical layers; 2) by means of changing environment, a system can “switch” to another homeostatic pattern. It is worth noting that those implements of diversification serve also as implements for strengthening the stability of a system.

Summarizing, the new form of intelligence, semantic intelligence, opens the door to the entirely new reading of the Moore’s law with regards to the issue about the match between structure and functionality.

The functional distinguishability of structurally identical species is successfully utilized by the computation which thus proceeds in non-recursive means as discussed in [1]. Indeed, it is implemented by non-linear steps executed in a non-homogeneous way whose generic property is algorithmic un-reachability from one another in any finite number of linear operations. This is another consequence of the decomposition theorem where the power spectrum comprises an irrational frequency along with the homeostatic pattern and the continuous band [1]. Moreover, the presence of a specific interplay among short- and long-range spatio-temporal correlations among reactions renders the entire system irreducible to linearly connected moduli where the linearity is the necessary fundament for a “hardware” to be able to execute any piece of algorithmic intelligence in a reproducible way. However, linear operations allow unlimited accumulation of matter/energy/information in any locality thus contradicting the very core of the idea of boundedness which puts bounds on accumulation and/or depletion of energy/matter/information beyond specific margins as a primary condition for stable long-term functioning of any system. On the contrary, the non-recursive computing is implemented by means of spontaneously executed natural processes which automatically maintain boundedness of rates and amplitudes in each and every spatio-temporal point.

As an immediate consequence, the number of logical operations and the number of hardware components for semantic intelligence are intertwined in a highly non-trivial and complex interplay whose general properties are diversity and non-extensivity.

In turn, these differences once again prompt to suggest that the diversity of properties and abilities of any new form of intelligence are still far ahead to be discovered and utilized. What is more exciting is that such things as laws and rules which hold for one type of intelligence, e.g. Moore’s law for algorithmic intelligence, transforms to new view point, that is non-extensivity and adaptabil-

ity of relation structure-functionality for the semantic intelligence.

4. Conclusions

The present paper is an example that practical rules such as the famous Moore's law hold for specific setting only and that the way of overcoming their limitations goes via fundamental changes of those settings. Thus, the replacement of the principle of locality with the principle of boundedness yields a cascade of consequences. The cascade starts with the central for the entire theory of boundedness decomposition theorem and passes through the grounded on it novel notion of the chemical potential. It culminates in a new approach to the matter about the match between software and hardware based on non-extensivity of the number of the logical operations and the hardware components, and the wide use of new materials as well. To compare, the principle of locality provides only proportionality between the number of logical operations and the hardware components.

Thus, despite its role for practical needs, the present paper appears as a methodological implement for delineating the deep and highly non-trivial role of the basic settings of any theory.

Conflicts of Interest

The author declares no conflicts of interest regarding the publication of this paper.

References

- [1] Koleva, M.K. (2012) Boundedness and Self-Organized Semantics: Theory and Applications. IGI-Global, Hershey, PA. <https://doi.org/10.4018/978-1-4666-2202-9>
- [2] Koleva, M. (2019) *Journal of Modern Physics*, **10**, 43-58. <https://doi.org/10.4236/jmp.2019.101005>
- [3] Koleva, M. (2020) *Journal of Modern Physics*, **11**, 767-778. <https://doi.org/10.4236/jmp.2020.116049>
- [4] Koleva, M. (2020) *Journal of Modern Physics*, **11**, 157-167. <https://doi.org/10.4236/jmp.2020.112010>
- [5] Koleva, M. (2015) *Journal of Modern Physics*, **6**, 1149-1155. <https://doi.org/10.4236/jmp.2015.68118>
- [6] Koleva, M. (2018) *Journal of Modern Physics*, **9**, 335-348. <https://doi.org/10.4236/jmp.2018.93024>

Multi-Bubble Universe Model: A Quantum-Relativistic Gravitational Theory of Space-Time

Massimo Auci^{1,2}

¹Maths and Physics Department, State European International School “Altiero Spinelli” Via Figlie dei Militari 25, Torino, Italy

²Space Science Department, Odisseo-Space Via Battistotti Sassi 13, Milano, Italy

Email: massimo.auci@gmail.com

How to cite this paper: Auci, M. (2021) Multi-Bubble Universe Model: A Quantum-Relativistic Gravitational Theory of Space-Time. *Journal of Modern Physics*, 12, 179-217.

<https://doi.org/10.4236/jmp.2021.123016>

Received: October 4, 2020

Accepted: February 7, 2021

Published: February 10, 2021

Copyright © 2021 by author(s) and Scientific Research Publishing Inc. This work is licensed under the Creative Commons Attribution International License (CC BY 4.0).

<http://creativecommons.org/licenses/by/4.0/>



Open Access

Abstract

A multi-bubble model of universe is presented, in which gravity is the result of the aging of electromagnetic dipoles produced in quantum fluctuations of the action inside a condensate of a particular type of balancing gravitons. In the model, the exchange of gravitons among the dipoles and the potential of vacuum balances the energy of the fluctuation. The effect is to create bubbles of space-time that by growing they expand the local vacuum. The model suggests that the universe originates from overlapping of bubbles of space-time associated with dipoles. Matter is originated during gravitons decay. The use of the Bridge Theory demonstrates how the attractive force field that emerges in each bubble is in the first approximation in accordance with Newtonian gravity at small, medium and large distances in accordance with the theory of General Relativity by also introducing a variable cosmological term that justifies some observed cosmological anomalies. The model overcomes the current concepts of Dark Energy and Dark Mass in favor of a gravity produced by the curvature of space-time of the bubble. The existence of the balancing gravitons provides an estimate of the actual amounts of Dark Energy, Dark Matter and matter measured in the current universe. The estimated theoretical mass of the balancing gravitons is consistent with the Kaluza-Klein gravitons of 2.68 TeV observed in the ATLAS experiment during Run #1. Moreover, the use of the observational data of the rotation speeds of two samples of galaxies allows to verify the good agreement of the real universe with the model, providing a possible explanation of the variability in the measurement of the Hubble constant.

Keywords

Bridge Theory, Cosmology, Dark Matter, Dark Energy, Gravitons, Relativity, Unification

1. Introduction

In history of cosmology [1], the assumption of the Lambda-CDM (Cold Dark Matter) model as describing the physical reality of the universe, naturally leads to a first difficulty in understanding the behavior of gravity on a galactic, extragalactic and cosmic scale [2]. A distribution of a large quantity of Dark Matter is imagined to exist and be gravitationally active influencing the halo of each galaxy, manifesting its presence through an anomalous rotation speed of the galactic halo itself. A second difficulty is the problem of the origin of the universe. All instrumental observations made on the Cosmic Microwave Background (CMB) are consistent with an initial inflationary scenario in which expansion was initially very fast, after which the universe slowed down and accelerated again as if was driven by antigravity produced by a hypothesized Dark Energy, so in light of the observations of the WMAP and Planck spacecrafts and of the recent measurements of the Hubble constant performed by different methods, all inconsistent with those obtained on the CMB, to believe that the Lambda-CDM model is able to describe the universe at every scale correctly do not seem easy.

A consistency at the Lambda-CDM model is given by the observation of an amount of ordinary visible baryonic matter contributing with $\Omega_b \cong 0.05$ at the baryonic density, at which is necessary to add an amount of yet not identified Dark Matter contributing with a $\Omega_{DM} \cong 0.25$ to density and of an amount of Dark Energy, probably associated to the vacuum energy with a $\Omega_{DE} \cong 0.7$, both sufficient to produce a flat universe expanding with a velocity growing in time. These two characteristics involve two fundamental aspects of physics. The first is related to the not confirmed existence of neutral bosonic particles habiting the galactic halos with a Dark Matter role, the second of a vacuum, not exactly empty, that actively participates at the total energy of the universe causing its expansion.

For this, there are some deep difficulties for the acceptance of the Lambda-CDM model in the present form, in fact on a galactic scale and beyond, it is very difficult to reconcile the model predictions with the direct observations. It would seem that a set of cosmological constants cannot be sufficient to describe perfectly the behavior of the single galaxies, of the clusters and of the universe itself in its early stages. Despite this, the historical experimental confirmation from LIGO and VIRGO [3] collaborations of the existence of the gravitational waves, and the confirmation of the existence of a gravitational redshift along the orbit at pericenter of S2, when the star is nearest the intense gravity produced by the massive black-hole in Sgr A [4], they should eliminate any doubts about the physical reality and the goodness of the Theory of General Relativity. Thus, it is necessary to assume gravity not as a fundamental pseudo-Newtonian force, but as an emerging force produced by the local curvature of space-time induced by the presence of masses and energy in the vacuum as predicted by the field equation in which gravity appears as a non-quantized field. In this sense, gravity seems to be an exception on the scenario of the fundamental forces. In particular,

if gravity is an effect and not a fundamental force, it is necessary to know why the curvature of space-time is produced and why it grows when the mass and density of energy grow in space-time, especially it is necessary to wonder why gravity is not a quantum field like other forces.

In this work, a new model of the universe is proposed and it is shown that the Theory of General Relativity reinterpreted in the context of a complete Bridge Theory (BT) [5] [6] is able to describe the universe without assuming the existence of real Dark Matter and real Dark Energy because their effects are emulated during the creation of space-time.

2. Why Is It Necessary to Try to Use Another Approach to Describe a New Cosmological Model?

One of the fundamental expected goals of modern physics is to discover gravity as a relativistic quantum force unified with other forces in nature. Two fundamental steps are needed to achieve this goal. The first is the experimental discovery of the existence of a quantum phenomenon associated with gravity or alternatively of a quantum theory of gravity describing the gravitational effects on each scale. The second is to understand as gravity can be unified with all the other forces, namely with the electromagnetic force. In both cases, to try to achieve these results it is necessary to start from a theory consistent with quantum theory, with relativity and with electromagnetic theory.

This work presents a model of universe in which electromagnetic forces and gravity are unified. The model developed with the use of quantum physics and relativity in the context of the BT is proved to be theoretically and phenomenologically consistent with the description of the electromagnetic quantum-relativistic phenomena as above hypothesized to be necessary. In any case, the use of BT based on real physical phenomena can be considered an interesting attempt to unify within a single non-speculative theory a quantum-gravitational phenomenology with electromagnetic forces.

2.1. The Dipole as an Electromagnetic Model of the Photon Exchanged during a Particle-Antiparticle Electromagnetic Interaction

The theoretical and phenomenological approach takes into account that in BT the electromagnetic interactions occur by means of the creation of real and virtual Dipole Electromagnetic Sources (DEMS), whose interaction energy is regulated by the wavelength defined by the minimum distance reached by the particles during their approach. The correctness of this approach proposed in terms of model in reference [7] and [8] and reviewed successively in Bridge Theory terms is guaranteed by the theoretical estimation of the Sommerfeld constant springing out by theory as a universal numerical constant independent by the values of the Planck constant, of the electron charge, of the light speed and by external adjustment of useful parameters.

The DEMS model demonstrates the initial conjecture [9] based on the role of the transverse component of the Poynting vector associated with the induction zone during the direct interaction of the particle-antiparticle pair, in generating the quantization. In synthesis, the electromagnetic dipole formed during a direct interaction has a non-zero dipole moment that gives it cylindrical symmetry in the Poynting vector field. The lack of spherical symmetry with respect to radial emission gives rise to a non-null transverse component of the Poynting vector associated with a rotating wave that localizes energy and momentum equal to that defined for a photon within the first wavefront. More exactly, inside the source zone of the DEMS defined by a spherical crown limited by the radii $\lambda/2 < r < 3\lambda/4$, an amount of energy formally and numerically in agreement with the photon hc/λ is localized. The first value of the action was calculated in a manner completely consistent with the DEMS model. The action value $h_1 = 6.626178 \times 10^{-34}$ J·s derived from the theoretical value of the Sommerfeld's constant calculated by the model, was subsequently improved in the more wide context of the BT by introducing the idea that the interacting charges, if referred to the dipole, cannot be approximated to a geometric points, so considering their angular dispersion was possible to provide an improved value $h_2 = 6.626075 \times 10^{-34}$ J·s of the action constant. This action value is in very good agreement with the current experimental value of the Planck constant $h_{\text{Planck}} = 6.626071 \times 10^{-34}$ J·s demonstrating that the DEMS model is independent from external conditions and allows a theoretical definition of the α^{-1} Sommerfeld's constant as a computable fundamental constant in an universe free to evolve without constraints. In this way, the DEMS behaves as a quantum mediator of the energy exchanged in a direct electromagnetic interaction, by emulating the quantized exchange of energy and momentum between the interacting particles.

2.2. The Role of the Uncertainty Principle in the Space-Time Creation

Considering that in BT the phase of production of a DEMS, called alpha phase (A), localizes the energy and momentum of the photon exchanged by the interacting particles, using the Poynting theorem is proved the existence of an uncertainty principle for observers external to the first wavefront in accordance with the Heisenberg principle, but also of an uncertainty principle for internal observers imbedded in the electromagnetic field of the DEMS, in this case, the pairs of variables position-momentum and time-energy within the dipole behave as conjugate variables because each pair is associated with the Poynting vector field of the DEMS, characterizing the localization and the propagation of the electromagnetic field. Thus, the electromagnetic field that fills the bubble within the wavefront defines the space-time of the bubble itself.

When the phase A ends, the photon exchange ends too. During this phase the interacting particles exchanged an energy equal to that of a photon with wavelength λ , from this instant the pair of particles begin to move away from each

other progressively increasing their mutual distance of interaction, *i.e.* they increase the wavelength of direct interaction up to infinity by bringing the DEMS up to zero energy. This final phase is called omega phase (Ω). It is necessary to ask ourselves how the energy of DEMS is stored and distributed in these two phases. In fact, during the alpha phase, the energy of interaction of the two particles is supplied externally by a process of acceleration, instead in the Ω phase, the first wavefront characterizing the DEMS energy emission is enclosing more and more space-time, while the wavelength that causally connects the two original interacting particles grows gradually reducing the electromagnetic energy of the actual DEMS. The difference in wavelength between the final and the initial signal defines the redshift of the original energy exchanged between the two interacting particles. If the energy conservation principle is not violated where did the missing energy go? In what other form of energy has the energy of the DEMS been transformed? This model suggests how the missing energy can become gravitational energy.

3. Multi-Bubble Universe Model

Considering the generalized uncertainty principle proposed in BT relative to the conjugate couples of variables energy-time and momentum-position measured by each observer, two independent cases can be considered:

1) The observer is not yet causally connected with the DEMS because it is moving externally to the first emitted wavefront of the DEMS in a pre-existing space-time, its position with respect to the DEMS is initially unknown. Reached by the wavefront the observer interacts with the DEMS through the wave. The interaction corresponds to an indirect measurement of the energy E and momentum P of the DEMS along the line of sight of the observer. In this case, the observations of momentum-position or of energy-time performed by each external observer, satisfy the Heisenberg's uncertainty principle. The relative observations of the position r and time t of both observers in order to the creation of the reciprocal DEMS, in agreement with BT are subject to the Lorentz-Einstein transformations. In this sense position and time of the observers depend on their relative movement with respect to the direct DEMS formation, the space-time in which each observer is imbedded is defined by the electromagnetic field produced by their interaction by means of the Planck action.

2) Two observers are placed in a pre-existing space-time and interacting with each other produce a new DEMS with respect to which they are placed inside the wave front emitted or equivalently, if a single observer is within the first wavefront of a DEMS the generalized uncertainty principle for internal observer in BT limits in both cases the measurable value of action of which the Planck constant is the upper limit, *i.e.* the direct interaction of a pair of particles or of a particle with one of the two particles of a DEMS, increasing the local action produces a weak perturbation of the pre-existing electromagnetic field rippling the space-time in terms of time-energy and position-momentum. The same phe-

nomenology is also suitable to describe a pair of particles created in a fluctuation of action which through the DEMS produced, it describes the creation of a new space-time bubble enveloped by the wavefront of the source. In this sense, the current universe can be considered an overlap of single bubbles.

Assuming the early universe to be all the space-time created inside a primordial bubble crossed in time by a web of direct and indirect interactions formed by DEMS connecting each particle with an antiparticle-observer, the space-time can be thought as an overlapping of bubbles. The Poynting's vector associated to the wavefront of each of these electromagnetic connections produces a directional pressure of radiation on the internal border of each local DEMS, with the effect to push on the resulting wavefront expanding the own space-time. Considering all the electromagnetic DEMS produced inside the universe, the resultant effect on the external border is a non-balanced pressure expanding it. When a direct connection produces a DEMS with wavelength λ , for the energy conservation principle, a part of the energy is involved in the DEMS production, if the DEMS is produced by a new pair of particles created from an action fluctuation, the amount of energy necessary for this creation must be taken somewhere, an energy supply that must exist before the emission of the pair and the formation of the DEMS, an energy made available from a field of *nothingness*, a sort of potential energy that feeds the source zone of the DEMS emitting a wave increasing the space-time of the bubble. The external side of the wavefront corresponds to the border of a local space-time of the DEMS on which act simultaneously two antagonist pressures: one negative produced by the subtraction of energy from the nothingness field and one positive which produces the expansion of the wavefront. The two pressures are perfectly balanced in a way such that after the first acceleration during the production of the source zone of the DEMS, the velocity of expansion of the wavefront is steady and equal to the light speed in each direction respect each observer in agreement with the relativity principle.

The existence of a field of nothingness besides the field of electromagnetic vacuum is suggested by the fact that a pair of existing particles can interact in the vacuum, that is, in a pre-existing space-time, but it can also be created together with their space-time by an action fluctuation. In this case, the creation of the pair would increase the energy of the universe in addition to its extent, and this would violate the principle of conservation of the energy.

3.1. Model of an Expanding Electromagnetic Space-Time Bubble

Using BT and the DEMS model in which is proved as in the source zone of the dipole is localized an amount of energy and momentum equivalent to that of a photon of equal wavelength, let

$$U = E + W \quad (1)$$

to be the total amount of energy of vacuum inside a DEMS,

$$E = hc/\lambda \quad (2)$$

describes the electromagnetic energy localized in the photon exchanged between particle and antiparticle and W the nothingness field that supplies the energy of the DEMS. In fact, for the conservation principle the electromagnetic energy (2) cannot be created but only transformed. After the creation the particles move apart each from other or annihilate in accordance with the conservation laws.

Following the theory, the creation of the pair is coinciding with a DEMS able of describing in BT the dual behavior of each particle [10]. The electromagnetic wave emitted by the source expands the electromagnetic bubble by pushing on the edge of the vacuum and inducing a constant radial resistance force σ_w in all directions. The total strength in the solid angle is given by

$$\frac{dW}{d\lambda} = 4\pi\sigma_w \quad (3)$$

which acts against the expansion of the wavefront such that the resultant radial strength of vacuum is null in each direction. This effect allows a wave propagation with a radial steady speed equal to light speed c . In fact, the wavefront grows up expanding with a force

$$\frac{dE}{d\lambda} = -\frac{hc}{\lambda^2} \quad (4)$$

Considering the forces (3) and (4), the total strength

$$\frac{dU}{d\lambda} = -\frac{hc}{\lambda^2} + 4\pi\sigma_w \quad (5)$$

is nulled for the wavelength λ_m characterizing the wavelength of the minimum of energy of the vacuum corresponding to the ground state U_0 of the energy (1), for each other value of wavelength the strength (5) is different by zero and the total vacuum energy is greater than the ground state. Considering a stretching of the wavelength, integrating the strength (5) between an initial and a final wavelength $[\lambda, \lambda']$, to conserve unchanged the energy of the ground state must be

$$\delta U = \left(\frac{hc}{\lambda'} + 4\pi\sigma_w\lambda' \right) - \left(\frac{hc}{\lambda} + 4\pi\sigma_w\lambda \right) = 0 \quad (6)$$

In agreement with the Equations (1), (2) and (3)

$$U = \frac{hc}{\lambda} + 4\pi\sigma_w\lambda \quad (7)$$

is the total vacuum energy inside the bubble of space-time of a DEMS.

In order to maintain the energy of the state (7) unchanged during the wavelength stretching, it is necessary that the transition occurs adiabatically. Assuming the state U as a constant value, the Equation (7) gives as solutions two wavelength corresponding to an initial and a final value of wavelength:

$$\lambda_{i,f} = \frac{U \pm \sqrt{U^2 - 16\pi\sigma_w hc}}{8\pi\sigma_w} \quad (8)$$

only when U is such a that

$$U \geq \sqrt{16\pi\sigma_w hc} \quad (9)$$

According to the Equation (9), considering an action fluctuation of arbitrary value H , is possible to define the energy of the vacuum as

$$U = 2\sqrt{4\pi\sigma_w(h+H)c} \tag{10}$$

the wavelengths (8) become

$$\lambda_{i,f} = \sqrt{\frac{(h+H)c}{4\pi\sigma_w}} \mp \sqrt{\frac{Hc}{4\pi\sigma_w}} \tag{11}$$

For $H = 0$ (no fluctuation), the Equation (11) gives $\lambda_m = \lambda_i = \lambda_f$, both the wavelengths are coinciding and are corresponding with the ground state of energy

$$U_0 = 2\sqrt{4\pi\sigma_w hc} \tag{12}$$

with

$$\lambda_m = \sqrt{\frac{hc}{4\pi\sigma_w}} \tag{13}$$

In this sense, electromagnetic energy (2) possibly emitted in a fluctuation through a local DEMS, must be supplied by an amount of energy of the nothingness field by means of an increase of action $H > 0$, *i.e.* the energy of the electromagnetic vacuum grows and it is $E > W$, therefore the wavelength of the DEMS would become lower than its limit value λ_m , but a quantity of energy is returned to the nothingness field inducing an adiabatic transition that reduces the DEMS energy stretching the wavelength from the initial value λ_i to the final value λ_f decreasing the electromagnetic energy and increasing the energy of the nothingness field in such a way that $E < W$. Using the Equation (7), (11) and (13), it is possible to verify the identity of the vacuum energy first and after the transition $U_i = U_f$ for each arbitrary fluctuation H proving the total energy (7) grows but the transition leaves it unchanged

$$U_{i,f} = 2\sqrt{4\pi\sigma_w(h+H)c} \tag{14}$$

Assuming fluctuations $h+H$ with values multiple of the Planck action constant, defining arbitrarily

$$H = (n-1)h \tag{15}$$

with $n \geq 1$, using Equation (11) only spontaneous transitions $\lambda_i \rightarrow \lambda_f$ occurring from an initial value

$$\lambda_i = (\sqrt{n} - \sqrt{n-1})\lambda_m \tag{16a}$$

towards a final value

$$\lambda_f = (\sqrt{n} + \sqrt{n-1})\lambda_m \tag{16b}$$

with a finite but not arbitrary increment of wavelength

$$\delta\lambda = 2\sqrt{n-1}\lambda_m \tag{17}$$

produced by adiabatic transitions able to maintain unchanged during the transition the in initial state of the vacuum energy (7). Using the Equations (14), (15)

and Equation (16) the electromagnetic and nothingness energies of the local vacuum become respectively

$$E_{i,f} = \frac{1}{2}U_0(\sqrt{n} \pm \sqrt{n-1}) \quad (18)$$

$$W_{i,f} = \frac{1}{2}U_0(\sqrt{n} \mp \sqrt{n-1}) \quad (19)$$

yielding for the total energy of vacuum (14)

$$U_{i,f} = U_0\sqrt{n} \quad (20)$$

which is a function of the multiplicity $n \geq 1$. In each case, in agreement with Equation (6) the transition occurs adiabatically

$$\delta U = U_f - U_i = 0 \quad (21)$$

implying during the transition using the Equation (18) and (19) and (21)

$$-\delta E = \delta W = U_0\sqrt{n-1} \quad (22)$$

i.e. each increase of wavelength (17) produces a decrease of the electromagnetic energy of the DEMS balanced by the increase of the energy of the nothingness field. The number n defines the energy of the fluctuation and the vacuum state (20). In the ground state $n=1$ the electromagnetic and nothingness energies are identical, each transition occurring not modifies the final wavelength of the DEMS which remains stable at the minimum energy, for this characteristic the quantum of energy that can be exchanged between the electromagnetic fields of the vacuum and the nothingness field is defined Balancing Graviton (BG) and it is associate to a boson particle G_{BG} with energy

$$E_{BG} = \sqrt{4\pi\sigma_w hc} . \quad (23)$$

Using the Equation (23), the Equation (12) becomes

$$U_0 = 2E_{BG} . \quad (24)$$

Vice versa, for fluctuations with $n > 1$, the electromagnetic energy (18) is greater than the nothingness energy (19) and a number of BG (23) are exchanged increasing the energy of the nothingness field, expanding space-time and maintaining unchanged the initial energy of the vacuum state after the fluctuation. Now defining usefully $n = N^2 + 1$ the integer number $N = 0,1,2,3,\dots$ is the number of BG exchanged between the electromagnetic field of the DEMS and the nothingness field. After the transition the final energy of the vacuum state is:

$$U = U_0\sqrt{N^2 + 1} . \quad (25)$$

Using the definition of the number of BG exchanged the Equation (22) becomes

$$-\delta E = \delta W = NU_0 . \quad (26)$$

Higher is the initial electromagnetic energy (18) with multiple fluctuations $n = 2,5,10,\dots$, greater is the number $N = \sqrt{n-1}$ of BG that are exchanged

during the adiabatic transition between the DEMS and the nothingness field, lower is the residual electromagnetic energy after the transition, in which the wavelength of the original DEMS is stretched of a length increase defined by the Equation (17) with a redshift

$$z = 2N \left(\sqrt{N^2 + 1} + N \right). \quad (27)$$

In other terms, by the exchange of $N \geq 1$ BG, the bubble with radius coinciding with the initial wavelength λ_i of the DEMS has a quantized expansion with an increase of radius up to λ_f and an increase of space-time, converting the part in excess of electromagnetic energy of the DEMS in energy of the nothingness field which corresponds to a growing tension on the internal border of the space-time. In this model the nothingness energy has the role of potential energy of the vacuum.

3.2. Balancing Gravitons and Action Fluctuations

In order to evaluate the constant strength σ_w is necessary to assume that with a very high level of electromagnetic energy density within an expanding primary spherical bubble, the nothingness field can have a number of BG with an energy enough high to produce new fluctuations forming each a new DEMS transforming the original space-time inside the primary bubble in an overlapping of sources equivalent to a gas of photons, an overlap of bubbles ping in which each photon has a wavelength less equal than that of the primary bubble. This condition originates a black-body spectrum with a characteristic cut-off wavelength as defined in BT. The Planck spectrum is characterized by the average temperature

$$T_{ave} = \frac{hc}{k_B \lambda_{ave}}$$

with electromagnetic emissions within two cutting frequencies, a lower frequency due to the upper wavelength of the bubble and an upper frequency beyond which the DEMS becomes a Micro-Black-Holes (MBH) [11]. Since is not correct to use directly the results obtained for a MBH in which gravity has been assumed as a Newtonian fundamental strength, it is possible to estimate the cut-off frequency *i.e.* the minimum value of wavelength, considering when the total electromagnetic energy localized by the DEMS becomes equivalent to all the energy carried by the impinging interacting particle and simultaneously equal to the Newtonian gravitational energy of the interacting pair of particles emerging by the interaction. To solve these three conditions:

$$\begin{cases} E = \frac{hc}{\lambda} \\ E = mc^2 \\ E = G_0 \frac{m^2}{\lambda} \end{cases} \quad (28)$$

where G_0 is an initial unknown value of the gravitational coupling constant acting inside the primary DEMS of space-time or in other terms, the early value of the gravitational constant in a primary bubble. Using the three previous equa-

tions in pairs of two, the Equation (28) yields a pseudo-Planck mass

$$m_{eq} = \sqrt{\frac{hc}{G_0}} \quad (29)$$

associated to the pseudo-Planck length defining the BG wavelength

$$\lambda_{BG} = \sqrt{\frac{hG_0}{c^3}} \quad (30)$$

Let the wavelength (13) $\lambda_m \equiv \lambda_{BG}$ to be the minimum non-zero wavelength associated at the minimum value of the nothingness energy achieving in space-time, the Equation (13) and (30) yield a constant force as the value of the total tension of space-time border when the bubble is forced to expanding

$$\frac{dW}{d\lambda} = \frac{c^4}{G_0} \quad (31)$$

Consequently, in the ground state the energy of the nothingness field and of the electromagnetic field of vacuum state are equal to the energy (23) of a BG, *i.e.*

$$E_{BG} = E_0 \equiv W_0 = \sqrt{\frac{hc^5}{G_0}} \quad (32)$$

Equation (32) is the energy of a collapsed DEMS not coinciding numerically with that one defined for a MBH because the effective value of G_0 to use in the Equation (32) is yet to evaluate.

Since the energy of the BG (32) is the largest amount of electromagnetic energy that can be produced and localized within a DEMS, but it is also the lower energy achievable for the nothingness field, a fluctuation of action $H > 0$ emerges under form of a one or more DEMS with high energy that cannot overcoming the energy limit of a BG, then emits the excess of energy in the form of an integer number of BG, the energy is absorbed from the field of nothing by stabilizing the electromagnetic energy of the DEMS, stretching the wavelength of the primary DEMS and expanding the bubble. After the fluctuation, the space-time is grown maintaining unchanged the initial total energy of vacuum. On the other hand, the nothingness field acquiring the energy of a great number of BG can re-provide energy to the electromagnetic field within the bubble, producing pairs of particles originating new DEMS and space-time inside the primary bubble. The process in its whole is a sort of energy recycling starting from the initial Zero Point Energy (ZPE) of the electromagnetic vacuum. For this way to behave, the BG exchange divides the energy between the electromagnetic field and the field of nothingness, keeping the total energy of the vacuum in constant balance. For the previous reason, the BG is here defined as a quantum of balance.

In the BG exchange, considering an adiabatic expansion in a space-time with $n \gg 1$, using the Equation (26), let

$$\delta E = -NU_0 \quad (33)$$

and

$$\delta W = NU_0 \quad (34)$$

to be respectively the electromagnetic energy subtracted and the energy acquired by the nothingness field under form of gravitational potential energy by means of the exchange of BG, using the Equation (33) and (34) the Equation (21) is verified ever null for each adiabatic transition occurring by the exchange of an arbitrary numbers N of BG, *i.e.* the transition occurring during the fluctuation leaves the final energy unchanged, but the number N of BG that define the total energy of the vacuum exchanged grows with the final effect of to stretch the wavelengths of the black-body spectrum as estimated with the (27).

4. Local Pseudo-Gravity

Considering a DEMS with an internal electromagnetic energy $E \ll E_{BG}$ and the Equation (7) in the form

$$U = E + \frac{c^4}{G_0} \lambda \quad (35)$$

where lower is the electromagnetic energy E , higher is the nothingness energy W , and as shown in **Figure 1** the total energy of vacuum U at right side of the events horizon grows expanding the wavelength of the corresponding DEMS. In the Eq. (35) the strength c^4/G_0 turn out to be a tension constant of the space-time fabric [12]. Considering only low energy events occurring inside a pre-existing space-time with a bubble of radius λ associated with the emission of pairs of particles, of pairs of gamma or at radio waves, the wavelength characterizing the event is stretched by the expansion of the bubble in which it is contained without the exchanging of BG with the nothingness field. In this case, the energetical degrade of the bubble can be considered the elapsed time from the origin of the bubble. Time in this context can be considered an emergent energetic fourth dimension produced by the variation of the local electromagnetic energy with the stretching of the wavelength of the bubble and the increasing of the total tension of space-time.

Considering a bubble stretched from λ to λ' with a continue redshift z , using the Equation (35) is possible to evaluate the electromagnetic energy measured by an observer along its sight line after the stretching of the bubble. Considering an electromagnetic energy variations, since $\delta U = 0$ it follows $-\delta E = \delta W$ calculated between two different wavelengths $\lambda' > \lambda$ with $-\delta E < E_{BG}$, it follows:

$$E - E' = \frac{c^4}{G_0} \lambda' - \frac{c^4}{G_0} \lambda \quad (36)$$

that yields

$$E' = E - z \frac{c^4}{G_0} \lambda \quad (37)$$

corresponding to the redshifted observed energy estimated starting from the initial value E reduced of an amount of energy proportional to the stretching work of the wavelength of the bubble.

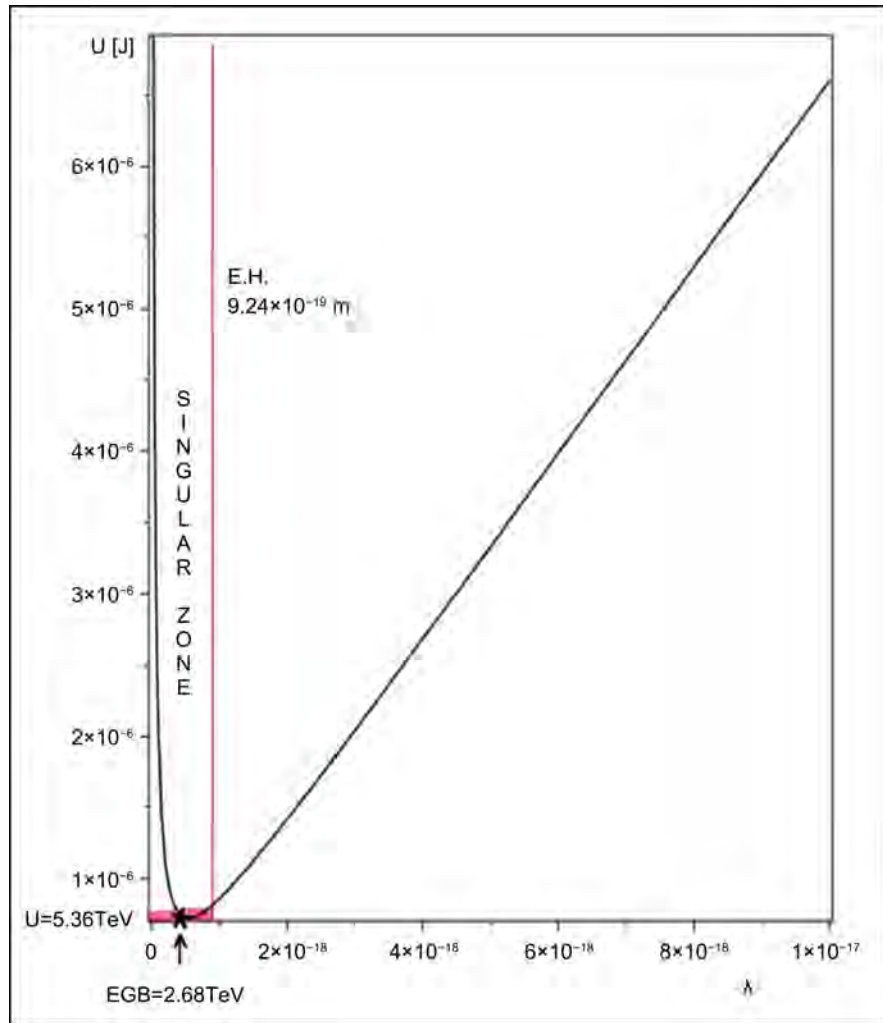


Figure 1. The total energy of the vacuum U as a function of the wavelength of the DEMS. The figure highlights the singular zone under the events horizon and the BG energy (32) as estimated below.

Considering each electromagnetic indirect or direct connection between moving observers obtained throughout a causal electromagnetic interaction described relativistically with the use of the Doppler equation [6]:

$$E_{\Gamma} = \frac{hc}{\lambda_0} = \frac{E^2 - P^2c^2}{2(E - Pc \cos \theta)} \tag{38}$$

where λ_0 is the generalized Compton wavelength of a photon exchanged inside the original DEMS along the sight line connecting one component of the DEMS and the observer. Combining the redshifted energy (37) and the observed energy (38), the energy of the photon E_{Γ} can be evaluated using the value of the original energy as proposed below.

4.1. Pseudo-Gravity Field

To describe the gravity phenomenology, it is necessary to consider an observer

like in the case (1) of paragraph 3, that is an observer placed externally to a DEMS in a pre-existent space-time. When the observer is reached by the electromagnetic wave of the DEMS, an indirect connection between DEMS and observer is realized. The effect is a causal connection of the observer with one of the two particles forming the primary DEMS, this new connection is a secondary DEMS imbedded in the pre-existing space-time involving the primary source and its observer. An exchange of a photon of energy (38) occurs. After the eventual alpha phase, the omega phase of the DEMS starts at $\theta = \frac{\pi}{2}$ and the interaction angle is every $\theta > \frac{\pi}{2}$, *i.e.* the interaction angle between the trajectories of motion of the two interacting components of the secondary DEMS can be settled as $\theta = \pi/2 + \varphi$ where φ it is a positive angle with respect to the radial line of sight, with which the observer moves away.

Using the definitions of total rest energy and of Compton energy given in Ref. [6], the numerator of the Equation (38) becomes

$$E^2 - P^2 c^2 \equiv \left(\frac{2hc}{\lambda_c} \right)^2 = \varepsilon^2 \quad (39)$$

which is the square of the rest energy of the interacting particles of the DEMS.

To describe a redshifted energy received along the sight line of the observer, is necessary to use the Equation (39) in which the energy characterizes the radius of the bubble. The rest energy (39) it is an invariant, so the Equation (38) for the received energy, becomes:

$$E_r = \frac{\varepsilon^2}{2 \left(\frac{hc}{\lambda} - z \frac{c^4}{G_0} \lambda \right) (1 + \beta \sin \varphi)} \quad (40)$$

Considering the electromagnetic vacuum within a bubble to be an initial space-time at temperature T , the successive casual production of new DEMS inside the primary bubble behaves as a gas of photons, that they will make it evolve up to become a black-body at the same mean temperature with a Planck spectrum associated to an average wavelength $\lambda_{ave} = hc/k_B T$.

The denominator of the Equation (40) allows to define as a function of the redshift z of the light received, the border which divides the region of gravity from that of antigravity. So, using the mean characteristic wavelength and the definitions (30) and (32), the ratio

$$\zeta_{BG} = \lambda_{BG}^2 / \lambda_{ave}^2 \equiv k_B^2 T^2 / E_{BG}^2 \quad (41)$$

represents a variable threshold that separates antigravitational from gravitational energy of the primary DEMS. In fact, using the Equation (41), the Equation (40) can be broken into three equations, each for a different zone of redshift in the same bubble at temperature T :

$$E_{\Gamma} = \begin{cases} \frac{hc}{\lambda_c} & z = 0 & \text{(a)} \\ \frac{G_0}{4c^4} \frac{\varepsilon^2}{\frac{1}{2}(\zeta_{BG} - z)(1 + \beta \sin \varphi)\lambda} > 0 & 0 < z < \zeta_{BG} & \text{(b)} \\ \frac{G_0}{4c^4} \frac{-\varepsilon^2}{\frac{1}{2}(z - \zeta_{BG})(1 + \beta \sin \varphi)\lambda} < 0 & z > \zeta_{BG} & \text{(c)} \end{cases} \quad (42)$$

Considering the space-time of a primary bubble, for each DEMS produced that emits inside, an observer can be placed within:

1) *Quantum zone*: at redshift $z = 0$ the particles with resting energy (39) are not relativistic, the observer is one of the two interacting particles inside the DEMS or it is imbedded in their space-time. The energy is described by the Equation (42-a) and is equivalent to the energy of a photon with Compton wavelength, exchanged between the observer and one of the two interacting particles;

2) *Anti-gravitational zone*: with redshift $0 < z < \zeta_{BG}$, the energy is positive and it is described by the Equation (42-b). The bubble is in very fast expansion. The observer and the particles acquire enough energy to escape, radially stretching the wavelength with which they interact;

3) *Gravitational zone*: with redshift $z > \zeta_{BG}$, the energy is negative and it is described by the Equation (42-c). Gravity is produced.

From the Equation (42-b) is evident that each bubble suffers a rapid expansion during the DEMS formation until the redshift does not satisfy the condition $\zeta_{BG} - z < 0$ as required in the Equation (42-c). Considering the Equation (41) and the definition of redshift, the previous inequality has solution $\lambda > 1.4656\lambda_{BG}$ corresponds to $z > \zeta_{BG} \cong 0.4656$. When that occurs, antigravity becomes gravity. Considering the Events Horizon (EH) of a BG with a radius equal to the Schwarzschild radius $r_{EH} = 2\lambda_{BG}$, for wavelength in the interval $1.4656\lambda_{BG} < \lambda \leq 2\lambda_{BG}$ the DEMS produced are every below their EH and only by wavelength $\lambda > 2\lambda_{BG}$ the energy of the electromagnetic field emitted can propagate as shown in **Figure 1**.

4.2. Effective Interaction Distance

Considering the Equation (42-c), let λ to be the minimum distance at which two particles start to interact and λ' the actual final distance achieved when the two particles move apart each to the other with speed β and angle φ , is possible to define the effective interaction distance as the radial distance

$$r = \frac{1}{2}(z - \zeta_{BG})(1 + \beta \sin \varphi)\lambda \quad (43)$$

which in the zone (3) for relativistic particles with $\varphi = \pi/2$, Equation (43) can be correctly approximated at $r \cong z\lambda$ and for non-relativistic particles at $r \cong z\lambda/2$ proving that two observers indirectly connected in zone (3) are placed at an effective interaction distance of the order of the difference between the

stretched final wavelength and the initial one. Considering an elapsed time from the end of the phase alpha, such that $\lambda' \gg \lambda$, the effective distance (43) is of the order of the final wavelength $r \approx \lambda'$, so the Equation (43) allows to describe the gravitational interaction energy (42-c) in terms of the actual final distance measured as a function of four parameters $(z, \zeta_{BG}, \beta, \varphi)$.

Using the definitions of entangled rest masses (A.2) given in **Appendix A** and using the distance (43), the energy (42-c) can be rewritten in the pseudo-Newtonian form

$$E_{\Gamma} = -G_0 \frac{\mu_1 \mu_2}{r} \quad (44)$$

Defining the gravitational potential as $\phi_i = E_{\Gamma} / \mu_j$, the evaluation of the gravitational field yields

$$\mathbf{g}_1 = -\text{grad} \phi_1 = -G_0 \frac{\mu_1}{r^2} \hat{\mathbf{r}} \quad (45)$$

and reciprocally, for the body #1

$$\mathbf{g}_2 = -\text{grad} \phi_2 = -G_0 \frac{\mu_2}{r^2} \hat{\mathbf{r}} \quad (46)$$

hence the mutual strength between two entangled particles of masses μ_i and μ_j placed at the effective distance (43) agrees with the Newtonian form of the universal gravitational law:

$$\mathbf{F} = -G_0 \frac{\mu_i \mu_j}{r^2} \hat{\mathbf{r}} \quad (47)$$

The Equation (47) becomes a singularity at the border when the effective interaction distance is zero at $z = \zeta_{BG}$ independently from the value of the black-body temperature. Using Equation (47) and Equation (43) it is easy to prove that identical pairs of interacting particles producing identical gravitational attractive force are not necessarily interacting at a same final wavelength. In fact, their effective interaction distances do not depend on the only real space position, because identical values of gravitational force can be produced by an infinity of different combinations of values of the four parameters and of the wavelength from which they depend. This can assign equal values of energy and of gravity strength at different pairs of particles also if they are placed at a different real reciprocal distance in space-time. It is important to highlight as Equation (47) describes the gravitational force between two interacting particles as if their actual distance were fixed. Considering the original DEMS, when the two interacting particles are in relative motion it is necessary to consider that the value of the wavelength corresponding to the initial direct interaction has not a fixed value, but changes continuously as a function of their characteristic red-shift. This changing occurs also for indirect interactions of observers connected through a DEMS by means of the propagation of the emitted electromagnetic wave. In this case, when the observer is achieved by the wave becomes connected at a DEMS and a direct interaction starts. In both cases it is necessary to correct

the strength for the changing of scale of the interaction.

4.3. Difference between Indirect and Direct Gravitational Interaction

Considering an observer in the case (1) of paragraph 3 placed in a position in space-time much far from a DEMS, its distance can be expressed as a multiple of the effective wavelength at which the DEMS emits a wave respect the observer. Assuming the travelled distance

$$r' = \xi r \quad (48)$$

where r is the effective wavelength (43) of the gravitational wave signal emitted by the DEMS and $\xi > 1$ a dimensionless fraction. When the wave signal reaches the observer a secondary DEMS with wavelength (48) starts to emit. The energy directly exchanged is of types (42-a). Successively, considering the relative motion of the two entangled partners, the interaction can be described by Equation (42-b) in which the bubble expands stretching its wavelength. When the condition $z > \zeta_{BG}$ is satisfied, the observer suffers an attractive force consistent with (47). In this case, the measured strength is attenuated than a factor $1/\xi^2$ compared to that of the primary DEMS

$$\Phi = -G_0 \frac{\mu_i \mu_j}{r'^2} \hat{r} = \frac{1}{\xi^2} \mathbf{F} \quad (49)$$

Using the Equation (49), it is easy to verify that considering identical interacting particles distributed in space-time, when the energy is shared by wave, each interaction switches from indirect to direct and the energy propagated is reduced of a factor $1/\xi$ per each interaction, while the gravitational force is reduced in strength of a factor $1/\xi^2$ at a time producing entanglement among all the particles involved. Considering a different multiplicity for each interaction, the signal intensity is attenuated by the creation of secondary DEMS that absorb and degrade energy more quickly than happens for propagated waves that do not meet matter.

4.4. Dynamic Correction of the Gravitational Strength

When a direct gravitational interaction (42-c) between two particles starts, their relative motion in space-time stretches the original wavelength settled by their initial causal contact modifying continuously the gravitational strength acting between the two particles. To describe the changing in scale of the force occurring at charge of the work done to stretch the initial wavelength, it is necessary to consider the variation of the energy (44) respect the wavelength, *i.e.* respect the distance of the initial direct interaction. As shown in **Appendix B**, the resultant effective gravitational force is given by:

$$\Psi = \frac{1}{2} (z + \zeta_{BG}) (1 + \beta \sin \varphi) \mathbf{F} \quad (50)$$

where the Equation (50) describes the correct radial force along the sight line of

the observer placed at an effective distance r from the particle with which it is entangled. Using the scalar dimensionless ratio

$$Z = \frac{\Psi}{F} \tag{51}$$

is possible to define the effective gravitational strength between two bodies in relative motion as represented in **Figure 2**. In other words, two particles placed at a direct interaction distance r as defined in Equation (43), are attracted each to the other with an effective strength

$$\Psi = -G_0 Z \frac{\mu_1 \mu_2}{r^2} \tag{52}$$

Equation (52) is homolog to the Newton's law but it is different in respect the Equation (47) by the presence of the ratio (51) that can be assumed generally different. Attributing the changing in scale at the value of the gravitational pseudo-constant $G = G_0 Z$, the Equation (52) allows to define the gravitational coupling pseudo-constant that varies in space-time with the change of parameters $(z, \zeta_{BG}, \beta, \phi)$. Using the Equations (51) and (52), let $b = \beta \sin \varphi$ with $0 < b < 1$ the speed projection, the value of the gravitational pseudo-constant is defined by the function

$$G = \frac{G_0}{2} (z + \zeta_{BG})(1+b) \tag{53}$$

Considering the local universe as represented in **Figure 2(b)**, respect an observer in a lab at the present time, the gravitational coupling constant (53) must coincide at the actual (starred*) standard value, *i.e.* $G^* = 6.67192 \times 10^{-11} \text{ N}\cdot\text{m}^2\cdot\text{kg}^{-2}$ [13]. Considering the set of reduced parameters $(z \geq \zeta_{BG}, \zeta_{BG}, 0)$, using the Equation (32) and (41) with an actual black body temperature $T = 2.73 \text{ K}$ of the

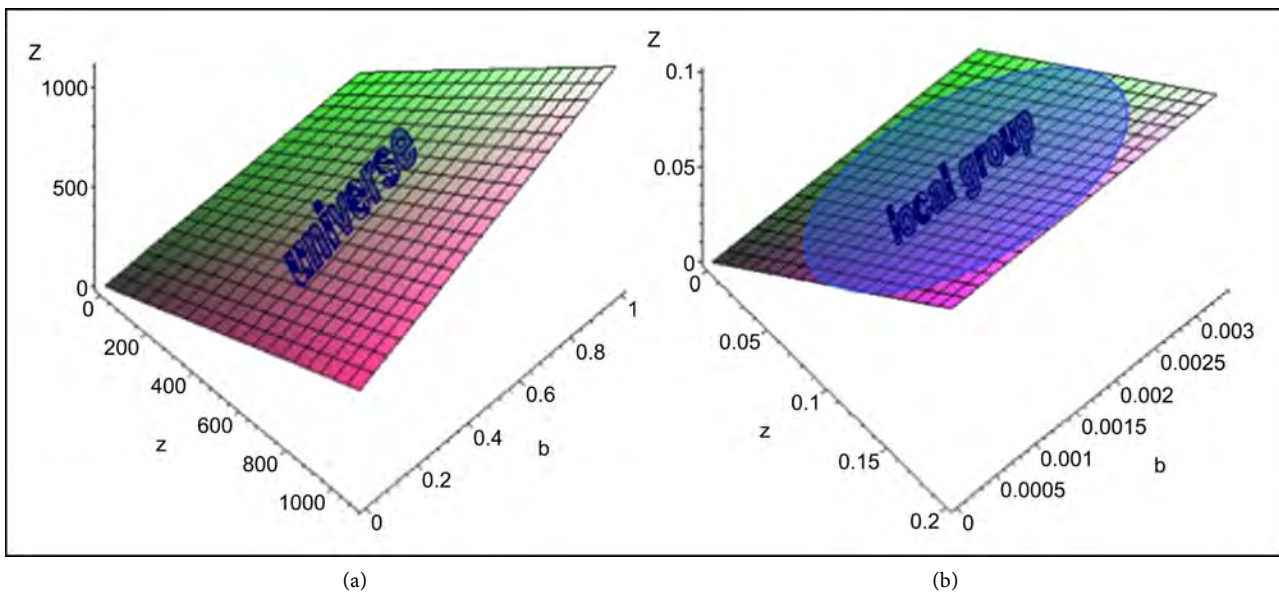


Figure 2. Representation of the variability of the Z scaling factor modulating the early gravitational coupling constant G_0 . (a) Scaling range for the whole universe. (b) scaling range for the local group.

CMB, the primordial gravitational coupling constant results to be $G_0 = 8.68 \times 10^{+21} \text{ N}\cdot\text{m}^2\cdot\text{kg}^{-2}$ with $z \geq \zeta_{BG} = 7.69 \times 10^{-33}$, from which, the nowadays value of the gravitational constant results to be as the expected actual one $G \geq G_0 \zeta_{BG} = 6.67 \times 10^{-11} \text{ N}\cdot\text{m}^2\cdot\text{kg}^{-2}$. Using the Equation (47), the local effective gravitational tension (50) between two interacting bodies can be rewritten in the Newtonian scalar form as

$$\Psi_{i,j} = -G \frac{\mu_i \mu_j}{r^2} \quad (54)$$

Considering as general fundamental cases, when the local interaction is relativistic $(\zeta_{BG}, \zeta_{BG}, 1)$ and when the local interaction is classic $(\zeta_{BG}, \zeta_{BG}, 0)$, Equation (54) yields in the first case

$$\Psi \cong -2G \frac{\mu_i \mu_j}{r^2} \hat{r} \quad (55)$$

and in the last

$$\Psi \cong -G \frac{\mu_i \mu_j}{r^2} \hat{r} \quad (56)$$

but are possible many variations, for example for a captured electron orbiting around a proton with $\varphi \cong 0$, it follows $b = 0$, assuming a vacuum temperature of 2.73 K with $z \cong \beta = \frac{1}{137} \gg \zeta_{GB}$ as suggested in reference [14], the Equation (53) gives a gravitational constant $G \cong G_0/274 = 3.17 \times 10^{+19} \text{ N}\cdot\text{m}^2\cdot\text{kg}^{-2}$ giving for the entangled masses $\mu_e \mu_p$ of a couple electron-proton in a hydrogen, a strength

$$\Psi \cong -G \frac{\mu_e \mu_p}{r_H^2} \cong 1.73 \times 10^{-17} \text{ N} \quad (57)$$

much greater than the Newtonian value of gravity, but lower than the Coulombian force which is of the order of 10^{-7} N .

5. Emergent Newtonian Gravity

The Equation (36) puts in evidence as gravity is produced by the conservation of the vacuum energy when the radius of the bubble, the wavelength of the DEMS, is stretched during the omega phase, *i.e.* when the wavelength of the direct interaction grows. To produce the gravity as a force between macroscopic body it is necessary to consider the strength between the particles with which the matter is formed. For example, a great number of hydrogen atoms are confined in a volume of space-time. Each proton and electron of the atoms interact electromagnetically with all the other particles of opposite charge. The resultant gravitational effects obtained adding up the fields emitted by each DEMS produced by the direct interaction between a positive and a negative charge, yields a resultant strength which value is varying with the energies localized by each DEMS and by their effective age in redshift terms. In this sense, if a DEMS is just formed on it does not act gravity. Using the generalized definitions (45) and (51), the total

gravitational field produced by the particles is

$$\Gamma = \sum_i Z_i \mathbf{g}_i \tag{58}$$

Extending the Equation (58) to an arbitrary equal number $N_p = N_e = N_H$ of protons and electrons forming a cloud of hydrogen, the gravitational field acting on an observer is given by

$$\Gamma = -G_0 m_p \sum_{j=1}^{N_p} \frac{Z_j}{r_j^2} \hat{\mathbf{r}}_j - G_0 m_e \sum_{k=1}^{N_e} \frac{Z_k}{r_k^2} \hat{\mathbf{r}}_k \tag{59}$$

Since a bounded couple proton-electron is a hydrogen atom, using its spatial average position r_i of the atom respect to the observer, Equation (59) becomes

$$\Gamma = -G_0 (m_p + m_e) \sum_{i=1}^{N_H} \frac{Z_i}{r_i^2} \hat{\mathbf{r}}_i \tag{60}$$

where considering the effective distance (46) of the observer from the moving center of mass of the cloud, is possible to define a mean function of the factors as

$$\sum_{i=1}^{N_H} \frac{Z_i}{r_i^2} = \frac{1}{r^2} \sum_{i=1}^{N_H} Z_i \cos^2 \chi_i = \frac{N_H \bar{Z}}{r^2} \tag{61}$$

where χ_i defines the angular distance of each atom from the center of mass of the cloud.

Equation (60) becomes

$$\Gamma = -G \frac{M_{cloud}}{r^2} \hat{\mathbf{r}} \tag{62}$$

where

$$M_{cloud} = N_H (m_p + m_e), \tag{63}$$

is the total mass of the hydrogen cloud, $G = G_0 \bar{Z}$ is the Modified Gravitational Constant (MGC) as defined in Equation (53) where \bar{Z} is the average ratio (51) calculated on all the hydrogen atoms. The gravity is produced from a spatial concentration of energy as an emergent real force which the effective strength depends not only from the mass and by the effective distance (46) but also from the effective MGC value which modulates the classical value of Newtonian gravity. Using the definition of effective distance (43), the redshift produced by the expansion of the bubble of space-time can be defined as

$$z = \zeta_{BG} + \frac{2r}{(1+b)\lambda_b}, \tag{64}$$

in agreement with (51) the scalar dimensionless ratio becomes

$$Z = \frac{r}{\lambda_b} + \zeta_{BG} (1+b) \tag{65}$$

with which using the gravitational force (62), the gravitational potential of a cloud of mass (63) becomes

$$\Phi = -G_0 \left[\lambda_b^{-1} + \frac{\zeta_{BG} (1+b)}{r} \right] M_{cloud} \hat{\mathbf{r}} \tag{66}$$

The consequences on large scale of the MGC in the Equation (66) can be much relevant, in fact considering two galaxies moving away at relativistic velocity, they are associated to a radial redshift $z = \beta$ with $\varphi \cong \pi/2$ and will show a gravitational attraction greater than the one previewed by the Newtonian gravitational law as if their mass was greater than of the visible one. In this case, the gravitational anomaly is able to simulate the presence of an exceeding mass. Conversely, two nearby interacting galaxies, with a relative not relativistic motion $\beta \cong 0$, would show a gravity equal the one expected considering their visible mass. This effect, if confirmed, would eliminate the need for Dark Matter in the galactic halos

6. Anomalous Rotational Velocity of Galaxies

Another interesting effect usually attributed to Dark Matter could be observed considering the matter orbiting around a gravitational attractor, like the case of stars or gas orbiting around a galactic nucleus or a black hole. Since the motion occurs tangentially with $\varphi \cong 0$ around the attractor, the orbital velocity of matter is directly proportional to the square root of the absolute value of the gravitational potential of the attractor. In this case, considering the Equation (66) is possible immediately to write

$$V_r = \sqrt{\left(\frac{G_0}{\lambda_b} + \frac{G}{r}\right)M} \quad (67)$$

Since the Equation (67) has got a velocity constant term, can be rewritten in the form

$$V_r = \sqrt{V_0^2 + G \frac{M}{r}} \quad (68)$$

where

$$V_0 = \sqrt{\frac{G_0}{\lambda_b} M} \quad (69)$$

can be interpreted as the anomalous rotational velocity of the matter orbiting at great distance from the center of mass and it is coinciding with the bubble contribute at the velocity of the halo. The effect is a flat velocity of the galactic halo, so considering a galaxy, its external rotational velocity is a constant value (69) depending only by the mass contained within the spherical shell centered in the center of mass and by the value of the wavelength λ_b of the redshifted gravitational wave associated at the maximum extension of the bubble of space-time containing the attractor, *i.e.* the wavelength λ_b is the radius of the local universe connected gravitationally with the galaxy.

In general, considering the modified gravitational field (66) which produces a strength acting on the rotating matter much intense than the Newtonian one, the squared of the velocity of rotation in the Newtonian approach gives a mass much greater than what it really is

$$M_{real} = M_{Newton} - \frac{V_0^2}{G} r. \tag{70}$$

In other terms, the orbital velocity gives an estimation of the Newtonian gravitational mass of an attractor greater than the one expected with the present theory. This fact provides a bubble associated with a galaxy with an effective mass energy formally in accordance with that estimated for an effective DEMS in Equation (37), in which a part of the initial energy became energy of the nothingness field which increases the tension of space-time of the galactic bubble

$$E' = E - \frac{c^2 V_0^2}{G} r \tag{71}$$

7. The Einstein Field Equation for the Multi-Bubble Universe

The gravity (54) is originated by the curvature of the local space-time of a DEMS produced by a concentration of energy inside the spherical wavefront but also from the relativistic motion of the two interacting observers which modifies the energy density in space-time. In this sense gravity is the final result of the interaction of two observers due to energy conservation of two particles electromagnetically entangled. To calculate the local curvature of the space-time of a single DEMS respect the centre of mass of the source, it is necessary to consider the total energy of the vacuum defined by the Equation (1). Defining the derivative of the volume of the first wavefront of the DEMS with respect the wavelength measured in the center of mass

$$\frac{dV}{d\lambda_0} = 4\pi\lambda_0^2 \tag{72}$$

and using Equation (72) and the strength (5) respect the center of mass, the scalar value of the energy density is

$$T = \frac{dU}{dV} = -\frac{hc}{4\pi\lambda_0^4} + \frac{\sigma_w}{\lambda_0^2} \tag{73}$$

Using the Equation (30) it is easy to obtain

$$\frac{8\pi G_0}{c^4} T = \frac{2}{\lambda_0^2} - \frac{1}{2} \frac{G_0 h}{c^3} \left(\frac{2}{\lambda_0^2} \right)^2 \tag{74}$$

where the left side, the Equation (74) is the track of the Einstein's tensor

$$\frac{8\pi G_0}{c^4} g^{\mu\nu} T_{\mu\nu} = g^{\mu\nu} R_{\mu\nu} - \frac{1}{2} g^{\mu\nu} g_{\mu\nu} R. \tag{75}$$

Since the track of the Ricci's tensor in Equation (75) is the scalar curvature R and for a four-dimensional space-time $g^{\mu\nu} g_{\mu\nu} = 4$, the Equation (75) can be rewritten in scalar terms as

$$\frac{8\pi G_0}{c^4} T = -R \tag{76}$$

consequently, from the Equation (74) and (76), by using the BG energy (31) and

the definition (41), the scalar curvature of a DEMS is

$$-R = \frac{2}{\lambda_0^2} (1 - \zeta_{BG}) \quad (77)$$

Equation (77) shows how for $\zeta_{BG} = 1$, corresponding to a gravitationally collapsed DEMS, the scalar curvature of space-time is zero as in a universe with zero energy density. This occurs because all the energy of the DEMS is transferred by means of the exchange of a BG to the energy of the field of nothingness, which behaves like a potential energy of space-time. The final effect is to maintain unchanged the total energy flattening the space-time. Vice versa in the case $\zeta_{BG} \ll 1$, the Equation (77) converges to the scalar curvature of the bubble of space-time with a radius equal to the wavelength of a DEMS referred to the own center of mass

$$-R \cong \frac{2}{\lambda_0^2} \quad (78)$$

Equation (78) corresponds to the curvature of the Beltrami pseudosphere with radius equal to the wavelength of the DEMS.

By using Equations (75), (76), the Equation (78) becomes

$$-R = g^{\mu\nu} R_{\mu\nu} - \frac{1}{2} g^{\mu\nu} g_{\mu\nu} R \quad (79)$$

and the Equation (77) can be rewritten in good approximation in the form

$$\frac{8\pi G_0}{c^4} g^{\mu\nu} T_{\mu\nu} = g^{\mu\nu} R_{\mu\nu} - \frac{1}{2} g^{\mu\nu} g_{\mu\nu} R + \frac{1}{4} \zeta_{BG} g^{\mu\nu} g_{\mu\nu} R \quad (80)$$

which, in space-time with $0 < \zeta_{BG} \ll 1$ is in agreement with the track of the Einstein's tensor (75) for a flat universe, associate to a close to zero cosmological term.

Equation (80) puts in evidence as the cosmological term is not a constant because it is varying with the amount of energy of the vacuum. In fact, considering a bubble with $\zeta_{BG} = 1$, the track of the field Equation (80) and the scalar curvature (77) yield a null vacuum tension $T = 0$ in an empty and flat bubble in which all energy is possessed by the field of nothingness. In each other case, the tensor associated to the field Equation (80) yields:

$$\frac{8\pi G_0}{c^4} T_{\mu\nu} = R_{\mu\nu} - \frac{1}{2} g_{\mu\nu} R + \frac{1}{4} \zeta_{BG} g_{\mu\nu} R \quad (81)$$

where the third term on the right side corresponds to the energy of vacuum produced inside the DEMS, *i.e.* the cosmological term is a variable.

7.1. Energy and Curvature of the Space-Time of a DEMS

In terms of electromagnetic wave energy density, applying the definition of generalized Compton wavelength given in [8]

$$\lambda_0 = \frac{2hc}{\varepsilon} \gamma (1 - \beta \cos \theta) \quad (82)$$

the scalar curvature (78) can be rewritten in the relativistic form

$$R = -\frac{\varepsilon^2}{2h^2c^2} \frac{1-\beta^2}{(1-\beta\cos\theta)^2} \quad (83)$$

which contains the energy of the photon exchanged between the two interacting particles, namely of the photon emitted by a DEMS towards an observer. The Equation (83) highlights how space-time curvature depends on the square of the rest energy located within the DEMS, but also on the dynamic conditions in which the interaction occurs. In fact, the maximum of the curvature is achieved during the phase of approaching of the two interacting particles. In this case, the incidence angle is $\theta \cong 0$, using the definition of entangled energy (2.A), the Equation (83) becomes

$$R = -\frac{\varepsilon_1\varepsilon_2}{2h^2c^2} \frac{1+\beta}{1-\beta} \quad (84)$$

in which for effect of the Doppler factor the curvature of the bubble increases during a relative high energy approach with $\beta \rightarrow 1$, but it is zero when in space-time, there is not electromagnetic energy density. Using Equation (84) in agreement with Equation (78) is possible to define the energy of the interaction as a function of the local curvature,

$$E = hc\sqrt{-\frac{R}{2}} = \gamma \frac{\varepsilon}{2}(1+\beta) \quad (85)$$

Equation (84) shows how curvature is a relativistic quantity, in fact, identical observers with different speeds feel different curvatures in presence of the same amount of energy. Following this idea for macroscopic bodies, the galaxies of a same cluster can be attracted to their common center of mass with different values of gravity, for effect of the difference among their masses but also by the different relative speed of each galaxy respect the center of mass. Speedy galaxies will experience high value of space-time curvature.

7.2. The Einstein's Tensor and the Cosmological Term for a Multi-Bubble Universe

To consider a whatever sphere of space-time in the universe with an arbitrary radius r and not a single DEMS of wavelength λ_0 , but a region in which many bubble can coexist in a space-time foam, using the Equations (5), (73) and (30) in the form

$$\frac{dV}{d\lambda_0} T = -\frac{hc}{\lambda_0^2} + \frac{c^4}{G_0} \quad (86)$$

that considering the derivative of the volume of the multi-bubble can be rewritten as

$$\frac{dV}{dr} \frac{dr}{d\lambda_0} T = -\frac{hc}{\lambda_0^2} + \frac{c^4}{G_0} \quad (87)$$

Using the Equation (B.7) in **Appendix B**, Equation (87) becomes

$$\frac{8\pi G_0 Z}{c^4} T = \frac{2}{r^2} \left(1 - \frac{G_0 h}{c^4} \frac{1}{\lambda_0^2} \right) \quad (88)$$

Using the definition of MGC and the definition (41), the Equation (88) can be rewritten as

$$\frac{8\pi G}{c^4} T = \frac{2}{r^2} (1 - \zeta_p) \quad (89)$$

where the effective gravitational pseudo-constant $G = G_0 Z$ depends by the space-time dynamics. Similarly, to what was done for the field Equation (81), the Equation (89) gives the Einstein's field equation for a spherical region of any radius

$$\frac{8\pi G}{c^4} T_{\mu\nu} = R_{\mu\nu} - \frac{1}{2} g_{\mu\nu} R + g_{\mu\nu} \Lambda \quad (90)$$

Considering the cosmological term at right hand of the Equation (90) its value is due to the nothingness field and as in Equation (89) decreases with the inverse of the squared of the distance from the center of mass of a whatever gravitational attractor, varying in time throughout the ζ_{BG} value, representing in the Equation (89) the Planck's antigravity-gravity threshold. This effect is justifying in peculiar conditions a rapid expansion of the considered multi-bubble universe without the necessity to suppose the existence of Dark Energy.

Assuming the nowadays value of ζ_{BG} , the scalar field is estimated to be for great distances in agreement with a positive near zero cosmological term

$$\Lambda = \frac{\zeta_{BG}}{2r^2} \approx \frac{3.8 \times 10^{-33}}{r^2} \approx 0 \quad (91)$$

decreasing with the squared of the radius r of the sphere, delimiting a generic space-time multi-bubble. The Equation (91) in the present era emulates the presence of a very low positive dark energy able to change locally with the redshift value respect the threshold of ζ_{BG} , producing in the multi-bubble contractive or expansive effects as predicted in the Equation (42). Considering the results given by the Planck Collaboration which given a measured Hubble constant value lower than $70 \text{ km}\cdot\text{s}^{-1}\cdot\text{Mpc}^{-1}$ [15] and other measures performed on standard candles [16], gravitational lenses [17] and direct parallax [18] that give measures greater than the same value, to exemplify, assuming $H_0 \approx 70 \text{ km}\cdot\text{s}^{-1}\cdot\text{Mpc}^{-1}$ the Equation (91) yields

$$\Lambda = \frac{\zeta_{BG} H_0^2}{2c^2} \approx 10^{-85} \text{ m}^{-2}. \quad (92)$$

8. Prediction and Structure of the Universe

To adapt the Multi-Bubble model to the real observed universe is essential to choose observational data relevant for this model. Is possible to consider the universe from the human point of view, *i.e.* from the Earth center. Each spacecraft observation can be considered made from a lab placed in the Earth center, so the infrared cosmic background corresponds to the emission of the surface of the

early universe that evolving stretches the primordial wavelength of the first bubble to the actual radius. Inside the universe, the action fluctuations produce new bubbles of space-time by expanding the primordial bubble originating the energy and the matter from which galaxies have taken origin. Considering this scenery is possible to place each galaxy on an ideal concentric spherical shell with a radius characterized by a peculiar value of redshift, so galaxies with equal redshift are positioned on the same ideal surface. Throughout the exchange of an integer number N of BG, the radii of each concentric sphere grows adiabatically in time of an amount $\delta\lambda = 2N\lambda_{BG}$ increasing the redshift of a corresponding amount estimated by the Equation (27) until the external shell becomes coinciding with the visible cosmic microwave background (CMB).

8.1. Estimation of the Amounts of Dark Energy, Dark Matter and Baryonic Matter Inside a Multi-Bubble Universe: Can G_{BG} Be a Kaluza-Klein Graviton G_{KK} ?

Considering the current CMB, what is observed from Earth can be considered to correspond to the spectral emission of the primordial bubble now redshifted towards the microwave electromagnetic spectrum. Before the creation of space-time, the nothingness field it exchanges energy with the electromagnetic field of vacuum through the exchange of BG mediators. The characteristic energy of a BG is estimated with the Equation (32) using the value of G_0 by resulting to be $E_{BG} \cong 2.68$ TeV (see **Figure 1**) perfectly in agreement with the mass energy limit of the Kaluza-Klein graviton G_{KK} observed in the channel $G_{KK} \rightarrow \gamma\gamma$ by the ATLAS collaboration [19].

It is necessary to remember that the BG is a spin-zero boson with the characteristics of a gravitationally self-collapsed DEMS, its radius is under the own EH and its energy is formally equal to that of Planck in which the value of the gravitational constant G is substituted by the primordial gravitational constant G_0 , *i.e.* its energy is considered a primordial pseudo Planck energy.

Considering each possible spherical bubble, if its radius is smaller or equal than the Schwarzschild radius of a BG: $r \leq 2\lambda_{BG}$ with $\lambda_{BG} \cong 4.62 \times 10^{-19}$ m, the bubble cannot be visible because it is ever under the own EH $r_{EH} \approx 10^{-18}$ m. Considering the condition (42-c), each graviton decaying produces a DEMS with a bubble influenced by antigravity only if its radius is within the range $\lambda_{BG} \leq r \leq 1.4656\lambda_{BG}$ or by gravity if $r > 1.4656\lambda_{BG}$. In both cases each bubble with a radius in the region $1.4656\lambda_{BG} < r \leq 2\lambda_{BG}$ is not observable because collapsed below the EH but become observable when $r > 2\lambda_{BG}$.

As examined in paragraph 3.1, if the vacuum is in the ground state with $n = 1$ no exchange of energy occur ($N = 0$), *i.e.* the energy of the vacuum remains unchanged, the radius of the bubble is steady and equal to λ_{BG} . Because the electromagnetic field and space-time do not exist externally, the black-body temperature in a not existing space-time is not defined and can be considered identically equal to zero. All the BG in the ground state are a condensate of MBH gra-

gravitationally active as discussed above, in order to the validity of the condition (42-c) but not visible because under their EH with radius of the order of 10^{-18} m. They represent the natural limit of the universe because externally to their radius space-time does not exist. Considering as zero time the BG decay into a DEMS in a gravity range $r > 1.4656\lambda_{BG}$, from that moment the radius of the BG it expands becoming an electromagnetic bubble with the emission of a high energy pair *lepton-lepton* or *gamma-gamma*, during the DEMS evolution three distinct zones with different range of radius and energy can be considered:

1) The Events Horizon Zone

Each BG is a MBH with Compton wavelength λ_{BG} associated to a DEMS with empty source zone defined by the spherical crown within the interval $\lambda_{BG} \leq 2r \leq 3\lambda_{BG}/2$. If only fluctuations of action with $n=1$ occur, the BG remain in the form of a non-observable condensate because under the own EH but gravitationally active for the own energy. The radius of the G_{BG} is of the order of the internal limit of the source zone of the DEMS: $r_{BG} = \lambda_{BG}/2$.

2) The Expansion Zone

When in the condensate fluctuations with $n > 1$ occur, the initial wavelength $\lambda_i = (\sqrt{n} - \sqrt{n-1})\lambda_{BG} < \lambda_{BG}$ is instantaneously adiabatically converted expanding the non-observable DEMS up to the final value of wavelength

$\lambda_f = (\sqrt{n} + \sqrt{n-1})\lambda_{BG} > 2\lambda_{BG}$ changing the energy of the DEMS but not the total energy of the space-time bubble. The energy of the original fluctuation it can be converted only in space-time beyond the events horizon producing in the bubble a mean Planck's spectrum temperature greater than zero. Thus, an observer positioned in space-time outside the EH sees the emission of pairs of particles or of pairs of photons only from a minimum distance $r > 2\lambda_{BG}$. The energy of the initial fluctuation evolves under form of a real DEMS with stretched wavelength $\lambda_f > 2\lambda_{BG}$ beyond the events horizon. In this case, the BG exchanged between the electromagnetic field and the field of nothingness, decaying turns into a pair of particles that have the possibility to escape from each other or annihilate themselves by increasing in any case the energy of the visible universe.

3) The Far Universe Zones

After successive fluctuations, the universe is expanded and space-time grew up to become the current universe. The cosmic background observed today from a distance $r = c/H_0$ is the primordial events horizon in which it is possible to observe the primordial quantum fluctuations under form of energy and matter emissions from the Schwarzschild surface of the primordial condensate.

To estimate the percentage of Dark Energy, Dark Matter and ordinary matter observed in the universe it is necessary to calculate the value of the Planck's threshold characterizing the cosmic background formation in three different situations:

a) Dark Energy. Is represented by the effects on the observable universe of the energy U_0 of each condensate component corresponding to a fluctuation

$n = 1$. The total energy is not observable because is under the events horizon, but is gravitationally active both in producing antigravity and gravity acting on the matter in the actual universe. Using the expansion zone (2), the typical maximum length characterizing the quantum fluctuations among the BG is $\lambda \cong \lambda_{BG}/2$. The use of the Equation (41) gives a threshold $\zeta_{BG}^{(DE)} \cong 4$.

b) Dark Matter. Is represented by the all energy spectrum emitted beyond the lower limit of the source zone under the events horizon. To estimate the contribute of the Dark Matter it is necessary consider the primordial Planck's threshold (41) characterizing the energy emitted in the source zone under the events horizon of each BG. These energy and matter cannot be observable but acts gravitationally on all energy and matter placed in space-time beyond the events horizon. Since the wavelength of each DEMS corresponds to the minimal distance R of interaction of a pair of particles emitted by the graviton during the decaying, the ratio $\rho = R/\lambda_i$ in the source zone of the DEMS is always within the interval $1 < \rho \leq 3/2$. Using the structural mean ratio estimated accurately in BT: $\bar{\rho} \cong 1.276$, for a spectrum produced by a pair of interacting particles with minimum interaction distance $R \cong \lambda_{BG}$, the Equation (41) gives $\zeta_{BG}^{(DM)} = \bar{\rho}^2 \cong 1.63$ with an upper limit of 2.25 imposed by the external boundary of the source zone $1 < \zeta_{BG}^{(DM)} \leq 9/4$.

c) Ordinary Energy and Matter. To estimate the energy associated to all the ordinary matter and electromagnetic energy of the bubble is necessary to calculate the Planck's threshold characterizing the energy that each DEMS emits in space-time, *i.e.* in the zone external to the EH $\lambda \geq r_{EH} = 2\lambda_{BG}$. Considering the energy emitted from the events horizon border towards space-time, the Equation (43) gives the threshold $\zeta_{BG}^{(M)} \cong 0.250$.

Considering the far universe zone (3), when the radius of the expanding bubble becomes the radius of the current multi-bubble universe and $r = c/H_0$, the far cosmic background observed is characterized by the overlapping of the three different effects described above. Using the definition of the ratio of the density of the universe to the critical density associated to the cosmological term:

$$\Omega_{\Lambda} = \frac{1}{3} \left(\frac{c}{H_0} \right)^2 \Lambda \tag{93}$$

with the Equation (92) is possible to estimate the percentages of energies produced during the expansion of the multi-bubble universe. Denoting with a star the primordial value of the Planck's threshold

$$\Omega_{\Lambda}^* = \frac{\zeta_{BG}^*}{6} \tag{94}$$

assuming as radius of the universe the Hubble value, dividing in two parts the primordial Planck's threshold as defined in the previous points (a) and (b)

$\zeta_{BG}^* = \zeta_{BG}^{(DE)} + \zeta_{BG}^{(DM)}$, Equation (94) yields

$$\Omega_{\Lambda}^* = \frac{5.63}{6} \cong 0.938 \tag{95}$$

respectively $\Omega_{\Lambda DE}^* \cong 0.667$ and $\Omega_{\Lambda DM}^* \cong 0.271$ non-visible because under the events horizon.

On the other hand, the total amount of energy associated to the ordinary visible baryonic matter and energy (C) is

$$\Omega_B^* = \frac{\zeta_{BG}^{(B)}}{6} = \frac{0.250}{6} \cong 0.0417 \tag{96}$$

Considering the sum of the three components: Dark Energy, Dark Matter (95) and ordinary energy (96) (see **Table 1** and **Figure 3**)

$$\Omega^* = \Omega_{\Lambda}^* + \Omega_B^* \cong 0.980 \approx 1 \tag{97}$$

the value (97) results lower than one, justifying the continued expansion weakly accelerated of the multi-bubble. A small positive or negative difference respect to $\Omega = 1$ is probably due to the chosen value of the primordial Planck's threshold for the Dark Matter, perhaps more correctly a little larger than that estimated for the statistical effects can occur on the events horizon. Surely, however, considering the external value of the source zone of the bubbles the model limits the total omega value to be less than 1.083.

Table 1. Omega values and percentages of energy and matter in the universe formation Estimated by the Multi-Bubble Model.

Type of Component	Percentage of Component Ω_i / Ω^* (%)	Density Ratio Contribute Ω^*
Dark Energy	68.06	0.6667
Dark Matter	27.69	0.2712 (<i>upper limit</i> 0.3750)
Ordinary Matter and EM Energy	4.25	0.0417
Total	100.00	0.9796 (<i>upper limit</i> 1.0834)

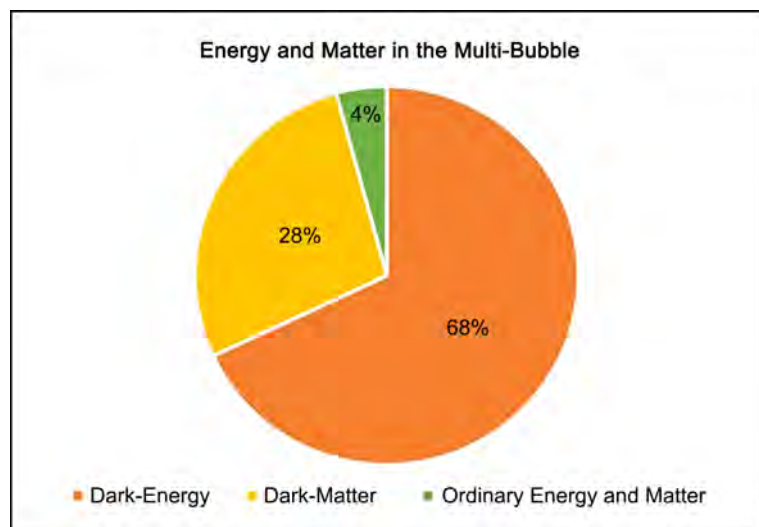


Figure 3. Distribution of energy and matter related to the index Ω_i / Ω^* of **Table 1**.

Considering only the cosmological variable term, is possible to deduce that in the early universe on the EH $r = r_{EH}$ its value was close to

$$\Lambda^* = \frac{\zeta_{BG}^*}{8\lambda_{BG}^2} \approx 3.4 \times 10^{+36} \text{ m}^{-2} \tag{98}$$

decreasing with the square of the temperature of the CMB

$$\Lambda = \frac{k_b^2}{8h^2 c^2} T^2 \tag{99}$$

at the current average value (92) close to zero. Equation (99) suggests as in different bubbles with different local temperatures the cosmological term can be different from the mean value (92), producing faster or slower expansions.

The recent measured values of omega are in very good agreement with the theoretically values estimated with the multi-bubble model presented in **Table 1**.

8.2. On the Estimation of the Actual Radius of the Gravitationally Active Universe

The estimation of the anomalous rotation velocities of the galaxies implies the estimation of the length λ_b characterizing the effective gravitational radius of the bubble of space-time in which the galaxy is been produced, *i.e.* the stretched value of the wavelength of the primitive bubble in which a galaxy has taken origin.

In order to analyze the sample of galaxies [20] in **Table 2**, all with a redshift very close to $z \sim 1$, *i.e.* all positioned on a spherical shell of radius equal to the distance of the galaxies from the observer, is necessary to consider to verify the linear relation between the squared of the flat velocity Y of each galaxy with its mass X . The evidence of their linear proportionality $R_1: Y = \alpha_{11}X + \alpha_{01}$ is shown in **Figure 4**. The linear regression coefficients are: $\alpha_{11} = 3.54 \times 10^{-37} \text{ km}^2 \cdot \text{s}^{-2} \cdot \text{kg}^{-1}$ and $\alpha_{01} = 1.12 \times 10^4 \text{ km}^2 \cdot \text{s}^{-2}$ at $R^2 = 0.9314$. Considering Equation (68) and (69) in the form

$$V_f^2 = \frac{G}{r_b} M + V_0^2 \tag{100}$$

let

$$\begin{cases} \frac{G}{r_b} = \alpha_{1j} \\ V_0^2 = \frac{G_0 M}{\lambda_b} = \alpha_{0j} \end{cases} \tag{101}$$

to be the regression coefficients of the Equation (100), using the Equations (68) and (70) is possible to define for the galaxies sample in **Table 2**.

$$\begin{cases} \bar{V}_0 = \sqrt{\alpha_{0j}} \\ \frac{\bar{\lambda}_b}{M} = \frac{G_0}{\alpha_{0j}} \\ \bar{r}_b = \frac{G}{\alpha_{1j}} \\ \bar{H}_b = \frac{c}{\lambda_b} \end{cases} \tag{102}$$

Table 2. Sample I: redshift $z_r \approx 1$.

Observed Galactic Parameters and Estimations of the Characteristics of the Bubble							
Galaxy	$\beta \equiv z_r$	M_z [$\times 10^9 M_\odot$]	M_x [$\times 10^{39}$ kg]	V_f [km/s]	V_f^2/M_x [$\times 10^{-30}$ km 2 ·s $^{-2}$ ·kg $^{-1}$]	λ_b [$\times 10^{51}$ m]	H_b [$\times 10^{-24}$ km·s $^{-1}$ ·Mpc $^{-1}$]
zmvvd_z1_87	0.896	3.31	6.59	96	1.40	6.20	1.49
zmus_z1_86	0.841	3.55	7.06	109	1.68	5.16	1.80
u3_5138	0.809	5.50	10.9	128	1.50	5.79	1.60
hiz_z1_258	0.838	5.62	11.2	117	1.22	7.09	1.31
zmus_z1_129	0.995	6.76	13.4	122	1.11	7.84	1.18
zmus_z1_125	0.998	8.91	17.7	141	1.12	7.74	1.20
zmus_z1_217	0.895	10,5	20.8	146	1.02	8.48	1.09
u3_25160	0.897	11.2	22.3	133	0.793	11.0	0.845
zmus_z1_166	0.975	12.9	25.6	148	0.855	10.2	0.912
u3_14150	0.896	12.9	25.6	144	0.809	10.7	0.863
zcos_z1_192	0.917	14.8	29.4	147	0.735	11.8	0.783
zmus_z1_119	0.839	21.9	43.5	179	0.736	11.8	0.785
zmus_z1_21	0.839	25.1	50.0	157	0.493	17.6	0.526
hiz_z1_258	0.838	25,7	51.1	173	0.585	14.8	0.624
zcos_z1_202	0.841	34,7	69.0	188	0.512	16.9	0.547
zcos_z1_690	0.927	38.9	77.4	208	0.559	15.5	0.596
zcos_z1_692	0.930	40.7	81.0	190	0.446	19.5	0.475
gs3_22005	0.954	52.5	104	215	0.443	19.5	0.472
Average		18.6	37.1	152	0.890	11.5	0.802

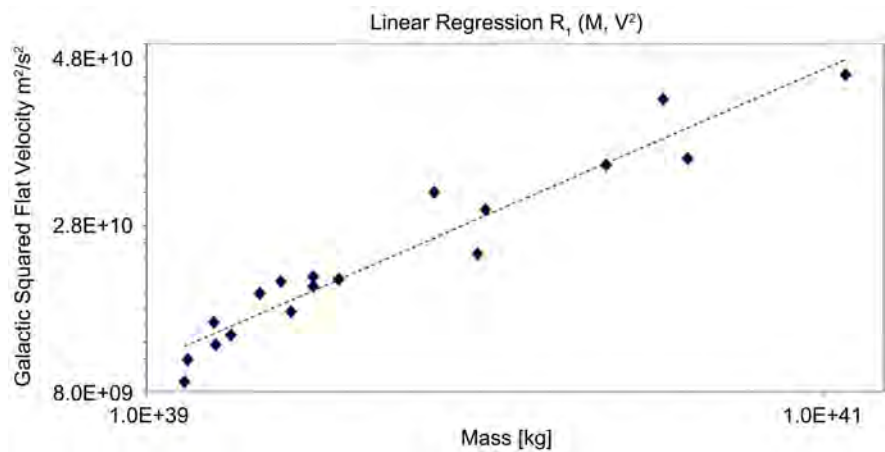


Figure 4. Linear regression of a sample of 18 galaxies with redshift $z \sim 1$.

respectively the average flat velocity of the galaxy, the current average wavelength of the gravitational wave signal per unit of mass associated to a bubble, the average galactic radius of the active galactic haloes and the average Hubble constant of expansion of the bubble associated to the effective universe radius. Considering the Equation (55) and assuming a radial movement in which galaxies go away from the observer, assuming: $b = 0$ and $z \cong 1$; using the values of G_0 and G the Equation (101) gives

$$R_1 \rightarrow \begin{cases} \bar{V}_0 \cong 110 \text{ km/s} \\ \bar{\lambda}_b/M \cong 7.8 \times 10^{+8} \text{ km/kg} \cong 7.6 \times 10^{+20} \text{ Mpc/M}_\odot \\ \bar{r}_b \cong 1.9 \times 10^{+17} \text{ km} \cong 6.1 \text{ kpc} \end{cases} \quad (103)$$

It is important to highlight as the Hubble constant of the bubble defined in the Equation (102) can be used to estimate the age of the first gravitational emission of the bubble, *i.e.* the elapsed time by the first quantum fluctuation which has produced the bubble in which the galaxy has taken origin. Its value is associated at the maximum extension of the bubble of space-time containing the galaxy, *i.e.* the wavelength λ_b is the radius of the real universe connected gravitationally with the galaxy.

Using the values in column seven of **Table 2**, is possible to note how the radius of the space-time gravitationally linked to each galaxy in the sample is greater than the estimated radius of the universe, because the gravitationally linked bubble extension is proportional to the mass of the galaxy, that is, at the number of quantum fluctuations that within the bubble produced the mass energy of the galaxy. To prove the hypothesis of the gravitational connection of galaxies with a space-time bubble larger than the current estimation of the universe radius is enough to consider a second heterogeneous sample of galaxies [21] in **Table 3**. In this case, although the galaxies have different redshifts that make them not comparable in terms of belonging to the same spherical shell with the same gravitational constant value $G = G_0 Z$, the linear regression analysis performed on the galactic rotation speed and mass data of the galaxies, shows an average behavior perfectly in accordance with the results of the previous sample in **Table 2**.

In fact, considering the linear regression law $R_2: Y = \alpha_{12}X + \alpha_{02}$ shown in **Figure 5**, the regression coefficients are: $\alpha_{12} = 3.00 \times 10^{-36} \text{ km}^2 \cdot \text{s}^{-2} \cdot \text{kg}^{-1}$ and $\alpha_{02} = 1.11 \times 10^4 \text{ km}^2 \cdot \text{s}^{-2}$ at $R^2 = 0.6462$, with which using the value α_{02}

$$R_2 \rightarrow \begin{cases} \bar{V}_0 \cong 110 \text{ km/s} \\ \bar{\lambda}_b/M \cong 7.8 \times 10^{+8} \text{ km/kg} \cong 7.6 \times 10^{+20} \text{ Mpc/M}_\odot \end{cases} \quad (104)$$

gives values totally in agreement with the results obtained with R_1 in Equation (103).

This unexpected but hoped-for compatibility between the two galaxies samples highlights a homology in galactic bubble structures relative to their age and extent in terms of gravitational interaction. Using Equation (55) and (68)

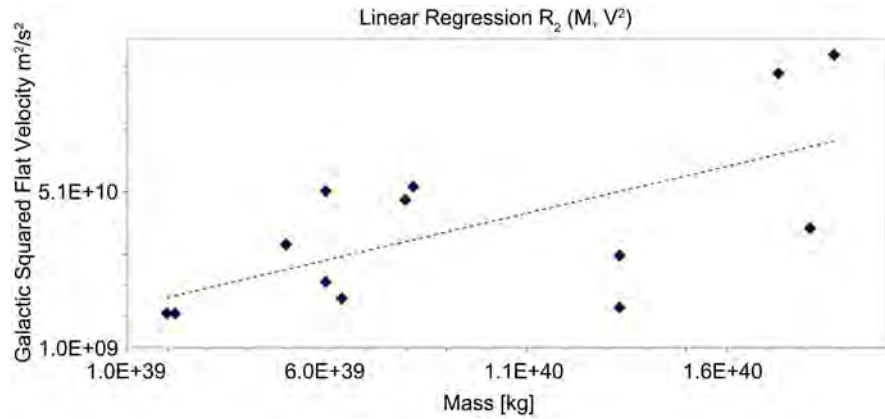


Figure 5. Linear regression of the sample II of 13 galaxies with different redshift.

$$\lambda_b^{-1} = \frac{V_0^2}{MG_0} \tag{105}$$

with which is possible to estimate $H_b^{-1} = \lambda_b/c$ which reciprocal is tabulated in last column of **Table 2** and **Table 3**, yielding the age of the quantum fluctuation from which each bubble has taken origin. The reciprocal value H_b is a characteristic Hubble constant of the bubble associated to the local redshift $z = H_b r/c \equiv r/\lambda_b$ as a function of the radius of a spherical shell inside the bubble giving the local Hubble law $v = H_b r$. While each quantum fluctuation is a boson, and in each bubble can be produced many fluctuations each producing a bubble, the primitive bubble expands like an overlap of bubbles with Hubble’s law depending on the radius of the spherical shell considered

$$v = \left(\sum_{j=1}^k H_{bj} \right) r = H_0 r \tag{106}$$

describing how the universe is seen expanding from an observer at any point in space-time. Following the pattern is evident that each bubble has a Hubble’s expansion constant which is variable with the number of fluctuations in the field of nothingness from which its matter originated and with the uncertainty due to the accuracy of the measurements of the velocities of own galactic halo. Using the data of the sample of 13 galaxies in **Table 3**, the evaluation of the average gravitational wavelengths of the galactic bubbles and consequently of the average galactic Hubble’s constant associated to the sample of galactic bubbles is

$$\bar{H}_b = (5.1 \pm 2.4) \times 10^{-24} \text{ km} \cdot \text{s}^{-1} \cdot \text{Mpc}^{-1} \tag{107}$$

Considering the space-time as a foam in which each bubble contributes to the expansion pushing matter on the borders of the bubbles, is possible estimate the average number of bubbles, *i.e.* of active galaxies along the direction of observation in the universe as the ratio between the Hubble’s constant value and the average galactic Hubble of the bubble (107), giving $k_g = H_0/\bar{H}_b$ in such a way that the standard Hubble’s constant is defined as

$$H_0 = \sum_{j=1}^{k_g} H_{bj} = k_g \bar{H}_b \tag{108}$$

Table 3. Sample II, heterogeneous z_r

Observed Galactic Parameters and Estimations of the Characteristics of the Bubble								
Galaxy	Type	$\beta \equiv z_r$ [$\times 10^{-3}$]	M_s [$\times 10^9 M_s$]	M_g [$\times 10^{39}$ kg]	V_f [km/s]	V_f^2/M_g [$\times 10^{-30}$ km ² ·s ⁻² ·kg ⁻¹]	λ_b [$\times 10^{51}$ m]	H_b [$\times 10^{-24}$ km·s ⁻¹ ·Mpc ⁻¹]
M33	Scd	-0.60	1.0	1.99	110	6.10	1.42	6.51
UGC7321	Sd	1.38	1.1	2.19	110	5.49	1.58	5.85
NGC253	Sc	0.86	2.5	4.97	≈185	6.86	1.26	7.32
NGC3044	Sc	4.30	3.0	5.97	149	3.71	2.34	3.95
M31	Sb	-1	3.0	5.97	226	8.58	1.01	9.15
NGC2403	Scd	0.43	3.2	6.36	130	2.65	3.28	2.83
Milky Way	Sb	-	4.0	7.96	220	6.08	1.43	6.49
NGC891	Sb	1.76	4.1	8.15	220	6.46	1.34	6.89
NGC4559	Scd	2.72	6.7	13.3	118	1.05	8.30	1.12
NGC6946	Scd	0.15	6.7	13.3	175	2.30	3.78	2.45
NGC2613	Sb	5.61	8.7	17.3	≈298	5.14	1.71	5.48
NGC5775	Sb	5.67	9.1	18.1	198	2.17	4.00	2.32
NGC5746	Sb	5.75	9.4	18.7	308	5.08	1.71	5.41
Averages						4.74	2.55	5.06

In **Figure 6** and **Figure 7** are plotted the values of the galactic Hubble constant for the two samples of galaxies used. Since the Equation (108) implies that the Hubble constant is not a true constant, because it depends on the random number of gravitationally active bubbles (primordial fluctuations) in the space-time zone in which the measurement is performed, the universe expands unevenly, and measurements obtained using different astrophysical methods in different regions of space-time can yield different results, requiring complex reinterpretations of the data [22].

As an example considering a measure performed on a space-time zone of the universe giving $H_0 = 75 \text{ km} \cdot \text{s}^{-1} \cdot \text{Mpc}^{-1}$, assuming the average value of $\bar{H}_b = (5.06 \pm 2.4) \times 10^{-24} \text{ km} \cdot \text{s}^{-1} \cdot \text{Mpc}^{-1}$ in **Table 3** is possible to estimate the approximate number of bubbles, *i.e.* the number of the gravitational active local bubbles as ratio between the value of the Hubble's constant and the average galactic Hubble constant of the primordial local bubble as $k_g = H_0 / \bar{H}_b \approx 1.5 \times 10^{25}$. This consideration suggests that in volumes of space-time with high density of energy and matter, a large number of primordial fluctuations were produced from the origin at the current time, each producing a bubble with energy and matter currently largely structured in galaxies, in this case, the Hubble constant may be greater than that measured in a space-time with a lower density of energy and matter, that is, the measurement of Hubble's constant is directional and depends on the time difference separating the space-time observed.

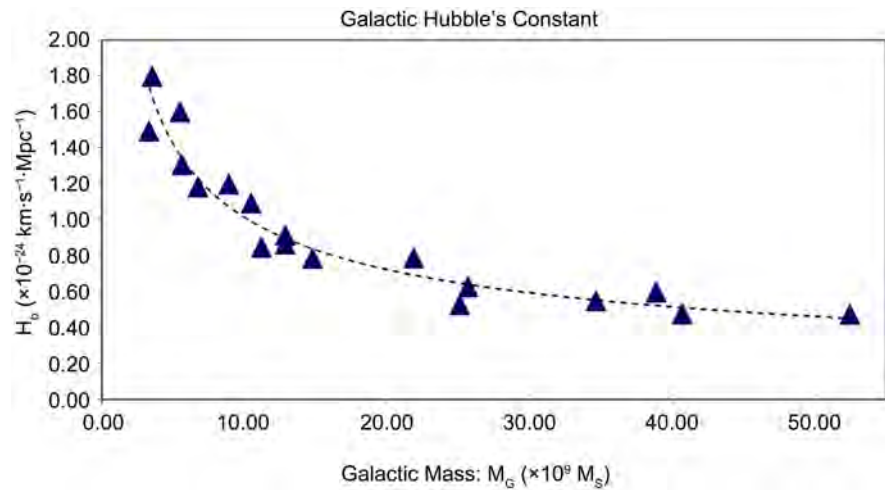


Figure 6. Galactic Hubble expansion constant associated to the sample one of galaxies as a function of the mass.

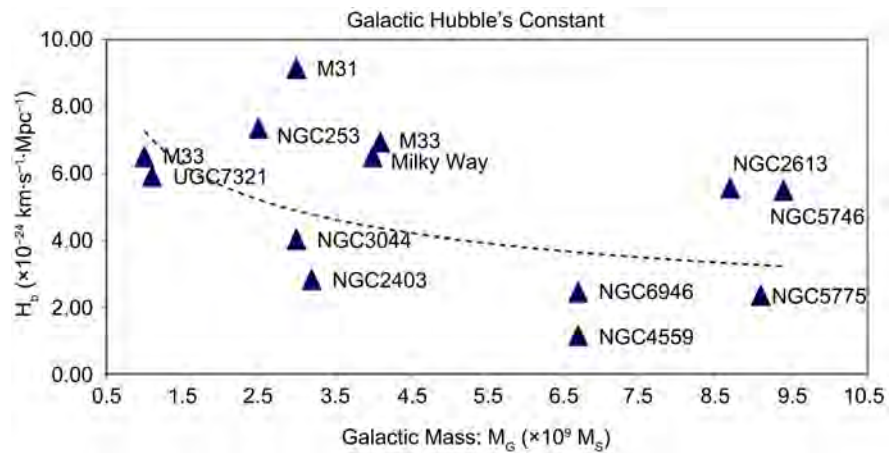


Figure 7. Galactic Hubble expansion constant associated to the sample two of galaxies as a function of the mass.

9. Conclusions

In this work, a gravitational theory has been developed within a space-time model based on the foundations of Bridge Theory, a theory that unifies quantum-relativistic phenomenologies and electro-gravitational forces. In fact, this model has strong roots in quantum theory and relativity theory, a way to rethink Maxwell's Electromagnetic Theory as the common basis of the entire physical world.

The model uses the notion of DEMS and describes space-time as a foam in which each bubble is a Dipole Electromagnetic Source (DEMS) that exchanges Balancing Gravitons (BG) with the potential energy of the vacuum. The exchange of BG, estimated to correspond in mass energy to Kaluza-Klein gravitons of 2.68 TeV observed in Run #1 in ATLAS, it helps to increase the electromagnetic energy and matter that powers galaxies in a spherical bubble of space-time, just a brick of the universe. The spontaneous creation of new bubbles keeps in

balance the negative and positive pressure in space-time that expands differently zones of universe according to the number of bubbles produced inside. The resulting effect leads the Hubble constant to have different values with direction without this implying the existence of a real Dark Energy in play, but only the presence of accelerations produced by the variability of the number of the expanding bubbles, *i.e.* by the variability of the distribution of the galaxies along the sight line of the observer. The dynamic evolution of each DEMS induces a local curvature of space-time that characterizes each bubble, so gravity acts on the whole matter within the bubble. Considering the universe as a foam of DEMS, gravity is proved to transcend the boundaries of the bubble acting on all matter of the universe in accordance with Einstein's field equation but with a modified gravitational constant changing value with a set of variables depending on the dynamics of the direct interaction and on the energy of the bubble. Within the bubbles, the Newtonian strength is modified by the continued change in the scale factor producing at great distances a more intense gravity. The resulting effect justifies abnormal rotations of galactic halos without using Dark Matter in the form of unknown particles or mechanically unjustified MOND theories, because it is the energy of the vacuum hidden under the fabric of the universe that acts gravitationally. In terms of General Relativity, the model is in accordance with the presence of a not constant lambda cosmological term nowadays very close to zero and of an omega term very close to one but not necessarily everywhere equal.

Conflicts of Interest

The author declares no conflicts of interest regarding the publication of this paper.

References

- [1] Rees, M.J. (2003) *Philosophical Transactions of the Royal Society of London. Series A: Mathematical, Physical and Engineering Sciences*, **361**, 2427-2434. <https://doi.org/10.1098/rsta.2003.1289>
- [2] Di Valentino, E., Melchiorri, A. and Silk, J. (2019) *Nature Astronomy*, **4**, 196-203. <https://doi.org/10.1038/s41550-019-0906-9>
- [3] Abbott, B.P., Abbott, R., Abbott, T.D., Acernese, F., Ackley, K., Adams, C., Adams, T., Addesso, P., Adhikari, R.X., Adya, V.B., *et al.* (2017) *Astrophysical Journal Letters*, **851**, L35.
- [4] GRAVITY Collaboration (2018) *Astronomy & Astrophysics*, **615**, L15.
- [5] Auci, M. and Dematteis, G. (1999) *International Journal of Modern Physics B*, **13**, 1525-1557. <https://doi.org/10.1142/S0217979299001569>
- [6] Auci, M. (2018) *Journal of Modern Physics*, **9**, 2206-2222. <https://doi.org/10.4236/jmp.2018.912139>
- [7] Auci, M. (1990) *Physics Letters A*, **148**, 399-404. [https://doi.org/10.1016/0375-9601\(90\)90488-A](https://doi.org/10.1016/0375-9601(90)90488-A)
- [8] Auci, M. (1990) *Physics Letters A*, **150**, 143-150.

-
- [https://doi.org/10.1016/0375-9601\(90\)90109-2](https://doi.org/10.1016/0375-9601(90)90109-2)
- [9] Auci, M. (1990) *Physics Letters A*, **135**, 86-88.
[https://doi.org/10.1016/0375-9601\(89\)90650-6](https://doi.org/10.1016/0375-9601(89)90650-6)
- [10] Auci, M. (2020) *SSRG International Journal of Applied Physics*, **7**, 7-15.
<https://doi.org/10.14445/23500301/IJAP-V7I2P102>
- [11] Auci, M. (2006) Self-Gravitational Red Shift Effect and Micro-Black Holes Production in Dipolar Electromagnetic Sources.
- [12] Estakhr, A.R. (2016) APS Annual Meeting of the Far West Section Vol. 61, Num. 17.
- [13] Prevedelli, M., Cacciapuoti, L., Rosi, G., Sorrentino, F. and Tino, G.M. (2014) *Philosophical Transactions of the Royal Society A*, **372**, Article ID: 20140030.
<https://doi.org/10.1098/rsta.2014.0030>
- [14] Auci, M. (2008) Fundamentality of the Sommerfeld's Fine Structure Constant in Bridge Theory and Consequences on the Fundamental Atomic Constants.
- [15] Aghanim, N., *et al.* (2020) *A&A*, **641**, A6.
<https://doi.org/10.1051/0004-6361/201833910>
- [16] Amendola, L. and Quartin, M. (2019) Measuring the Hubble Function with Standard Candle Clustering.
- [17] Jee, I., *et al.* (2019) *Science*, **365**, 1134-1138. <https://doi.org/10.1126/science.aat7371>
- [18] Croft, R.A.C. (2020) Direct Geometrical Measurement of the Hubble Constant from Galaxy Parallax: Predictions for LSST/VRO and WFIRST.
- [19] Aad, G., *et al.* (2014) *Physical Review D*, **90**, Article ID: 052005.
- [20] Di Teodoro, E.M., Fraternali, F. and Miller, S.H. (2016) *Astronomy & Astrophysics*, **594**, A77. <https://doi.org/10.1051/0004-6361/201628315>
- [21] SIMBAD, Astronomical Data Base.
- [22] Verde, L., Treu, T. and Riess, A.G. (2019) *Nature Astronomy*, **3**, 891-895.
<https://doi.org/10.1038/s41550-019-0902-0>

Appendix A: Definition of Entangled Masses

From Ref. [6] the relativistic energy of the interacting particles forming a DEMS at rest is

$$\varepsilon = \sqrt{(E_1 + E_2)^2 - \|\mathbf{P}_1 + \mathbf{P}_2\|^2} c^2 = \sqrt{\varepsilon_1^2 + \varepsilon_2^2 + 2\varepsilon_1\varepsilon_2\gamma_1\gamma_2(1 - \beta_1\beta_2 \cos \vartheta)} \quad (\text{A.1})$$

where ϑ is the angle between the momenta \mathbf{P}_1 and \mathbf{P}_2 of the two colliding particles with respect to the lab-frame S . Equation (A.1) can be also considered equal to a mixed rest energy of the two interacting particles in such a way the squared rest energy can be expressed as the product of two entangled mass energy terms

$$\varepsilon^2 = 4\mu_1\mu_2c^4 \quad (\text{A.2})$$

each defining the entangled rest mass of one of the two particles

$$\mu_i = \frac{\varepsilon_i}{2c^2} \sqrt{\frac{\varepsilon_1 + \varepsilon_2}{\varepsilon_2} + 2\gamma_1\gamma_2(1 - \beta_1\beta_2 \cos \vartheta)} \quad i = 1, 2 \quad (\text{A.3})$$

in fact, the observer cannot distinguish the rest energies of a single interacting particle because each particle is entangled with the other or with the observer with which it produces the DEMS. For two identical interacting particles with same rest energy $\varepsilon_1 \equiv \varepsilon_2 = \varepsilon$ if they are at rest, the Equation (A.3) becomes

$$\mu = \frac{\varepsilon}{c^2} \quad (\text{A.4})$$

Appendix B: Effective Gravity on the Boundary of the Bubble

Considering a DEMS with an optic wavelength $\lambda = h/p$ produced by the direct interaction of an impinging particle with $\beta = pc/E$ and approaching angle θ , with a antiparticle at rest placed in the lab frame S . After the creation of the DEMS occurring during the incoming phase A in which the source zone localize and emits the energy and the momentum under form of an impulsive electromagnetic signal in radial expansion, begins the successive destroying Ω phase in which the spatial distance between the two interacting particles grows stretching the value of the effective wavelength of the DEMS at a value $\lambda' > \lambda$. Using Eq. (46) and (47), the force felt by an external observer #1 when it is reached up by the electromagnetic signal emitted by the body #2 is given by:

$$\mathbf{F} = \mu_1\mathbf{g}_2 = -G \frac{\mu_1\mu_2}{r^2} \hat{\mathbf{r}} \quad (\text{B.1})$$

where r is the effective distance at which observer and particle interact independently by the value of the original wavelength emitted by the DEMS. Assuming for the two bodies an ordinary redshift $z \geq z_{BG}$, Equation (B.1) is the work done by the electromagnetic forces contrasted by the tension of the vacuum to propagate the original energy of the DEMS. Considering the total strength acting on the observer at the moment in which the wavelength achieves it and the direct interaction starts as

$$\mathbf{F} = -grad(E_r) = -\frac{dE_r}{d\lambda} \frac{d\lambda}{dr} \hat{\mathbf{r}} \quad (\text{B.2})$$

the tension of the space-time, depends by wavelength variation, *i.e.* from the scale variation of the distance of direct interaction

$$\Psi = -\frac{dE_r}{d\lambda} \hat{\mathbf{r}} \quad (\text{B.3})$$

due to the stretching of the wavelength, hence starting from the definition of the Newtonian force like gradient, is possible to write

$$\mathbf{F} = \Psi \frac{d\lambda}{dr} \quad (\text{B.4})$$

from which using the Equation (B.1)

$$\Psi = -G_0 \frac{\mu_1 \mu_2}{r^2} \frac{dr}{d\lambda} \hat{\mathbf{r}} \quad (\text{B.5})$$

Assuming as distance the Equation (43) and the definition (41), using the red-shift definition follows:

$$\frac{dr}{d\lambda} = \frac{1}{2} \left(\frac{d\lambda'}{d\lambda} - 1 + \frac{\lambda_{BG}^2}{\lambda^2} \right) (1 + \beta \cos \phi). \quad (\text{B.6})$$

considering $\lambda' = (1+z)\lambda$ and using the Equation (41) the Equation (B.6) becomes

$$Z = \frac{dr}{d\lambda} = \frac{1}{2} (z + \zeta_{BG}) (1 + \beta \cos \phi) \quad (\text{B.7})$$

that used in the Equation (B.5) rewritten in terms of wavelength *i.e.* in terms of the initial direct interaction distance gives:

$$\Psi = -\frac{2(z + \zeta_{BG})}{(z - \zeta_{BG})^2 (1 + \beta \cos \phi)} G_0 \frac{\mu_1 \mu_2}{\lambda^2} \hat{\mathbf{r}} = T \boldsymbol{\varphi} \quad (\text{B.8})$$

where

$$\boldsymbol{\varphi} = -G_0 \frac{\mu_1 \mu_2}{\lambda^2} \hat{\mathbf{r}} \quad (\text{B.9})$$

is an ideal value of the gravitational force between the two interacting particles in a bubble with wavelength λ . Using the Equation (47), the Equation (B.8) can be also rewritten in the form

$$\Psi = Z\mathbf{F} \quad (\text{B.10})$$

The Equation (B.10) corresponds to the Equation (50).

On the Poincaré Algebra in a Complex Space-Time Manifold

Nathalie Debergh^{1*}, Gilles D'Agostini², Jean-Pierre Petit²

¹Department of Agronomy, Haute Ecole Charlemagne, Huy, Belgium

²Manaty Research Group, Glanon, Dijon, France

Email: *nathalie.debergh@hech.be

How to cite this paper: Debergh, N., D'Agostini, G. and Petit, J.-P. (2021) On the Poincaré Algebra in a Complex Space-Time Manifold. *Journal of Modern Physics*, 12, 218-228.

<https://doi.org/10.4236/jmp.2021.123017>

Received: December 27, 2020

Accepted: February 7, 2021

Published: February 10, 2021

Copyright © 2021 by author(s) and Scientific Research Publishing Inc.

This work is licensed under the Creative Commons Attribution International License (CC BY 4.0).

<http://creativecommons.org/licenses/by/4.0/>



Open Access

Abstract

We extend the Poincaré group to the complex Minkowski space-time. Special attention is paid to the corresponding algebra that we achieve through matrices as well as differential operators. We also point out the generalizations of the two Casimir operators.

Keywords

Complex Minkowski Manifold, Poincaré Group, Lie Algebraic Methods Applied to Physics

1. Introduction

Complex numbers are known to be powerful mathematical tools to describe physical phenomena. Usually, their role is limited to intermediate calculations and they are not welcome in final results. However, sometimes these results do depend on these numbers in the sense that they explicitly appear in the final equations.

To our knowledge, complex energies first appeared as intrinsic components of the physical paradigm in the relativistic Kemmer-Duffin-Petiau equation [1], dealing with vector mesons. When they are subject to a sufficiently strong magnetic field ($B > \frac{m^2}{e}$), their energies, whose squares are given by¹ [2]

$$E^2 = m^2 + 2eB \left(n + \frac{1}{2} + s \right); n = 0, 1, 2, \dots; s = 0, \pm 1 \quad (1)$$

become purely imaginary ones.

More recently, some cosmological models [3] used an imaginary time. They

¹Here and all along this paper, we take the velocity of light equal to 1.

all conjecture a join between areas of imaginary time and areas of real time. Somehow, real time emerges from imaginary time, the latest being helpful to remove gravitational singularities.

This idea is clearly not unanimous because an imaginary time is most of the time seen as non-physical, even heretical. Also voices [4] rose to emphasize the inconsistency of such a transition between imaginary and real times which still remains vague. Some attempts have been performed to specify it. For instance, in [5], imaginary time stands before the Planck time and is related to imaginary energies seen as pure information. Thus, an imaginary time is compatible with the fact that time does not go by and the information, which in a sense, replaces matter, is retained until time rotates and becomes real. To cite the authors of [5], this imaginary time is analogous to the moment when the music is burned on a CD but not yet listened to. It can wait indefinitely until one decides to put the CD in a drive: time then becomes real and follows its arrow.

We think that imaginary time and, by extension, complex space-time coordinates, are one of the most promising tracks for generalizing relativistic quantum mechanics.

One of the advances of complex numbers in this direction is the concept of Minkowski complex space-time. A first attempt with emphasis on specific aspects of twistors has been performed in [6]. In the present paper, we come back to this idea but with a different metric. In fact, the metric considered in [6] involved a *complex* space-time interval while we want to limit ourselves to a *real* one. We could compare this to the wavefunction role in usual quantum mechanics. Indeed this function, although complex, appears on a real form, like the square of its modulus, when physics concepts must be discussed.

More precisely, the key idea involved by our proposal of (3 + 1)-D complex Minkowski manifold is to extend spatial as well as time coordinates to complex numbers with a *Hermitian* metric given by

$$ds^2 = \eta_{\mu\nu} \overline{dx^\mu} dx^\nu \quad (2)$$

with

$$\eta = \text{diag}(1, -1, -1, -1); x^\mu = \{t, x, y, z\}; \mu, \nu = 0, 1, 2, 3 \quad (3)$$

Here the notation $\overline{x^\mu}$ refers to the complex conjugate of x^μ while the *diag* notation means that we consider a diagonal matrix.

The purpose of this paper is to investigate this (3 + 1)-D Minkowski manifold and, in particular, to see what would the Poincaré group/algebra become when coordinates are complex numbers.

To do so, we first have to consider a (6 + 2)-D real manifold by considering real as well as imaginary parts of the involved complex numbers. This is the subject of the next Section. Then, we use the corresponding coadjoint action to put in evidence the transformation laws on momenta which are nothing else than basis operators for the algebra. Sections 4 and 5 are devoted to the differential realization of these momenta in the real as well as the complex cases. The trans-

formations of the group are then available in Section 6. We point out the Casimir operators in Section 7 and finally conclude in Section 8.

2. The Extended Poincaré Group/Algebra

As well known the Lorentz group $O(1,3)$ preserves

$$X^T \eta X \tag{4}$$

where η has been defined in (3) while

$$X^T = (t, x, y, z) = \{x^\mu, \mu = 0, 1, 2, 3\}$$

(X^T refers here to the transposition of X).

If we now consider complex coordinates x^μ , Equation (4) is replaced by ($X_C^\dagger \equiv (\overline{X_C})^T$)

$$X_C^\dagger \eta X_C; X_C^T = (t, x, y, z) = \{x^\mu, \mu = 0, 1, 2, 3\} \tag{5}$$

The Lie group $U(1,3,C)$ is, by definition, the one leaving the quadratic form (5) invariant.

This quadratic form (5) is equivalent to the orthogonal one

$$X_R^T G X_R \tag{6}$$

with

$$X_R^T = \{x_R^\mu, x_I^\mu, \mu = 0, 1, 2, 3\} = \{x^A, A = 0, 1, 2, \dots, 7\} \tag{7}$$

and

$$G = \text{diag}(1, -1, -1, -1, 1, -1, -1, -1) \tag{8}$$

We obviously have

$$x^\mu = x_R^\mu + i x_I^\mu \tag{9}$$

The Lie group preserving (6) is $O(2,6)$.

Even if the quadratic forms are formally equivalent, the two groups $U(1,3,C)$ and $O(2,6)$ have a different number of parameters (16 for $U(1,3,C)$ and 29 for $O(2,6)$). This finding, that might be surprising at first sight, will be explained in a next Section.

Due to the embedding of $U(1,3,C)$ in $O(2,6)$, we focus on the larger group.

Consequently, we define the extended Poincaré group on the (6 + 2)-D real Minkowski space as the set of the following (9 by 9) matrices

$$g = \begin{pmatrix} L & \alpha \\ 0 & 1 \end{pmatrix} \tag{10}$$

where the 8-vector

$$\alpha^T = (\alpha^A, A = 0, 1, 2, \dots, 7)$$

is associated with (real) translations in the (6 + 2)-D manifold and L is the (8 by 8) matrix of the $O(2,6)$ group *i.e.*

$$GL^T GL = I \tag{11}$$

The Lie algebra corresponding to (10) is the vector space of the matrices given by

$$Z = \begin{pmatrix} \omega & \gamma \\ 0 & 0 \end{pmatrix}; \gamma^T = (\gamma^A, A = 0, 1, 2, \dots, 7) \tag{12}$$

Here the coefficients γ^A are real numbers and ω is the matrix of the $so(2,6)$ algebra defined by

$$G\omega^T G = -\omega \tag{13}$$

In details, we have

$$\omega = \sum_{A,B=0}^7 J_{AB} j^{AB} \tag{14}$$

where J_{AB} are real numbers and j^{AB} are the (28) basis matrices of $so(2,6)$ namely

$$j^{AB} = \varepsilon(AB)e^{AB} - \varepsilon(BA)e^{BA} \tag{15}$$

(no summation on repeated indices). In Equation (15), the numbers $\varepsilon(AB)(= \pm 1)$ are constrained by

$$\varepsilon(AB)\varepsilon(CD)\delta^{BC} = G^{BC}\varepsilon(AD); \varepsilon(AB)\varepsilon(CD)\delta^{AD} = G^{AD}\varepsilon(CB) \tag{16}$$

while the notation e^{AB} stands for a 8 by 8 matrix made of “0” everywhere except a “1” at the intersection of the $(A+1)^{th}$ line and the $(B+1)^{th}$ column.

Noticing that

$$e^{AB}e^{CD} = \delta^{BC}e^{AD} \tag{17}$$

we come easily to the $so(2,6)$ commutation relations

$$[j^{AB}, j^{CD}] = G^{BC}j^{AD} + G^{BD}j^{CA} + G^{AC}j^{DB} + G^{AD}j^{BC}; j^{AB} = -j^{BA} \tag{18}$$

We will come back to this algebra in Section 4. Let us just conclude this one by mentioning that the adjoint representation of the extended Poincaré group is, by definition, given by

$$Z' = gZg^{-1} \tag{19}$$

This leads to

$$\omega' = L\omega L^{-1} \tag{20}$$

as well as to the following relation

$$\gamma' = -L\omega L^{-1}\alpha + L\omega \tag{21}$$

3. The Coadjoint Representation: Transformation Laws of the Momenta

Here we follow Souriau’s approach [7], one of us has already successfully applied it [8] to Kaluza 5-D space-time. By analogy with what has been done in the $so(1,3)$ case, we define a torsor μ of the extended Poincaré group by the

identity

$$\mu(Z) \equiv \frac{1}{2} \text{Tr}(M\omega) + (GP)^T \gamma \tag{22}$$

where

$$\mu \equiv \{P, M\}, P \in \mathbf{R}^8, GM^T G = -M \tag{23}$$

We require the invariance

$$\mu'(Z') = \mu(Z) \tag{24}$$

or, in other words

$$\frac{1}{2} \text{Tr}(M\omega) + (GP)^T \gamma = \frac{1}{2} \text{Tr}(M'L\omega L^{-1}) + P'^T G(-L\omega L^{-1}\alpha + L\omega) \tag{25}$$

where we have used Equations (20)-(21) of the adjoint representation.

The relation (25) implies the following transformation on the momenta P:

$$P' = LP \tag{26}$$

Thus, Equation (25) reduces to

$$\frac{1}{2} \text{Tr}(M\omega) = \frac{1}{2} \text{Tr}(M'L\omega L^{-1}) - P'^T G\omega L^{-1}\alpha$$

Remembering that the last term is the product of a transposed 8-vector and an 8-vector, we can rewrite this relation as

$$\frac{1}{2} \text{Tr}(M'L\omega L^{-1}) = \frac{1}{2} \text{Tr}(M\omega) + \text{Tr}(G\omega L^{-1}\alpha P'^T)$$

which, after usual manipulations on the trace, leads to

$$\frac{1}{2} \text{Tr}(L^{-1}M'L\omega) = \frac{1}{2} \text{Tr}(M\omega) + \text{Tr}(L^{-1}\alpha P'^T G\omega)$$

or, in an equivalent way

$$\text{Tr}(L^{-1}M'L\omega) = \text{Tr}(M\omega) + \text{Tr}(L^{-1}\alpha P'^T G\omega) - \text{Tr}(P\alpha^T GL\omega) \tag{27}$$

We thus come to the conclusion that

$$M' = LMGL^T G + \alpha P'^T L^T G - LP\alpha^T G \tag{28}$$

Equations (26) and (28) provide the transformation laws of the momenta.

4. Differential Realization of the Momenta: The (6 + 2)-D Real Poincaré Algebra

Let us take a look at the result (26). If we write the transformations on the coordinates through the group as (cf. Equation (10))

$$X' = LX + \alpha \tag{29}$$

they can be inverted following

$$X = GL^T GX' - GL^T G\alpha \tag{30}$$

This implies that

$$\nabla' = GLG\nabla \tag{31}$$

where ∇ is the 8D-gradient

$$\nabla^T = \left\{ \frac{\partial}{\partial x^A}, A = 0, 1, 2, \dots, 7 \right\} \tag{32}$$

Comparing with (26), it is obvious to conclude that

$$P = CG\nabla \quad (C = \text{constant})$$

With the conventions (7) and

$$\partial_A \equiv \frac{\partial}{\partial x^A}$$

the momenta P are thus

$$P_A = C\partial_A; P^A = C\partial^A = CG^{AB}P_B \tag{33}$$

We recover the momenta of usual Quantum Mechanics if the constant C is fixed as $C = i\hbar$ and A limited to the first four values. However, for simplicity, we fix here $C = 1$ so that

$$P_A = \partial_A; P^A = G^{AB}P_B \tag{34}$$

In the same way, the momenta M satisfying (28) can be realized through a matrix similar to ω (see Equation (14))

$$M = \sum_{A,B=0}^7 J_{AB}j^{AB}$$

but with

$$J^{AB} = x^A\partial^B - x^B\partial^A, A, B = 0, 1, 2, \dots, 7 \tag{35}$$

In other words, we have

$$M = XP^T G - PX^T G$$

And it is straightforward to convince ourselves of (28) to be satisfied by using (26) and (29).

It is then easy to find out the commutation relations of the (6 + 2)-D Poincaré algebra by using

$$[x^A, \partial^B] = -G^{AB} \tag{36}$$

They read

$$[J^{AB}, J^{CD}] = G^{BC}J^{AD} + G^{BD}J^{CA} + G^{AC}J^{DB} + G^{AD}J^{BC} \tag{37}$$

in agreement with Equation (18) and

$$[J^{AB}, P^C] = -G^{AC}P^B + G^{BC}P^A \tag{38}$$

$$[P^A, P^B] = 0 \tag{39}$$

5. The (3 + 1)-D Complex Poincaré Algebra

By making use of the change of variables (9), we can define linear combinations of the J^{AB} as well as the P^A operators in order to restore the extended Poincaré algebra in a (3 + 1)-D complex manifold. These linear combinations write

$$M^{\mu\nu} = -J^{\mu\nu} - J^{(\mu+4)(\nu+4)} \tag{40a}$$

$$M_I^{\mu\nu} = -J^{\mu(\nu+4)} - J_{\nu(\mu+4)} \tag{40b}$$

$$N^{\mu\nu} = -J^{\mu\nu} + J^{(\mu+4)(\nu+4)} \tag{40c}$$

$$N_I^{\mu\nu} = -J^{\mu(\nu+4)} + J_{\nu(\mu+4)} \tag{40d}$$

$$P_C^\mu = \frac{1}{2}(P^\mu - iP^{\mu+4}); \overline{P}_C^\mu = \frac{1}{2}(P^\mu + iP^{\mu+4}) \tag{40e}$$

They lead to the following realizations in terms of complex coordinates x^μ and their derivatives

$$\partial_\mu = \frac{\partial}{\partial x^\mu} = \left(\frac{\partial}{\partial t}, \frac{\partial}{\partial x}, \frac{\partial}{\partial y}, \frac{\partial}{\partial z} \right), \partial^\mu = \frac{\partial}{\partial x_\mu} = \left(\frac{\partial}{\partial t}, -\frac{\partial}{\partial x}, -\frac{\partial}{\partial y}, -\frac{\partial}{\partial z} \right) \tag{41}$$

$$M^{\mu\nu} = -x^\mu \partial^\nu + x^\nu \partial^\mu - \overline{x^\mu \partial^\nu} + \overline{x^\nu \partial^\mu} \tag{42a}$$

$$M_I^{\mu\nu} = -ix^\mu \partial^\nu - ix^\nu \partial^\mu + i\overline{x^\mu \partial^\nu} + i\overline{x^\nu \partial^\mu} \tag{42b}$$

$$N^{\mu\nu} = -\overline{x^\mu \partial^\nu} + \overline{x^\nu \partial^\mu} - x^\mu \overline{\partial^\nu} + x^\nu \overline{\partial^\mu} \tag{42c}$$

$$N_I^{\mu\nu} = -i\overline{x^\mu \partial^\nu} + i\overline{x^\nu \partial^\mu} + ix^\mu \overline{\partial^\nu} - ix^\nu \overline{\partial^\mu} \tag{42d}$$

$$P_C^\mu = \partial^\mu, \overline{P}_C^\mu = \overline{\partial^\mu} \tag{42e}$$

It was already evident through Equations (40) but it is even more obvious here that $M^{\mu\nu}$, $N^{\mu\nu}$, $N_I^{\mu\nu}$ are antisymmetric on their indices and thus there are six of them for each category while $M_I^{\mu\nu}$ is symmetric leading to ten different operators. These 28 operators are real ones: only the four P_C^μ are complex and have to be supplemented by their conjugates.

The corresponding commutation relations are then

$$[M^{\mu\nu}, M^{\alpha\beta}] = \eta^{\alpha\nu} M^{\beta\mu} + \eta^{\beta\nu} M^{\mu\alpha} + \eta^{\alpha\mu} M^{\nu\beta} + \eta^{\beta\mu} M^{\alpha\nu} \tag{43a}$$

$$[M^{\mu\nu}, M_I^{\alpha\beta}] = -\eta^{\alpha\nu} M_I^{\beta\mu} - \eta^{\beta\nu} M_I^{\mu\alpha} + \eta^{\alpha\mu} M_I^{\nu\beta} + \eta^{\beta\mu} M_I^{\alpha\nu} \tag{43b}$$

$$[M_I^{\mu\nu}, M_I^{\alpha\beta}] = -\eta^{\alpha\nu} M^{\beta\mu} + \eta^{\beta\nu} M^{\mu\alpha} + \eta^{\alpha\mu} M^{\nu\beta} - \eta^{\beta\mu} M^{\alpha\nu} \tag{43c}$$

$$[M^{\mu\nu}, N^{\alpha\beta}] = \eta^{\alpha\nu} N^{\beta\mu} + \eta^{\beta\nu} N^{\mu\alpha} + \eta^{\alpha\mu} N^{\nu\beta} + \eta^{\beta\mu} N^{\alpha\nu} \tag{43d}$$

$$[M_I^{\mu\nu}, N^{\alpha\beta}] = -\eta^{\alpha\nu} N_I^{\beta\mu} - \eta^{\beta\nu} N_I^{\mu\alpha} + \eta^{\alpha\mu} N_I^{\nu\beta} + \eta^{\beta\mu} N_I^{\alpha\nu} \tag{43e}$$

$$[N^{\mu\nu}, N^{\alpha\beta}] = \eta^{\alpha\nu} M^{\beta\mu} + \eta^{\beta\nu} M^{\mu\alpha} + \eta^{\alpha\mu} M^{\nu\beta} + \eta^{\beta\mu} M^{\alpha\nu} \tag{43f}$$

$$[M^{\mu\nu}, N_I^{\alpha\beta}] = \eta^{\alpha\nu} N_I^{\beta\mu} + \eta^{\beta\nu} N_I^{\mu\alpha} + \eta^{\alpha\mu} N_I^{\nu\beta} + \eta^{\beta\mu} N_I^{\alpha\nu} \tag{43g}$$

$$[M_I^{\mu\nu}, N_I^{\alpha\beta}] = \eta^{\alpha\nu} N^{\beta\mu} + \eta^{\beta\nu} N^{\mu\alpha} - \eta^{\alpha\mu} N^{\nu\beta} - \eta^{\beta\mu} N^{\alpha\nu} \tag{43h}$$

$$[N^{\mu\nu}, N_I^{\alpha\beta}] = -\eta^{\alpha\nu} M_I^{\beta\mu} + \eta^{\beta\nu} M_I^{\mu\alpha} + \eta^{\alpha\mu} M_I^{\nu\beta} - \eta^{\beta\mu} M_I^{\alpha\nu} \tag{43i}$$

$$[N_I^{\mu\nu}, N_I^{\alpha\beta}] = \eta^{\alpha\nu} M^{\beta\mu} + \eta^{\beta\nu} M^{\mu\alpha} + \eta^{\alpha\mu} M^{\nu\beta} + \eta^{\beta\mu} M^{\alpha\nu} \tag{43j}$$

$$[M^{\mu\nu}, P_C^\alpha] = \eta^{\alpha\mu} P_C^\nu - \eta^{\alpha\nu} P_C^\mu; [M^{\mu\nu}, \overline{P}_C^\alpha] = \eta^{\alpha\mu} \overline{P}_C^\nu - \eta^{\alpha\nu} \overline{P}_C^\mu \tag{43k}$$

$$[M_I^{\mu\nu}, P_C^\alpha] = i\eta^{\alpha\mu} P_C^\nu + i\eta^{\alpha\nu} P_C^\mu; [M_I^{\mu\nu}, \overline{P_C^\alpha}] = -i\eta^{\alpha\mu} \overline{P_C^\nu} - i\eta^{\alpha\nu} \overline{P_C^\mu} \quad (43l)$$

$$[N^{\mu\nu}, P_C^\alpha] = \eta^{\alpha\mu} \overline{P_C^\nu} - \eta^{\alpha\nu} \overline{P_C^\mu}; [N^{\mu\nu}, \overline{P_C^\alpha}] = \eta^{\alpha\mu} P_C^\nu - \eta^{\alpha\nu} P_C^\mu \quad (43m)$$

$$[N_I^{\mu\nu}, P_C^\alpha] = -i\eta^{\alpha\mu} \overline{P_C^\nu} + i\eta^{\alpha\nu} \overline{P_C^\mu}; [N_I^{\mu\nu}, \overline{P_C^\alpha}] = i\eta^{\alpha\mu} P_C^\nu - i\eta^{\alpha\nu} P_C^\mu \quad (43n)$$

$$[P_C^\alpha, P_C^\beta] = [P_C^\alpha, \overline{P_C^\beta}] = [\overline{P_C^\alpha}, \overline{P_C^\beta}] = 0 \quad (43o)$$

The usual Poincaré algebra is recovered through Equations (42a), (43k) and (43o). It is now realized through complex variables and corresponds to the proposal made by one of us in [8]. We can also recognize the algebra $u(1,3,C)$ through the operators (42a)-(42b) and their commutation relations (43a)-(43c). The operators (42c)-(42d) are the complement of $u(1,3,C)$ in $so(2,6)$.

6. Transformations of the Extended Poincaré Group

Now that the algebraic content is clear, let us come to the group approach subtended by the transformations (29).

We recognize in (29) eight real translations associated with α , or, in an equivalent way, four complex ones. The contributions of the matrix L can be understood as follows:

1) Twelve transformations of “boost” type *i.e.* “rotations” between a (real or imaginary) time component and three (real or imaginary) space components:

$$\begin{cases} t'_a = \cosh(\theta_{ab}^{0j}) t_a - \sinh(\theta_{ab}^{0j}) x_b^j \\ x_b'^j = -\sinh(\theta_{ab}^{0j}) t_a + \cosh(\theta_{ab}^{0j}) x_b^j \end{cases} \quad (44)$$

with $j = 1, 2, 3; a = R, I; b = R, I$.

2) Twelve rotations between (real or imaginary) space components:

$$\begin{cases} x_a'^k = \cos(\theta_{ab}^{jk}) x_a^k + \sin(\theta_{ab}^{jk}) x_b^j \\ x_b'^j = -\sin(\theta_{ab}^{jk}) x_a^k + \cos(\theta_{ab}^{jk}) x_b^j \end{cases} \quad (45)$$

with $j = 1, 2, 3, j \neq k; a = R, I; b = R, I$.

3) Four rotations between real and imaginary parts of one of the components:

$$\begin{cases} t'_R = \cos(\theta^{00}) t_R - \sin(\theta^{00}) t_I \\ t'_I = \sin(\theta^{00}) t_R + \cos(\theta^{00}) t_I \end{cases} \quad (46a)$$

$$\begin{cases} x'_R{}^j = \cos(\theta^{jj}) x_R^j + \sin(\theta^{jj}) x_I^j \\ x'_I{}^j = -\sin(\theta^{jj}) x_R^j + \cos(\theta^{jj}) x_I^j \end{cases} \quad (46b)$$

Let us rewrite these results within the complex coordinates:

$$t' = e^{i\theta^{00}} t; x'^j = e^{-i\theta^{jj}} x^j \quad (47)$$

These equations are remarkable in the sense that they show that the complexification enables the connection between the Lorentz components. Indeed we know [9] that the Lorentz group has four components: $L_+^\uparrow, L_-^\uparrow = PL_+^\uparrow, L_+^\downarrow = PTL_+^\uparrow$

and $L_-^\downarrow = TL_+^\uparrow$. Each of the three last ones is related to the first one by acting on it with a discrete symmetry, either the parity operator P or the time-reversal operator T . Two objects in “mirror symmetry” are necessarily linked by a rotation in a higher dimensional space and that’s exactly what happens here: the complexification allows these dimensions to exist in order to relate a coordinate and its opposite (which corresponds to $\theta^{\mu\mu} = \pi$).

Similar discussions can be made with the complex algebra. We will just mention here that if the $U(1,3,C)$ operators perform transformations such as boosts or rotations on the four complex coordinates x^μ , the other 12 ones (corresponding to exponentiations of $N^{\mu\nu}$ or $N_i^{\mu\nu}$) realize, in addition, a complex conjugation. It is actually the reason why, despite of the fact that the quadratic forms (5) and (6) are equivalent, the Lie groups $U(1,3,C)$ and $O(2,6)$ are not isomorphic.

7. The Casimir Operators

The number of Casimir operators associated with the inhomogeneous group $ISO(2,6)$ (which is the one subtended by our approach in the real space) is equal to 4 [10].

We put here explicitly in evidence two of them *i.e.* the ones generalizing the two Casimirs of the Poincaré algebra.

The first Casimir operator is

$$C_1 = P^T GP \tag{48}$$

It is indeed invariant under the transformation (26). Another way to be convinced of the form (48) is to rewrite it in details

$$C_1 = P^A P_A = 4P_C^\mu P_{C\mu} \tag{49}$$

and verify that it commutes with each of the 36 operators of the extended Poincaré algebra by using Equations (38)-(39) or (43k)-(43o) depending on whether we choose to work with eight real coordinates or four complex ones.

By analogy with the real case, we can thus define the mass of a particle living in the complex Minkowski space-time by

$$\left| E^2 \right| - \left| \mathbf{p}^2 \right| = m^2; E = P_C^0, p^j = P_C^j \tag{50}$$

a relation which simplifies when the system is at rest and gives

$$E = m e^{i\phi} \tag{51}$$

This is the complex version of the famous Einstein relation² $E = m$.

The second Casimir operator requests more calculations. We indeed need to introduce the following 3-rank tensor

$$W^{ABC} = J^{AB} P^C - J^{AC} P^B + J^{BC} P^A \tag{52}$$

It is antisymmetric on the two first indices as well as on the two last ones but is (evidently) symmetric on A and C . It thus gives rise to 56 operators.

²Recall that $c = 1$.

Let us take a while to mention that, in the real case, these operators reduce to the four well known ones

$$W_\mu = \frac{1}{2} \varepsilon_{\mu\nu\lambda\alpha} J^{\nu\lambda} P^\alpha \tag{53}$$

namely the four components of the Pauli-Lubanski pseudo-vector. No need to say that, here, there is no interest to go through the dual to obtain a similar writing, as this will lead to a pseudo-tensor of rank 5.

So let us focus on the operators (52). It is easy (even if laborious) to convince ourselves that they are such that

$$\begin{aligned} [W^{ABC}, J^{DE}] = & G^{AD} W^{BCE} - G^{AE} W^{BCD} - G^{BD} W^{ACE} \\ & + G^{BE} W^{ACD} + G^{CD} W^{ABE} - G^{CE} W^{ABD} \end{aligned} \tag{54a}$$

$$[W^{ABC}, P^D] = 0 \tag{54b}$$

and

$$\begin{aligned} [W^{ABC}, W^{DEF}] = & G^{AD} (W^{BCE} P^F - W^{BCF} P^E) + G^{AE} (W^{BCF} P^D - W^{BCD} P^F) \\ & + G^{AF} (W^{BCD} P^E - W^{BCE} P^D) + G^{BD} (W^{AEF} P^C - W^{CEF} P^A) \\ & + G^{BE} (-W^{ADF} P^C + W^{CDF} P^A) + G^{BF} (W^{ACE} P^D - W^{ACD} P^E) \\ & + G^{CD} (-W^{ABF} P^E + W^{ABE} P^F) + G^{CE} (-W^{ABD} P^F + W^{ABF} P^D) \\ & + G^{CF} (W^{DAB} P^E - W^{EAB} P^D) \end{aligned} \tag{54c}$$

The two first relations show that

$$C_2 = W^{ABC} W_{ABC} \tag{55}$$

does commute with each of the 36 generators of the extended Poincaré algebra and, consequently, is the second Casimir operator.

Its interpretation goes through the so-called “little groups” technics *i.e.* restricting ourselves to particular momenta P . If the rest is considered, only two P operators do not vanish:

$$P^0 = 2m \cos \phi; P^4 = 2m \sin \phi \tag{56}$$

This implies the following form for C_2

$$\begin{aligned} C_2 = & 4m^2 (J_{12}^2 + J_{31}^2 + J_{23}^2 + J_{15}^2 + J_{16}^2 + J_{17}^2 + J_{25}^2 \\ & + J_{26}^2 + J_{27}^2 + J_{35}^2 + J_{36}^2 + J_{37}^2 + J_{56}^2 + J_{57}^2 + J_{67}^2) \\ & - 4m^2 (\cos \phi)^2 (J_{14}^2 + J_{24}^2 + J_{34}^2 + J_{45}^2 + J_{46}^2 + J_{47}^2) \\ & - 4m^2 (\sin \phi)^2 (J_{01}^2 + J_{02}^2 + J_{03}^2 + J_{05}^2 + J_{06}^2 + J_{07}^2) \\ & - 4m^2 \sin \phi \cos \phi (\{J_{01}, J_{14}\} + \{J_{02}, J_{24}\} + \{J_{03}, J_{34}\} \\ & + \{J_{05}, J_{45}\} + \{J_{06}, J_{46}\} + \{J_{07}, J_{47}\}) \end{aligned} \tag{57}$$

We notice that the only J^{AB} that does not appear in (57) is J^{04} namely the rotation on time. We also recover the spin interpretation of the real case except that we

have here 20 possibilities for one spin algebra ($so(3)$) to be put in evidence. This is evidently due to the increasing of spatial dimensions which are now 6.

8. Conclusions

We have extended the Poincaré group as well as its algebra to a complex Minkowski space. Beyond the real operators corresponding to transformations of the real coordinates, our approach shows that supplementary imaginary as well as complex operators appear to form with the previous ones a 36-dimensional real or complex algebra according to choosing 8 real coordinates or 4 complex ones.

What are the unirreps of the extended Poincaré algebra? What physical implications could have this complex algebra? What would be a complex version of usual quantum mechanics?

These questions remain open at this stage and will be the subject of further considerations.

Data Availability

The data that support the findings of this study are available within this article.

Conflicts of Interest

The authors declare no conflicts of interest regarding the publication of this paper.

References

- [1] Petiau, G. (1936) *Classe des Sciences*, **8**, 16.
- [2] Velo, G. and Zwanziger, D. (1969) *Physical Review*, **186**, 1337.
- [3] Hartle, J.B. and Hawking, S.W. (1983) *Physical Review D*, **28**, 2960. <https://doi.org/10.1103/PhysRevD.28.2960>
- [4] Deltete, R.J. and Guy, R.A. (1996) *Synthese*, **108**, 185-203. <https://doi.org/10.1007/BF00413497>
- [5] Bogdanoff, G. and Bogdanoff, I. (2002) *Annals of Physics*, **296**, 90-97. <https://doi.org/10.1006/aphy.2001.6212>
- [6] Hansen, R.O., Newman, E.T., Penrose, R. and Tod, K.P. (1978) *Proceedings of the Royal Society of London A*, **363**, 445-468. <https://doi.org/10.1098/rspa.1978.0177>
- [7] Souriau, J.M. (1997) Structure of Dynamical Systems. In: *Progress in Mathematics*, Springer, Boston, Vol. 149. <https://doi.org/10.1007/978-1-4612-0281-3>
- [8] Petit, J.P. (2018) *Progress in Physics*, **14**, 38.
- [9] Srinivasa Rao, K.N. (1988) The Rotation and Lorentz Groups and Their Representations for Physicists. Wiley, New-Delhi, p. 213.
- [10] Chaichian, M., Demichev, A.P. and Nelipa, N.F. (1983) *Communications in Mathematical Physics*, **90**, 353-372. <https://doi.org/10.1007/BF01206887>

A New Formula of Redshift vs. Space Expansion and Dark Energy

Olivier Serret

ESIM Engineer, Cugnaux, France

Email: o.serret@free.fr

How to cite this paper: Serret, O. (2021) A New Formula of Redshift vs. Space Expansion and Dark Energy. *Journal of Modern Physics*, 12, 229-253.

<https://doi.org/10.4236/jmp.2021.123018>

Received: December 23, 2020

Accepted: February 17, 2021

Published: February 20, 2021

Copyright © 2021 by author(s) and Scientific Research Publishing Inc. This work is licensed under the Creative Commons Attribution International License (CC BY 4.0).

<http://creativecommons.org/licenses/by/4.0/>



Open Access

Abstract

The speed away of stars and galaxies is traditionally calculated from the relativistic formula according to the measurement of the redshift. It is demonstrated here another formula for this speed away of stars and galaxies, from this same redshift z . After having exposed critiques on the demonstration and the relativistic use which require the assumption of an expanding universe by itself, it is proposed within the framework of neo-Newtonian mechanics the formula $V = \frac{z}{1+z}c$ where V is the speed from the source. This formula has the double characteristic of being equivalent to relativistic predictions for low redshifts, but of deviating from them by up to 17% for high redshifts. It is consistent with the observation of the anisotropy of the Universe and the Cosmic Microwave Background. It helps to explain Pioneer anomalies. It is compatible with the constancy in the majority of cases of interference phenomena. Finally, it provides a new analysis grid for the observation of supernovae, galaxies and distant pulsars, thus opening up new fields of research on the increase in distances attributed to dark energy and also in other areas of the cosmology.

Keywords

Redshift, Blueshift, Dark Energy, Radial Velocity, Expansion of the Universe, Anisotropy, Hubble Law, Pioneer Spacecraft, Photon, Wavelength, Frequency, Variable Speed, Celerity of Light

1. Introduction

In the past, the stars did not exactly follow the supposedly perfectly circular trajectory, it was necessary to imagine the existence of epicycles ... until new elliptical trajectories were accepted. Today, the distant galaxies not having to exceed

the speed of light in spite of the law of Hubble, it is imagined a space which would create itself its own space, and the distant supernovae not following exactly the speed away calculated there, it is imagined the existence of a repulsive dark energy ... unless we come to accept a new formula for the speeds away as a function of the redshift. This is what we will try to demonstrate in this article.

After having recalled the definitions and uses of redshift and wavelength, we will analyze the research status on the relativistic redshift formula. Then we will propose the neo-Newtonian derivation to get to the expression of a slightly modified formula. Finally, we will discuss the consequences or not of this change of formula.

2. Definition and Context

The redshift, noted z , is the fringe shift measured on light and electromagnetic waves from moving objects. From this measurement, first the speed away for stars and galaxies is calculated and then their distance is deduced using Hubble's "law".

Yet, at the horizons of the Universe, by correlating with the distances derived from their luminosity, supernovae appear to be at distances greater than those calculated by the redshift method (see **Figure 1**). To explain this additional distance speed and therefore this additional distance, it is invoked the existence of a dark energy with a repulsive effect, dark energy which has so far not been able to be directly apprehended. And more simply, why not question the formulas used to calculate the very fast speeds and the far distances?

Light and electromagnetic waves in general are characterized by their wavelength λ , their propagation speed c and their frequency f .

We can characterize them only by two out of three parameters because they are related to each other by the relation:

$$\lambda = c/f \tag{1}$$

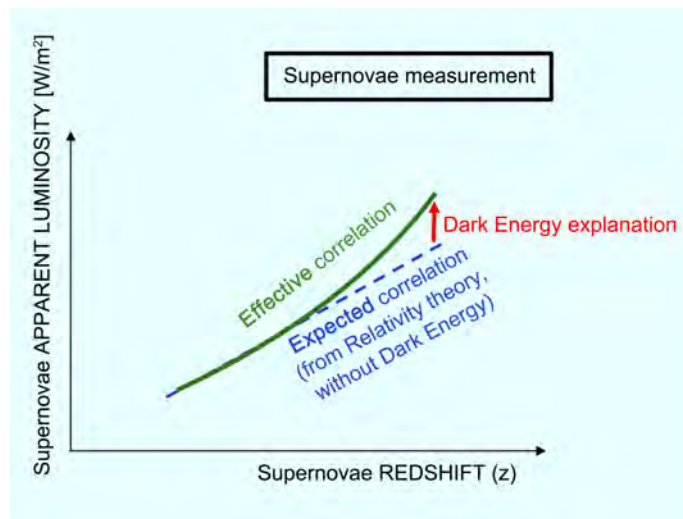


Figure 1. Schematic explanation of Dark Energy.

Since the speed of light in vacuum is assumed to be constant, it has become customary to characterize the electromagnetic waves by only one parameter, the wavelength λ (*i.e.* a distance). Yet this is the frequency (*i.e.* a time, or more exactly the inverse of time) that we perceive or directly measure. For example, an optical detector does not measure a length, but is excited at certain frequencies. This is why in this article we will favor the explanation by frequencies f (rather than by wavelengths λ).

3. Analysis of the Relativistic Redshift Formula

The relativistic expression allowing to deduce the distance speed V from the redshift z is as follows:

$$V = -\frac{(1+z)^2 - 1}{(1+z)^2 + 1}c \quad (2)$$

This formula comes up against two difficulties.

3.1. The Derivation Itself

The usual demonstration goes through the following intermediate step [1] [2] [3] [4]:

$$\lambda_{obs} = \frac{c - V}{f_{obs}} \quad (3)$$

The problem is that the theory of Relativity postulates that the speed linking the two quantities λ_{obs} and f_{obs} is constant and therefore that the numerator must be equal to c in any frame of reference. This means that V should be zero, which is contradictory with a moving source.

There are also few much more complex derivations, but the one we have seen [5] is also open to criticism (in this video, there is a mix between Galilean formulas and relativistic formulas and the Equation (3) is implicit).

3.2. The Expansion of Space Itself

Even admitting the validity of the previous derivation, the relativistic formula only allows to relate the redshift to the speed by making an additional assumption, namely the expansion of space itself. This additional assumption does not appear necessary as long as the source does not move away at very high speeds because it is used a simplified formula. But when they are faced with very high speed or high z 's, they end up with an inconsistency that can only be overcome by posing the strange hypothesis of a space that expands by itself. Without this additional assumption, the relativistic Equation (2) of the redshift leads to an inconsistent situation on the propagation speeds [see **Appendix 1**].

4. The Neo-Newtonian Derivation

4.1. The Neo-Newtonian Mechanic

So what formula should be used between the distance velocities and the fringe

shifts received from high- z stars and galaxies? The proposal falls within the framework of neo-Newtonian mechanics which is none other than Newtonian mechanics but without the principle of equivalence between inert mass and gravitational mass: thus, the increase of inertial mass as a function of the speed prevents the photon from exceeding the celerity c ; this means that the speed of the photon would not be constant in any frame of reference. The purpose of this article is not to detail Newtonian Mechanics, the reader may consult it in the **RELATED LINKS [a]**. And as in Newtonian mechanics, it is assumed that the photon is a body of matter that can move in a vacuum, and that there is a fixed or barycentric frame R_0 .

4.2. The Method of the Derivation

The derivation is based on the redshift understood as an effect of the Doppler-Fizeau effect. The **Doppler-Fizeau effect** can be described as the effect produced by a moving source of electromagnetic waves in which there is an apparent upward shift in frequency for observers towards whom the source is approaching and an apparent downward shift in frequency for observers from whom the source is receding. Here is a simplified derivation of the speed away as a function of redshift, the general derivation is given in **Appendix 2**. Let us take the usual and simplified case of a photon emitted from a source which moves away while the observer is motionless in the fixed frame of reference R_0 . The photons (A) then (B) are emitted according to the time interval T_{source} at the celerity c in the reference frame of the source, but according to neo-Newtonian mechanics they move at the speed $(c - V)$ in the fixed reference frame R_0 (see **Figure 2**)

$$v_{photon/R_0} = c_{photon/source} - |v_{source/R_0}| \tag{4}$$

with $|v_{source/R_0}| > 0$.

There are two ways to calculate the distance between photons (A) and (B):

- The first way is to note that the distance λ between the photons (A) and (B) is the distance D_A traveled by the photon (A) during the time T_{source} added to the distance d_{source} traveled by the source until the emission photon (B) (see **Figure 3**)

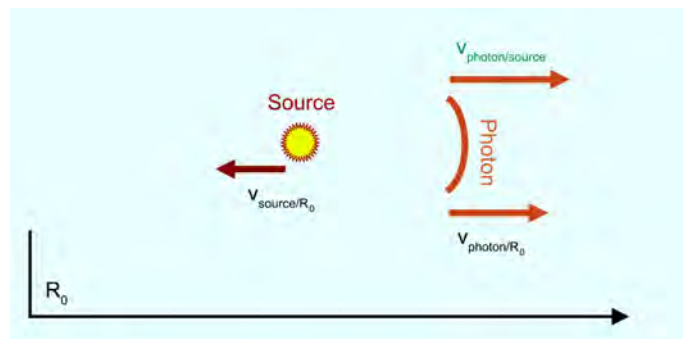


Figure 2. Velocities of the photon: in black/ R_0 and in green/source S.

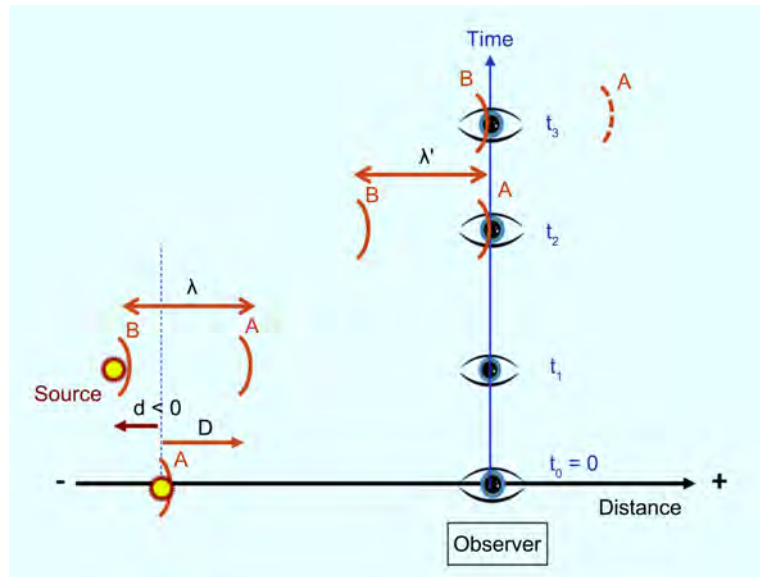


Figure 3. Photons from the moving source to the observer.

$$\lambda = D_A + |d_{source}| \tag{5}$$

$$\lambda = v_{A/R_0} * T_{source} + |v_{source/R_0} * T_{source}| \tag{6}$$

- The second way is to consider that the distance between the photons is the propagation distance of the photon (B) until it reaches the position where the photon (A) had been observed at the time of the emission of (B):

$$\lambda' = v_{B/R_0} * T_{obs} \tag{7}$$

$$\lambda' = v_{B/R_0} / f_{obs} \tag{8}$$

In neo-Newtonian mechanics, there is no variation in distance or time depending on the speed of the frame of reference, the distance between two photons is the same whether it is calculated from the observer or from the source.

$$\lambda' = \lambda \tag{9}$$

The frequency being the inverse of the period, the redshift is defined from the frequencies by:

$$1 + z = \frac{f_{source}}{f_{obs}} \tag{10}$$

we then get (see details of the calculation in **Appendix 2**):

$$v_{source} = -\frac{z}{1+z} c \tag{11}$$

And in the case where the speed of the source with respect to the frame of reference R_0 is directed in the same direction as the photon, the formula is then

$$v_{source} = z \cdot c \tag{12}$$

In both cases, it is a Doppler-Fizeau effect applied to electromagnetic waves, without expansion of the space itself.

5. Discussion

5.1. The Difference with the Relativistic Speed Prediction

Compared to the relativistic redshift formula, the new speed away remains lower than the previous one until it reaches 17% deviation at $z = 1.4$ as shown in **Figure 4**. This is not incompatible with the current estimate of $\pm 10\%$ of distance [6]. And that means that the neo-Newtonian formula is closer to relativistic predictions than to Newtonian predictions. However, note that for usual values up to $z = 0.02$ (*i.e.* according to Hubble's law up to 240 million light years), the difference does not exceed 1% (See **Table 1**). And for slightly smaller values up to $z = 0.01$ we find within 1% the usual approximation

$$v_{source} = -z \cdot c \tag{13}$$

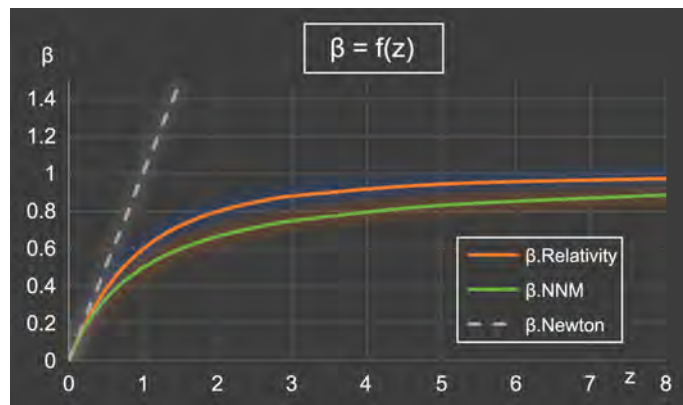


Figure 4. Velocities in Relativity theory, Newtonian mechanics and neo-Newtonian mechanics.

Table 1. Comparison of velocities.

VELOCITY	$\beta = z$	Relativity	Neo Newtonian	Difference	
z	[km/s]	[km/s]	[km/s]	[km/s]	[%]
0	0	0	0	0.0	0.0%
0.001	300	300	300	0.1	0.0%
0.005	1500	1496	1493	4	0.2%
0.01	3000	2985	2970	15	0.5%
0.02	6000	5940	5882	58	1%
0.1	30,000	28,507	27,273	1234	4%
0.5	150,000	115,385	100,000	15,385	13%
1	300,000	180,000	150,000	30,000	17%
1.6	480,000	222,680	184,615	38,065	17%
2	600,000	240,000	200,000	40,000	17%
5	1,500,000	283,784	250,000	33,784	12%
8	2,400,000	292,683	266,667	26,016	9%
15	4,500,000	297,665	281,250	16,415	6%
1000	300,000,000	299,999	299,700	299	0%

Thus, the difference in prediction with the relativistic values of speed only appears significant for very large redshift values z exceeding unity.

5.2. A Universe Which Does Not Expand Itself

In the relativistic demonstration of redshift it is implied a space which expands itself. This assumption is also found with the law of Hubble which would like that the galaxies located on the cosmic horizon, to 13.8 billion light years, would go in the future faster than the speed of the light except to consider also that space would expand on its own. And this space would be expanding between galaxies but not within galaxies, as evidenced by the image of raisin bread in an oven [7]. This strange hypothesis is akin to “creationism”. The derivation of the neo-Newtonian formula does not come up against these difficulties. With a source moving away from a fixed observer, we calculate the distance d traveled by the source, and we calculate the distance L that the photon (B) travels. When we make the difference δ of the distances, it is zero. And for blueshift with a source that approaches a fixed observer, the difference δ in distances is also zero. In these two cases, with neo-Newtonian mechanics there is no longer any need to consider an expanding space (see **Appendix 3**).

5.3. Interference of Light Waves

Having a variable frequency and a variable propagation speed makes it possible to have an unchanged wavelength. This is why this generally does not change the light interference phenomena and why it is difficult to see it by this means (see **Appendix 4**).

5.4. The Existence of a Fixed Frame of Reference

The hypothesis of a fixed or barycentric frame of reference R_0 is consistent with the latest observations on the anisotropy of the Universe [8] [9] [10] (see **Figure 5**) who measured that the solar system is moving at 390 km/s compared to the Diffuse Cosmological Background, the Galaxy having to move at 630 km/s (more than two million km/h). This Cosmic Microwave Background (CMB) would thus play this role of reference frame R_0 .

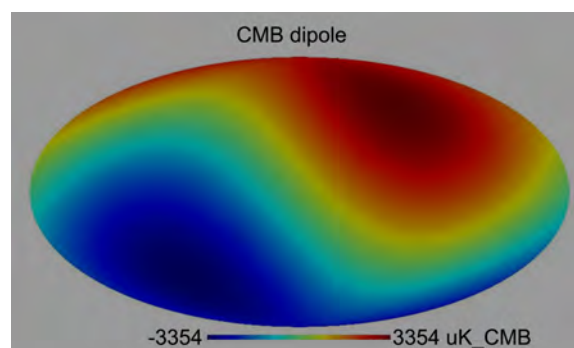


Figure 5. Dipolar anisotropy of the CMB (COBE measurement) before treatment [11]. Color bar: red for redshift, blue for blueshift.

5.5. Proof by the Pioneer Spacecrafts

The Pioneer spacecrafts had two characteristics, their very high speed at 37 km/s after the passage of Jupiter and the absence of stabilization or correction of the flight (which the Voyager spacecraft are equipped with). Examination of the trajectory of the two Pioneer spacecraft had detected complementary retrograde acceleration—that is, an unexplained slowing down. Officially this anomaly was solved by decreeing that this acceleration came from a continuous jet of photons emitted by each spacecraft. Nevertheless, in a previous article [e], we had shown that this anomaly could also be easily explained by taking the empirical relation:

$$1 + z = \frac{1}{1 - |\beta|} \quad (14)$$

β was then oriented in the other direction, but this formula is strictly equivalent to that demonstrated in this article. So this new formula for redshift helps explain the Pioneer anomaly or rather conversely, Pioneer spacecrafts demonstrate the validity of this formula for redshift.

5.6. A New Paradigm

Having a lower distance velocity does not necessarily mean that the distances would be lower. Indeed, relativistic cosmology is based on Hubble's law, with a Hubble constant which is paradoxically not constant over time and whose value differs depending on the measurement method used. The greater than expected distances and speeds prevalent by dark energy proponents could just as easily mean a current slowing of the expansion due to gravity. Recall that a traditional explosion also implies that all bodies move away from each other in proportion to their respective distance. No longer correlating the speed of the redshift with Hubble's law would make it possible to have another interpretation of distance, for example for quasars whose apparent luminosity is poorly explained [12]. This would allow us to re-examine the age of the Universe by taking into account the age of stars estimated to be over 14 billion years old [13]. The different distances (luminous, covariant, angular, proper and cosmological), all linked by the redshift z , could surely be simplified by considering that basically there are in relation to the observer only two distances, that of emission and that where the body is now. These are just examples of possible developments. Having a new paradigm opens up the fields of the possible with new areas to test, study and interpret

6. Conclusions

We have derivated within the framework of neo-Newtonian mechanics the value V of the speed from the source in function of the redshift to get to a new formula:

$$V = \frac{z}{1+z} c.$$

This formula has the double characteristic of being equivalent to relativistic predictions for low redshifts, but of deviating from them by up to 17% for high redshifts.

What can be the consequences of future research?

For any observed physical phenomenon, we seek an explanation. For example:

1) As the speed of expansion of the Universe cannot exceed the speed of light, it is assumed that space itself is expanding.

2) As the light interference remains identical despite the movement of the source, it is assumed that the speed of light would be constant in any frame of reference.

3) As our Galaxy being in motion with respect to the Cosmic Microwave Background (in contradiction with the isotropy of the theory of Relativity), it is assumed that it would be subjected to the Dipole Repeller.

4) As the Pioneer spacecrafts seem to be slowing down more than expected, it is assumed that they would be slowed down by their own flow of photons.

5) As distant supernovae appear less bright than expected, it is assumed that there is a dark energy that makes them accelerate.

Faced with these difficulties of interpretation, we propose here a change of paradigm, namely that resulting from neo-Newtonian mechanics:

1) We have expressed and demonstrated a slightly different formula relating the redshift to the speed of movement of the source. Thus, it is no longer necessary to imagine an expanding space by itself, which does not prevent galaxies from moving away from each other as a result of an explosive-type phenomenon.

2) We have shown that a variable frequency and speed of propagation depending on the movement of the source can explain a constant wavelength and therefore stable light interferences.

3) The observed anisotropy of the Universe can be explained very well by considering the Cosmic Microwave Background as the expression of a fixed or barycentric frame R_0 .

4) The slight blueshift effect of Pioneer spacecrafts is proof of the validity of this new redshift formula:

5) The Universe retains many mysteries, and not just about distant supernovae and quasars.

This new analysis grid proposed here (within Neo-Newtonian Mechanics) would allow any researcher interested in it to shed new light on his research, to test it and would surely open up the field of possibilities.

Acknowledgements

I would like to thank BGD for the reading and for the support.

Conflicts of Interest

The author declares no conflicts of interest regarding the publication of this paper.

References

- [1] Vincent, M. (2012) Validation des principes de la relativité restreinte (3/3). ENS

- Lyon.
<http://culturesciencesphysique.ens-lyon.fr/ressource/validation-relativite-restreinte-3.xml>
- [2] Chodorowski, M.J. (2011) *Monthly Notices of the Royal Astronomical Society*, **413**, 585-594. <https://arxiv.org/abs/0911.3536>
<https://doi.org/10.1111/j.1365-2966.2010.18154.x>
 - [3] Langlois, D. (2011) Introduction à la relativité, cours et exercices. Vuibert, p. 30.
 - [4] Semay, C. and Silvestre-Brac, B. (2016) Relativité restreinte, bases et applications. Dunod, p. 179.
 - [5] Guth, A. (2013) 3. The Doppler Effect and Special Relativity. MIT.
<https://www.youtube.com/watch?v=tJ2AJJMcQXs>
 - [6] Luri, X., *et al.* (2018) *A&A*, **616**, 2-19.
<https://www.aanda.org/articles/aa/pdf/2018/08/aa32964-18.pdf>
 - [7] Courtois, H. (2020) Voyage sur les flots de galaxies, Laniakea et au-delà. Dunod.
 - [8] Rubin, V.C. (1977) Is There Evidence of Anisotropy in the Expansion of the Universe? Cambridge University Press, Cambridge.
<https://doi.org/10.1017/S0252921100053549>
 - [9] Colin, J., *et al.* (2019) *A&A*, 3-7. <https://arxiv.org/pdf/1808.04597.pdf>
 - [10] Migkas, K., *et al.* (2020) *A&A*, **636**, p. 42.
<https://doi.org/10.1051/0004-6361/201936602>
 - [11] NASA, LAMDA-DMR Images.
https://lambda.gsfc.nasa.gov/product/cobe/dmr_image.cfm
 - [12] Arp, H. (1967) *Astrophysical Journal*, **148**, p. 321.
<https://ui.adsabs.harvard.edu/abs/1967ApJ...148..321A/abstract>
<https://doi.org/10.1086/149159>
 - [13] Bond, H.E., *et al.* (2013) *The Astrophysical Journal Letters*, **765**, 1-2, 4.
<https://doi.org/10.1088/2041-8205/765/1/L12>

Related Links

- a Presentation *Let's free Newtonian Mechanics from the equivalence "principle"!*
<https://www.gsjournal.net/Science-Journals/Research%20Papers-Relativity%20Theory/Download/7499>
- b Lorentz derivation *How to Demonstrate the Lorentz Factor: Variable Time vs. Variable Inertial Mass*
http://file.scirp.org/pdf/JMP_2015022510573131.pdf
Reply to "A Simple Derivation of the Lorentz Transformation"
http://file.scirp.org/pdf/JMP_2017121915203275.pdf
Lorentz transformation derivation criticism
<https://www.youtube.com/watch?v=koPnW0mXcvI>
- c Force *Net Force $F = \gamma^3 ma$ at High Velocity*
http://file.scirp.org/pdf/JMP_2016042814580505.pdf
- d Velocities *Velocity Addition Demonstrated from the Conservation of Linear Momenta, an Alternative Expression*
http://file.scirp.org/pdf/JMP_2015050609513342.pdf
Mass of Inertia and Kinetic Energy
<http://gsjournal.net/Science-Journals/Research%20PapersRelativity%20Theory/Download/4113>
An improvement of the accuracy of Fizeau's experiment
<http://gsjournal.net/Science-Journals/Research%20Papers-Relativity%20Theory/Download/7247>
The new speed composition $u = v + w/\gamma^2$ in agreement with Fizeau's experiment
<http://gsjournal.net/Science-Journals/Research%20Papers-Relativity%20Theory/Download/7247>
- e Redshift *XXXX*
Present one
The Pioneer Anomaly explained by the Processing of the Doppler Effect
<http://gsjournal.net/Science-Journals/Research%20Papers-Relativity%20Theory/Download/7330>
Redshift derivation criticism
- f Michelson experiment *Which derivation for the result of the MMX (Michelson & Morley Experiment) in translation with respect to the observer?*
<https://www.gsjournal.net/Science-Journals/Research%20Papers-Relativity%20Theory/Download/7808>
- g Sagnac effect *A Non-Relativistic Explanation of the Sagnac Effect*
https://file.scirp.org/pdf/JMP_2019041715043977.pdf
- h Muons Lifetime *Muon Lifetime would depend of its Energy*
<http://www.mrelativity.net/Papers/51/Muons%20Serret%20Millennium.pdf>
- i Mercury perihelion *About the ovoid orbits in general, and perihelion precession of Mercury in particular (2)*
<http://www.mrelativity.net/Papers/51/Mercury%20Millennium%20Serret%205%20janvier%202018.pdf>
- j Light deflection *Hipparcos did not measure directly the light bending!*
<http://gsjournal.net/Science-Journals/Research%20Papers-Mechanics%20/%20Electrodynamics/Download/6998>
Gravitational Light Deflection: could Relativity be Invalidated by GAIA?
<http://mrelativity.net/Papers/51/Light%20deflection%20SERRET%20Millennium%20Aout%202018.pdf>
-

Continued

k	Shapiro time delay	<i>Shapiro Time Delay derivates from Refraction</i> http://www.mrelativity.net/Papers/51/Shapiro%20SERRET%20Millennium%20journal%20202018.pdf
l	Dark Matter	<i>The flat rotation curve of our galaxy explained within Newtonian mechanics</i> https://physicessays.org/browse-journal-2/product/1240-7-olivier-serret-the-flat-rotation-curve-of-our-galaxy-explained-within-newtonian-mechanics.html
m	Dark Energy	<i>Gravity vs. Dark Energy, about the Expansion of the Universe</i> http://file.scirp.org/pdf/JMP_2018011714405269.pdf
n	Gravitational waves	<i>Gravitational waves or particle radiation?</i> https://www.physicessays.org/browse-journal-2/product/1588-12-olivier-serret-gravitational-waves-or-particle-radiation.html

Appendix 1: Criticism of the Derivation of the Relativistic Redshift Formula

Let us have

- An observer without motion (he is in his own frame)
- A source moving at the velocity v_{source} (in the observer's frame). So

$$\beta = \frac{v_{source}}{c} \quad (1.1)$$

Relativistic equation hereafter

$$1+z = \sqrt{\frac{1+\beta}{1-\beta}} \quad (1.2)$$

is equivalent to

$$\beta = \frac{(1+z)^2 - 1}{(1+z)^2 + 1} \quad (1.3)$$

The links between the frequencies and the periods are

$$1+z = \frac{f_{source}}{f_{obs}} \quad (1.4)$$

$$1+z = \frac{T_{obs}}{T_{source}} \quad (1.5)$$

We'll check two cases, the redshift and the blueshift one.

1) Edshift Case

See specific configuration of **Figure 6**.

- The distance of emission source of the photon (B) at the time $t_1 = T_{source}$:

$$d_{source} = v_{source} (t_1 - t_0) \quad (1.6)$$

$$d_{source} = -\beta \cdot c \cdot T_{source} \quad (1.7)$$

with v_{source} and so $\beta < 0$.

- And the length traveled by the photon (B) to reach the observer is

$$L = v_{photon} (t_2 - t_1) \quad (1.8)$$

$$L = c \cdot (T_{obs} - T_{source}) \quad (1.9)$$

And with the Equation (1.5)

$$L = c \cdot ((1+z) - 1) \cdot T_{source} \quad (1.10)$$

$$L = c \cdot z \cdot T_{source} \quad (1.11)$$

2) Blueshift Case

See specific configuration of **Figure 7**.

- The distance of emission source of the photon (B) at the time $t_1 = T_{source}$:

$$d_{source} = \lambda \quad (1.12)$$

$$\lambda = v_{photon} T_{source} \quad (1.13)$$

$$\lambda = c T_{source} \quad (1.14)$$

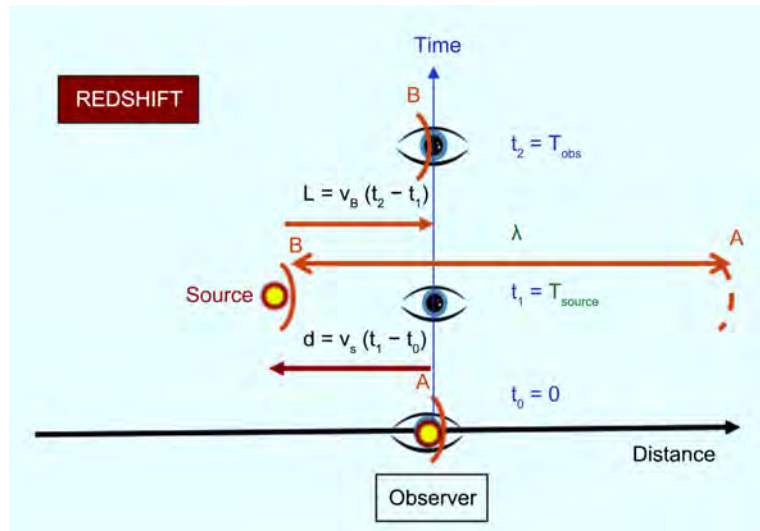


Figure 6. Redshift case/SR.

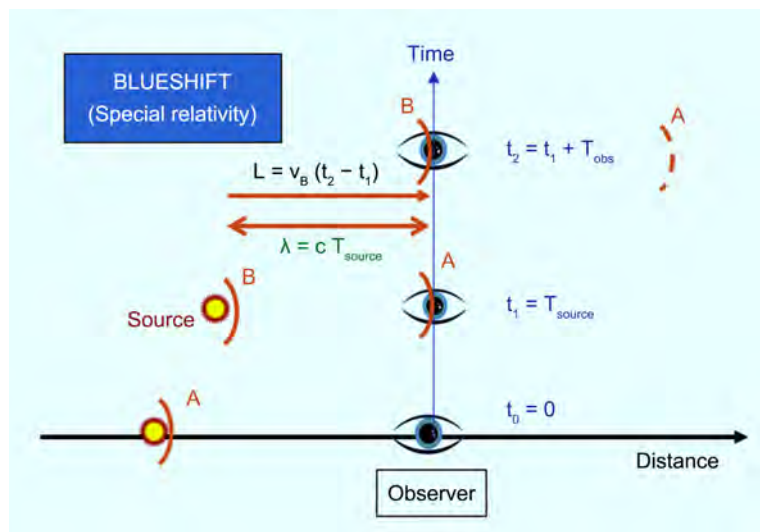


Figure 7. Blueshift case/Special Relativity.

Then

$$d_{source} = cT_{source} \tag{1.15}$$

- And the length traveled by the photon (B) to reach the observer is 16

$$L = v_{photon}(t_2 - t_1) \tag{1.16}$$

$$L = c \cdot T_{obs} \tag{1.17}$$

$$L = c \cdot (1 + z) \cdot T_{source} \tag{1.18}$$

Numerical application (with for example $T_{source} = 1$ second):

Let us apply in **Table 2** previous formulas with some example of z and with the difference of length:

$$\delta = L - |d| \tag{1.19}$$

Table 2. Relativistic numerical application.

T = T source = 1 second for example	Blueshift		Redshift	
shift z	-0.5	-0.1	1	10
Distance of B source from A:				
β source (SR)	-0.60	-0.10	0.60	0.98
d: distance of emission of B from O	c T	c T	-0.6 c T	-0.98 c T
Length traveled by photon B:				
T observed/T source = (1 + z)	0.5	0.9	2	11
L: Length traveled by photon B	0.5 c T	0.9 c T	c T	10 c T
Difference δ	-0.5 c T	-0.1 c T	0.4 c T	9.02 c T

So to explain the redshift, you need to suppose a Universe expansion (for example a Universe expansion of $0.4 * c * T$ for $z = 1$).

And to explain the blueshift, you need to suppose a Universe contraction (of $-0.1 * c * T$ for $z = -0.1$)!

→ **Without a Universe which would expand by itself, the relativistic formula of redshift is uncoherent!**

Appendix 2. Derivation of the Neo-Newtonian Formula of Redshift

Let us have a coordinate system oriented according to the propagation of the photons. According to the motion of the Source and the motion of the Observer, there are 4 cases. We illustrate 2 cases (see **Figure 8** and **Figure 9**).

A2.1. The Hypotheses

1) About the source:

Let us have a source emitting photon (A) at time t_0 and photon (B) at time t_1 . By definition, the source period T_{source} is

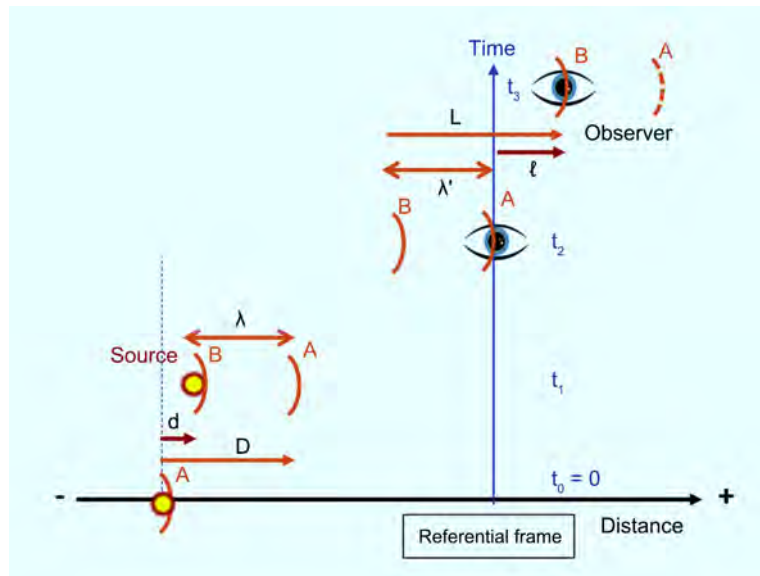


Figure 8. Source motion to the right & Observer motion to the right.

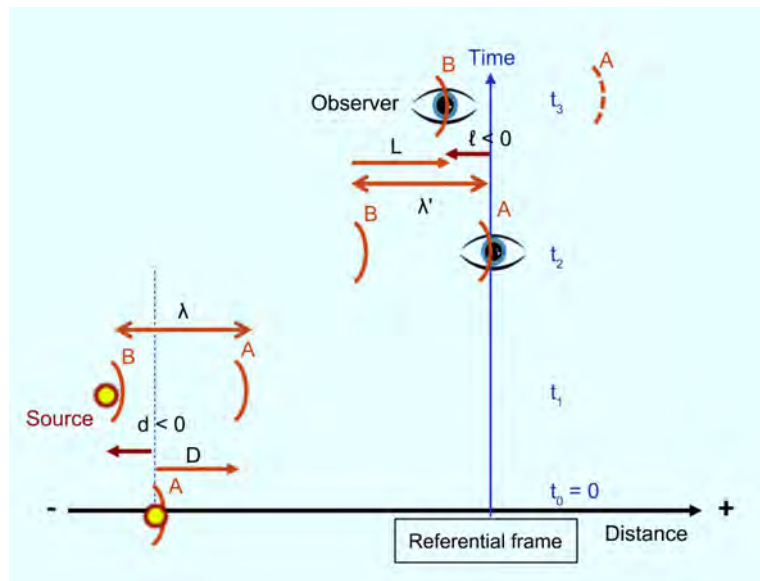


Figure 9. Source motion to the left & Observer motion to the left.

$$T_{source} = t_1 - t_0 \quad (2.1)$$

d_{source} is the distance traveled by the source at the velocity v_{source} during a period T_{source}

$$d_{source} = v_{source} \cdot T_{source} \quad (2.2)$$

D_A is the distance traveled by the photon (A) at the velocity v_A during a period T_{source}

$$D_A = v_A \cdot T_{source} \quad (2.3)$$

λ is the distance between photon (A) and photon (B)

$$\lambda = D_A - d_{source} \quad (2.4)$$

Please note these are algebraic value. If d_{source} is positive, λ will be lower than D_A . If d_{source} is negative, λ will be greater than D_A (please check **Figure 8** with t_1 for d_{source} positive, and **Figure 9** with t'_1 with d_{source} negative).

2) About the observer:

Let us have an observer receiving photon (A) at time t_2 and photon (B) at time t_3

By definition, the observer period T_{obs} is

$$T_{obs} = t_3 - t_2 \quad (2.5)$$

l_{obs} is the distance traveled by the observer at the velocity v_{obs} during a period T_{obs}

$$l_{obs} = v_{obs} \cdot T_{obs} \quad (2.6)$$

L_B is the distance traveled by the photon (B) at the velocity v_B during a period T_{obs}

$$L_B = v_B \cdot T_{obs} \quad (2.7)$$

λ' is the distance between photon (A) and photon (B)

$$\lambda' = L_B - l_{obs} \quad (2.8)$$

Please note these are algebraic value. If l_{obs} is positive, λ' will be lower than L_B . If l_{obs} is negative, λ' will be greater than L_B (please check **Figure 8** at t_3 for l_{obs} positive, and **Figure 9** at t'_3 for l_{obs} negative).

Because the motion of the source is continuous, the velocities of the photons are all the same

$$v_B = v_A \quad (2.9)$$

Because the velocities of the photons are the same, the distance between photons remain the same

$$\lambda' = \lambda \quad (2.10)$$

What is perceived is the frequency, not the wave length. So the redshift z is, with f for frequency

$$1 + z = \frac{f_{source}}{f_{obs}} \quad (2.11)$$

Remark 1: In Newtonian mechanics and so in Neo Newtonian Mechanics,

there is no difference of length whatever it is measured from the Observer frame or from the Referential frame.

Remark 2: when c is constant please note Equation (2.11) is equivalent to

$$1 + z = \frac{\lambda_{obs}}{\lambda_{source}} \tag{2.12}$$

By definition of the frequency

$$f = \frac{1}{T} \tag{2.13}$$

And let us define V the distance speed of the source from the observer by

$$V \cong v_{source} - v_{obs} \tag{2.14}$$

In Neo-Newtonian Mechanics, the velocities cannot be directly added for very high velocities. In the present case, we consider that the source and the observer are in usual velocity, so we can use the approximatively equal symbol.

A2.2. Derivation

Using Equations (2.4), (2.3), (2.2)

$$T_{source} = \frac{\lambda}{v_A - v_{source}} \tag{2.15}$$

Using equations (2.6), (2.7), (2.8), (2.9), (2.10)

$$T_{obs} = \frac{\lambda'}{v_B - v_{obs}} \tag{2.16}$$

Using equations (2.9) and (2.10)

$$T_{obs} = \frac{\lambda}{v_A - v_{obs}} \tag{2.17}$$

Using Equations (2.11) and (2.13)

$$1 + z = \frac{T_{obs}}{T_{source}} \tag{2.18}$$

Then using Equations (2.15) and (2.17)

$$1 + z = \frac{v_A - v_{source}}{v_A - v_{obs}} \tag{2.19}$$

$$v_A - v_{obs} + z(v_A - v_{obs}) = v_A - v_{source} \tag{2.20}$$

$$z(v_A - v_{obs}) = v_{obs} - v_{source} \tag{2.21}$$

So using Equation (2.14)

$$V \cong -z(v_A - v_{obs}) \tag{2.22}$$

- When V is positive, the source gets closer to the observer, it is the blueshift.
- When V is negative, the source gets away from the observer, it is the redshift.

Lest us now consider 2 cases, either the photon is moving in the same direction than the source ($v_{source} > 0$), either the photon is moving in the opposite

direction from the source ($v_{source} < 0$).

In Neo-Newtonian Mechanics, a photon cannot go faster than the asymptotic limit s , which means that the faster velocity of the photon is c .

$$\begin{cases} \text{if } [v_{source} > 0] \text{ then } [v_A = c] \\ \text{if } [v_{source} < 0] \text{ then } [v_A \cong c + v_{source}] \end{cases} \quad (2.23a-b)$$

Please note that in the second case, v_A is not greater but lower than c , because $v_{source} < 0$.

1) $v_{source} > 0$ (see **Figure 10**)

Using Equations (2.22) and (2.23 a)

$$V \cong -z(c - v_{obs}) \quad (2.24)$$

Please note that usually $v_{obs} \ll c$, then we get

$$V \cong -z \cdot c \quad (2.25)$$

That means that when the source is coming toward us relatively to the absolute frame, we will get a blueshift except if the Earth is moving away faster than the source.

Physically, this is not the usual case.

2) $v_{source} < 0$ (see **Figure 11**)

Using Equations (2.22) and (2.23b)

$$V \cong -z(c + v_{source} - v_{obs}) \quad (2.26)$$

Then with Equation (2.14)

$$V \cong -z(c + V) \quad (2.27)$$

$$(1 + z)V \cong -z \cdot c \quad (2.28)$$

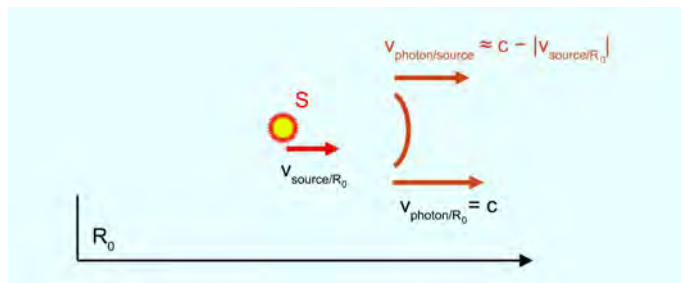


Figure 10. Photon going in the same direction as the source S.

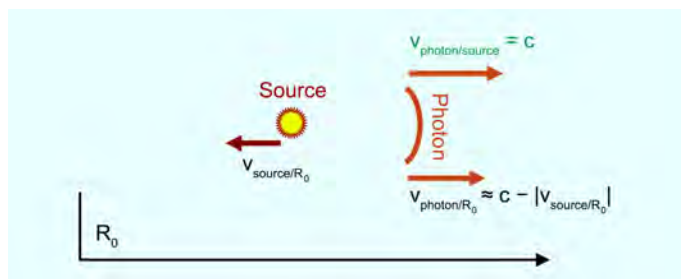


Figure 11. Photon going in the opposite direction of the source S.

So we get the general formula of the redshift with the algebraic value V :

$$V \cong -\frac{z}{1+z}c \quad (2.24)$$

- When z is positive, V is negative, the source moves away from the observer, it is the redshift.
- When z is negative, V is positive, the source moves toward the observer, it is the blueshift.

Please note that when $z \ll 1$, then we get

$$V \cong -z \cdot c \quad (2.30)$$

Appendix 3. Derivation of the Neo-Newtonian Redshift Formula

Let us have

- An observer without motion (he is in his own frame)
- A source moving at the velocity v_{source} (in the observer's frame). So

$$\beta = \frac{v_{source}}{c} \tag{3.1}$$

NNM equation hereafter for the redshift, when the axis is oriented with the photon

$$1 + z = \frac{1}{1 + \beta} \tag{3.2}$$

Is equivalent to

$$\beta = -\frac{z}{1 + z} \tag{3.3}$$

Period from redshift

$$1 + z = \frac{f_{source}}{f_{obs}} \tag{3.4}$$

$$1 + z = \frac{T_{obs}}{T_{source}} \tag{3.5}$$

We'll check two cases, the redshift and the blueshift one.

1) Redshift case

See specific configuration of **Figure 12**.

- The distance of emission source of the photon (B) at the time $t_1 = T_{source}$:

$$d_{source} = v_{source} (t_1 - t_0) \tag{3.6}$$

$$d_{source} = \beta \cdot c \cdot T_{source} \tag{3.7}$$

with $v_{source} < 0$ and so $\beta < 0$.

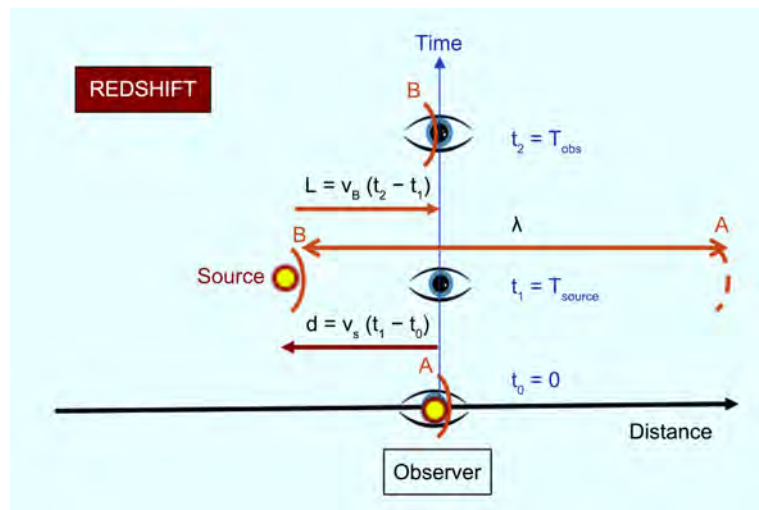


Figure 12. Redshift case/NNM.

- And the length traveled by the photon (B) to reach the observer is

$$L = v_{\text{photon}} (t_2 - t_1) \tag{3.8}$$

for the redshift ($v_{\text{source}} < 0$) using the Equation (2.23b) already seen

$$v_{\text{photon}} \cong c + v_{\text{source}} \tag{2.23b bis}$$

with $v_{\text{source}} < 0$

$$L = (c + v_{\text{source}}) \cdot (T_{\text{obs}} - T_{\text{source}}) \tag{3.9}$$

Using Equations (3.1) and (3.2):

$$c + v_{\text{source}} = c + \beta \cdot c \tag{3.10}$$

$$1 + \beta = \frac{1}{1 + z} \tag{3.11}$$

So

$$c + v_{\text{source}} = \frac{c}{1 + z} \tag{3.12}$$

And using Equation (3.5)

$$z \cdot T_{\text{source}} = T_{\text{obs}} - T_{\text{source}} \tag{3.13}$$

Then from Equation (3.9)

$$L = \frac{c}{1 + z} \cdot (z \cdot T_{\text{source}}) \tag{3.14}$$

$$L = c \cdot \frac{z}{1 + z} \cdot T_{\text{source}} \tag{3.15}$$

So in the case of the redshift, δ is the difference

$$\delta = L - |d| \tag{3.16}$$

$$\delta = c \cdot \frac{z}{1 + z} \cdot T_{\text{source}} - (|\beta| \cdot c) T_{\text{source}} \tag{3.17}$$

According to NNM, for the redshift when the axe is oriented with the photon:

$$|\beta| = \frac{z}{1 + z} \tag{3.18}$$

Then

$$\delta = 0 \tag{3.19}$$

2) Blueshift case

See specific configuration of **Figure 13**.

- The distance of emission source of the photon (B) at the time $t_1 = T_{\text{source}}$:

$$\lambda = D - d \tag{3.20}$$

$$\lambda = v_{\text{photon}} \cdot T_{\text{source}} - v_{\text{source}} \cdot T_{\text{source}} \tag{3.21}$$

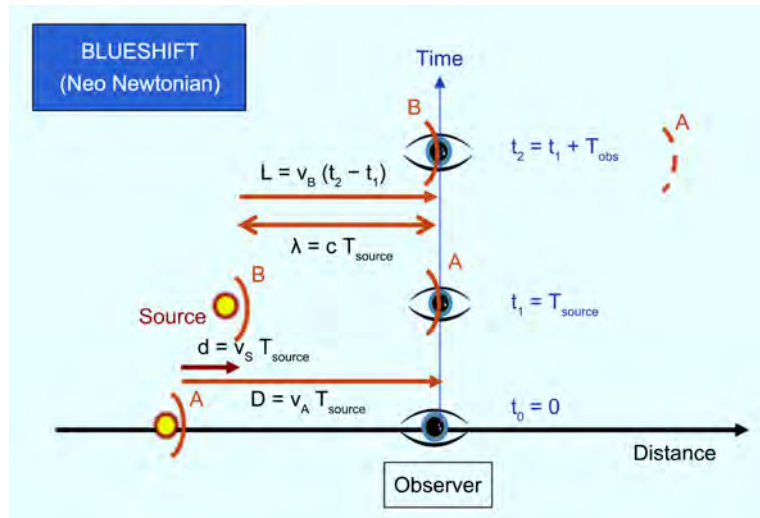


Figure 13. Blue shift case/Neo Newtonian Mechanics.

for the redshift ($v_{source} > 0$) using the Equation (2.23a) already seen

$$v_{photon} = c \tag{2.23a bis}$$

$$\lambda = c \cdot T_{source} + z \cdot c \cdot T_{source} \tag{3.22}$$

with $z < 0$

$$\lambda = c(1 + z) \cdot T_{source} \tag{3.23}$$

- And the length traveled by the photon (B) to reach the observer is

$$L = v_{photon} (t_2 - t_1) \tag{3.24}$$

$$L = v_{photon} T_{obs} \tag{3.25}$$

Using Equation (3.3)

$$T_{obs} = (1 + z) T_{source} \tag{3.26}$$

$$L = c \cdot (1 + z) \cdot T_{source} \tag{3.27}$$

So in the case of the blueshift:

$$\delta = L - \lambda \tag{3.28}$$

$$\delta = c \cdot (1 + z) T_{source} - c(1 + z) \cdot T_{source} \tag{3.29}$$

$$\delta = 0 \tag{3.30}$$

Numerical applications (with $T_{source} = 1$ second).

Let us apply in **Chart 3** previous formulas with some example of z and with the difference of length δ with:

$$\text{for the blueshift, } \delta = L - |\lambda| \tag{3.31}$$

$$\text{for the blueshift, } \delta = L - |d| \tag{3.32}$$

Chart 3. Neo-Newtonian numerical application.

T = Tsource = 1 second	BLUESHIFT		REDSHIFT		
	shift z	-0.5	-0.1	1	10
Distance of B source from A					
β source (NNM)	-1.00	-0.11	0.50	0.91	
d: distance of emission of B from O			-0.5 c T	-0.91 c T	
λ: distance from B to A	(0.5 c) T	(0.9 c) T			
Length traveled by photon B:					
T observed/Tsource = (1 + z)	0.5	0.9	2	11	
L: Length traveled using Tobs	c (0.5 T)	c (0.9 T)	0.5 c T	0.91 c T	
Difference δ	0	0	0	0	

Appendix 4. Interferences

$$1 + z = \frac{f_{source}}{f_{obs}} \quad (4.1)$$

1) According to NNM for the redshift

$$\text{if } [v_{source} < 0] \text{ then } [v_A \cong c - |v_{source}|] \quad (4.2)$$

$$v_{source} = \frac{z}{1+z} c \quad (4.3)$$

So

$$v_A \cong c \left(1 - \frac{z}{1+z} \right) \quad (4.4)$$

$$v_A \cong c \frac{1}{1+z} \quad (4.5)$$

$$\lambda_{obs} = \frac{v_A}{f_{obs}} \quad (4.6)$$

$$\lambda_{obs} \cong \left(c \frac{1}{1+z} \right) \left(\frac{1+z}{f_{source}} \right) \quad (4.7)$$

$$\lambda_{obs} \cong \frac{c}{f_{source}} \quad (4.8)$$

$$\lambda_{obs} \cong \lambda_{source} \quad (4.9)$$

2) And according to NNM for the blueshift

$$\text{if } [v_{source} > 0] \text{ then } [v_A = c] \quad (4.10)$$

$$\lambda_{obs} = \frac{v_A}{f_{obs}} \quad (4.11)$$

$$\lambda_{obs} = c \left(\frac{1+z}{f_{source}} \right) \quad (4.12)$$

$$\lambda_{obs} \neq \lambda_{source} \quad (4.13)$$

Particle Physics Problems Addressed with Simple Mathematics Related to General Relativity

T. R. Mongan

Sausalito, CA, USA

Email: tmongan@gmail.com

How to cite this paper: Mongan, T.R. (2021) Particle Physics Problems Addressed with Simple Mathematics Related to General Relativity. *Journal of Modern Physics*, 12, 254-259.
<https://doi.org/10.4236/jmp.2021.123019>

Received: December 22, 2020

Accepted: February 19, 2021

Published: February 22, 2021

Copyright © 2021 by author(s) and Scientific Research Publishing Inc. This work is licensed under the Creative Commons Attribution International License (CC BY 4.0).

<http://creativecommons.org/licenses/by/4.0/>



Open Access

Abstract

Existing particle physics models do not account for dark matter and neutrino mass, or explain the three generations of fundamental fermions. This analysis uses simple mathematics, related to general relativity, to address these problems. The paper does *not* address the very difficult problem of quantizing general relativity.

Keywords

Quantum Mechanics, General Relativity, Standard Model

1. Introduction

Particle physics models fail to account for dark matter, and the Standard Model for fundamental particles of ordinary matter faces several problems. First, since neutrinos oscillate between neutrino states when propagating through space, the Standard Model must be modified to accommodate neutrino mass. Second, the Standard Model does not explain why three, and only three, fundamental fermions are in each Standard Model charge state e , $(2/3)e$, and $-(1/3)e$, where e is electron charge. Third, the Standard Model involves point particles with spin angular momentum \hbar , or $\hbar/2$. Angular momentum is usually defined for rotating objects extended in space and, regarding point particles with angular momentum, we might ask what is rotating. Fourth, infinite energy density of point particles is a problem. These problems are reframed below using simple mathematics related to general relativity.

2. Dark Matter from Elbaz-Novello Quantized Friedmann Equation

It is often assumed all four forces governing the universe were unified early in the history of the universe. When initial force symmetry broke, the gravitational structure constant $\frac{Gm_p^2}{\hbar c} = 5.9 \times 10^{-39}$, with $\hbar = 1.05 \times 10^{-27} \text{ g}\cdot\text{cm}^2/\text{sec}$, $c = 3 \times 10^{10}$

cm/sec, and proton mass $m_p = 1.67 \times 10^{-24} \text{ g}$, is the ratio of the strengths of gravity and the strong force after inflation. In flat, homogeneous, and isotropic post-inflationary space with matter density ρ , a strong gravity model for dark matter [1] approximates the strong force as an effective strong gravity acting

only on matter, with strength $G_s = \left(\frac{M_p}{m_p}\right)^2 G = 1.7 \times 10^{38} G$, gravitational constant $G = 6.67 \times 10^{-8} \text{ cm}^3/(\text{g}\cdot\text{sec}^2)$, and Planck mass $M_p = \sqrt{\frac{\hbar c}{G}} = 2.18 \times 10^{-5} \text{ g}$.

The strong gravity Friedmann equation $\left(\frac{dR}{dt}\right)^2 - \left(\frac{8}{3}\right) 8\pi G_s \rho R^2 = -c^2$ describes local curvature of spaces defining closed massive systems bound by effective strong gravity. Because strong force at short distance is involved, quantum mechanical analysis is necessary. The Schrodinger equation resulting from Elbaz-Novello quantization [2] [3] of the Friedmann equation for closed massive systems bound by effective strong gravity is

$$-\frac{\hbar^2}{2\mu} \frac{d^2}{dr^2} \psi - \frac{2G_s \mu M}{3\pi r} \psi = -\frac{\mu c^2}{2} \psi \quad (1)$$

where $M = 2\pi^2 \rho r^3$ is conserved mass of closed systems with radius r and μ an effective mass. Equation (1) is identical in mathematical form to the Schrodinger equation for the hydrogen atom and can be solved immediately. Ground state curvature energy $-\frac{\mu}{2\hbar^2} \left(\frac{2G_s \mu M}{3\pi}\right)^2$ of Equation (1) must equal $-\frac{\mu c^2}{2}$ for consistency with the corresponding Friedmann equation, so effective mass $\mu = \frac{3\pi \hbar c}{2G_s M}$. Ground state solutions of Equation (1) describe stable closed systems bound by effective strong gravity, with zero orbital angular momentum and

radius $\langle r \rangle = \frac{G_s M}{\pi c^2} = \frac{\hbar M}{\pi c m_p^2}$. Geodesic paths inside these stable ground state closed systems created by effective strong gravity are all circles with radius $\langle r \rangle = \frac{\hbar M}{\pi c m_p^2}$, so matter within these closed systems is permanently confined

within a radius $\langle r \rangle$. No matter can enter or leave them after they form, to increase or decrease the amount of matter in those closed systems, so they constitute rigid impenetrable spheres of dark matter interacting only gravitationally. Assuming velocity-independent rigid sphere scattering [4], (self-interaction collision cross-section)/mass ratio for dark matter particles is $\frac{\sigma}{M} = \frac{4\pi(2r)^2}{M}$.

Consider values of $\frac{\sigma}{M}$ between $0.015 \text{ cm}^2/\text{g}$ and $0.025 \text{ cm}^2/\text{g}$, near the estimated [5] $\frac{\sigma}{M} = 0.015 \text{ cm}^2/\text{g}$. Inserting dark matter particle radius/mass relation $\langle r \rangle = \frac{\hbar M}{\pi c m_p^2}$ into rigid sphere (self-interaction collision cross-section)/mass relation $\frac{\sigma}{M} = \frac{4\pi(2r)^2}{M}$ yields $M = \left[\left(\frac{\sigma}{M} \right) \frac{\pi}{16} \left(\frac{c}{\hbar} \right)^2 m_p^3 \right] m_p$. Values of $\frac{\sigma}{M}$ between $0.015 \text{ cm}^2/\text{g}$ and $0.025 \text{ cm}^2/\text{g}$ indicate dark matter particle mass between 10.5 GeV and 17.5 GeV , consistent with Kelso/Hooper/Buckley analysis [6]. Estimated nucleon mass equivalent $A = \left(\frac{\sigma}{M} \right) \frac{\pi}{16} \left(\frac{c}{\hbar} \right)^2 m_p^3$ of dark matter particles ranges from 11.2 to 18.7 , with radii $r = \left(\frac{A}{\pi} \right) \left(\frac{\hbar}{m_p c} \right)$ ranging from $0.75 \times 10^{-13} \text{ cm} = 0.75 \text{ F}$ to $1.25 \times 10^{-13} \text{ cm} = 1.25 \text{ F}$.

If $\frac{\sigma}{M} = 0.02 \text{ cm}^2/\text{g}$, dark matter particles have mass $14 \text{ GeV} = 14.9 m_p$, radius 1.00 F , and density $6 \times 10^{15} \text{ g/cm}^3$. Then, if all four forces were unified in the early post-inflationary universe, as the universe continued expanding prior to force symmetry breaking, matter density in the universe steadily dropped. When matter density fell to $6 \times 10^{15} \text{ g/cm}^3$, matter could coalesce into close-packed dark matter spheres accounting for 74% of all matter (88% of dark matter).

Impenetrable spheres of dark matter are the ultimate defense against gravitational collapse, suggesting a core of close-packed spheres of dark matter is at the center of black holes, rather than a singularity. Close-packed spheres of n dark matter particles have radius $R_n = \sqrt[3]{n} \frac{\hbar M}{\pi c m_p^2} = \sqrt[3]{n} \times 10^{-13} \text{ cm} = \sqrt[3]{n} \text{ F}$ and Schwarzschild radius $R_s = \frac{29.9 G n m_p}{c^2} = 3.7 n \times 10^{-51} \text{ cm}$, smaller than the physical radius of the sphere until $\sqrt[3]{n} \times 10^{-13} \text{ cm} = 3.7 n \times 10^{-51} \text{ cm}$ or $n = 1.4 \times 10^{56}$, indicating minimum mass for accretionary black holes is $2.1 \times 10^{57} m_p = 3.5 \times 10^{33} \text{ g}$, or about 1.75 times the solar mass. Surface temperature of black holes with mass near the solar mass is about 10^{-9} K , about a billion times less than the cosmic microwave background temperature, so black hole evaporation will only occur far in the future. Discovery of black holes with mass less than a solar mass would invalidate this analysis.

3. Standard Model Particles Described by Solutions of Einstein Equations

This section describes Standard Model particles with mass as small radius solutions of Einstein's equations.

Fundamental fermions with mass m and Compton wavelength $l = \frac{\hbar c}{mc^2}$ can be treated as spherical shells with radius $\frac{l}{4}$ rotating around an axial core cen-

tered on the axis of rotation, with half of any fermion charge on the shell surface at distance of the Planck length $l_p = \sqrt{\frac{\hbar G}{c^3}} = 1.62 \times 10^{-33}$ cm from the axis of rotation. Fundamental fermions can then be represented as Godel solutions of Einstein's equations, with average matter density ρ equal average fermion mass density, pressure $\left(\frac{1}{2}\right)\rho c^2$ from negative vacuum energy density $-\left(\frac{1}{2}\right)\rho c^2$, and effective internal gravitational constant G_f determined by

$$\omega = 2\sqrt{\pi G_f \rho} \tag{2}$$

Rotation axis orientation is unknown until z component of fermion angular momentum is measured, so fermion mass appears sinusoidally distributed on a disk of radius $(l/4)$ perpendicular to the line of sight.

Considered as spheres with radius $(l/4)$ their Compton wavelengths l , fundamental fermions have three associated geometric quantities, volume $\sim l^3$, surface area $\sim l^2$, and diameter $\sim l$. Mass and pressure distribution in fundamental fermions identifies three wavelengths in each charge state as solutions of a cubic equation $Al^3 + Bl^2 + Cl = 0$. Describing mass and pressure distribution in terms of surface and linear elements requires shell thickness and core radius l_p . In each charge state $\frac{ne}{3}$, with $n = 0, 1, 2$ or 3, total fermion mass is the sum of mass equivalent of pressure, $\frac{m}{2}$, in the volume, mass equivalent of surface pressure $\frac{\pi}{4}Sl^2$, and core mass Ll , so

$$\frac{4}{3}\pi\rho\left(\frac{l}{4}\right)^3 = \frac{4}{3}\pi\frac{\rho}{2}\left(\frac{l}{4}\right)^3 + 4\pi S\left(\frac{l}{4}\right)^2 + 2L\left(\frac{l}{2}\right). \tag{3}$$

Writing (3) as

$$Al^3 - Bl^2 - Cl = 0 \tag{4}$$

with $A = \frac{\pi}{96}\rho$, $B = \frac{\pi S}{4}$, and $C = 2L$, the discriminant $B^2C^2 - 4AC^3$ is positive regardless of the sign of B and the equation has three real roots corresponding to three fermion Compton wavelengths in a charge state. Nickalls [7] showed wavelengths l satisfying Equation (4) correspond to projections on the l axis, defined by an angle Θ , of vertices of an equilateral triangle. Θ is the angle between two lines starting at the center of the triangle, one parallel to the l axis and one extending to the rightmost vertex of the equilateral triangle. Nickall's parameters $l_N = -\frac{B}{3A} = -\frac{8S}{\rho}$, $\delta^2 = l_N^2 - \frac{C}{3A} = l_N^2 - \frac{64L}{\rho}$, $3l_N = l_1 + l_2 + l_3$, and $\delta^2 = \frac{(l_1 - l_N)^2}{4} + \frac{(l_2 - l_3)^2}{12}$, identify roots $l_1 = l_N + 2\delta \cos \Theta$, $l_2 = l_N - \delta(\cos \Theta - \sqrt{3} \sin \Theta)$, and $l_3 = l_N - \delta(\cos \Theta + \sqrt{3} \sin \Theta)$ corresponding to fermion Compton wavelengths in a charge state. Three positive Compton wavelengths in each charge state require negative surface mass equivalent density

$S = -\frac{\rho l_N}{8}$, $\delta^2 < l_N^2$ in each charge state, and positive mass per unit core length $L = \frac{\rho}{64}(l_N^2 - \delta^2)$. Negative S results from positive shell vacuum energy density $\left(\frac{1}{2}\right)\rho c^2$, opposite the negative vacuum energy density $-\left(\frac{1}{2}\right)\rho c^2$ in the volume, and negative pressure equivalent mass inside the shell counters positive pressure equivalent mass in the volume. With no net pressure at the fermion surface, no force acts to increase or decrease fermion size, as necessary for stable fundamental fermions identified as Godel solutions within our universe.

Fermion spheres with radius $\frac{l}{4}$ and core radius l_p have moment of inertia $I = \frac{2}{5} \frac{m}{2} \left(\frac{l}{4}\right)^2 + \frac{2}{3} \frac{\pi}{4} S l^2 \left(\frac{l}{4}\right)^2 + \frac{1}{2} L l l_p^2$, with negligible last term because $l_p \ll l$. Angular velocity $\omega = \frac{\hbar}{2I} = \frac{8c}{0.2l - l_N}$ and tangential speed of points on the spherical shell equator as a multiple of the speed of light $\frac{v_T}{c} = \frac{\omega l}{4c} = \frac{2l}{0.2l - l_N}$. $\frac{v_T}{c} > 1$ for lowest mass fermions in each charge state, allowing closed time-like curves within those Godel solutions, is acceptable in fundamental fermions unchanging from creation to annihilation. From Equation (2), $\frac{G_f}{G} = \frac{3l^4}{l_p^2 (0.2l - l_N)^2}$.

Ground state fundamental fermions, the constituents of atoms and molecules, differ from higher mass fundamental fermions in the same charge state by having core mass less than total mass, tangential speeds $\frac{v_T}{c} > 1$, and larger internal gravitational constants. With fine structure constant $\frac{e^2}{\hbar c} = \frac{1}{137}$, electrostatic potential energy of fundamental fermions from repulsion between equal surface charges near the rotation axis is $\left(\frac{ne}{6}\right)^2 \bigg/ \left(\frac{l}{2}\right) = n^2 \frac{me^2}{9\hbar c} = n^2 \frac{m}{1233}$. If electrostatic potential energy is the same for all charged ground state fundamental fermions and electron mass $m_e = 0.511$ MeV, up quark mass $m_u = 4m_e = 2.04$ MeV and down quark mass $m_d = 9m_e = 4.60$ MeV, well within quark mass error bars. All charged fundamental fermion masses and charges then relate to electron charge and mass.

Treating massive Standard Model bosons as Godel solutions is simpler than for fermions. W^\pm and Z bosons can be described as uniform spheres rotating around a core, with radius l_p , surrounding the spin axis. Again, core term contribution is negligible, so the moment of inertia is approximately $I = \frac{2}{5} m r^2$, where r is boson radius $\frac{l}{4}$. Fundamental bosons have angular momentum $\hbar = I\omega$, so their angular velocity is $\omega = \frac{40\hbar}{ml^2} = 40 \frac{c}{l}$ and Equation (2) results in

$\frac{G_i}{G} = \frac{25}{3} \left(\frac{l}{l_p} \right)^2$. Higgs bosons can be treated as static Einstein solutions of general

relativity with matter energy density ρc^2 and positive vacuum energy density $\frac{1}{2} \rho c^2$, opposite the negative vacuum energy density of Gödel solutions. The

Friedmann equation for radius of such closed, homogeneous, isotropic systems with internal gravitational constant G_i is

$$\left(\frac{dR}{dt} \right)^2 - \frac{8\pi G_i}{3} \left[\rho c^2 \left(\frac{R_0}{R} \right)^3 + \frac{1}{2} \rho c^2 \right] \left(\frac{R}{c} \right)^2 = -c^2, \text{ with } \frac{dR}{dt} = 0, R = R_0 = \frac{l_H}{4}, \text{ and}$$

Higgs Compton wavelength l_H , resulting in $\frac{G_i}{G} = \frac{1}{12} \left(\frac{l_H}{l_p} \right)^2$.

4. Magnetic Moments of Fundamental Particles

Magnetic moments of fundamental particles with fractional charge fe , mass m ,

and spin $s\hbar$ are approximately $\mu = \frac{fes\hbar}{m}$ [8]. Fractional charge fe circling

the spin axis at distance l_p from the axis, with velocity v , produces a current

$$I = \frac{fev}{2\pi l_p}. \text{ Treating particle cores as solenoids with } N \text{ turns surrounding the}$$

spin axis, charged fundamental fermions and bosons have magnetic moment

$$\frac{N}{2} fevl_p \text{ and } N = \frac{2s\hbar}{vml_p}. \text{ So, electrons require } N = \frac{(0.2l - l_n)\hbar}{8mcl_p^2}.$$

Conflicts of Interest

The author declares no conflicts of interest regarding the publication of this paper.

References

- [1] Mongan, T.R. (2011) Dark Matter from “Strong Gravity”—Consistent with CRESST, CoGenT, and DAMA/LIBRA. <https://arxiv.org/abs/0706.3050>
- [2] Elbaz, E., Novello, M., Salim, J.M., Motta da Silva, M.C. and Klippert, R. (1997) *General Relativity and Gravitation*, **29**, 481-487. <https://doi.org/10.1023/A:1018834800025>
- [3] Novello, M., Salim, J.M., Motta da Silva, M.C. and Klippert, R. (1996) *Physical Review D*, **54**, 6202. <https://doi.org/10.1103/PhysRevD.54.6202>
- [4] Schiff, L.I. (1995) *Quantum Mechanics*. 2nd Edition, McGraw-Hill, New York.
- [5] Hennawi, J.F. and Ostriker, J.P. (2002) *The Astrophysical Journal*, **572**, 41. <https://doi.org/10.1086/340226>
- [6] Kelso, C., Hooper, D. and Buckley, M. (2012) *Physical Review D*, **85**, Article ID: 043515. <https://arxiv.org/abs/1110.5388>
- [7] Nickalls, R. (1996) *The Mathematical Gazette*, **77**, 354-359. <https://doi.org/10.2307/3619777>
- [8] Holstein, N. (2006) *American Journal of Physics*, **74**, 1104. <https://doi.org/10.1119/1.2345655>

Theoretical Evidence for Wave Nature of Micro Particle and New Theory of Its Collective Motion in Material

Takahisa Okino

Department of Applied Mathematics, Faculty of Science & Engineering, Oita University, Oita, Japan
Email: okino@oita-u.ac.jp

How to cite this paper: Okino, T. (2021) Theoretical Evidence for Wave Nature of Micro Particle and New Theory of Its Collective Motion in Material. *Journal of Modern Physics*, 12, 260-283.
<https://doi.org/10.4236/jmp.2021.123020>

Received: January 2, 2021

Accepted: February 20, 2021

Published: February 23, 2021

Copyright © 2021 by author(s) and Scientific Research Publishing Inc.
This work is licensed under the Creative Commons Attribution International License (CC BY 4.0).

<http://creativecommons.org/licenses/by/4.0/>



Open Access

Abstract

Since a material is composed of micro particles, investigating behavior of those particles is essentially dominant for materials science. The diffusivity of diffusion equation is relevant to not only a collective motion of micro particles but also a motion of single particle. An elementary process of diffusion was thus theoretically investigated in a local space and time. As a result, the investigation concluded that the wave nature of micro particle results from denying the mathematical density theorem of a real time in the Newton mechanics. In other words, the basic theory of quantum mechanics is established in accordance with the cause-and-effect relationship in the Newton mechanics, for the first time, regardless of the de Broglie hypothesis. In relation to the collective motion of micro particles, the new diffusion theory was also reasonably established using the universal expression of diffusivity obtained here. In the present paper, the new findings indispensable for the fundamental knowledge in physics are thus systematically discussed in accordance with the theoretical frame in physics.

Keywords

Diffusion, Fick's Laws, de Broglie's Hypothesis, Schrödinger's Equation, Matter-Wave

1. Introduction

There is occasionally an important relation in natural phenomena where it is universally valid under a given condition. When we cannot reveal the theoretical evidence, it has been accepted as a law or a principle in physics. Further, the equation derived theoretically from its law or principle has been accepted as a basic

one in physics, where it corresponds to a theorem in mathematics. In accordance with such theoretical frame, physics has developed until now.

The basic theory in physics lies in Newton's laws established under the condition of having the common time between arbitrary coordinate systems. Einstein's relativity [1], which is one of the modern physics, was established in 1905 by denying the absolute time in the Newton mechanics in accordance with the constant principle of light speed c . However, Newton's laws are still acceptable as dominant ones in physics under the condition of $v \ll c$, where v is a speed of a body with mass m .

On the other hand, the quantum theory, which is the other modern physics, was established by accepting the de Broglie hypothesis [2] of

$$mv = p = h/\lambda, \quad (1)$$

where h, λ are the Planck constant [3] and a wave length of matter-wave defined here. In the Newton mechanics, both the particle nature and wave one are not simultaneously accepted. The conception of matter-wave is thus extremely novel. We had not understood the cause-and-effect relationship between the Newton mechanics and the quantum mechanics until recently. In the following, it will be thus revealed that the quantum mechanics is theoretically established by denying the mathematical density theorem of a real time in the Newton mechanics.

In 1923, de Broglie assumed that the result mc^2 of Einstein's relativity and the photon energy $h\nu$ of the Planck theory relevant to a light of frequency ν are equivalent to each other. Further, he assumed that c/ν corresponds to λ of a matter-wave, if we accept the replacement of $c \rightarrow v$ in the relation $mc = h\nu/c$ obtained here. After that, the experimental results revealed that an electron has an intrinsic nature like a wave [4]. In relatively recent years, the experimental results revealed that an atom or a molecule has also an intrinsic nature like a wave [5]. However, we did not confirm whether such a micro particle satisfies Equation (1) or not, even if it had an intrinsic nature like a wave. Further, we did not understand the theoretical evidence that a micro particle in the Newton mechanics has a wave nature.

For a micro particle with mass m , the wave equation $\Psi(t, x, y, z)$ given by

$$i\hbar \frac{\partial}{\partial t} \Psi(t, x, y, z) = -\frac{\hbar^2}{2m} \langle \tilde{\nabla} | \nabla \rangle \Psi(t, x, y, z) \quad (2)$$

was derived by Schrödinger in 1926 from Equation (1) [6]. It was revealed that the Schrödinger Equation (2) is applicable to behavior of an arbitrary micro particle. This indicates indirectly that Equation (1) is valid for those micro particles. As far as Equation (2) is derived from Equation (1), however, understanding of the correlation between the quantum mechanics and the Newton mechanics is essentially impossible. Therefore, the correlation between them has been understood as an afterthought for a long time by using the correspondence principle between a physical quantity in the Newton mechanics and the corresponding operator in the quantum mechanics. From a viewpoint of the theoretical frame in the fundamental physics, therefore, the quantum theory is still incom-

plete, as far as the cause-and-effect relationship between the quantum mechanics and the Newton mechanics is not revealed.

For a collective motion of micro particles in the space-time (t, x, y, z) , Fick's first law relevant to the diffusion flux $|J_F\rangle$ given by

$$|J_F\rangle = -D|\nabla\rangle C \quad (3)$$

was proposed in 1855, where $C(t, x, y, z)$ and D are a concentration of micro particles and a diffusivity [7]. Fick's second law was accepted as a nonlinear partial differential equation of

$$\Omega C = 0, \text{ for } \Omega = \frac{\partial}{\partial t} - \langle \tilde{\nabla} | D \nabla \rangle, \quad (4)$$

where $\langle \tilde{\nabla} | = -|\nabla\rangle^\dagger$ is used because of the Hermite conjugate of the Dirac bracket for a differential operator. In physics, Equation (3) shows that the diffusivity D is a proportional factor of a concentration gradient to the diffusion flux $|J_F\rangle$. In mathematics, Equation (4) shows that D is an operator in the operator Ω . As far as we accept Equations (3) and (4), therefore, we cannot understand the physical essence of D from their equations.

Here, the new findings are as follows.

1) The diffusion equation, having been accepted as the Fick second law since 1855, was theoretically derived from the mathematical theory of Markov's process [8] [9] [10]. It was then found that the elementary quantity of diffusivity D corresponds to the angular momentum and is expressed as $D = \hbar/2m$ [11] [12] [13]. The universal expression of diffusivity, which is applicable to any diffusion problem, was also derived.

2) The diffusion equation using $D = \hbar/2m$ for a micro particle in an isolated local space was transformed into the wave Equation (2) of Schrödinger by denying the mathematical density theorem of a real time in the Newton mechanics [11] [12] [13]. The wave nature of an arbitrary micro particle was, for the first time, theoretically revealed in accordance with the cause-and-effect relationship between the quantum mechanics and the Newton mechanics. Further, it was theoretically revealed that Equation (1) of matter-wave is not a hypothesis but a basic equation in physics [12] [13].

3) The general solutions of nonlinear diffusion equation, which had never been solved since 1855, were reasonably obtained [14]. As a result, the new diffusion theory of a multi-components system was reasonably established in relation to the transformation from a diffusion equation of a moving coordinate system into that of a fixed one, and vice versa [9] [10].

As far as a material is composed of micro particles, investigating behavior of those particles is indispensable for research subjects in the materials science. In the following, it will be theoretically confirmed that the theory of diffusion plays an important role for fundamental problems in the materials science.

2. Theoretical Frame in Classical Quantum Theory

From a viewpoint of theoretical frame in physics, fundamental problems in the

classical quantum theory are briefly discussed in accordance with a time series in the following.

In the space-time (t, x, y, z) , the Markov process [8] in mathematics is applicable to such behavior as a collective motion of micro particles in an isolated physical system. As a result, the diffusion equation of

$$\frac{\partial}{\partial t} C(t, x, y, z) = D \langle \tilde{\nabla} | \nabla \rangle C(t, x, y, z) \quad (5)$$

was theoretically obtained as a nonlinear partial differential equation [9] [10]. In the isolated local space, the diffusivity D relevant to a micro particle with mass m is then obtained as

$$D = \frac{(\Delta r)^2}{2\Delta t} = \frac{\Delta r p}{2m}, \text{ for } r = \sqrt{x^2 + y^2 + z^2}, \quad (6)$$

where $p (= mv)$ is a momentum of micro particle. Equation (6) shows that the diffusivity satisfies the relation of parabolic law. Further, a micro particle in the isolated local space has an angular momentum because of the term $\Delta r p$. In other words, the micro particle makes a circuit on the surface of isolated local space. This corresponds to phenomena known as a lattice vibration or a thermal vibration of atoms in a material.

The diffusion Equation (5) derived here is a moving coordinate system judging from the derivation process. It will be revealed that we can transform it into the relation (4) of a fixed coordinate system, and vice versa. It will be also revealed that the diffusivity expression obtained here plays a complementary role for incompleteness of the theoretical frame in the quantum theory.

As seen from the atomic hypothesis of Dalton in 1803 and the law of Avogadro in 1811, the chemists in those days thought that a material is composed of atoms or molecules as fundamental particles. On the other hand, the velocity distribution function of Maxwell in 1859 or Boltzmann in 1968 was reported in physics as a problem of mechanical elastic collision between these fundamental particles. The theoretical frame developed here was relevant to a theory between the thermodynamics and the Newton mechanics, where the averaged impulse resulting from collisions between micro particles corresponds to a thermodynamic pressure of macro quantity in physics. Further, the equipartition of energy reported in 1876 was the theory that a mechanical energy of micro particle corresponds to an absolute temperature of macro quantity in the thermodynamic state [15].

By assuming a micro particle as a component of material, it seemed in those days that the equipartition of energy reveals what a material is composed of fundamental particles. However, it was found that the equipartition of energy cannot explain the theory of specific heat in a low temperature region. In the end of 19 century, therefore, there was no such firm theory in physics that a material is composed of atoms and/or molecules as fundamental particles.

In circumstances mentioned above, Planck in 1900 [3] reported the theoretical relation indicating what the light of electromagnetic wave has a nature like a

particle. We cannot originally accept a picture having simultaneously a particle nature and a wave one in the classical physics. After that, however, Einstein in 1905 [16] and Compton in 1923 [17] revealed that the light has both a wave nature and a particle one.

On the other hand, in relation to the Brown motion relevant to a random movement of pollen in water, Einstein in 1905 [18] revealed that the self-diffusion phenomena of water molecules are visualized by behavior of pollen. In other words, the relation of diffusivity obtained here shows that a material is composed of atoms and/or molecules as fundamental particles. As mentioned later in a head of Einstein's paradox, however, there is a problem in the theoretical frame developed then. In addition, Langevin in 1908 [19] also derived a similar relation to Einstein's theory from analyzing an equation of motion for a micro particle.

In accordance with the empirical equation of radiant light reported by Balmer in 1885 [20], Bohr in 1913 [21] proposed a model of atomic structure under the quantum condition and the frequency condition. In the model, an electron moves on a specific circular orbit r_n ($n=1,2,\dots$) around the nucleus and it jumps from an orbit to an adjacent orbit through the radiation or absorption of energy $\Delta E = h\nu$. Using a momentum p of electron, the notation

$$\Delta r = r_n - r_{n-1} \quad (r_0 = 0) \quad \text{and the angular momentum } |L\rangle \text{ yielding}$$

$$|L\rangle = |r \times p\rangle \rightarrow |\Delta L\rangle = |r_n \times p_n\rangle - |r_{n-1} \times p_{n-1}\rangle, \quad \Delta L = \sqrt{\langle \Delta L | \Delta L \rangle},$$

the quantum condition is rewritten as

$$\Delta L = \Delta r p = \hbar. \quad (7)$$

After the Bohr model, the experimental results of Frank and Hertz in 1914 [22] suggested that an electron of the Bohr model moves on a specific circular orbit around the nucleus concerned. Further, it was experimentally revealed that the electronic beam has diffraction phenomena of a wave characteristic [4]. Based on the experimental results, it is considered that an electron of the Bohr model has a wave nature as a matter-wave. When an electron of the Bohr model satisfies the relation of

$$\lambda = 2\pi\Delta r, \quad (8)$$

it moves stably on a specific circular orbit as a stationary wave. Here, if we eliminate Δr from Equations (7) and (8), Equation (1) reasonably obtained.

It was thus found that Equation (1) is valid for an electron of the Bohr model. Here, we think the function φ of progressive wave in the space-time $(t, |r\rangle)$ given by

$$\varphi = A \exp[i(\langle k | r \rangle - \omega t)], \quad (9)$$

where the notations $A, \langle k |$ and ω are an amplitude of vibration of a frequency ν , a wave number vector of $k = \sqrt{\langle k | k \rangle} = 2\pi/\lambda$ relevant to a wave length λ and angular velocity of $\omega = 2\pi\nu$. In that case, Equations (1), (7) and (8) satisfy the relation $k = 2\pi/\lambda = 1/\Delta r$ relevant to the progressive wave then. It was thus

confirmed that Equation (1) is valid also for a motion of free electron. At this point, as far as we discuss the motion of an electron, Equation (1) is not a hypothesis but a basic equation in accordance with the theoretical frame in physics.

In circumstances mentioned above, de Broglie in 1923 [2] proposed Equation (1) as a hypothesis applicable to an arbitrary micro particle. After that, Schrödinger in 1926 [2] derived a wave Equation (2) from using Equation (1). It was found that the Schrödinger equation is applicable to behavior of an arbitrary micro particle. The Schrödinger equation is directly derived from the relation of matter-wave then. The theoretical evidence that a micro particle in the Newton mechanics has a wave nature has never been revealed since 1926. The theoretical frame of the quantum mechanics is thus still incomplete without revealing the causality for the Newton mechanics.

3. Consistency of Quantum Theory with Basic Theory in Physics

The basic idea in physics lies in the Newton mechanics. For example, Einstein's relativity was established by denying the absolute time in the Newton mechanics. In the following, it will be revealed that we can establish the quantum theory by denying the mathematical density theorem of a real time in the Newton mechanics.

As a formal problem between Equations (2) and (5), if we rewrite $D \rightarrow i\hbar/2m$ and $C \rightarrow \hbar\Psi$ in Equation (5), it is transformed into Equation (2). If the transformation from the diffusion equation relevant to a picture of micro particles into the wave equation of Schrödinger relevant to a wave picture is theoretically possible, we can then obtain the evidence that a micro particle in the Newton mechanics has a wave nature. In history, therefore, the transformation from Equation (5) into Equation (2) was investigated by the giant figures in physical society like Einstein, Bohm and others. However, the attempt was not successful. It is considered that the root cause of failure lies in having accepted the diffusion equation as a law of Fick without physical essence of diffusivity.

Here, the Fick second law shows that the diffusivity is related to a micro particle in the diffusion region. Nevertheless, we cannot grasp the physical essence of diffusivity relevant to a micro particle from the Fick laws. About that matter, as mentioned above, Okino began by deriving the diffusion equation from the mathematical theory of Markov process in order to grasp the physical essence of diffusivity. In the following, the fundamental theory in physics will be developed using Equation (6) obtained then.

Applying the equipartition of energy to a free electron in a material gives the relation of

$$\Delta rp = \alpha (k_B T + \varepsilon) \Delta t, \quad (10)$$

where k_B , ε and α are the Boltzmann constant, a correction term for the uncertain principle at $T = 0$ and a degree of freedom of micro particle, for example, $\alpha = 3$ in case of a mono-atomic molecule. Since the free electron satisfies

also the relation of $\Delta r p = \hbar$, $\Delta t (= \hbar / \alpha (k_B T + \varepsilon))$ depends only on an absolute temperature. Here, note that there is no characteristic quantity of a free electron in Equation (10) in spite of the discussion about the free electron itself. This means that Equation (10) is valid also for an arbitrary micro particle in a material [13] when the equipartition of energy is applied to it. It is, therefore, revealed that Equation (7) of

$$\Delta L = \Delta r p = \hbar$$

becomes also valid for an arbitrary micro particle in a material [11] [12] [13].

By substituting Equation (7) into Equation (6), the elementary quantity of diffusivity yielding

$$D = \frac{\Delta L}{2m} = \frac{\hbar}{2m} \quad (11)$$

is obtained in the isolated local space. In the following, the wave nature of an arbitrary micro particle will be revealed using Equation (11).

When d is a distance between two micro particles A and B of the same kind in the isolated local space, it is necessary to observe a reflected light of wave length $\lambda < d$ for the discrimination of A from B. If d is very small, a high energy of $\hbar c / \lambda$ is necessary for the discrimination. As a result, we cannot then discriminate them because of a turbulence caused by the high energy. In that situation, we consider an elastic collision problem between the above micro particle A and B in the following, where the particle A moves with a velocity $v_A = v_0$ and the particle B is in the rest state of the velocity $v_B = 0$.

If we can identify the difference between the micro particles A and B in the space and time given by $(\Delta t_A, \Delta r_A)$ and $(\Delta t_B, \Delta r_B)$, the particle A reaches $v_A = 0$ from a velocity $v_A = v_0$ with the acceleration $a_A = -\infty$ because of $\lim_{\Delta t_A \rightarrow 0} \left\{ \Delta r_A / (\Delta t_A)^2 \right\}$ and subsequently the particle B reaches $v_B = v_0$ from the velocity $v_B = 0$ with the acceleration $a_B = \infty$ because of $\lim_{\Delta t_B \rightarrow 0} \left\{ \Delta r_B / (\Delta t_B)^2 \right\}$.

On the other hand, if we cannot identify the difference between them, it seems that the particle A reaches $v_A = 0$ from a velocity $v_A = v_0$ with the acceleration $a_A = -\infty$ and subsequently the particle A reaches $v_A = v_0$ again from the velocity $v_A = 0$ with the acceleration $a_A = \infty$. For the behavior of the particle A in the collision time Δt_C between $0 < \Delta t_C < \Delta t_A + \Delta t_B$, the acceptance of $a_A = \infty$ between $0 < \Delta t < \Delta t_B$ indicates that we must accept the relation of $\Delta t \rightarrow i\Delta t$ in accordance with the definition of acceleration $\lim_{\Delta t \rightarrow 0} \left\{ \Delta r / (\Delta t)^2 \right\}$, resulting from the impossibility of the discrimination of A from B between $0 < \Delta t < \Delta t_B$ [11] [12] [13].

The matter mentioned here is equivalent to denying the mathematical density theorem of a real time in the Newton mechanics. In other words, there is a minimum unit time ε_t as a real time and the relation of $\Delta t \rightarrow i\Delta t$ is reasonably acceptable in the region of $\Delta t < \varepsilon_t$ [11]. Generally, as can be seen from rewriting a partial differential equation into the difference equation, it means a re-

lation valid in a local space-time $(\Delta t, \langle \Delta r |) = (\Delta t, \Delta x, \Delta y, \Delta z)$. The relation of $\Delta t \rightarrow i\Delta t$ is thus valid only in such a local space-time. If $t \rightarrow it$ is valid, the general solution of partial differential equation becomes not a complex value function but a complex function then.

In accordance with the discussion mentioned above, accepting the impossibility of discrimination between two particles of the same kind in a local space corresponds to accepting the relation of differential operator given by

$$\frac{\partial}{\partial t} = \lim_{\Delta t \rightarrow 0} \frac{\Delta}{\Delta t} \rightarrow \lim_{\Delta t \rightarrow 0} \frac{\Delta}{\pm i \Delta t} = \mp i \frac{\partial}{\partial t}$$

in the present theory. It was revealed that there is no conception of acceleration for a motion of micro particle in a local space [13]. As shown in the relation of matter-wave, however, the conception of velocity is still valid in a local space. Therefore, judging from the correlation between differential operators expressed by

$$\frac{1}{v_x} = \lim_{\Delta t \rightarrow 0} \frac{\Delta t}{\Delta x} = \frac{\partial}{\partial x} t \rightarrow \lim_{\Delta x \rightarrow 0} \frac{\pm i \Delta t}{\Delta x} = \pm i \frac{\partial}{\partial x} t,$$

the relation of differential operator of

$$\frac{\partial}{\partial x} \rightarrow \pm i \frac{\partial}{\partial x}$$

should be consequently valid. It will be found that the imaginary operator shown here corresponds to a real eigenvalue of the Hermite operator. In addition, as seen from the above discussion, note that a local space is clearly real and $\Delta r \rightarrow \pm i \Delta r$ is not valid then.

A plus or a minus sign of the above imaginary operators is determined from eigenvalues of Equation (9). When $\pm i |\nabla\rangle$ operates on Equation (9), we determine $|\nabla\rangle \rightarrow -i |\nabla\rangle$ like the obtained eigenvalue corresponds to the direction of movement of progressive wave. In a similar manner, we determine $\frac{\partial}{\partial t} \rightarrow i \frac{\partial}{\partial t}$. Thus, the differential operators in the Newton mechanics corresponds to

$$\begin{cases} \frac{\partial}{\partial t} \rightarrow i \frac{\partial}{\partial t} \\ |\nabla\rangle \rightarrow -i |\nabla\rangle \end{cases} \quad (12)$$

in the quantum mechanics in accordance with the causality [11] [12] [13].

Substituting Equations (11) and (12) into Equation (5) yields the Schrödinger Equation (2) by rewriting $C \rightarrow \hbar \Psi$. In this case, it is revealed that Ψ becomes a complex value function then [11]. Judging from the transformation of the diffusion equation of micro particles into the wave equation of Schrödinger, at this point, it was theoretically revealed that an arbitrary micro particle has a wave nature. Therefore, Equation (8) of

$$\lambda = 2\pi \Delta r$$

is valid not only for a free electron but also for an arbitrary micro particle.

Hereinbefore, since it was theoretically revealed that Equations (7) and (8) are valid for an arbitrary micro particle, eliminating Δr from their equations yields the relation of matter-wave expressed by Equation (1). In accordance with the theoretical frame in physics, at this point, Equation (1) proposed by de Broglie as a hypothesis is now not a hypothesis but a basic equation in physics. Hereafter, the relation of matter-wave should not be thus named a hypothesis except the historical description.

In the above theoretical development, for a micro particle in a material, the relation of

$$\lambda = h / \sqrt{\alpha m (k_B T + \varepsilon)} \quad (13)$$

was obtained as a new expression of matter-wave [13]. It is considered that Equation (13) is applicable to the diffusion theory based on the matter-wave. For example, when the averaged distance between micro particles in a material is expressed as $2a$, a micro particle under the condition of $m < \hbar^2 / \alpha a^2 (k_B T + \varepsilon)$ cannot exist in a local space and it moves through interstices between micro particles while repeating collisions with other micro particles. As can be seen from the definition of diffusivity given by Equation (6), the behavior of such micro particles as satisfying $m < \hbar^2 / \alpha a^2 (k_B T + \varepsilon)$ should be expressed not by diffusion Equation (5) but by the wave equation expanded into the many-body problem in the quantum mechanics. As an example, the tunnel effect is known as such a case if the number of collision times is too few in a thin film.

In the past, the correlation between the quantum mechanics and the Newton mechanics has been discussed as an afterthought in accordance with the correspondence principle between an operator in the quantum mechanics and the corresponding physical quantity in the Newton mechanics. For example, the relations of a momentum p and energy E in the Newton mechanics have been accepted as

$$\begin{cases} p = -i\hbar\nabla \\ E = i\hbar\frac{\partial}{\partial t} \end{cases} \quad (14)$$

in the quantum mechanics. In accordance with the causality for the Newton mechanics discussed above, Equation (12) shows that Equation (14) is reasonably derived as

$$\begin{cases} p_x = h/\lambda_x = \frac{h}{2\pi\Delta x} \rightarrow \lim_{\Delta x \rightarrow 0} \hbar \frac{\Delta}{\Delta x}, & p_x = \hbar \frac{\partial}{\partial x} \rightarrow p_x = -i\hbar \frac{\partial}{\partial x} \\ E = h\nu = \frac{h}{2\pi\Delta t} \rightarrow \lim_{\Delta t \rightarrow 0} \hbar \frac{\Delta}{\Delta t}, & E = \hbar \frac{\partial}{\partial t} \rightarrow E = i\hbar \frac{\partial}{\partial t} \end{cases}$$

from $p_x = h/\lambda_x$ ($\lambda_x = 2\pi\Delta x$) and $E = h\nu$, ($\nu = 1/2\pi\Delta t$) in the present theory.

4. Importance of Derivation of Diffusion Equation

Hereinbefore, it was found that the theory of elementary process of diffusion

plays a dominant role for understanding a physical essence having been disregarded in the classical quantum theory. On the other hand, analyzing a diffusion equation relevant to a collective motion of micro particles has been widely performed as a basic theory in the materials science. In that situation, there are extremely serious misunderstanding problems in the existing diffusion theory having been widely accepted for a long time [23] [24]. In the following, therefore, the new diffusion theory will be developed in accordance with the general theory in the mathematical physics [9] [10].

1) *Theoretical frame of Fick's laws*

Fick proposed in 1855 that the thermal conduction equation derived by Fourier in 1822 is applicable to the diffusion phenomena for a collective motion of micro particles [7]. In that case, the Fick first law of diffusion flux $|J_F\rangle$ corresponding to the thermal flux of Fourier was then defined as Equation (3) of

$$|J_F\rangle = -D|\nabla\rangle C(t, x, y, z).$$

And the Fick second law of diffusion equation in a broad sense, corresponding to the thermal conduction equation of Fourier, was defined as Equation (4) of

$$\partial_t C(t, x, y, z) = \langle \tilde{\nabla} | D \nabla \rangle C(t, x, y, z).$$

It seems that the reason for the proposal of laws in those days results from the realization of parabolic law shown in experimental profiles of distribution relevant to a concentration as well as a temperature in a material.

When Fick's laws were proposed, Gauss's diversion theorem was already reported in 1813. As shown in the following, therefore, judging from the theoretical frame in physics, it is inadequate that we accept each of equations (3) and (4) as an independent law.

For a differentiable spatial vector $|A(x, y, z)\rangle$ in a region V within a single closed surface S , Gauss's diversion theorem shows that the correlation between a volume integral and a surface integral yielding

$$\iiint_V \langle \tilde{\nabla} | A \rangle dV = \iint_S \langle n | A \rangle dS \quad (15)$$

is valid, where $\langle n |$ is a unit vector perpendicular to a surface element dS .

When Gauss's diversion theorem is applied to a flux vector $|J(t, x, y, z)\rangle$ relevant to a physical quantity $C(t, x, y, z)$ per a unit volume in the region V , as far as there is no sink and source of $C(t, x, y, z)$ in the region V , the relation of

$$\iint_S \langle n | J(t, x, y, z) \rangle dS = -\iiint_V \frac{\partial}{\partial t} C(t, x, y, z) dV \quad (16)$$

is physically valid in relation to the law of material conservation. Equations (15) and (16) yield the well-known continuous equation given by

$$\frac{\partial}{\partial t} C(t, x, y, z) + \langle \tilde{\nabla} | J(t, x, y, z) \rangle = 0. \quad (17)$$

Here, we should mathematically consider a degree of freedom for a diffusion flux because of $\langle \tilde{\nabla} | J(t) \rangle = \langle \tilde{\nabla} | J_{\text{eq}} \rangle = 0$ for $|J(t)\rangle$ dependent only on a time

t and $|J_{\text{eq}}\rangle$ independent of the space-time. The diffusion flux should be thus expressed as

$$|J(t, x, y, z)\rangle = |J_{\text{F}}\rangle + |J(t)\rangle + |J_{\text{eq}}\rangle. \quad (18)$$

In the following, it will be revealed that $|J(t)\rangle$ and $|J_{\text{eq}}\rangle$ are indispensable for understanding diffusion phenomena [9] [10].

If we substitute Equations (3) or (18) into Equation (17), Equation (4) is reasonably obtained. Judging from the theoretical frame in physics, therefore, Equation (4) is not a law but a basic equation then, if we accept Equations (3) or (18) as a law. However, Fick's first law of Equation (3) is unsuitable as a universal law because of $|J(t)\rangle = |J_{\text{eq}}\rangle = 0$. On the other hand, if we accept Equation (4) as a law, Equations (3) or (18) is obtained by comparing it with Equation (17). In this case, Equations (3) or (18) is a basic equation judging from the theoretical frame in physics.

As mentioned above, the only diffusion Equation (4) would be accepted as a law relevant to diffusion phenomena in those days. At present, however, the diffusion Equation (4) is also not a law but a basic equation in physics because of the theoretical derivation [9] [10].

2) Theoretical expression of diffusivity

The diffusion Equation (5) was theoretically derived as a basic equation of moving coordinate system from a behavior of micro particle in an isolated local space. The diffusivity obtained here was expressed as Equation (6) then, and further it was also expressed as Equation (11) resulting from applying the equipartition of energy to a free electron in a material. In general, each of diffusion particles in local spaces is physically different conditions from each other. In a case where Equations (4) or (5) is applied to a whole diffusion region, we must consider a dependence of the space-time (t, x, y, z) on the diffusivity. However, a thermal effect on a diffusion particle in a material and a mechanical interaction between a diffusion particle and the surrounding other micro particles have not been incorporated into Equations (6) or (11) yet.

For a micro particle in a state of activation energy Q in a material at a temperature T , we incorporate the Boltzmann factor $\exp[-Q/k_{\text{B}}T]$ relevant to an existence probability of the diffusion particle into Equation (11) [25]. When a micro particle interacts with the surrounding other particles, we also incorporate the potential energy U of an external force $|F\rangle$ operating on the micro particle into the Boltzmann factor. The universal expression of diffusivity is thus expressed as

$$D = \frac{\hbar}{2m} \exp\left[\frac{U-Q}{k_{\text{B}}T}\right], \quad U = -\int Fdr \quad \text{for} \quad Fdr = \langle F|dr\rangle. \quad (19)$$

Judging from Equation (6) in a local space, a jumping velocity $|v_{\text{p}}\rangle$ of a micro particle from a local space to another one is obtained as a diffusivity gradient of

$$|v_{\text{p}}\rangle = |\nabla\rangle D = -\frac{|F\rangle}{k_{\text{B}}T} D. \quad (20)$$

When there are N elements in a diffusion region, we assume a concentration C^j of a $j(=1,2,\dots,N)$ element, which is normalized by total number of diffusion particles. Rewriting the concentration and diffusivity of equation (4) into C^j and D^j , the diffusion equation of a j element becomes

$$\frac{\partial}{\partial t} C^j(t, x, y, z) = \langle \tilde{\nabla} | D^j \nabla \rangle C^j(t, x, y, z), \quad (21)$$

where the normalized condition of $\sum_{j=1}^N C^j = 1$ is valid, as far as there is no sink and source in the diffusion region.

For a k element among N elements in the diffusion region, the relation of

$$\sum_{j=1}^N \langle \tilde{\nabla} | (D^j - D^k) | \nabla \rangle C^j(t, x, y, z) = 0 \quad (22)$$

is valid because of the normalized condition of $\sum_{j=1}^N C^j = 1$. Since the term $|\nabla \rangle C^j$ in Equation (22) is linearly independent of each other, the relation of $D^j - D^k = 0$ is mathematically valid in Equation (22). In other words, the relation of

$$\tilde{D} = D^1 = \dots = D^j = \dots = D^N \quad (23)$$

is thus valid in interdiffusion problems for a N elements system. Here, note that Equation (23) means not a relation of physical diffusivities but that of mathematical operators valid only in Equation (21) [9] [10].

Equation (21) is thus rewritten as

$$\frac{\partial}{\partial t} C^j(t, x, y, z) = \langle \tilde{\nabla} | \tilde{D} \nabla \rangle C^j(t, x, y, z). \quad (24)$$

As a matter of course, when we substitute initial and/or boundary values of a j element into the general solution \tilde{D} of Equation (24), Equation (23) shows that the physical solution D^j is then obtained by the replacement of $\tilde{D} \rightarrow D^j$ and $D^j \neq D^k$ is valid if $j \neq k$.

3) General solutions of nonlinear diffusion equation

The general solutions of nonlinear diffusion equation had never been reported in the history of diffusion. In other words, even general solutions of the one-dimensional space yielding

$$\frac{\partial}{\partial t} C(t, x) = \frac{\partial}{\partial x} \left\{ D \frac{\partial}{\partial x} \right\} C(t, x) \quad (25)$$

had been impossible. In 1894, Boltzmann transformed Equation (25) into the nonlinear ordinary differential equation of

$$-\frac{\xi}{2} \frac{dC}{d\xi} = \frac{d}{d\xi} \left\{ D \frac{dC}{d\xi} \right\} \quad (26)$$

in the parabolic space $\xi = x/\sqrt{t}$ [26]. The general solutions of Equation (26) had never been also reported until recently [14] [27] [28].

Diffusion experiments have been widely performed using a diffusion couple

for the one-dimensional space. The essence of diffusion theory is still kept in even that case. In the following, therefore, the analytical theory of diffusion equation is developed in case of the space-time (t, x) . In that case, the normalized condition of $\sum_{j=1}^N C^j = 1$ mentioned above is valid on a cross section perpendicular to the diffusion direction, as far as the shape variation of diffusion specimen is negligible as usual experiments.

In accordance with the usual analytical method of differential equation, the general solutions of equation (26) were reasonably obtained as

$$D^\pm(\xi) = D_m - D_\Delta \operatorname{erf} \left(\frac{\xi}{2\sqrt{D_{\text{int}\pm}}} - \frac{\xi_{\text{IF}}}{2\sqrt{D_{\text{int}+}}} + \operatorname{erf}^{-1} \left(\frac{D_m - D_{\text{IF}}}{D_\Delta} \right) \right) \quad (27)$$

$$C^\pm(\xi) = C_m - C_\Delta \operatorname{erf} \left(\frac{\xi}{2\sqrt{D_{\text{int}\pm}}} - \frac{\xi_{\text{IN}}}{2\sqrt{D_{\text{int}-}}} + \operatorname{erf}^{-1} \left(\frac{C_m - C_{\text{IN}}}{C_\Delta} \right) \right). \quad (28)$$

in the previous work [14]. Here, the notation \pm corresponds to \pm of the parabolic coordinate $\xi (= x/\sqrt{t})$, where the origin $x = 0$ of a fixed coordinate system is set at the initial junction interface in a diffusion couple composed of materials A ($x < 0$) and B ($x > 0$). The physical constants in Equations (27) and (28) determined from an initial and/or boundary values of diffusivity and concentration at $\xi = \xi_A$ and $\xi = \xi_B$ in the diffusion region $\xi_A \leq \xi \leq \xi_B$ are as follows:

$$D_m = (D_A + D_B)/2, \quad D_\Delta = (D_A - D_B)/2,$$

$$C_m = (C_A + C_B)/2, \quad C_\Delta = (C_A - C_B)/2,$$

$$\xi_{\text{IF}} = 0, \quad \xi_{\text{IN}} = 2\sqrt{D_{\text{int}-}} (\sqrt{D_A} - \sqrt{D_B}) / (\sqrt{D_A} + \sqrt{D_B}), \quad D_{\text{IF}} = \frac{D_A - D_B}{\ln D_A - \ln D_B},$$

$$C_{\text{IN}} = C_m - C_\Delta \frac{D_m - D_{\text{IF}}}{D_\Delta}, \quad D_{\text{int}+} = \frac{D_A + D_B}{2}, \quad D_{\text{int}-} = \sqrt{D_A D_B}.$$

In addition, when the physical field around a diffusion particle is considered to be uniform, the diffusivity D is accepted as a physical constant D_0 . In that case, Equation (26) is rewritten as

$$-\frac{\xi}{2} \frac{dC}{d\xi} = D_0 \frac{d^2C}{d\xi^2}. \quad (29)$$

On the other hand, the diffusivity expression of Equation (27) then becomes

$$D_A = D_B = D_0 \rightarrow D^\pm(\xi) = D_0$$

and the concentration profile of Equation (28) is expressed as

$$C^\pm(\xi) \rightarrow C(\xi) = C_m - C_\Delta \operatorname{erf} \left(\frac{\xi}{2\sqrt{D_0}} \right). \quad (30)$$

Here, Equation (30) itself is the general solution of Equation (29). Therefore, the general solution of Equation (29) is included in those of Equations (27) and (28) as an especial case.

The uniqueness of mathematical solution of differential equation reveals that physical solutions are determined as having no alternative by substituting initial and/or boundary values into their general solutions. Therefore, if we substitute the initial and/or boundary values relevant to j element for interdiffusion problems of a N elements system into the general solutions of Equations (27) and (28), the physical solutions of j element among N elements are possible. The analytical problems of nonlinear diffusion were thus fundamentally solved. Further, when there is an inhomogeneous term in the given diffusion equation, it is necessary to obtain a particular solution relevant to the Green function for solving the differential equation, in addition to the general solutions of Equations (27) and (28).

The solutions of Equations (27) and (28) were already reported in 2011 [14]. Nevertheless, the importance has not yet been universally known to researchers. As mentioned later, there has been such a situation that misunderstanding theory is widely accepted for a long time in the existing diffusion field [24]. In the following, therefore, the application of Equations (27) and (28) to actual problems is briefly explained here.

In the diffusion experiments, we can obtain not a diffusivity profile but an only concentration profile. When the diffusivity is physically considered to be such a constant value as a case of a self-diffusion or an impurity-diffusion, we can determine the diffusivity unknown quantity by fitting Equation (30) to the concentration profile of j element obtained from experiments, using the given initial concentration values for Equation (30).

In general, a diffusivity of j element for a diffusion system of L elements in a material A depends on (t, x) in case of Equation (25). There had been no mathematical methods to determine a diffusivity of j element in a diffusion system of L elements. In accordance with the present method, however, D_A^j of j element in the material A is reasonably obtained by using Equations (27), (28) and (30).

Here, we suppose experiments of a diffusion couple, where it is smoothly jointed at an initial interface between the material A mentioned above and a pure material B composed of k element among L elements in the material A. As a matter of course, the initial value of concentration C_A^j of j element in the material A is known. In that case, the diffusivity values applicable to initial and/or boundary ones in the material B are determined as

$$D_B^l = D_{\text{imp}}^l(\text{B}), \dots, D_B^k = D_{\text{self}}^k(\text{B}), \dots, D_B^j = D_{\text{imp}}^j(\text{B}), \dots, D_B^l = D_{\text{imp}}^l(\text{B})$$

by fitting Equation (30) to concentration profiles obtained from usual experiments for an impurity diffusion of $j(\neq k)$ element and a self-diffusion of k element in the pure material B, regardless of the present diffusion couple.

Subsequently, if we substitute the diffusivity $D_B^j = D_{\text{imp}}^j(\text{B})$ or $D_B^k = D_{\text{self}}^k(\text{B})$ obtained above to Equation (28), the only diffusivity D_A^j or D_A^k is unknown value then, because of the given initial concentration C_A^j , $C_B^j = 0$ or C_A^k , $C_B^k = 1$. By fitting Equation (28) to the experimental concentration profile of j or

k in the present diffusion couple, the diffusivity value D_A^j or D_A^k is thus determined.

For a diffusion couple between the above material A and a new material B composed of M elements, we suppose that there are N ($L \leq N, M \leq N$) elements in the diffusion region. In that case, a diffusivity value D_B^k of k element in the material B is also determined by the analytical method mentioned above. Therefore, if $j = k$ is valid in the diffusion region, substituting the diffusivity values D_A^j, D_B^k determined here into Equation (27) gives a diffusivity profile in the diffusion system of N elements, and also substituting those diffusivity values and the given initial and/or boundary values C_A^j, C_B^k of concentration into Equation (28) yields a concentration profile.

If $j \neq k$ and $C_A^j = 0$ (or $C_B^k = 0$) is valid, by replacing the above diffusivity value D_A^j (or D_B^k) with a diffusivity value $D_{\text{imp}}^j(\text{A})$ (or $D_{\text{imp}}^k(\text{B})$), which is determined from experiments for an impurity diffusion of j (or k) element in the material A (or B), we can obtain the physical solutions of Equations (27) and (28).

For the analysis of interdiffusion problems, it is thus extremely important that the general solutions of Equations (27) and (28) are theoretically obtained.

4) Coordinate system of diffusion equation

Generally, there is no such a conception as a migration or a concentration for the space in physics. However, if we consider a thermodynamic influence on a material in the region V within a single closed surface S , the expanding or the shrinking S is physically conceived. In that case, the observer on the surface S seems that the space migrates relatively against the observer itself and the original region V changes.

For the diffusion region space except the volume of micro particles themselves in the diffusion region, the conception of a vacancy flux and a vacancy concentration is widely accepted also in the existing diffusion theory. The conception of a relative migration of diffusion region space and its rate for a whole diffusion region are thus physically accepted.

The diffusion flux $|J(t)\rangle$ of Equation (18), considered as a mathematical problem relevant to a degree of freedom resulting from applying $|J(t, x, y, z)\rangle$ dependent on time t to the Gauss divergence theorem, means a relative migration of diffusion region space. When the origin of a moving coordinate system $(t', x', y', z') = (t', |r'\rangle)$ moves with a velocity $|v\rangle$ against that of a fixed one $(t, x, y, z) = (t, |r\rangle)$, the relation of

$$|r\rangle = |r'\rangle + \int_0^{t'} |v\rangle dt + |r_0\rangle \quad (31)$$

is valid under the condition of $t' = t$ and $|r'\rangle = 0, |r\rangle = |r_0\rangle$ at $t' = t = 0$.

Using Equation (31), the relations between differential operators in their coordinate systems are expressed as

$$\partial_t = \partial_{t'} + \langle \tilde{v} | \nabla' \rangle, \quad |\nabla\rangle = |\nabla'\rangle. \quad (32)$$

Substituting Equation (32) into Equation (4) of

$$\frac{\partial}{\partial t} C(t, x, y, z) = \langle \tilde{\nabla} | D \nabla \rangle C(t, x, y, z)$$

expressed as a fixed coordinate system $(t, x, y, z) = (t, |r\rangle)$, the relation of

$$\begin{aligned} \frac{\partial}{\partial t'} C(t', x', y', z') &= \langle \tilde{v} | \nabla' \rangle C(t', x', y', z') + \left\{ \langle \tilde{\nabla}' | D \rangle | \nabla' \rangle + D \langle \tilde{\nabla}' | \nabla' \rangle \right\} C(t', x', y', z') \\ &= D \langle \tilde{\nabla}' | \nabla' \rangle C(t', x', y', z') + \left\{ \langle \tilde{v} | + \langle \tilde{\nabla}' | D \rangle \right\} | \nabla' \rangle C(t', x', y', z') \end{aligned} \quad (33)$$

is valid.

Since the diffusion region space itself is continuous and has no mass, the relation of

$$\langle \tilde{v} | + \langle \tilde{v}_p | = 0$$

is physically valid between $|v\rangle$ of Equation (31) and $|v_p\rangle$ of Equation (20). Thus, the second term in Equation (33) disappears because of $\langle \tilde{v}_p | = \langle \tilde{\nabla}' | D$, and Equation (33) becomes Equation (5) of

$$\frac{\partial}{\partial t'} C(t', |r'\rangle) = D \langle \tilde{\nabla}' | \nabla' \rangle C(t', |r'\rangle)$$

in the moving coordinate system. As a matter of course, the inverse transformation is also possible [9] [10]. At this point, Equation (4) is now not a law but a basic equation in physics because of the theoretical derivation of Equation (5).

Rewriting Equation (33) into

$$\frac{\partial}{\partial t'} C(t', x', y', z') - \langle \tilde{\nabla}' | \{ |v\rangle + D | \nabla' \rangle \} C(t', x', y', z') = 0,$$

and if we compare it with Equation (17), a diffusion flux $|J'\rangle$ of

$$|J'\rangle = |J_F'\rangle + |v_p\rangle C + |J_{eq}'\rangle \leftarrow |J_F'\rangle = -D | \nabla' \rangle C, \quad |v_p\rangle = -|v\rangle \quad (34)$$

is obtained as a moving coordinate system, using a diffusion flux $|J_{eq}'\rangle$ independent of the space-time. Further, when $|v\rangle = 0 (= -|v_p\rangle = 0)$ is valid in Equation (31), since the moving coordinate system $(t', x', y', z') = (t', |r'\rangle)$ is consistent with the fixed coordinate system $(t, x, y, z) = (t, |r\rangle)$ then, the diffusion flux of Equation (34) is rewritten as

$$|J\rangle = |J_F\rangle + |J_{eq}\rangle \quad (35)$$

in the fixed coordinate system.

The Brown motion reveals that micro particles move randomly also under the condition of concentration gradient zero like a pure material. As far as Equation (3) is accepted as a law, the theoretical equation of diffusion flux is impossible then, because of $| \nabla \rangle C = 0$. In the existing diffusion theory, therefore, the self-diffusion has been understood from diffusion phenomena of isotope elements of extremely small quantities introduced into a pure material concerned. In the strict sense of the word, however, that corresponds to a diffusion problem relevant to the impurity diffusion.

In the present diffusion theory, the theoretical equation of self-diffusion is given by

$$J_x(t, x, y, z) = -\int \partial_i C(t, x, y, z) dx, \text{ for } |J(t, x, y, z)\rangle = |J_{\text{eq}}\rangle, \quad (36)$$

where $J_x(t, x, y, z)$ is the x component of the diffusion flux $|J(t, x, y, z)\rangle$ [9] [23]. Therefore, judging from the discussion mentioned here, the diffusion flux $|J_{\text{eq}}\rangle$ is thus indispensable for understanding the diffusion theory in case of concentration gradient $|\nabla\rangle C = 0$.

The well-known Kirkendall effect (K-effect Δx_{eff}) reveals that the jointed interface of diffusion couple shifts from the initial position to the diffusion direction in the interdiffusion problems [29]. At the same time, the phenomena indicate that the diffusion region space migrates in a diffusion region. Further, the matter also indicates that the moving and fixed coordinate systems of diffusion equation are indispensable for understanding diffusion phenomena. In the following, the formative mechanism of the K-effect is discussed.

In case of the one-dimensional space for Equation (31), using the relation of

$$x = x' + \int_0^{t'} v_x dt \quad (37)$$

valid between the coordinate systems under the condition of $x = x' = 0$ on the initial interface jointed at $t = t' = 0$, the problem between the coordinate systems of diffusion equations is discussed in the following.

The solution of diffusion equation corresponds to a concentration profile of the experiments carried out at a high temperature T_E . On the other hand, experimental data are usually obtained at a room temperature T_R . In order to compare the solution with the corresponding experimental data, therefore, it is necessary to grasp a thermal behavior of the diffusion region space between $T_R \leq T \leq T_E$.

The number of diffusion particles diffusing for $x > 0$ direction is generally different from one diffusing for $x < 0$ direction. In other words, if vacancies are rich in the diffusion region of $x > 0$ compared to their thermal equilibrium values, they are poor in the diffusion region of $x < 0$, and vice versa. In the state of $T = T_E$ just after diffusion experiments, it is considered that the coordinate origin $x' = 0$ at $t = t' = 0$ shifts from the initial position $x = 0$ to $x = l_E$ at $t = t_E$ as given by

$$l_E = \int_0^{t_E} v_x dt. \quad (38)$$

Vacancies in the vacancy rich region diffuse into the vacancy poor region during the temperature fall of $T_E \rightarrow T_R$ like the diffusion region space reaches a thermal equilibrium state. In that case, it is also considered that a quantity Q of vacancies flows from a vacancy rich region to the specimen surface, because of the specimen surface of a sink of vacancies. At the same time, a quantity Q of vacancies flows from the specimen surface to a vacancy poor region, because of the specimen surface of a source of vacancies then.

The formative mechanism of the K-effect depends on a material characteristic

of a specimen used as a diffusion couple. In the above discussion, the K-effect is expressed by the relation of

$$\Delta x_{\text{eff}} = Q/S, \quad (39)$$

where S is a cross section of specimen used as a diffusion couple [30] [31] [32]. In addition, the theoretical equation of the K-effect yielding

$$\Delta x_{\text{eff}} = \alpha_{\text{eff}} (N-1) \sum_{j=1}^N \{C_A^j - C_B^j\} \sqrt{D_\gamma^j t} \quad (40)$$

is valid in accordance with the parabolic law then, where the suffix γ means $\gamma \rightarrow A$ if $C_A^j \geq C_B^j$ or $\gamma \rightarrow B$ if $C_A^j < C_B^j$ and α_{eff} is a parameter dependent on a material characteristic used for the diffusion couple [9].

5) Einstein's paradox

Using the van't Hoff law relevant to an osmotic pressure, the Stocks law in a fluid, and the Fick first law relevant to a diffusion flux, Einstein theoretically investigated behavior of the well-known Brown motion of pollen in water and he obtained the expression of diffusivity yielding

$$D = RT/kN_A, \quad (41)$$

where R , N_A and k are the gas constant, the Avogadro constant and a proportional constant of an external force $|F\rangle$ used as $|F\rangle = -k|v_p\rangle$ for a micro particle moving with a velocity $|v_p\rangle$. As a result, it was revealed that a self-diffusion of water molecules is visualized by the behavior of pollen. In other words, it was revealed that a material is composed of such a fundamental particle as an atom and/or a molecule.

Einstein conceived then that the diffusion flux $|J\rangle$ becomes

$$|J\rangle = |v_p\rangle C \quad (42)$$

under the condition of a mechanical equilibrium state for diffusion particles, where the diffusion particle moves with a velocity $|v_p\rangle$ during an interaction of $|F\rangle = -k|v_p\rangle$. Here, substituting Equation (42) into the continuous Equation (17) yields not the diffusion equation but the well-known Euler's equation in a liquid given by

$$\partial_t C = -\langle \tilde{\nabla} |v_p\rangle C. \quad (43)$$

The theoretical frame developed here by Einstein is apparently inconsistent. In the following, the Einstein's paradox is revealed as a problem of coordinate systems of diffusion equation.

There was no discussion about coordinate systems of diffusion equation in those days. The diffusion flux $|J\rangle = |v_p\rangle C$ used here should be accepted as $|J'\rangle = |v_p\rangle C$ of a moving coordinate system. In that case, $|J'_F\rangle + |J'_{\text{eq}}\rangle = 0$ is valid in Equation (34) and we have $|J'_F\rangle = 0$ then because of neglecting $|J'_{\text{eq}}\rangle$ in those days. Therefore, Einstein obtained Equation (41) in such a thermal equilibrium state that the relation of $\lim_{v_p \rightarrow 0} \{J'_F/v_p C\} = 1$ is valid.

In the present theory, Equation (41) is directly obtained from substituting

$|F\rangle = -k|v_p\rangle$ into Equation (20) because of $R = N_A k_B$. The present theory yields Equation (41) regardless of whether the diffusion system is in a thermal equilibrium state or not.

If we compare the present theory to a carved statue by single knife, Einstein's theory corresponds to one by assembling complicated pieces of wood. The matter discussed here gives evidence that the new diffusion theory is meaningful for a fundamental physics.

6) *Historical misunderstanding problems in diffusion theory*

In relation to having been no conception of a moving or a fixed coordinate system for diffusion equation, misunderstanding problems have been widely accepted in the existing diffusion theory. Further, in relation to analyzing a diffusion equation, mathematically wrong methods for solving a differential equation have been also widely accepted for a long time.

In the following, interdiffusion problems in case of $N = 2$ for Equation (24) are discussed in order to reveal misunderstanding problems.

As mentioned above, it is apparent that the discussion about a moving or a fixed coordinate system for diffusion equation is indispensable for understanding diffusion theory. The K-effect affords an experimental evidence for the correlation between those coordinate systems. Nevertheless, a relation of diffusion flux, which is similar to Equation (34) of a moving coordinate system, has been widely accepted as a fixed coordinate system in the existing diffusion theory [33].

In the history of diffusion, the relation of $\tilde{D} = D^I = D^{II}$ between operators in a differential Equation (24) was misunderstood as a relation of physical diffusivity in the interdiffusion problems. If the relation $D^I = D^{II}$ is accepted as a physical diffusivity, it was then considered that understanding of the K-effect is impossible. Thereupon, the wrong conception of intrinsic diffusion was caused for interdiffusion phenomena in those days. In other words, the new intrinsic diffusivities $D_{\text{in}}^I, D_{\text{in}}^{II}$ satisfying the relation $D_{\text{in}}^I \neq D_{\text{in}}^{II}$ were thus phenomenologically incorporated into the theory of interdiffusion problems.

Based on the conception of intrinsic diffusion, Darken proposed a relation of

$$\tilde{D} = D_{\text{in}}^I C^{II} + D_{\text{in}}^{II} C^I, \quad (44)$$

where \tilde{D} was accepted as not an operator but a physical diffusivity [34]. The so-called Darken equation has been widely used for numerical analyses of interdiffusion problems [35] [36] [37]. It was, however, reported that Equation (44) is not mathematically valid because of mathematical errors in the derivation process [24]. Before that, it is believed that such conception of an intrinsic diffusion is an illusion conceived in those days, judging from the conception of operator \tilde{D} and further from the physical essence of diffusivity resulting from the derivation of diffusion equation.

The misunderstood matters relevant to the K-effect, the intrinsic diffusion, the Darken equation, and *etc.* have been widely accepted for a long time in the diffusion field. In fact, they have been plausibly explained in the fundamental text-

books [38] [39]. Misunderstanding theory in the existing diffusion field causes thus serious problems for not only researchers but also students. It is, therefore, required that the existing fundamental textbooks are suitably revised as soon as possible, also taking account of problems of coordinate systems of the diffusion equation.

5. Discussion and Conclusions

As far as a material is composed of micro particles, investigating behavior of those particles is indispensable for research subjects in the materials science. In that case, the Schrödinger Equation (2) has been applied to the research subjects for a few micro particles. On the other hand, the diffusion Equation (4) has been applied to research subjects for a collective motion of micro particles relevant to the Avogadro constant. Here, note that the diffusivity of diffusion equation is a physical quantity relevant to a single micro particle in a material then. It is, therefore, reasonable that the diffusivity correlates with the Schrödinger equation.

The Newton mechanics gives a source of theories in physics. In the modern physics, Einstein's relativity was established by denying the absolute time in the Newton mechanics. On the other hand, the quantum theory of another modern physics was established regardless of the Newton mechanics in those days. After that, the correlation between the quantum mechanics and the Newton mechanics has been understood as an afterthought for a long time through the correspondence principle between the physical quantity in the Newton mechanics and the corresponding mathematical operators in the quantum mechanics.

Judging from the theoretical frame in physics, it is considered that the quantum theory is still incomplete without revealing the causality for the Newton mechanics. From a viewpoint of fundamental physics, it is necessary to reveal theoretical evidence for the wave nature of an arbitrary micro particle in accordance with the cause-and-effect relationship in the Newton mechanics.

The diffusion equation having been accepted as a law for a long time since 1855 is formally transformed into the Schrödinger equation as mentioned in the text. Since the diffusion equation shows that the diffusivity depends on behavior of a micro particle in an isolated local space in a material, the transformation of the diffusion equation into the Schrödinger equation is thus reasonably accepted. It is, however, apparent that the theoretical transformation is impossible as far as we accept the Fick laws as it is. Before investigating the theoretical transformation between them, therefore, we must first grasp the physical essence of diffusivity itself.

Recently, the diffusion Equation (5) was reasonably derived from the mathematical theory of Markov process. As a result, it was first theoretically revealed that the diffusivity D correlates to the angular momentum as expressed by $D = \hbar/2m$ for a micro particle with mass m in an isolated local space. In other words, it was found that a diffusion particle makes a circuit on the surface of a local space in a material.

On the other hand, it was also revealed that the impossibility of discrimination between two micro particles of the same kind in close vicinity to each other is equivalent to denying the mathematical density theorem of a real time in the Newton mechanics. It was thus revealed that the time t in the Newton mechanics has a time ε_t of minimum unit as a real time. In future, the conception of the time ε_t may be accepted as a dominant conception in the fundamental physics.

As a result, it was also revealed that the differential operators $\partial/\partial t$ and $|\nabla\rangle$ in the Newton mechanics becomes $i\partial/\partial t$ and $-i|\nabla\rangle$ in the quantum mechanics. By rewriting $\partial/\partial t \rightarrow i\partial/\partial t$, $|\nabla\rangle \rightarrow -i|\nabla\rangle$ and $D \rightarrow \hbar/2m$ in the diffusion Equation (5), the Schrödinger Equation (2) is reasonably obtained. At this point, for the first time in physics, the wave nature of an arbitrary micro particle was theoretically revealed through the transformation from the diffusion equation relevant to a picture of micro particle into the wave equation of Schrödinger relevant to a wave picture. We could thus reasonably understand the necessity of quantum theory for behavior of a micro particle in accordance with the cause-and-effect relationship in the Newton mechanics.

In addition, it was also revealed that the well-known relation of matter-wave is valid as not a hypothesis but a basic equation in physics. Further, the validity of the matter-wave Equation (1) was not only reasonably revealed but also the new Equation (13) was theoretically obtained. In future, Equation (13) will be useful for understanding behavior of micro particles in a material.

Further, the derivation of diffusion equation first revealed that a moving coordinate system as well as a fixed coordinate system for the diffusion equation is essentially indispensable for understanding diffusion phenomena. The discussion about coordinate system of diffusion equation indicated that the wrong theory of diffusion has been accepted for a long time in the existing field. Concretely, the conception of intrinsic diffusion coefficient supposed to understand the Kirkendall effect is not essentially accepted judging from the basic theory of mathematical physics. In accordance with the transformation theory between those coordinate systems and the general solutions of a nonlinear diffusion equation, the new diffusion theory was reasonably established.

In history, most of laws, principles, and basic equations in physics were yielded in Europe and they have been widely accepted in the world. In such circumstances, it was revealed in the Asia country that the equations having been accepted as Fick's laws and de Broglie's hypothesis for a long time are now basic ones in physics, and further that the wave nature of an arbitrary micro particle can be reasonably explained by the conception of a time ε_t of minimum unit as a real time in the Newton mechanics. The conception of a time ε_t recalls the old word “刹那 (*setuna*)” of oriental idea to our mind then.

The basic equations shown in **Figure 1** are ones described in the usual textbooks on physics. As a result, the Figure shows that the theoretical derivation of diffusion Equation (5) plays a dominant role for understanding not only a basic theory of diffusion but also a root evidence for the validity of quantum theory.

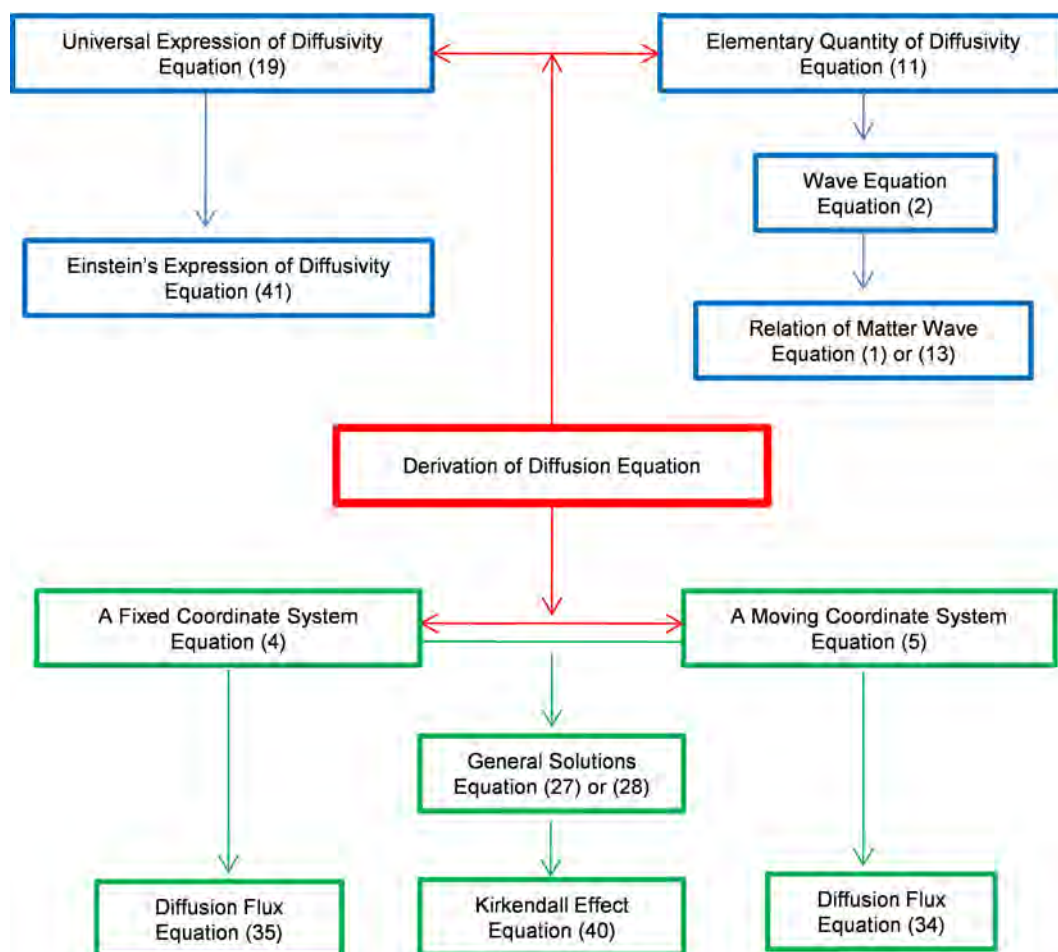


Figure 1. Basic equations resulting from derivation of diffusion equation. The basic equations, which should be accepted as new representations except the existing Equations (1), (2) and (4), are shown in the Figure. The derivation of diffusion equation is thus extremely meaningful in the fundamental physics.

From a viewpoint of the theoretical frame in physics, the matters discussed in the present paper are extremely fundamental ones as shown in the physical textbooks for students. We must have a responsibility to develop the physical truth in the textbooks. From a viewpoint of the physical education for younger people, therefore, we thus hope that researchers planning to write a fundamental textbook on physics would publish it taking account of the matters discussed above.

Conflicts of Interest

The author declares no conflicts of interest regarding the publication of this paper.

References

- [1] Einstein, A. (1905) *Annalen der Physik*, **17**, 132-148. <https://doi.org/10.1002/andp.19053220607>
- [2] de Broglie, L. (1923) *Nature*, **112**, 540. <https://doi.org/10.1038/112540a0>

- [3] Planck, M. (1900) *Verhandlungen der Deutschen Physikalischen Gesellschaft*, **2**, 237-245.
- [4] Thomson, G.P. (1927) *Nature*, **119**, 890. <https://doi.org/10.1038/119890a0>
- [5] Shimizu, F. (2000) *Physical Review Letters*, **86**, 987-990. <https://doi.org/10.1103/PhysRevLett.86.987>
- [6] Schrödinger, E. (1926) *Annals of Physics*, **79**, 361-376. <https://doi.org/10.1002/andp.19263840404>
- [7] Fick, A. (1855) *Philosophical Magazine*, **10**, 31-39. <https://doi.org/10.1080/14786445508641925>
- [8] Markov, A.A. (1960) *American Mathematical Society Translations Series 2*, **15**, 1-14. <https://doi.org/10.1090/trans2/015/01>
- [9] Okino, T. (2015) *Journal of Modern Physics*, **6**, 2109-2144. <https://doi.org/10.4236/jmp.2015.614217>
- [10] Okino, T. (2019) *Applied Physics Research*, **11**, 82-87. <https://doi.org/10.5539/apr.v11n1p82>
- [11] Okino, T. (2013) *Journal of Modern Physics*, **4**, 612-615. <https://doi.org/10.4236/jmp.2013.45088>
- [12] Okino, T. (2018) *Journal of Modern Physics*, **9**, 1007-1028. <https://doi.org/10.4236/jmp.2018.95063>
- [13] Okino, T. (2019) *International Journal of Fundamental Physical Sciences*, **9**, 48-54. <https://doi.org/10.14331/ijfps.2019.330131>
- [14] Okino, T. (2011) *Materials. Transactions*, **52**, 2220-2227. <https://doi.org/10.2320/matertrans.M2011137>
- [15] Boltzmann, L. (1876) *Wiener Berichte*, **74**, 533-560.
- [16] Einstein, A. (1905) *Annalen der Physik*, **17**, 891-921. <https://doi.org/10.1002/andp.19053221004>
- [17] Compton, A.H. (1922) *Physical Review*, **21**, 483-503. <https://doi.org/10.1103/PhysRev.21.483>
- [18] Einstein, A. (1905) *Annalen der Physik*, **18**, 549-560. <https://doi.org/10.1002/andp.19053220806>
- [19] Langevin (1908) *Comptes Rendus de Academie des Science (Paris)*, **146**, 530-533.
- [20] Balmer, J.J. (1885) *Annalen der Physik*, **261**, 80-87. <https://doi.org/10.1002/andp.18852610506>
- [21] Bohr, N. (1913) *Philosophical Magazine*, **26**, 1-25. <https://doi.org/10.1080/14786441308634955>
- [22] Frank, J. and Hertz, G. (1914) *Verhandlungen der Deutschen Physikalischen Gesellschaft*, **16**, 357-467.
- [23] Okino, T. (2012) *Journal of Modern Physics*, **3**, 1388-1393. <https://doi.org/10.4236/jmp.2012.310175>
- [24] Okino, T. (2013) *Journal of Modern Physics*, **4**, 1350-1353.
- [25] Boltzmann, L. (1872) *Wiener Berichte*, **63**, 275-370.
- [26] Boltzmann, L. (1894) *Annual Review of Physical Chemistry*, **53**, 959-964. <https://doi.org/10.1002/andp.18942891315>
- [27] Okino, T., Shimosaki, T., Fukuda, R. and Chou, H. (2012) *Defect and Diffusion Forum*, **322**, 11-31. <https://doi.org/10.4028/www.scientific.net/DDF.322.11>
- [28] Okino, T. (2012) *Journal of Modern Physics*, **3**, 255-259.

- <https://doi.org/10.4236/jmp.2012.33034>
- [29] Smigelskas, A.D. and Kirkendall, E.O. (1947) *Transactions of the Metallurgical Society of AIME*, **171**, 130-142.
- [30] Okino, T. (2014) *Applied Physics Research*, **6**, 1-7.
<https://doi.org/10.5539/apr.v6n2p1>
- [31] Okino, T., Chou, H. and Yamada, K. (2017) *Journal of Modern Physics*, **8**, 903-918.
<https://doi.org/10.4236/jmp.2017.86056>
- [32] Chou, H., Yamada, K. and Okino, T. (2018) *Journal of Modern Physics*, **9**, 130-144.
<https://doi.org/10.4236/jmp.2018.92009>
- [33] Manning, J.R. (1973) Theory of Diffusion. *Seminar of American Society for Metals*, Metal Park Ohio, 14 October 1974, 1-23.
- [34] Darken, L.S. (1948) *Transactions of the Metallurgical Society of AIME*, **175**, 184-201.
- [35] Hoshino, H., Iijima, Y. and Hirano, K. (1982) *Acta Materialia*, **21**, 674-682.
<https://doi.org/10.2320/matertrans1960.21.674>
- [36] Ke Haung, D., Keiser Jr., D. and Sohn, Y. (2013) *Metallurgical and Materials Transactions A*, **44**, 738-746. <https://doi.org/10.1007/s11661-012-1425-9>
- [37] Durand, A., Peng, L., Laplanche, G., Morris, J.R., Gerge, E.P. and Eggeler, G. (2020) *Intermetallics*, **122**, Article ID: 106789.
<https://doi.org/10.1016/j.intermet.2020.106789>
- [38] Shewmon, P.G. (1963) *Diffusion in Solids*. Series in Materials Science and Engineering, McGraw-Hill, New York.
- [39] Mehrer, H. (2007) *Diffusion in Solid*. Springer-Verlag, Berlin.

Quantization of the 1-D Forced Harmonic Oscillator in the Space (x, v)

Gustavo V. López, Omar J. P. Bravo

Departamento de Física, Universidad de Guadalajara, Blvd. Marcelino García Barragan y Calzada Olímpica, Guadalajara, Jalisco, México

Email: gulopez@cencar.udg.mx, hase12@hotmail.com

How to cite this paper: López, G.V. and Bravo, O.J.P. (2021) Quantization of the 1-D Forced Harmonic Oscillator in the Space (x, v) . *Journal of Modern Physics*, 12, 284-294.

<https://doi.org/10.4236/jmp.2021.123021>

Received: January 14, 2021

Accepted: February 22, 2021

Published: February 25, 2021

Copyright © 2021 by author(s) and Scientific Research Publishing Inc.

This work is licensed under the Creative Commons Attribution International License (CC BY 4.0).

<http://creativecommons.org/licenses/by/4.0/>



Open Access

Abstract

The quantization of the forced harmonic oscillator is studied with the quantum variable (x, \hat{v}) , with the commutation relation $[x, \hat{v}] = i\hbar/m$, and using a Schrödinger's like equation on these variable, and associating a linear operator to a constant of motion $K(x, v, t)$ of the classical system, The comparison with the quantization in the space (x, p) is done with the usual Schrödinger's equation for the Hamiltonian $H(x, p, t)$, and with the commutation relation $[x, \hat{p}] = i\hbar$. It is found that for the non-resonant case, both forms of quantization bring about the same result. However, for the resonant case, both forms of quantization are different, and the probability for the system to be in the excited state for the (x, \hat{v}) quantization has fewer oscillations than the (x, \hat{p}) quantization, the average energy of the system is higher in (x, \hat{p}) quantization than on the (x, \hat{v}) quantization, and the Boltzmann- Shannon entropy on the (x, \hat{p}) quantization is higher than on the (x, \hat{v}) quantization.

Keywords

Forced Harmonic Oscillator, (x, \hat{v}) Quantization, Constant of Motion

1. Introduction

The usual quantum mechanics formulation is done in the space (x, \hat{p}) [1], where $\hat{p} = -i\hbar\partial/\partial x$ is the linear operator associated to the classical generalized linear momentum of the motion of a particle of mass "m", where the commutation relation $[x, \hat{p}] = i\hbar$ [2] is satisfied. A linear operator is associated to the classical Hamiltonian, $\hat{H}(x, \hat{p}, t)$, to form the so called Schrödinger's equation [3]

$$i\hbar \frac{\partial \Psi}{\partial t} = \hat{H}(x, \hat{p}, t) \Psi, \quad (1)$$

where $\Psi = \Psi(x, t)$ is the wave function. This formulation has had enormous success to explain and to predict most microscopic behavior of the nature [4]. However, despite this enormous success, Hamiltonian-Lagrangian mathematical formulation has some details, even for 1-D problem where one knows that the Lagrangian (therefore the Hamiltonian) always exists [5]. First, from the expression to obtain the generalized linear momentum given the Lagrangian, $L(x, \dot{x}, t)$ for the system,

$$p(x, \dot{x}, t) = \frac{\partial L}{\partial \dot{x}}, \quad (2)$$

it is not always possible to obtain explicitly $\dot{x} = \dot{x}(x, p, t)$ to be able to get the explicit expression for the Hamiltonian from the Legendre's transformation [6],

$$H(x, p, t) = \dot{x}(x, p, t)p - L(x, \dot{x}(x, p, t), t). \quad (3)$$

Second, when one is dealing with classical dissipative systems [7],

$$\frac{d(mx)}{dt} = F(x, \dot{x}), \quad (4)$$

either it is not possible to find its Hamiltonian, or two different Hamiltonians are possible to find for the system [8] [9] [10] [11] [12]. Last one, for those problems of variable mass systems,

$$\frac{d(m(x, \dot{x}, t)\dot{x})}{dt} = F(x), \quad (5)$$

which are not invariant under Galileo's transformations and Sommerfeld modification is not consistent, to find the Hamiltonian for this system [13] requires to start from the "Inverse Problem of the Mechanics".

Therefore, one has the necessity to find some extension of the known quantization arised from the Hamilton-Lagrangian approach. In this way, there is already a proposition [14] [15] of using a function $K(x, v, t)$ that could be a constant of motion of the classical system, and to associate a linear operator to the velocity of the form

$$\hat{v} = -i \frac{\hbar}{m} \frac{\partial}{\partial x}, \quad (6)$$

such that $[x, \hat{v}] = i\hbar/m$, and to associate a linear operator

$$K(x, v, t) \rightarrow \hat{K}(x, \hat{v}, t), \quad (7)$$

which can be used to form the Shrödinger's like equation

$$i\hbar \frac{\partial \Psi}{\partial t} = \hat{K}(x, \hat{v}, t) \Psi. \quad (8)$$

The usual Quantum Mechanics is formulated through the Shrödinger's Equation (1), given in terms of the Hamiltonian associate to the system. However, in this paper, we intend to use the approach (8) as a possible alternative and extended way for the Quantum Mechanics, and this is done by studying the 1-D forced harmonic oscillator to determine whether or not there is a difference on

the quantization, and hopefully to see if the approach (8) could have with these result and experimental verification.

2. Analytical Approach for $K(x, v, t)$

The forced harmonic oscillator is classically characterized by Newton's equation

$$\frac{d(m\dot{x})}{dt} = -m\omega_0^2 x + \alpha \cos(\omega t + \varphi), \quad (9)$$

where “ m ” is the mass of the particle, ω_0 is the natural frequency of oscillation (when $\alpha = 0$), and α is the amplitude of the forced force. The well-known solution of this problem is

$$x(t) = \begin{cases} C_1 \cos \omega_0 t + C_2 \sin \omega_0 t + \frac{\alpha \cos(\omega t + \varphi)}{m(\omega_0^2 - \omega^2)}, & \omega \neq \omega_0 \\ C_1 \cos \omega_0 t + C_2 \sin \omega_0 t + \frac{\alpha \sin(\omega_0 t + \varphi)}{2m\omega_0}, & \omega = \omega_0 \end{cases} \quad (10)$$

where one has the non-resonant case ($\omega \neq \omega_0$) and the resonant case ($\omega = \omega_0$). The velocity is known by making the differentiation of (10) with respect the time, and the constants C_1 and C_2 are determined by the initial condition ($x(0), v(0)$). For the non-resonant case, these constants are

$$C_1 = x \cos \omega_0 t - \frac{v}{\omega_0} \sin \omega_0 t - \frac{\alpha}{m(\omega_0^2 - \omega^2)} \left\{ \cos(\omega t + \varphi) \cos \omega_0 t + \frac{\omega}{\omega_0} \sin(\omega t + \varphi) \sin \omega_0 t \right\} \quad (11a)$$

and

$$C_2 = x \sin \omega_0 t + \frac{v}{\omega_0} \cos \omega_0 t - \frac{\alpha}{m(\omega_0^2 - \omega^2)} \left\{ \cos(\omega t + \varphi) \sin \omega_0 t - \frac{\omega}{\omega_0} \sin(\omega t + \varphi) \cos \omega_0 t \right\} \quad (11b)$$

For the resonant case ($\omega = \omega_0$), one has

$$C_1 = x \cos \omega_0 t - \frac{v}{\omega_0} \sin \omega_0 t + \frac{\alpha}{2m\omega_0} \left\{ -t \sin(\omega_0 t + \varphi) \cos \omega_0 t + t \cos(\omega_0 t + \varphi) \sin \omega_0 t + \frac{1}{\omega_0} \sin(\omega_0 t + \varphi) \sin \omega_0 t \right\} \quad (12a)$$

and

$$C_2 = x \sin \omega_0 t + \frac{v}{\omega_0} \cos \omega_0 t - \frac{\alpha}{2m\omega_0} \left\{ t \sin(\omega_0 t + \varphi) \sin \omega_0 t + t \cos(\omega_0 t + \varphi) \cos \omega_0 t + \frac{1}{\omega_0} \sin(\omega_0 t + \varphi) \cos \omega_0 t \right\} \quad (12b)$$

Now, by choosing a constant of motion of the form

$$K_{\alpha}^{(nr,r)}(x, v, t) = \frac{1}{2} m \omega_0^2 (C_1^2 + C_2^2), \quad (13)$$

where “nr” means non-resonant and “r” means resonant, it follows that

$$\lim_{\alpha \rightarrow 0} K_{\alpha}^{(nr,r)}(x, v, t) = \frac{1}{2} m v^2 + \frac{1}{2} m \omega_0^2 x^2, \quad (14)$$

Which represents the usual energy of the harmonic oscillator, independently of the non-resonant case or resonant case. This constant of motion can be written as

$$K_{\alpha}^{(nr,r)}(x, v, t) = K_0(x, v) + W_{\alpha}^{(nr,r)}(x, v, t), \quad (15)$$

where K_0 and $W_{\alpha}^{(nr,r)}$ are defined as

$$K_0(x, v) = \frac{1}{2} m v^2 + \frac{1}{2} m \omega_0^2 x^2, \quad (16)$$

$$W_{\alpha}^{(nr)}(x, v, t) = \frac{1}{2} m \omega_0^2 \left[A^2 \cos^2(\omega t + \varphi) - 2Ax \cos(\omega t + \varphi) + B^2 \sin^2(\omega t + \varphi) + \frac{2Bv}{\omega_0} \sin(\omega t + \varphi) \right], \quad (17)$$

and

$$W_{\alpha}^{(r)}(x, v, t) = \frac{1}{2} m \omega_0^2 \left[a^2(t) - \frac{2a(t)v}{\omega_0} \cos(\omega_0 t + \varphi) - \frac{2bv}{\omega_0} \sin(\omega_0 t + \varphi) + 2a(t)b \cos(\omega_0 t + \varphi) \sin(\omega_0 t + \varphi) - 2a(t)x \sin(\omega_0 t + \varphi) + b^2 \sin^2(\omega_0 t + \varphi) \right], \quad (18)$$

where one has made the definitions

$$A = \frac{\alpha}{m(\omega_0^2 - \omega^2)}, \quad B = \frac{\alpha \omega}{m \omega_0 (\omega_0^2 - \omega^2)} \quad (19a)$$

and

$$a(t) = \frac{\alpha t}{2m\omega_0}, \quad b = \frac{\alpha}{2m\omega_0^2}. \quad (19b)$$

To solve Equation (8), one observes that the eigenvalues problem for the operator \hat{K}_0 ,

$$\hat{K}_0(x, \hat{v})\Phi = E\Phi, \quad (20)$$

has exactly the same solution of that one given by the Hamiltonian problem, $(\hat{p}^2/2m + m\omega_0^2 x^2/m)\Phi = E\Phi$ where the solution is the set $\{E_n^{(0)}, \Phi_n(x)\}_{n \geq 0}$,

$$E_n^{(0)} = \hbar \omega_0 (n + 1/2) \quad (21a)$$

and

$$\Phi_n(x) = A_n e^{-\xi^2/2} H_n(x), \quad \xi = \sqrt{\frac{m\omega_0}{\hbar}} x, \quad A_n = \left(\frac{m\omega_0}{\pi \hbar} \right)^{1/4} \frac{1}{\sqrt{2^n n!}}. \quad (21b)$$

Using Dirac's notation [16], where $\Phi_n(x) = \langle x | n \rangle$, with $|n\rangle$ characterizing the n th-state, and then one has the eigenvalue problem written as

$$\hat{K}_0 |n\rangle = E_n^{(0)} |n\rangle. \tag{22}$$

Therefore, one can propose the solution of the Schrödinger's Equation (8) with the operator constant of motion \hat{K} ,

$$i\hbar \frac{\partial |\Psi(t)\rangle}{\partial t} = \{ \hat{K}_0(x, \hat{v}) + W_\alpha^{(nr,r)}(x, \hat{v}, t) \} |\Psi(t)\rangle, \tag{23}$$

of the form

$$|\Psi(t)\rangle = \sum_{n=0}^{\infty} C_n(t) |n\rangle. \tag{24}$$

Taking into consideration (22), the orthogonality of the states ($\langle m|n\rangle = \delta_{mn}$), one obtains the following equation for the coefficients

$$i\hbar \dot{C}_m(t) = E_m^{(0)} C_m(t) + \sum_{n=0}^{\infty} C_n(t) W_{mn}^{(nr,r)}(t), \tag{25}$$

where $W_{mn}^{(nr,r)}(t)$ represents the matrix element

$$W_{mn}^{(nr,r)}(t) = \langle m | W_\alpha^{(nr,r)} | n \rangle. \tag{26}$$

The Equation (25) can be simplified using the new variable

$$C_k(t) = e^{-iE_k^{(0)}t/\hbar} D_k(t). \tag{27}$$

The equations for these new coefficients are

$$i\hbar \dot{D}_m(t) = \sum_{n=0}^{\infty} e^{i\omega_{mn}t} D_n(t) W_{mn}^{(nr,r)}(t), \tag{28}$$

where $C_k(0) = D_k(0)$ and the probability to find the system in the state $|k\rangle$ is $|C_k(t)|^2 = |D_k(t)|^2$. Matrix elements are much easier to calculate by using the non-Hermitian ascent “ a^\dagger ” and descent “ a ” operators,

$$a = \sqrt{\frac{m\omega_0}{2\hbar}} x + i\sqrt{\frac{m}{2\omega_0\hbar}} \hat{v}, \quad a^\dagger = \sqrt{\frac{m\omega_0}{2\hbar}} x - i\sqrt{\frac{m}{2\omega_0\hbar}} \hat{v}, \tag{29}$$

with the known properties [17]

$$[a, a] = [a^\dagger, a^\dagger] = 0, \quad [a, a^\dagger] = 1, \tag{30a}$$

and

$$a^\dagger |n\rangle = \sqrt{n+1} |n+1\rangle, \quad a |n\rangle = \sqrt{n} |n-1\rangle. \tag{30b}$$

For non-resonant case (nr), after calculating the matrix elements, using the orthogonality of the states, and making some rearrangements, one gets the equations for the real and imaginary parts of the coefficients, $D_k(t) = X_k(t) + iY_k(t)$, as

$$\begin{aligned} \dot{X}_k &= -c\sqrt{k} [\cos(\omega t + \varphi) \cos \omega_0 t Y_{k-1} + \cos(\omega t + \varphi) \sin \omega_0 t X_{k-1}] \\ &\quad - c\sqrt{k+1} [\cos(\omega t + \varphi) \cos \omega_0 t Y_{k+1} - \cos(\omega t + \varphi) \sin \omega_0 t X_{k+1}] \\ &\quad + d\sqrt{k} [\sin(\omega t + \varphi) \cos \omega_0 t X_{k-1} - \sin(\omega t + \varphi) \sin \omega_0 t Y_{k-1}] \\ &\quad - d\sqrt{k+1} [\sin(\omega t + \varphi) \cos \omega_0 t X_{k+1} + \sin(\omega t + \varphi) \sin \omega_0 t Y_{k+1}] \\ &\quad + a_1 \cos^2(\omega t + \varphi) Y_k + b_1 \sin^2(\omega t + \varphi) Y_k \end{aligned} \tag{31a}$$

$$\begin{aligned}
\dot{Y}_k = & +c\sqrt{k} [\cos(\omega t + \varphi) \cos \omega_0 t X_{k-1} - \cos(\omega t + \varphi) \sin \omega_0 t Y_{k-1}] \\
& + c\sqrt{k+1} [\cos(\omega t + \varphi) \cos \omega_0 t X_{k+1} + \cos(\omega t + \varphi) \sin \omega_0 t Y_{k+1}] \\
& + d\sqrt{k} [\sin(\omega t + \varphi) \cos \omega_0 t Y_{k-1} + \sin(\omega t + \varphi) \sin \omega_0 t X_{k-1}] \\
& - d\sqrt{k+1} [\sin(\omega t + \varphi) \cos \omega_0 t Y_{k+1} - \sin(\omega t + \varphi) \sin \omega_0 t X_{k+1}] \\
& + a_1 \cos^2(\omega t + \varphi) X_k + b_1 \sin^2(\omega t + \varphi) X_k,
\end{aligned} \tag{31b}$$

where a_1 , b_1 , c and d have been defined as

$$a_1 = \frac{\alpha^2 \omega_0^2}{2m\hbar(\omega_0^2 - \omega^2)^2}, \quad b_1 = \frac{\alpha^2 \omega^2}{2m\hbar(\omega_0^2 - \omega^2)^2} \tag{32b}$$

$$c = \frac{\alpha \omega_0^2}{\omega_0^2 - \omega^2} \frac{1}{\sqrt{2m\hbar\omega_0}}, \quad d = \frac{\alpha \omega}{\omega_0^2 - \omega^2} \sqrt{\frac{\omega_0}{2m\hbar}}. \tag{32b}$$

For the resonant case (r), one can in addition make the following change of coefficients

$$D_k(t) = e^{-i\alpha^2 t^3/24m\hbar} \tilde{D}_k(t) \tag{33}$$

to eliminate the quadratic time dependence appearing in the expression (18) and (19b). Note that $D_k(0) = \tilde{D}_k(0)$ and $|D_k(t)|^2 = |\tilde{D}_k(t)|^2$. Doing the same as it was done above, the real and imaginary parts of these new coefficients,

$\tilde{D}_k = \tilde{X}_k + i\tilde{Y}_k$, obey the equations

$$\begin{aligned}
\tilde{X}_k = & +f(t)\tilde{Y}_k - \sqrt{k} \{ [h(t)\tilde{X}_{k-1} - g(t)\tilde{Y}_{k-1}] \sin \omega_0 t + [h(t)\tilde{Y}_{k-1} \\
& + g(t)\tilde{X}_{k-1}] \cos \omega_0 t \} + \sqrt{k+1} \{ [h(t)\tilde{X}_{k+1} + g(t)\tilde{Y}_{k+1}] \sin \omega_0 t \\
& - [h(t)\tilde{Y}_{k+1} - g(t)\tilde{X}_{k+1}] \cos \omega_0 t \}
\end{aligned} \tag{34a}$$

$$\begin{aligned}
\tilde{Y}_k = & -f(t)\tilde{X}_k + \sqrt{k} \{ [h(t)\tilde{X}_{k-1} - g(t)\tilde{Y}_{k-1}] \cos \omega_0 t - [h(t)\tilde{Y}_{k-1} \\
& + g(t)\tilde{X}_{k-1}] \sin \omega_0 t \} + \sqrt{k+1} \{ [h(t)\tilde{X}_{k+1} + g(t)\tilde{Y}_{k+1}] \cos \omega_0 t \\
& + [h(t)\tilde{Y}_{k+1} - g(t)\tilde{X}_{k+1}] \sin \omega_0 t \}
\end{aligned} \tag{34b}$$

where the functions f , h , and g have been defined as

$$f(t) = \frac{\alpha^2}{8m\hbar\omega_0} \sin^2 \omega_0 t + \frac{\alpha^2 t}{4m\omega_0\hbar} \cos(\omega_0 t + \varphi) \sin(\omega_0 t + \varphi), \tag{35a}$$

$$g(t) = \frac{\alpha}{2\hbar} \left[\frac{1}{\omega_0} \sin(\omega_0 t + \varphi) + t \cos(\omega_0 t + \varphi) \right], \tag{35b}$$

and

$$h(t) = \frac{\alpha \omega_0 t}{2\hbar} \sin(\omega_0 t + \varphi). \tag{35c}$$

The dynamical systems (31) and (34) are solved by Runge-Kutta method a 4th-order.

3. Analytical Approach for $K(x, p, t)$

The Hamiltonian of the forced harmonic oscillator is [18]

$$H(x, p, t) = H_0(x, p) + \alpha x \cos(\omega t + \varphi), \quad (36)$$

where H_0 is given by

$$H_0(x, p) = \frac{p^2}{2m} + \frac{1}{2}m\omega_0^2 x^2. \quad (37)$$

The solution of the eigenvalue problem

$$H_0\Phi = E\Phi \quad (38)$$

is well known [19], and its solution is the same as (21). Therefore, to solve the Schrödinger's Equation (1), one proposes a solution of the form

$$|\Psi(t)\rangle = \sum_{n=0}^{\infty} e^{-iE_n^{(0)}t/\hbar} D_k(t)|n\rangle, \quad (39)$$

which, after substituting in the Schrödinger's equation, using the eigenvalues and the orthogonality between any two states, and making some rearranging, the following dynamical systems is brought about for the real and imaginary parts of the coefficients, $D_k(t) = x_k(t) + iy_k(t)$,

$$\begin{aligned} \dot{x}_k &= -\lambda \left[\sqrt{k} x_{k-1} - \sqrt{k+1} x_{k+1} \right] \cos(\omega t + \varphi) \sin \omega_0 t \\ &\quad - \lambda \left[\sqrt{k} y_{k-1} + \sqrt{k+1} y_{k+1} \right] \cos(\omega t + \varphi) \cos \omega_0 t \end{aligned} \quad (40a)$$

$$\begin{aligned} \dot{y}_k &= -\lambda \left[\sqrt{k} y_{k-1} - \sqrt{k+1} y_{k+1} \right] \cos(\omega t + \varphi) \sin \omega_0 t \\ &\quad + \lambda \left[\sqrt{k} x_{k-1} + \sqrt{k+1} x_{k+1} \right] \cos(\omega t + \varphi) \cos \omega_0 t, \end{aligned} \quad (40b)$$

where the constant λ has been defined as

$$\lambda = \alpha \sqrt{\frac{\hbar}{2m\omega_0}}. \quad (41)$$

These equations are also solved by using Runge-Kutta method at 4th-order.

4. Boltzmann-Shannon Entropy and Energy

Besides the probability to find the system in the state $|n\rangle$ at the time " t ", $|D_k(t)|^2$, for the analysis of the dynamics of the system in the spaces (x, \hat{v}) and (x, \hat{p}) , one can also consider the Boltzmann-Shannon entropy,

$$S(t) = -\sum_{k=0}^l |D_k(t)|^2 \ln |D_k(t)|^2, \quad (42)$$

and its average over an evolution time " T ",

$$\bar{S} = \frac{1}{T} \int_0^T S(t) dt, \quad (43)$$

as parameter which characterize the quantum dynamics of the system. This parameter gives us an indication of how many states enter in the dynamics evolution of the system. Therefore, it gives an indication of the information lost in the dynamics due to the increasing of the entropy in the quantum system. In addi-

tion, one can also consider the expectation value of the energy

$$\langle E \rangle(t) = \langle \Psi | \begin{pmatrix} \hat{H}_0 \\ \hat{K}_0 \end{pmatrix} | \Psi \rangle = \hbar\omega_0 \sum_{n=0}^l n |D_n(t)|^2 + \frac{1}{2} \hbar\omega_0, \quad (44)$$

and its average value over the evolution time of the system,

$$\bar{E} = \frac{1}{T} \int_0^T \langle E \rangle(t) dt. \quad (45)$$

This parameter gives information about how the energy is distributed among the states and how many of them are involved in the quantum dynamics.

In this way, solving the dynamical systems (31), (34), and (40), the evolution of the probabilities $|D_k(t)|^2$'s are gotten. Thus, the Boltzmann-Shannon entropy (42), the expectation value of the energy (44) and their average values (43) and (45) can be calculated and can be compared for the quantization in the spaces (x, v) and (x, p) .

5. Results

One considers a proton with mass $m = 1.6726219 \times 10^{-27}$ kg oscillating with a frequency $\omega_0 = 2\pi \times 10^9$ Hz on a one-dimensional line, and interacting with a periodic force of amplitude $\alpha = 10^{-13}$ Newtons with frequency ω and phase $\varphi = 0$. The initial conditions of the system are

$$C_k(0) = D_k(0) = \tilde{D}_k(0) = \delta_{k0}, \quad k = 0, \dots, 11 \quad (46)$$

that is, the system is on the ground state, and one selects ten excited possible state of the system. For the non-resonant case ($\omega \neq \omega_0$), the resulting dynamics from expressions (1) and (8) are exactly the same. There is not excitation of the system at all since the system remains in the ground state in both cases. For the resonant case ($\omega = \omega_0$), **Figure 1** shows the probabilities of having the system on the ground state ($k = 0$) and on the first excited state ($k = 1$) for the quantization on the space (x, v) , solid lines, and the quantization on the space (x, p) , dotted lines. As one can see, for the Hamiltonian quantization approach (H) there are much more oscillations of the probabilities than the quantization of the constant of motion approach (K), that is, there are more transitions per unit time in the H-approach case than in the K-approach case. One must note that the probability to have the system in the first excited state for the K-approach case is totally different from the H-approach case.

Figure 2 shows the average value of the energy as a function of the strength of the forced force (α). As one can see, this average value is always higher for H-approach case (the usual Quantum Mechanics approach) than for the K-approach case (our pretended extension for the Quantum Mechanics). However, the difference on the average energy value for both approaches is quite small and maybe out of experimental verification. This difference is expected since for the H-approach the Hamiltonian is not a constant of motion, but for the K-approach one has a quantization with a constant of motion of the system.

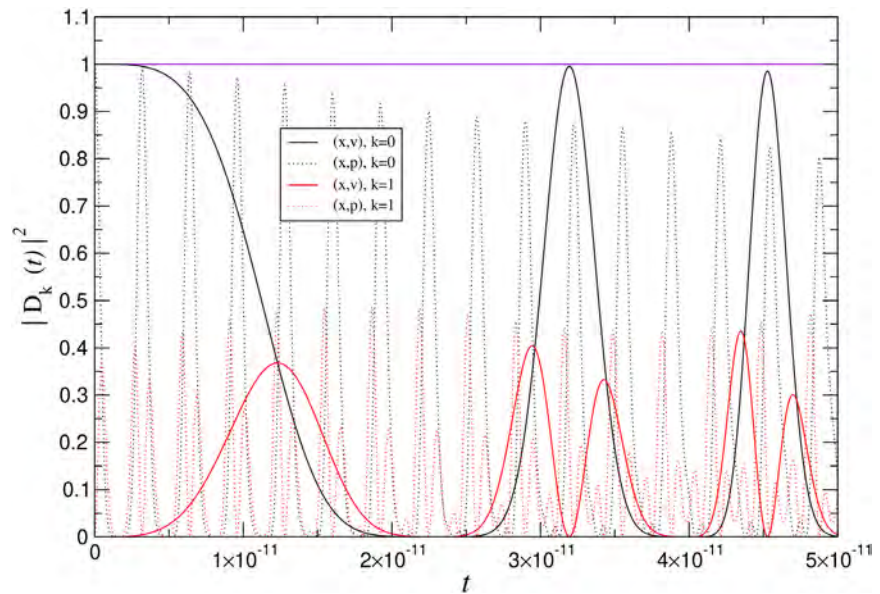


Figure 1. Ground state and first excited state evolution.

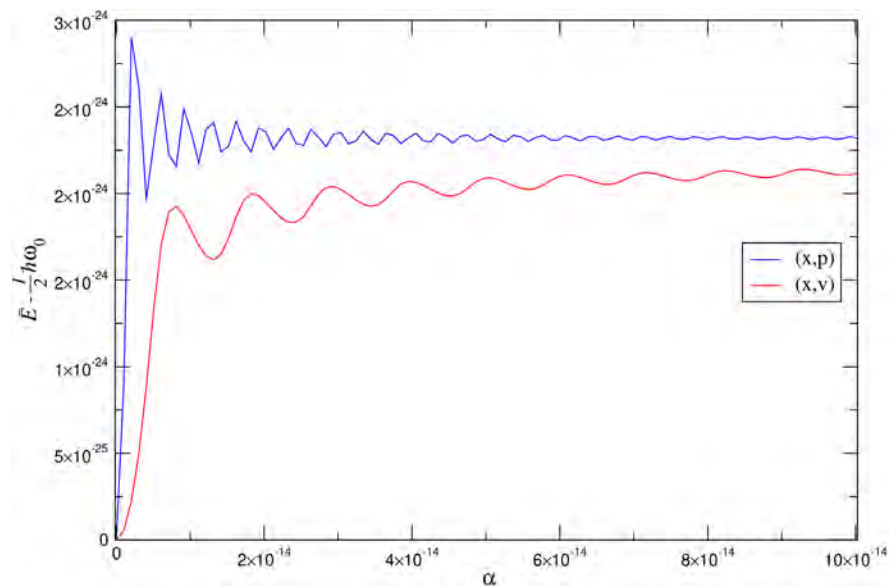


Figure 2. Average energy of the system.

Figure 3 shows the average value of the Boltzmann-Shannon entropy as a function of the strength of the forced force (α). Notice that, having total number of 11 states, the possible maximum entropy is 2.398. As the previous case, this parameter is always higher for the H-approach case than for the K-approach case due to the same reason that the Hamiltonian is not a constant of motion and K is indeed a constant of motion of the system. However, this difference is not so small and maybe could be used as a good parameter for experimental proposes. This difference means that the H-approach case brings about more complex behavior in the quantum dynamics than the K-approach case, and that the H-approach case losses more information than the K-approach case.

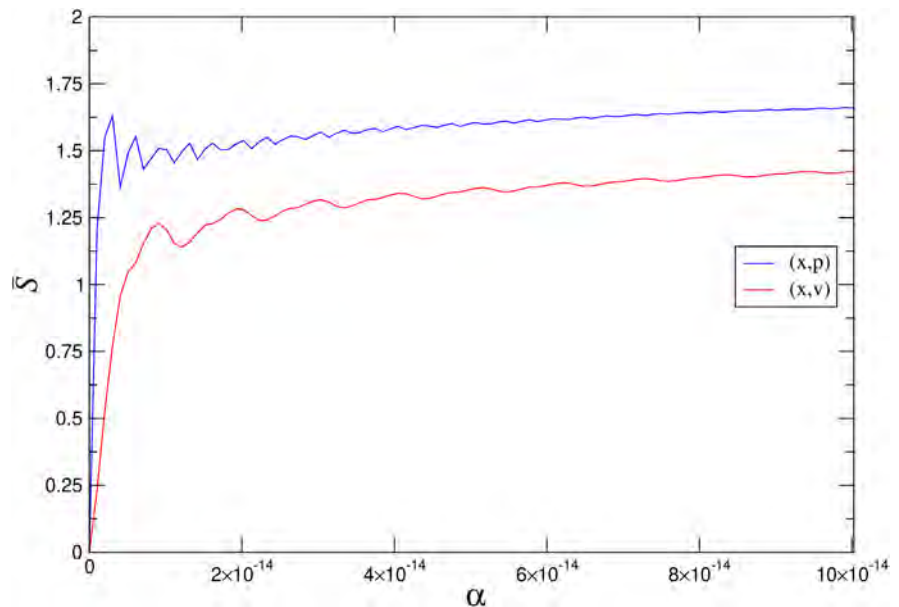


Figure 3. Average Boltzmann-Shannon entropy.

6. Conclusion

The quantization of the 1-D forced harmonic oscillator was carried out with the operators (x, \hat{v}) using the assigned linear operator to a constant of motion $K(x, v, t)$ of the classical case. The restriction imposed on this constant was that it must be reduced to the known energy expression when the forced force is zero. This quantization was compared with the usual quantization with the operators (x, \hat{p}) and the associated Hamiltonian $H(x, p, t)$ of the classical case. It was shown that the probabilities to find the system in the state $|n\rangle$, $|D_n(t)|^2$, has less oscillations in the K-quantization than in the H-quantization. In addition, the average values of the energy and the average value of the Boltzmann-Shannon entropy are lower in the K-quantization than in the H-quantization. Since the difference in the average value of the energy is quite small, this parameter does not look good to measure experimentally. However, the difference in the entropy is significant and it represents a good parameter to look experimentally.

Conflicts of Interest

The authors declare no conflicts of interest regarding the publication of this paper.

References

- [1] Von Neumann, J. (1932) *Mathematical Foundations of Quantum Mechanics*, Volume 183. Princeton University Press, Princeton.
- [2] Born, M. (1926) *Zeitschrift für Physik*, **38**, 803. <https://doi.org/10.1007/BF01397184>
- [3] Schrödinger, E. (1926) *Physical Review*, **28**, 1049-1070. <https://doi.org/10.1103/PhysRev.28.1049>

- [4] Spielman, I. (2017) *Nature*, **545**, 293-294. <https://doi.org/10.1038/545293a>
- [5] Darboux, G. (1894) *Lecons sur la Théorie Générale des Surfaces*, volume 3. Gauthier-Villars, Paris.
- [6] Goldstein, H. (1978) *Classical Mechanics*, Volume I, II. Addison-Wesley, Boston.
- [7] López, P., López, G.V. and López, X.E. (2007) *International Journal of Theoretical Physics*, **46**, 1100. <https://doi.org/10.1007/s10773-006-9260-7>
- [8] López, P., López, G.V. and López, X.E. (2011) *Advanced Studies in Theoretical Physics*, **5**, 253-268.
- [9] Man'ko, V.I., Dodonov, V.V. and Skarzhinsky, V.D. (1981) *Hadronic Journal*, **4**, 1734.
- [10] Man'ko, V.I., Dodonov, V.V. and Skarzhinsky, V.D. (1982) *Il Nuovo Cimento B*, **69**, 185. <https://doi.org/10.1007/BF02721265>
- [11] Griselda, A., López, G.V. and Martínez-Prieto, R.M. (2018) *Journal of Applied Mathematical and Physics*, **6**, 1382. <https://doi.org/10.4236/jamp.2018.66115>
- [12] Motensinos, M. and Torres del Castillo, G.F. (2004) *Physical Review A*, **70**, Article ID: 032104. <https://doi.org/10.1103/PhysRevA.70.032104>
- [13] López, G.V. (1998) *Journal of Theoretical Physics*, **37**, 1617-1623. <https://doi.org/10.1023/A:1026628221912>
- [14] Lopez, G.V. (2012) *Journal of Modern Physics*, **3**, 777-785. <https://doi.org/10.4236/jmp.2012.38102>
- [15] López, G. and López, P. (2006) *International Journal of Theoretical Physics*, **45**, 753. <https://doi.org/10.1007/s10773-006-9064-9>
- [16] Dirac, P. (1939) *Mathematical Proceedings of the Cambridge Philosophical Society*, **35**, 416-418. <https://doi.org/10.1017/S0305004100021162>
- [17] Leventhal, J.J. and Burkhardt, C.E. (2008) Harmonic Oscillator Solution Using Operator Methods. https://doi.org/10.1007/978-0-387-77652-1_7
- [18] Lifshitz, E.M. and Landau, L.D. (1970) *Course of Theoretical Physics*, Volume I.
- [19] Messiah, A. (1966) *Quantum Mechanics*, Volume I. John Wiley & Sons, Hoboken, Ch. XII.

Electric Charge, Matter Distribution, and Baryon Asymmetry from Holographic Principle

T. R. Mongan

84 Marin Avenue, Sausalito, CA, USA
Email: tmongan@gmail.com

How to cite this paper: Mongan, T.R. (2021) Electric Charge, Matter Distribution, and Baryon Asymmetry from Holographic Principle. *Journal of Modern Physics*, 12, 295-299.
<https://doi.org/10.4236/jmp.2021.123022>

Received: January 26, 2021

Accepted: February 23, 2021

Published: February 26, 2021

Copyright © 2021 by author(s) and Scientific Research Publishing Inc. This work is licensed under the Creative Commons Attribution International License (CC BY 4.0).

<http://creativecommons.org/licenses/by/4.0/>



Open Access

Abstract

Explaining baryon asymmetry (*i.e.*, matter dominance) in the universe has been a vexing problem in physics. This analysis, based on the holographic principle, identifies fractional electric charge with the state of bits of information on the event horizon. Thermodynamics on the event horizon at the time of baryogenesis then estimates observed baryon asymmetry.

Keywords

Electric Charge, Baryon Asymmetry, Holographic Principle

1. Introduction

Baryon asymmetry (matter dominance) in the universe has been difficult to explain. This paper is based on the holographic principle [1], a direct consequence of quantum mechanics, general relativity, black hole thermodynamics, and Shannon information theory, indicating only a finite number (about 10^{122}) of bits of information encoded on the event horizon will ever be available to describe our observable universe. The two possible states of each bit, positive and negative, can be identified with fractional charge in the universe. Describing Standard Model fermions as spheres with radius $1/4$ their Compton wavelength [2] indicates charge $\pm \frac{e}{6}$ associated with each bit, where e is electron charge. Thermodynamics on the event horizon at the time of baryogenesis and energy difference between bit states then estimates observed baryon asymmetry. Similar treatment of baryon asymmetry [3] used a specific preon model not relevant to this analysis.

2. Charge and the Holographic Principle

Fundamental particles in the Standard Model have charge $\pm \frac{ne}{3}$, where $n = 0, 1, 2$ or 3 . Considering fundamental fermions as spheres with radius $1/4$ their Compton wavelength [2] requires surface charge $\pm \frac{ne}{6}$ at each end of the spin axis to insure identical electrostatic potential energy of first-generation fermions. So, identifying states of each bit of information available to describe the observable universe as $\frac{e}{6}$ or $-\frac{e}{6}$ accounts for charge in the universe. Origin of the universe by quantum fluctuation from nothing [4] requires equal number of plus and minus charged bits to ensure a charge-neutral universe and charge conservation, a precondition for gauge invariance and Maxwell's equations. In any physical system, energy must be transferred to change state of information bits. Protons have charge e and anti-protons have charge $-e$. Regardless of how bits of information on the horizon specify protons or anti-protons, bit configurations specifying protons must differ in 6 bits from configurations specifying anti-protons. Since $\frac{e}{6}$ bits and $-\frac{e}{6}$ bits do not have the same energy, the number of protons and anti-protons created in the early universe must be slightly different. If $\frac{e}{6}$ bits have lower energy than $-\frac{e}{6}$ bits, there must be more matter than anti-matter in the universe and this analysis estimates that baryon asymmetry.

3. Matter Distribution in the Universe

At the fundamental level, information specifies time evolution of matter distribution in the universe. Observations indicate our universe is a closed Friedmann universe, dominated by vacuum energy in the form of a cosmological constant and so large it is approximately flat [5]. If Hubble constant $H_0 = 67.8 \text{ km}\cdot\text{sec}^{-1}\cdot\text{Mpc}^{-1}$, critical density $\rho_{crit} = \frac{3H_0^2}{8\pi G} = 8.64 \times 10^{-30} \text{ g/cm}^3$, where $G = 6.67 \times 10^{-8} \text{ cm}^3/(\text{g}\cdot\text{sec}^2)$. Matter accounts for 30.8% of energy in today's universe, today's matter density in the universe is $\rho_0(0) = 0.308\rho_{crit} = 2.66 \times 10^{-30} \text{ g/cm}^3$, and vacuum energy density $\rho_v = (1 - 0.308)\rho_{crit} = 5.98 \times 10^{-30} \text{ g/cm}^3$. Cosmological constant $\Lambda = \frac{8\pi G\rho_v}{c^2}$, where $c = 3 \times 10^{10} \text{ cm/sec}$, and there is an event horizon in the universe at radius $R_H = \sqrt{\frac{3}{\Lambda}} = 1.64 \times 10^{28} \text{ cm}$. The holographic principle then indicates only $N = \frac{\pi R_H^2}{\ln(2)l_p^2} = 4.69 \times 10^{122}$ bits of information on the event horizon will ever be able to describe our observable universe, where Planck length $l_p = \sqrt{\frac{\hbar G}{c^3}} = 1.62 \times 10^{-33} \text{ cm}$ and Planck's constant $\hbar = 1.05 \times 10^{-27} \text{ g}\cdot\text{cm}^2/\text{sec}$.

With no source or sink for information outside a closed universe, the amount

of information available to describe the observable universe remains constant. In a closed universe, the total quantity of matter in the universe is conserved, there are only N bits of information available and mass per bit of information, approximately 10^{-67} g, is mass $M_H = \frac{4}{3}\pi R_H^3 \rho_0(0) = 4.92 \times 10^{55}$ g divided by the number of bits N .

Information on the horizon specifying distribution of mass within the observable universe at any instant is of little use to an observer, because signals traveling at light speed take about 17 billion years to reach the observer. However, as shown below, baryon asymmetry can be estimated using only information on the horizon at the time of baryogenesis. Since mass associated with each bit of information is only about 10^{-67} g, the analysis is consistent with protons and anti-protons having indistinguishable masses.

4. Baryon Asymmetry

Temperature at time of baryon formation (baryogenesis) was

$$T_B = \frac{2m_p c^2}{k} = 2.18 \times 10^{13} \text{ }^\circ\text{K}, \text{ where Boltzmann constant}$$

$$k = 1.38 \times 10^{-16} \left(\frac{\text{g}\cdot\text{cm}^2}{\text{sec}^2} \right) / ^\circ\text{K} \text{ and proton mass } m_p = 1.67 \times 10^{-24} \text{ g. Scale factor of}$$

$$\text{the universe at baryogenesis was } R_B = R_0 \left(\frac{2.725}{T_B} \right) \approx 10^{15} \text{ cm, where } 2.725 \text{ }^\circ\text{K is}$$

today's cosmic microwave background temperature and $R_0 \approx 10^{28}$ cm is today's scale factor. Time t_b of baryogenesis, in seconds after the end of inflation, is found

$$\text{from Friedmann's equation } \left(\frac{dR}{dt} \right)^2 - \left(\frac{8\pi G}{3} \right) \epsilon \left(\frac{R}{c} \right)^2 = -\kappa c^2. \text{ After inflation, the}$$

universe is so large it is almost flat, and curvature parameter $\kappa \approx 0$. Energy

$$\text{density is } \epsilon(R) = \epsilon_r \left(\frac{R_0}{R} \right)^4 + \epsilon_m \left(\frac{R_0}{R} \right)^3 + \epsilon_v, \text{ where } \epsilon_r = 4.4 \times 10^{-34} \left(\frac{\text{g}}{\text{cm}^3} \right) c^2, \epsilon_m,$$

and ϵ_v are today's radiation, matter, and vacuum energy densities. Vacuum energy density was negligible in the early post-inflationary universe, and radiation

dominated before radiation/matter equality, when $R \ll 10^{-5} R_0$. Integrating

$$\left(\frac{dR}{dt} \right)^2 - \left(\frac{8\pi G}{3c^2} \right) \epsilon_r R_0^4 = \left(\frac{dR}{dt} \right)^2 - \left(\frac{A}{R} \right)^2 = 0, \text{ where } A = \sqrt{\frac{8\pi G \epsilon_r R_0^4}{3c^2}}, \text{ from the}$$

$$\text{end of inflation at } t=0 \text{ to } t \text{ gives } \frac{1}{2} (R^2 - R_i^2) = At, \text{ where } R_i \text{ is scale factor}$$

$$\text{at the end of inflation. So } t_B = \frac{R_B^2 - R_i^2}{2A} \approx \frac{R_B^2}{2A} \approx 10^{-7} \text{ sec, if } R_B \gg R_i. \text{ Distance from any point in the universe to the particle horizon for that point [6] is}$$

$$d_B = cR_B \int_0^{t_B} \frac{dt'}{R(t')} = \left[\frac{cR_B}{A} \sqrt{R_i^2 + 2At} \right]_0^{t_B} = \frac{cR_B}{A} \left[\sqrt{R_i^2 + 2At_B} - R_i \right]. \text{ Since } R_B \gg R_i,$$

$$d_B \approx cR_B \sqrt{\frac{2t_B}{A}} \approx 10^4 \text{ cm.}$$

Surface gravity on particle horizon at baryogenesis is

$$g_{HB} = \frac{4\pi G}{3c^2} \varepsilon(R_B) d_B \approx \frac{4\pi G}{3c} \frac{\varepsilon_r R_0^4}{AR_B^2} \tag{1}$$

and associated horizon temperature [7] [8] is

$$T_{HB} = \frac{\hbar}{2\pi ck} g_{HB} \approx 6 \times 10^{-7} \text{ K} \tag{2}$$

Temperature at any epoch is uniform throughout a postinflationary homogeneous isotropic Friedman universe, and causal horizon at baryogenesis is distance d_B from every point in the universe. Temperature at every point on the causal horizon for every point in the universe is the same because surface gravity of the uniform sphere within the horizon is the same at every point on every horizon. Bits on all causal horizons are in thermal equilibrium, only two quantum states are accessible to those bits, and equilibrium statistical mechanics establishes occupation probabilities of bit states in thermal equilibrium at temperature T_{HB} proportional to their corresponding Boltzmann factors. So, if energy of $\frac{e}{6}$ bits on the horizon at baryogenesis is $E_{bit} - E_d$ and energy of $-\frac{e}{6}$ bits is $E_{bit} + E_d$, proton/antiproton ratio at baryogenesis is

$$\left(e^{\frac{E_{bit}-E_d}{kT_{HB}}} / e^{\frac{E_{bit}+E_d}{kT_{HB}}} \right)^6 = e^{\frac{12E_d}{kT_{HB}}} \approx 1 + \frac{12E_d}{kT_{HB}} \text{ and proton excess is } \frac{12E_d}{kT_{HB}}.$$

Energy released when a bit on the horizon drops from $-\frac{e}{6}$ state to $\frac{e}{6}$ state raises another bit from $\frac{e}{6}$ to $-\frac{e}{6}$ state, and that is the mechanism for charge conservation. Energy must be transferred by massless quanta with wavelengths related to the size of the universe. With no reliable definition of size (as opposed to scale factor) of an open universe, this analysis only applies to a closed Friedmann universe, in particular one like ours that is so large it is approximately flat. The only macroscopic length characteristic of the horizon of a closed Friedmann universe with radius (scale factor) $R(t)$ is circumference $2\pi R(t)$. If energy $2E_d$ to change the state of bits associated with a mass quantum within the universe (and corresponding bits on the horizon) at baryogenesis equals the energy of massless quanta with wavelength characteristic of a closed Friedmann universe with radius R_B

$$2E_d = \frac{\hbar c}{R_B} \tag{3}$$

Using Equations (1), (2), and (3), proton excess at baryogenesis is

$$\frac{12E_d}{kT_{HB}} = \left(\frac{24\pi c^2}{R_0} \right) \left(\frac{2.725}{T_B} \right) \sqrt{\frac{3}{8\pi G \varepsilon_r}}. \text{ Dependence on } R_0 \text{ arises because } R_B \text{ the radius of the universe at baryogenesis, depends on } R_0, \text{ today's cosmic microwave background temperature } 2.725 \text{ K, and temperature } T_B \text{ at baryogenesis. For } R_0 \approx 10^{28} \text{ cm, proton excess is } 1.8 \times 10^{-9}. \text{ WMAP [9] estimated baryon density to cosmic}$$

microwave background photon density ratio as 6.1×10^{-10} . At baryogenesis, the number of proton states with six $\frac{e}{6}$ bits approximately equals the number of anti-protons states with six $-\frac{e}{6}$ bits, and when almost all protons and antiprotons annihilate to two photons the ratio of baryon to photon states is $\frac{1}{3}(1.8 \times 10^{-9}) = 6 \times 10^{-10}$, in agreement with WMAP.

5. Conclusion

Using the holographic principle, states of information bits on the event horizon describing matter distribution within the universe are identified with fractional electric charge. Describing fundamental fermions in the Standard Model as spheres with radius 1/4 their Compton wavelength and half their charge on the surface at each end of their spin axis, combined with thermodynamics on the event horizon at the time of baryogenesis, explains baryon asymmetry.

Acknowledgements

This note was inspired by discussions with the young scientist James Bartley Mongan.

Conflicts of Interest

The author declares no conflicts of interest regarding the publication of this paper.

References

- [1] Bousso, R. (2002) *Reviews of Modern Physics*, **74**, 825. <https://doi.org/10.1103/RevModPhys.74.825>
- [2] Mongan, T.R. (2020) *Journal of Modern Physics*, **11**, 1993-1998. <https://doi.org/10.4236/jmp.2020.1112126>
- [3] Mongan, T.R. (2012) *Journal of Modern Physics*, **3**, 581-584. <https://doi.org/10.4236/jmp.2012.37079>
- [4] Mongan, T.R. (2001) *General Relativity and Gravitation*, **33**, 1415-1424. <https://doi.org/10.1023/A:1012065826750>
- [5] Mongan, T.R. (2015) Holography, Large Scale Structure, Supermassive Black Holes and Minimum Stellar Mass. arXiv: 1301.0304.
- [6] Islam, J. (2002) *An Introduction to Mathematical Cosmology*. 2nd Edition, Cambridge University Press, Cambridge, p. 73.
- [7] Padmanabhan, T. (2010) *AIP Conf. Proc.*, **1241**, 93. [arXiv:0911.1403].
- [8] Padmanabhan, T. (2009) A Dialogue on the Nature of Gravity. [arXiv: 0910.0839].
- [9] Bennet, C.L., *et al.* (2003) *The Astrophysical Journal Supplement Series*, **148**, 1.

Time-Neutrality of Natural Laws Challenged: Time Is Not an Illusion but Ongoing Energy-Driven Information Loss

Helmut Tributsch^{1,2*}

¹Institute for physical and theoretical Chemistry, Free University, Berlin, Germany

²Helmholtz Centre Berlin for Materials and Energy, Berlin, Germany

Email: helmut.tributsch@alice.it

How to cite this paper: Tributsch, H. (2021) Time-Neutrality of Natural Laws Challenged: Time Is Not an Illusion but Ongoing Energy-Driven Information Loss. *Journal of Modern Physics*, 12, 300-327. <https://doi.org/10.4236/jmp.2021.123023>

Received: January 21, 2021

Accepted: February 23, 2021

Published: February 26, 2021

Copyright © 2021 by author(s) and Scientific Research Publishing Inc. This work is licensed under the Creative Commons Attribution International License (CC BY 4.0).

<http://creativecommons.org/licenses/by/4.0/>



Open Access

Abstract

It is shown that the time of entropy increase, here called action time, is caused by a dynamically understood energy. It drives time by decreasing its presence per state, that is by abandoning order, information, and creating entropy. This mechanism can be derived from basic principles via the Lagrange-Euler formalism, just considering the properties of really experienced, oriented time and thus abandoning the paradigm of time neutrality. It describes nature driven by a dynamically understood principle of least action, which is identified as manifestation of fundamental irreversibility in nature. This readily explains the second law of thermodynamics and also yields the entropy law for non-linear irreversible thermodynamics: maximum entropy production within the restraints of the system. Dynamic energy-driven time, action time, and time asymmetry is generated via the process of erasing information and liberating its energy irreversibly as heat. It is not an illusion but information-based reality. It is the loss of information to the past and different from clock-time, which is just an artificial scale, using information for tracking real time, action time. Energy-driven fundamental irreversibility of nature can better describe experienced reality and opens the way to understand and finally imitate the self-organizing creativity in nature. It also draws far reaching consequences for understanding quantum physics, gravitation and cosmology as well as biology. From the point of view of irreversibility, nature turns out to be more elegant, simpler and rationally understandable. For the first time, it can be explained in a few words what energy and nature basically represent and why it must have been information, which has started the universe.

*Retired (Personal Profile: www.helmut-tributsch.it).

Keywords

Time-Invariance, Energy, Time, Entropy, Information, Irreversibility, Self-Organization, Nature

1. Introduction

Time-neutrality, that is time translation symmetry and time reversal symmetry, of natural laws with entropy increase towards higher probability as the only practically conceivable time ordinate has shaped the world view of physics. A recent BBC production with the title: “Are you experiencing time wrong?”, dealing with the question, why we are only experiencing time moving forward, while physics says that time can move in either direction [1], highlights the conflict, which the public still feels when confronted with this time concept of physics. It is additionally underlined by a famous historic statement: Einstein, shortly before his death, wrote in 1955 in a letter to the son and sister of his deceased friend Michele Besso: “...the distinction between past, present and future only has the meaning of an illusion, though a persistent one”.

The explanation, given by present physics, that natural phenomena develop in direction of increasing entropy and maximum probability can be accepted, because they are evident in nature. But what do they mean in reality and what exactly is their relation to the claimed time neutral fundamental physical laws? The Lagrange function, which is expected to fully describe a developing system and also energy itself are traditionally treated as scalar, non-oriented quantities. They are expected to allow dynamic development in either direction, forward and backward in time. Accepting, that entropy increase in one direction only prevails, anticipates that a phenomenon such as a directional time already exists, because one can observe the increase of entropy in dependence on the time we experience. This phenomenon of entropy increase can, however, not be derived from time-neutral fundamental laws without additional assumptions. Both, the Boltzmann approach (H-theorem) [2] to derive entropy increase, as well as modern Markovian (memory loss) treatments [3] of time-neutral systems abandon information on the past to show that time-neutral natural phenomena finally only continue to proceed in one direction (which only is a mathematical consequence of omitting information, which in a physical system has an energy content). Other attempts to demonstrate time symmetry breaking tacitly assume, besides of coarse-graining (information loss), feedback processes to show development of chaotic, directional properties [4]. They require a distinction between “before” and “after”, which in a time-neutral world is not possible (see also later). Statistical reasoning within time-reversible deterministic physics alone cannot explain a time arrow [5]. A humiliating consequence of this situation is that present science, although very advanced in many respects, cannot derive the important second law of thermodynamics, entropy increase in a closed space,

from time-neutral initial conditions without additional assumptions (not talking about the impossibility to derive an entropy law for non-linear irreversible thermodynamics). So, what is time in reality and why, in practice, it appears to be oriented?

Our clocks need energy to function, but the time they show, the length of their oscillation periods, which are allowed to proceed in form of sequences of oscillations, only depends on natural and material constants. This is also true for the Planck time, the shortest recognized time interval, which only depends on gravitation constant, light velocity and the quantum constant of action. These constants do not produce changes themselves, but their involvement in determining oscillation lengths can be used to generate and measure time periods, which is of course an important technical tool as a scale for a visualization of time in form of progressing and periodically repeating numbers, in form of information. The link to practical life is, as well known, provided by measuring astronomical periods, days, years with clock-time.

This publication attempts to answer the questions, what the time of entropy increase actually is and what relation it has to time neutrality and energy turnover. It further investigates what causes the second law of thermodynamics, what is the time for self-organization in space and in biology and what relation time has to energy and entropy, to which it has been linked in quantum theory via the uncertainty relation [6]. Basing on the identified energy-driven time arrow consequences for understanding nature are discussed.

2. Results

2.1. What Is the Time of Entropy Increase?

Let us consider a real system which is proceeding asymmetrically, increasing its entropy S from S_1 to S_2 , for example an expanding gas. Tacitly, present science is assuming that something like a path for time is existing, along which systems can move forward or backward, while respecting intricate behavior within space-time properties. A directional orientation of such processes arises because they are expected to develop in direction of higher probability (lower information content) and are thus imprinting the experienced orientation of time. What is the origin of such a drive? Information is linked to thermodynamic entropy (see later). The difference in entropy generated, the entropy gain, can be multiplied with the absolute temperature T :

$$TS_2 - TS_1 = T\Delta S \quad (1)$$

and yields the not any more available (entropic) energy $T\Delta S$ (e.g. low temperature environmental heat). We now can ask the question, where this entropic energy came from. Considering the first law of thermodynamics, energy conservation, it cannot arise from nothing, and it could only have been generated from somehow available energy. How did entropy increase with time consequently arise? It was generated from originally available, free energy. Time dependent entropy increase is thus ultimately driven by energy turnover. Since no other

physical driving element is evident, which may aim at generating entropy, this available free energy must consequently have the property to drive the process, for which time is required. Free energy must decrease its internal order and information content to generate energy in its not any more available, entropic form in a condition of highest probability.

Two different approaches, the presently accepted and the here proposed one, for the same event of entropy production are here confronted. The traditional one (used in present physics) applies a mathematical statistical argument, which calculates, how likely it is that a proposition becomes true. The higher the probability of an event, the more likely it will be that the event will occur. This drives the process along the time path we experience. The second approach, presented here, argues that one is dealing with a physical system, which is subject to physical law, in this case controlled by energy with its properties and its law of conservation. The system must follow natural laws. The author's standpoint: the system concerned is a process determined by laws of physics, the function of which can be described by mathematical formalisms. It is itself not an abstract mathematical process. Therefore, it follows physical regularity towards maximum probability, which can be statistically-mathematically described. Here, physical law has priority over mathematical reasoning. A physical system cannot follow mathematical reasoning without a supporting and direction and rate controlling physical law. The conclusion derived from (1), that a dynamic energy is driving entropy increase, is valid. There must be a physical process aiming simultaneously at maximum entropy (disorder) and energy conservation. It can only be action producing free energy. In contrast to present understanding (energy is treated as a scalar quantity, not interested in performing work) energy should therefore not only have the ability to do work, but also the interest to do it. It should have directional properties, interest in entropy production, in decreasing its information content. Can an appropriate mathematical formalism for such a here expected behavior of energy, which obviously contradicts time-neutrality, be derived from basic principles in support of such a conclusion?

2.2. Reconsidering Noether's Symmetry Approach

In order to question time-neutrality in basic laws, it is necessary to deal with the Lagrange-Euler formalism, which is presently used to calculate dynamic and energetic processes in all relevant field of physics, ranging from particle physics to dynamics and Relativity Theory. It is also unavoidable to reinvestigate time invariance considerations which were based on time neutrality and symmetry. Emmy Noether, in 1912, demonstrated that conservation laws can be deduced from symmetry and invariance laws [7]. This way energy conservation was also deduced from time neutrality and symmetry. The mathematical derivation deviates in this case somewhat from standard Noether's theorem since time is not considered to be a generalized coordinate. By totally differentiating the Lagrange function L , which should entirely describe a system, reorganizing the relation

and considering the validity of the Euler-Lagrange-equation, one yields the well-known equation (q = degree of freedom, generalized coordinate; the point on it indicates time derivative) (e.g. [8]):

$$\frac{d}{dt} \left[\frac{\partial L}{\partial \dot{q}} \dot{q} - L \right] = - \frac{\partial L}{\partial t} \quad (2)$$

It equates the total time derivation of energy E

$$E = \frac{\partial L}{\partial \dot{q}} \dot{q} - L \quad (3)$$

with the negative partial time derivation of the Lagrange function (which describes the system via the principle of least action and the Euler-Lagrange equations), or, rearranged, yields:

$$- \frac{dE}{dt} = \frac{\partial L}{\partial t} \quad (4)$$

$$\frac{\partial L}{\partial t} = \text{time asymmetry} \quad (4a)$$

The partial derivative of the Lagrange function (4a) is considered to express time asymmetry against displacement or translation in time. Traditionally, time invariance against displacement (time neutrality and symmetry with respect to orientation) for the Lagrange function is assumed and time asymmetry (4a) consequently set zero [8]. Basing on time-neutral fundamental laws, E and L are presently considered to be scalar quantities, just numbers. Formulas derived from them can consequently describe dynamic motion both in positive and negative time direction. The time axis is just a preexisting path, which can be used in both directions. Based on such preconditions an assumption of zero time asymmetry ((4a) set zero) was seen justified. The Lagrange function as well as energy, understood as scalar quantities, can accompany a natural system both into the future and into the past. This led to a formal derivation of the law of energy conservation: the right side of Equation (4), time asymmetry (4a), was set zero (compare [8]), since invariance with respect to displacement of the Lagrange function in time was assumed. Consequently, the total derivative of energy is zero. Energy E correspondingly results to be a constant, is conserved in time. This is the well-known conservation law for energy.

Since energy conservation has also been again and again confirmed experimentally, its validity is, of course, undebated (it is later also shown to automatically result from the here derived mechanism). But is this additional confirmation of energy conservation via conventionally “assumed” time neutrality and time symmetry and invariance acceptable and correct? Energy conservation itself does not exclude that free, available energy has other degrees of freedom to show dynamic function on the way to entropy formation and time asymmetry (the total derivative of energy in Equation (4) implies also additional implicit time dependencies, which have to be considered). What is this additional physical property of energy which implements and expresses this time dependence and

thus the actually experienced directional time flow and time asymmetry?

2.3. The Correspondence between Dynamic Energy and Time Asymmetry

Lived time in presence and in the past behaves differently compared with time in the future. We cannot move back into the past and changes performed in the past have an effect on the future. This, however, does not happen in the opposite direction. An energy system, described by the Lagrange function, which started to convert energy in the past, while respecting energy conservation, will have generated different amounts of entropic energy depending on its subsequent position on the time axis. If one accepts these facts about time, which we are experiencing, there is no invariance and symmetry with respect to displacement in time for the Lagrange function. The ratio of free and entropic energy of a system, which a Lagrange function is describing, varies with time and its information (negentropy) content will change, decrease, accordingly along the time axis. The laws or equations that describe a system at time t and $t \pm dt$ are not identical. The behavior is also different in forward and backward direction. Only a behavior in forward direction is actually observed.

Consequently, in Equation (4), the time asymmetry (4a), the partial derivation of the Lagrange function with respect to time, can definitively not be set zero (which would mean zero asymmetry and invariance against displacement in time). During history of physics the convention of time neutrality, the ability of a system to develop in either time direction, forward and backward, has won over experimental facts, deducible from experience with lived time, as just discussed. This practical experience with lived time should have excluded, that time asymmetry as expressed by (4a) in (4) can be set zero. As a consequence, equation (4) gets an entirely different significance. It describes a situation, in which a dynamic energy property (total derivation of energy with respect to time) is related to an asymmetry in time behavior (4a).

What does this here now differently to be interpreted Equation (4) exactly mean for the understanding of energy properties in relation to time asymmetry? Mathematically, Equation (4) equates a partial time derivative of the Lagrange function (time asymmetry) with the negative (decreasing) value of the total time derivative of energy. This means that something decreasing within energy and described by its total derivative is responsible for and driving time asymmetry. A partial time derivative only considers changes with respect to time, omitting their effect on other variables. The total derivative also considers all additional implicit time dependencies (such as on turnover of information, order—see later).

A remarkable consequence of abandoning the experimentally unjustified claim of time neutrality and time symmetry is, that the well-known, established Equation (4), derivable from basic principles, then precisely explains what causes time asymmetry: The necessary consequence derivable from Equation (4) and its correct, experimentally backed interpretation is, that nature is acting in such a

way, that the decreasing total derivative of energy is related to and defines the degree of time asymmetry as expressed by the partial time derivation of the Lagrange function in Equation (4). The right interpretation of this Equation (4) can only be that the quality of free, available energy changes during energy turnover and thus generates time asymmetry by causing and driving an oriented time. A change in free energy, while energy is conserved, is actually observed during energy turnover. Free energy with a high information content, order (e.g. a chemical fuel), changes into energy with a lower information content (entropic energy (1), e.g. environmental heat), while energy in its totality is conserved.

Since the Lagrange function L is expected to fully describe the system, Equation (4) expresses that energy (a function of L (3)) with its intrinsic dependencies totally controls the time behavior of the system via its properties. This draws a drastic consequence: nature is not exposed to time neutrality but driven by energy. No new assumption was required, but an experimentally unproven convention (time neutrality and invariance against displacement) dropped in favor of considering experimental facts on lived time, as we experience it. This excludes, as also discussed above (in subsection 2.1.), with different arguments, that a purely mathematical-statistical criterion for attainment of highest probability (and time orientation) is applicable separate from a physical law, which prescribes that. According to (4) it is free energy, with its dynamic property (contained in its total derivative), which is determining the physical law which generates irreversible changes and time asymmetry by approaching a situation of maximum probability. Equation (4) additionally expresses that this dynamic energy property is inseparably related to the degree of time asymmetry (4a). A dynamically behaving energy is responsible for time asymmetry! Via Equation (4) it is related to and causes time asymmetry. Both, energy and time, react as dynamic quantities. Since time asymmetry was deduced from a critical evaluation of time, which we observe and experience, and since the Lagrange formalism is accepted to describe essential aspects of nature, this is a refutation and disproof of the convention of time neutrality and time symmetry within (another disproof of time neutrality follows later).

Here, it is evident, where an obvious, drastic change in understanding nature is needed. Free energy is not a scalar, a simple number, as expected for time symmetry (with (4a) set zero) and able to react in positive and negative time direction. Energy has, in contrast, dynamic, vectorial properties and its behavior is inseparably linked with time asymmetry (according to Equation (4) and meaning (4a)). Relation (4) was strictly derived from established theoretical understanding, but the conventional assumption of time neutrality ((4a) set zero) excluded due to the above discussed experimental facts on lived time. As a consequence, energy must be related to an oriented time, must produce changes over time and must also generate the time asymmetry itself as described by Equation (4). A dynamic energy and an active, directional time are, inevitably, interrelated and linked. Time neutrality or time symmetry (defined as (4a) set zero), which

has never been supported by experimental evidence, is therefore experimentally disproved and identified as persistent convention, which should be overcome.

The negative sign in Equation (4) indicates that some implicit component of available energy must be able to decrease along with development of time subject to time asymmetry (while respecting energy conservation). The total derivative of energy mathematically considers this implicit dependence on a time dependent variable (below shown to be information). What is ultimately enforcing such a decrease in a property of energy along the time axis? What law the time dependent energy follows is found by rearranging Equation (4) and integrating it to:

$$-\int dE \partial t = \int \partial L dt \quad (5)$$

The right side now expresses the time evolution of changes in the Lagrange function, which arise as a consequence of time asymmetry. These are the changes experienced as real time flow, here to be called “action time”. What does Equation (5) say in terms of energy? The left side is showing the negative (decreasing) time integral over a total differential energy quantity. It is the decreasing differential “action” (energy times time). This is exactly what the principle of least action is expressing for an infinitesimal section of energy. Equation (5) tells us consequently, that the asymmetric development of the Lagrange function in time (right side), and thus of the physical system, is following and the consequence of the principle of least action (left side). Time flow and changes caused by time are the consequence of fulfilling the principle of least action.

That the principle of least action is applied and works in nature as a fundamental principle is a three centuries long experience in physics. According to Equation (5) it definitely describes a dynamic law, expressing, that, via the principle of least action, nature is fundamentally dynamic and time-asymmetric. A time-orienting change in the Lagrange function follows from a “dynamic” principle of least action. Such a fundamentally dynamic property of this principle is in present physics not considered as such, because energy and time are just treated as numbers, scalar quantities. For this reason, the meaning of the principle of least action has remained enigmatic. In contrast, Equation (5) here implies, that energy has the ability to approach a minimum in some of its qualities (included in the total derivative), following the principle of least action. Energy, subject to the dynamic principle of least action, has to have dynamic properties and, according to Equations (4) and (5), is inseparably linked to and drives time asymmetry. This way, the principle of least action gets a significance, which has never been recognized in the past: the principle of least action expresses that nature is fundamentally irreversible with a dynamic energy generating a directional time, the time we are experiencing. It is a flow of action (energy times time), as expressed in (5). It is not clock-time, which is used to follow this flow of action in an averaged way via oscillating mechanisms, cleared from the drive of energy (see mathematical distinction later).

What is new with an energy, which has dynamic properties? It is in clear contradiction to present handling energy as a scalar quantity with the potential to

perform work, but no interest in doing it. It is also in clear contradiction with the concept of time neutrality and time invariance against displacement and inversion, which allows to describe energy systems to act both in positive and negative time direction. However, an engineer will understand that energy is needed to produce movement in experienced time direction and the public understanding of “having energy” equally implies dynamic action. Aristotle, who lived in the 4th century BC, already argued along this line: “Time is the measure of a movement that takes place from a before to an after”. His idea of time did not describe any illusion, but he recognized experienced movement, energy-driven reality, as an expression of time. He described action as generated by a stone rolling down a hill (following the principle of least action) and stated that passing time is linked to such movements (as expressed in (5)). Since movements are linked to energy turnover, time is linked to a “dynamic” energy. All together makes sense because it reflects reality.

Let us recall, what could be learned up to now in order to find out what decreasing energy property is accompanying the drive, responsible for the time-orientation in free energy. When energy is responsible for the dynamics of a system, described by the Lagrange function L , then Equation (4) also expresses that there is no time invariance against displacement in time ((4a) cannot be set zero). An energy system therefore develops in direction of increasing entropy and generates time asymmetry. Equation (5) in addition tells that this occurs via the principle of least action. This means that energy acts as a dynamic variable and that the time generated is directional (which is also experimentally observed). It also describes that the time-related properties of a system (described by L) are exclusively determined by dynamic time dependent properties of energy (which presently is excluded by the concept of a scalar energy quantity). This supports the arguments presented above in subchapter 2.1. Energy consequently not only has the property of being conserved (as experimentally proven, and later confirmed for the presented formalism), it simultaneously has an additional dynamic time dependent property itself (considered in the total derivative of energy in Equation (4)). The same is then, of course also true for the Lagrange function. Both have to be considered to act as dynamic variables, entirely in contrast to their present role as scalar quantities. By becoming time oriented they abandon the world of time-neutrality. Energy is not consumed, not decreasing in quantity. What time dependent property contained in energy and considered by its total derivative in Equation (4) is then actually, between free energy and entropic energy, changing and driving time? During entropy production information is abandoned and energy is involved. What is the role of information in such an energy conversion process?

2.4. Entropy Formation and Energy Driven Information Loss

It is well known that thermodynamic entropy S and information entropy I are related via (k is the Boltzmann constant) (e.g. [9]).

$$S = k \ln 2I \quad (6)$$

An increase of entropic energy $T\Delta S$ is, since energy is conserved, linked to a corresponding turnover and decrease of free energy ΔE . An increase of information entropy I is linked to a decrease (negative sign) of actual information I_{act} . Replacing thermodynamic entropy S for information entropy I (6) and considering that an increase of information entropy I is linked to a decrease (negative sign) of actual information I_{act} , the working ability of available energy can be calculated. It is subject to a decrease in contained actual information I_{act} (within free energy) according to the following relation:

$$\Delta E \rightarrow T\Delta S = -kT \ln 2\Delta I_{\text{act}} \quad (7)$$

In this relation $kT \ln 2$ is the energy needed to activate 1 bit. It is again liberated as thermodynamic heat (entropic energy), when erased. With the above considerations (subchapters 2.1. and 2.2.) identifying free energy as the origin and driving source of entropy increase and of oriented time, it means that the turnover of free energy is linked to a decrease of information. During an energy conversion process, energy itself is conserved, but information (order) within the original free energy is decreasing. This decrease in the information content is considered in the total time derivative of energy (Equation (4)) and is therefore directly linked to the generation of time asymmetry. The product is chaotic, entropic energy with a negligible level of order or information left. This abandonment of information from free, available energy, during production of entropic, chaotic energy, is responsible for the generation of time intervals which are adding to time asymmetry. The process of entropy increase in combination with a progressing time can therefore be attributed to a free energy with the property of aiming at a reduction of presence per state, which is equivalent to a diminution of order, information, as described by relation (7). Practical examples are heat dissipated into the environment or an excited molecule releasing energy in smaller quantities via various pathways.

Such a decrease in information, which free, available energy, $E(t) = E(I_{\text{act}}(t))$, experiences during energy turnover, on its way to entropic energy, is obviously considered in the overall energy balance and in energy conservation. Since the work of Szilard [10] it is known that the minimum energy required to store 1 bit of information is $kT \ln 2$. Landauer [11] has shown that erasure of 1 bit of information generates heat and increases thermodynamic entropic energy by $kT \ln 2$. Free energy already contains the information (e.g. stored in chemical bonds of fuels, which create the ability to do work) and when erased its energy is still there as entropic energy in the form of low temperature heat. Energy conservation is therefore also fulfilled for the total time derivative of $E(t)$ in Equation (4), which expresses, how dynamic energy drives time asymmetry via decreasing contained information and increasing entropy. The information lost during entropy formation (7) was originally still available for free energy and its turnover is the origin and thrust of energy-driven changes.

2.5. What Exactly Is Experienced Time?

Since science has based natural laws on time neutrality and considers time to be an illusion, numerous attempts have been undertaken to make real, experienced time more understandable (e.g. [12] [13] [14] [15] [16]). They yielded deeply rooted considerations, studied wise comments on time since antiquity and discussed intelligent statements from experience, but essentially remained futile, because explaining lived time as a consequence of time neutrality and from the viewpoint of relativistic time paradoxes turned out to be practically impossible. For most observers, it remained therefore an open question what experienced time actually is.

According to the considerations presented here, science itself causes the problem. Science has simply to drop the persistent convention of time neutrality and time neutrality and symmetry in fundamental laws. It is a heritage from historic times, when formulation and understanding of dynamic laws were still too complicated. The time of entropy increase and the entropy increase itself are not compatible with time neutrality and the concept of time as an illusion. Time is caused by free energy, which has to be considered dynamic and time-oriented. Subject to this new interpretation time is the

“energy-driven flow of action observed in nature”,

as expressed by relations (5), with L and E here being dynamic variables. Action time (the flow of action subject to the principle of least action) as described by (5), is progressing in an inhomogeneous way, within large and small processes, which may proceed simultaneously or in consequence. Since energy, via the processes activated in generating action time, thereby loses information (7), time is also the

“ongoing loss of information about the past”.

Progressing time is, in fact, a process of information loss due to energy turnover.

Since action-time, with its turnover of action and information respectively, is, in nature, occurring locally and temporarily inhomogeneous, clock-time is to be used and calibrated as a scale for defining and measuring an averaged progress of action-time. Also, our brain may be doing this with changes going on in the environment.

The energy-driven time, “action time”, is directional and makes natural processes fundamentally irreversible. Energy, consequently, by generating action, via the principle of least action (relation (5)), drives a time, which is oriented and provides a flow of information turnover. This can be mathematically derived by inserting the expression (7) describing the information to be lost from active, free energy on its way to entropic energy into Equation (4) and considering that free energy still disposes of this information (changed sign). This relates the information-based quality of energy and its turnover to asymmetric time evolution. One yields:

$$-\frac{dE}{dt} = -\frac{dE}{dI_{\text{act}}} \frac{dI_{\text{act}}}{dt} = -kT \ln 2 \frac{dI_{\text{act}}}{dt} = \frac{\partial L}{\partial t} \quad (8)$$

This formula (8) shows that asymmetric time evolution, the partial time derivative of the (dynamic) Lagrange function L , is directly related to the decrease of a property of energy E , which turns out to be the loss of information I_{act} (including its energetic value $kT \ln 2$) according to Equation (7). Again, $kT \ln 2$ is the energy for creating one bit of information, which is then released as entropic energy (e.g. environmental heat) when the information is again erased.

When free energy is turned over on its way to entropic energy, energy itself is conserved, but information is lost. Since information stored in energy itself has an energy content which is then reappearing as entropic energy, turnover of information works in accordance with overall energy conservation. Energy is not lost in the process and the reason for energy conservation, which was previously veiled, becomes obvious.

How are we experiencing time flow around us? Energy turnover is linked with information turnover (8). When a new energy source is appearing in parallel, more information will initially be there, which equally will be gradually lost during energy turnover, and this will go on with more and different energy sources in the environment or the living body. An observer experiences, via the energy-phenomena observed, time-displaced sequences of images of varying information content (Equation (8)). It is like seeing successive complex images adding to a movie. Experiencing time is actually like seeing a movie. Energy driven, changing information turnover is a key to understand passing time as a reality, an information-based energy-driven reality. Since energy turnover proceeds under permanently varying conditions, such information will typically be different and characteristic for past, presence and future. A distinction between them, as in daily practice, is clearly possible and can be documented via information. In addition, turnover of action and information (including erasing it) respectively (Equations (5) and (8)) are invariant during relativistic transformation. We are not dealing with an illusion and relativity paradoxes, as found for clock-time, disappear for action time.

This conclusion obviously contradicts the above-mentioned statement by Einstein on time (clock-time) as an illusion. According to arguments presented here experienced time is not an illusion (nor is it clock-time) but is information-based reality! A continuously generated flow and turnover (erasing) of information, which accompanies the parallel flow of action, generates action-time, which is not an illusion.

A block-universe understands time differently: Relativity Theory is based on time-neutral natural laws and Einstein calculated and commented on clock-time, which is not energy driven, not the real time accompanying changes discussed here, but a normalized scale, contradicting equation (4), which defines the origin of time asymmetry. Clock-time is a kind of frozen time, a strange contrast to the time really experienced. It was nevertheless used to design the fourth dimension of space-time and was exposed to relativity considerations (Einstein insisted that

time is clock-time). According to the formalism developed here clock-time is just a scale and has not the potential to tell us how energy converting systems are actually behaving in their own dynamic way.

During the rise of Relativity-Theory the Nobel prize winning French philosopher Henri Bergson attacked Einstein accusing him of “spreading metaphysics over science by describing time and its formulas as a time not lived by human experience”. Einstein replied that “there is no (separate) time for philosophers” [17]. Here it was shown that such time for philosophers (and reflecting people) exists. It is action time, which is not subject to relativistic changes (see later). The considerations developed in this paper give Bergson right. Time (clock-time) as an illusion does not support and explain real life. Action time (5), which is described here as the experienced, energy-driven, information erasing time phenomenon (8), is clearly different from clock-time, which is based on a different foundation but, of course, useful and necessary for registering and calibrating averaged changes. Since its information comes from and involves energy, action time (5) communicates the message of energy phenomena. Clock-time, on the other hand, is not the real time, but a kind of “alias”. It has nothing to do with energy turnover and uses combinations of natural constants and material properties to measure, via chains of oscillation periods, an averaged progress of energy-driven real time flow (action time) in the environment, ultimately calibrated for practical use with periodical astronomical phenomena.

2.6. Real Time (Action Time) Means Erasing Information, Clock-Time Just Using It

What is the mathematical relation between real time (action time) and clock-time? In order to better understand what action time, defined as time evolution of changes in the Lagrange function, means and what its relation to clock-time is, the rearrangement and integration of formula (4) to yield (5) should now be repeated with formula (8). One obtains:

$$-\int dE \partial t = -\int (kT \ln 2) dI_{\text{act}} \partial t = \int \partial L dt = \text{action time} \quad (9)$$

It describes action time as the loss of information dI_{act} to the past, but multiplied with the energy $E' = kT \ln 2$, which is liberated when erasing one bit and turned over into entropic energy (heat). This means that free energy has to be turned over and thereby information to be erased to generate action time. It has the dimension of action (energy times time, where time has the meaning of clock-time) and is relativistic invariant.

In order to obtain clock-time, action time (with the dimension of a flow of action) has to be divided by the energy turned over per bit, $E' = kT \ln 2$. The result is shown in the following equation:

$$-\int \frac{dE}{E'} \partial t = -\int dI \partial t = \int \frac{\partial L}{E'} dt = \text{clock-time} \quad (10)$$

Clock-time is, as deducible from relation (10), providing information, but this information is not turned over, erased. It is simply, since energy E and Lagrange

function L were neutralized as dynamic variables, used as a scale providing information. It is also used in this simple function for defining the fourth dimension in space-time. No energy turnover and corresponding information loss or erasure is involved in this case. No time asymmetry is involved any more. Clock-time is therefore only useful for registering an averaged, energy-driven progress of action-time (9). It is just a tool for measurement and as a scale subject to relativistic changes. These changes have, however, no significance for energy turnover and time asymmetry, as described by (4) and (5), which follow action time (9). In conclusion, it can be said that action time (9) flows, driven by the principle of least action, while clock-time (10) is frozen, just a scale, invented by humans.

2.7. How Humans Are Experiencing Time

Let us now consider how humans experience time and were and still are dealing with it. Many energy conversion processes are all the time occurring in the environment as well as in the human body itself. Geological processes, life activities, weather phenomena and social events are continuously proceeding and consuming (useful) energy. This occurs via a turnover of information (8), which is thereby finally erased and liberated as heat.

Physically, this means that information from the environment or the human body, which was present before, is gone and new information, from ongoing additional energy turnover, is available. Humans and other living organisms have learned to experience the phenomenon of vanishing older and newly made available information from their environment as time flow. Since it turned out to be crucial for their living activities humans attempted to measure and subdivide time and found that periodical natural phenomena were especially useful for this purpose. They followed and studied the movement of the sun and marked the cast shadow. They also studied the movement of the moon. This resulted in useful calendars for daily and annual activities. Since Kepler empirically formulated his laws and later Newton provided the mathematical tool to calculate them it is known that the formula for the time periods of cycling planets and satellites only depend on system constants and natural constants. They do not contain any reference to energy turnover.

Later humans developed artificial clocks, which are also based on periodical phenomena (pendulum movement, quartz oscillation, atomic transition), which require energy for visualization, but the time periods they apply have again nothing to do with energy. Clocks, like planetary cycles, provide information (10) useful for monitoring changes in the environment. The information used in this case is however not erased, but allows to monitor energy driven action time (9) in an averaged, calibrated way via the provided scale.

Different from energy-driven real time (action time), clock-time, as a scale, follows its own laws. Itself it does not reflect the flow of action and of information lost to the past, as seen from (10) in comparison with (9) for action time.

Clock-time is a kind of standardized, energy-neutral scale (10), applied for monitoring the ongoing energy-driven erasure of information in the environment (9).

It is the author's conviction that mayor problems in physics started to arise, when clock-time, with concepts basing on time neutrality and incomprehension of the dynamic role of energy (4), was identified with action-time, the really lived time: Einstein commented: "time is what the clock shows". It would be more correct to say: "time is what clocks partially imitate".

As a pure scale, not involving erasure of information, clock-time is changeable, subject to relativistic transformation, with conclusions to be drawn, which are presently shaping the concept of our universe. They are known to be to a significant extent paradox and counterintuitive. Examples: Within the presently favored block universe the most distant galaxies, already approaching light velocity, will be experiencing nearly time standstill (and higher life there expecting this also for our own galaxy). In contrast, the here derived energy-driven action time (9) is invariant. Life in these galaxies, subject to the same energy laws, will proceed equally fast there. The mentioned notion of galaxies wandering off with close to light velocity (velocity even doubled (!) when referred to opposite universe position) may also be treated with caution, since time-neutral quantum physics could not properly consider irreversible energy loss (red-shift) for spreading photons via entropy generation (see later). Time travel, with all its paradoxes, is inevitably fiction as well. Energy consuming travelers would have to travel with action time (9). It is relativistic invariant, functioning via erasing of information and not with frozen clock-time (10), within which they would only accompany information into the past or into the future. This information from clock-time, as a scale, can be compressed or stretched, because subject to relativistic transformation, and therefore causes counterintuitive paradoxes, which have nothing to do with reality.

2.8. Information-Based Proof of Time Asymmetry in Energetic Processes

After such far-reaching conclusions, which indicate that clock-time is not expressing essential energy-related reality but only acting as a scale, a reevaluation of the responsible basic claim—absence of time neutrality in natural laws—is appropriate (test of validity of Equation (4) as drive for time asymmetry). An additional critical test is now possible for verification whether abandoning time neutrality and time displacement invariance is justified and consistent with present knowledge about energy behavior. For this purpose, one can use the derived Equation (8) to evaluate its deeper meaning. By insisting on (experimentally not supported) time-neutrality and time-symmetry (the partial derivative of the Lagrange function (4a) in (8) set zero) it follows from (8) that dI_{act}/dt then equals zero and as a consequence acting information I_{act} in free energy would always stay constant. Acting information would thus remain conserved during energy turnover. Such a conclusion, derived from basic Equations (2) to (4) while just still insisting on time neutrality of natural laws, is entirely in conflict

with our understanding of energy turnover from valuable free energy (high order, high information content) to not any more valuable entropic energy (low order, low information content). It thus disproves the here hypothetically assumed time neutrality on experimentally verified grounds. It is entirely incompatible with our understanding about energy. It is also in conflict with our knowledge about information, which is not a quantity, for which a conservation law is known or even applicable.

In turn, the experimental fact that information is erased, not remaining constant, during energy turnover proves time asymmetry and disproves time symmetry ((4a) set zero) according to Equation (8).

In a time-neutral universe, as it is claimed to exist today, energy turnover, as we know it from long-term experience, would simply not work, since free, available energy must lose information on its way to entropic energy (e.g. low temperature heat). Time neutrality is thus entirely inconsistent with known, relevant properties of energy and information. Formula (8) also indicates that information turnover is essential for energetic processes and is the key towards performing work. The here presented test, together with the above discussed asymmetry of lived time, again underlines the justifiability of challenging fundamental time neutrality as a claim which contradicts reality and contributes to an imaginary model of nature and our universe.

In this context, it is appropriate to ask what it exactly is what makes energy with high information content (free energy) much more valuable and active than the same amount of energy with low information content (entropic energy). It is the intricate structure of chemical bonds, the profound and complicated physical nature of electromagnetic or gravitational fields, the complex electron distribution in excited molecular states, which get mechanisms to work via the elaborate information they contain and make available. Such information is lost on the way to entropic energy, because information is erased and its energy content released in form of not anymore useful entropic energy. It is obvious that it is the quality of information contained in energy which is determining its value as energy source. This information is lost and erased during energy turnover, used to perform work or dissipated as heat, and this process contributes, according to Equation (9), to the progress of real time, action time. Real time, action time, is an energy-driven information phenomenon which, because it strikingly designed the environment, has shaped the existence of living beings. Clock-time (10), as a frozen scale provides information, but does not erase it. It can be used to track, calibrate and measure action time, which may proceed inhomogeneous in time and space (9), from outside the information erasing systems. But itself clock-time cannot give deeper insight into fundamental properties of energetic processes which generate experienced time.

2.9. Thermodynamic Entropy Laws Follow without Additional Assumptions

According to relation (8) abandonment of actual information, erasing it, from

energy systems, which reflects the occurring changes, is thus related to asymmetric time evolution (4a) and entropy increase (7). Progressing time, action time, is linked to an ongoing erasing and deletion of information. It is obvious, that the important second law of thermodynamics, the time dependent increase of entropy in a closed space, automatically follows from such energy-time properties, as expressed by (8) and considering (7). The information content in the system decreases (entropy increases) and generates time asymmetry while energy in its entirety is conserved. It is a dynamic energy and not higher probability, which is ultimately responsible for time orientation. Via relations (8) and (9) this is a straightforward result. It is significant to point out again, that the presently favored time-neutral formalism does not allow derivation of this important empirical second law of thermodynamics without additional assumptions. Here, the difference simply is, that the paradigm of time neutrality ((4a) set zero, which is an experimentally unproven convention) was abandoned considering the known properties of lived time, and taking into account that, while the total energy is being conserved, the information, lost due to entropy generation, must have originated from free, available energy. A derivation of the second law of thermodynamics from basic principles (Equation (4)) succeeded, though with the message, that nature is fundamentally irreversible.

The flow of information, abandoned and erased from an energy converting system, which aims at a decrease of energy's information content (order), is also the key to distinguish between a "before" and an "after" (with different information contents) for facilitating feedback in self-organization processes. Because of the relation between information turnover and time flow (8) it is information which ultimately links past and present (a distinction which is not available in a time-neutral, time-invariant world) during build-up of local order at the expense of entropy production. It is the energy-driven, information handling action time (9) which pushes open the door to the creative world of non-linear irreversible thermodynamics facilitating impressive terrestrial and galactic phenomena as well as biological nature and life. It should, by allowing better understanding, at the longer term, also help to develop bio-analogue energy and material technology, which has been so successful in nature, but is subject to complex self-organization processes, which fail subject to time neutrality. What entropy law do such self-organized non-linear processes follow?

Equation (8) with Equation (7) state that for dynamic systems far from equilibrium a reduction and erasing of information, equivalent to entropy production, becomes rate limiting. This has a significant consequence. Self-organized, feedback-driven systems will accelerate this rate and finally maximize the rate of information loss (entropy gain) within their restraints. It means they follow an entropy law and an aim:

“maximum entropy (energy) turnover within the constraints of the system”.

A hurricane will aim at harvesting maximum energy from the sea environment and will grow in power accordingly, but slow down after landfall due to

changing constraints.

This entropy law for non-linear irreversible processes gives important new insight (see also discussion later), which could up to now not be derived from reversible thermodynamics, due to rate limitation of chemical processes via statistically occurring collisions with (scalar) activation energies to be surpassed (of course still valid as approximation near equilibrium).

Biological systems must follow this aim of maximum entropy production as well (an aim is hitherto strictly denied in biological science), but its implementation is not only balanced by given restraints of the systems, but additionally guided and controlled by the evolved and superposed genetic code. They are teleological systems due to these feedback processes involved, as already recognized in 1943 for cybernetic systems [18] (e.g. regulatory and purposive electronic devices). They are subject to a purely materialistic purpose generated by the systems themselves.

Why was it so easily possible to derive the second law of thermodynamics and the entropy law for non-linear irreversible thermodynamics from dynamic energy-time considerations (Equations (4), (7) and (8))? These laws are dealing with energy systems developing in time. Consequently, a dynamic relation between energy and time was needed to understand and describe them. Equation (8) could provide it, not however a concept of time-neutral natural laws with a scalar energy quantity, which has no interest reacting in time, which as clock-time in addition was treated as frozen.

3. Summary and Discussion

3.1. Time Is the Track of Energy-Driven Information Loss

Physics today, while insisting on time-neutrality and time-neutral fundamental laws, takes note of the phenomenon of entropy increase over time as a striking natural process and accepts that time practically proceeds via mechanisms, which aim at maximum probability and measures it with clocks. The time response of clocks has nothing to do with energy turnover. The time progress they measure only expresses sequences of time intervals of oscillating systems the oscillation period of which is determined by natural constants and material parameters. This clock-time, embedded and manipulated within General Relativity Theory, became a crucial element in constructing a block-universe, in which time is considered merely to be an illusion, depending on relative movements [19]. Equation (10) explains, why clock-time is indeed an illusion: The information it expresses is just a scale. It does neither reflect changes nor orientation, which energy turnover traces, which requires erasing information, which releases $kT \ln 2$ in entropic energy for each bit, as relation (9) describes for action time.

As suspected at the beginning of subchapter 2.5., the claimed time neutrality for natural laws and time paradoxes from Relativity Theory were essential stumbling blocks on the way to understanding time. The considerations presented here, which rely on a re-interpretation of the Lagrange-Euler formalism on the

basis of experimental facts on experienced time, derive, that this experienced time is an expression of a fundamentally irreversible nature. Time is generated and pushed by energy (expressed by Equation (4)), which is causing movements and changes, and is not at all an illusion. Equation (4), when expressed by “dynamic” quantities of Lagrange function and energy (and not by scalar quantities, as characteristic for a time-neutral world), is the origin of an energy-driven time, which is oriented, and thus the basis of time asymmetry. Free energy, by decreasing its order and erasing information, and thereby producing entropic energy, generates this oriented time as a flow of action, action time (Equation (5) and (9)). This energy-driven time flow is caused as a process of erasing information on the past. During generation of action-time via such a mechanism, intervals, measurable as passed clock-time, are apparently inevitable. They simply show up during the process of formation of energetic products of lower information content (entropic energy $T\Delta S$). Time (measurable as clock-time) is required for erasing information and converting energy into entropic energy, environmental heat.

On the basis of such results time is not a pre-existing time-neutral axis in positive and negative time direction, as presently assumed. It is an oriented dimension created by continuous information turnover as a consequence of energy turnover, or, more precise, by abandonment and erasure of information contained in available energy. In this respect time is clearly an information phenomenon. Its function is dealing with and providing information. Real time in nature (here called action time (9)) is the ongoing process of information loss to the past and ultimate expression of nature’s dynamics and creativity. Such complex information processes are not accessible for clock-time, which is a designed and calibrated information scale (10) useful only for keeping track of action time (9).

Energy-driven, information handling processes generate “action time” (5) (9) and make up the changing world we are seeing around us as a sequence of changing information images (expressed by (8)). Clocks, working via oscillations determined by natural constants and material parameters, are however needed to monitor action time in an averaged and calibrated way. They are constructed not to measure the flux of abandoned information (action time) during “lived” time, but simply provide information on changes in form of a time scale (10). These clocks measure the progress of action-time, but do not any more give access to relevant properties of energy systems. When atomic clocks are sent flying around the globe the observed microsecond shift [20] is real, but here expected to be an effect of calibration and relativity changes due to changed parameters during travel affecting atomic oscillations only. It is not a change in real time, action time, which is an energy phenomenon and of different nature. Technical installations, which work with clocks, have, of course, to consider such deviations, when required.

When the real time in nature, action time (expressed in (5) (9)), is to be transformed to a moving system, the energy-driven flow of action (or turnover

of abandoned, erased information) has to be transformed, and action as well as turnover of abandoned information remain invariant. Relativity paradoxes disappear for energy converting systems. The clock-time of the block-universe [21] is not the real time—it is indeed an illusion (as claimed by its proponents themselves), an artificial time scale shaped by natural and system constants defining oscillation periods and subject to characteristic relativistic transformation. It has, as its mathematical description (10) clearly shows, neither to do with time asymmetry (defined as the partial time derivation of the Lagrange function (4a)), nor with energy-driven systems (the total time derivative of energy). In order to describe relevant natural systems, the time must get the property of thereby simultaneously abandoning information as action-time does (9) and energy converting systems do.

The scientific strategy applied here to question time neutrality was based on a simple, transparent procedure: starting from the established Lagrange and Euler-Lagrange formalism (Equations (2)-(4)) and energy-entropy notions (1), the time-symmetry claim (4a) for Equation (4) was questioned and disproved basing on experimental facts on lived time. Time asymmetry, the partial derivation of the Lagrange function with respect to time (right side of relation (4)) cannot be set zero because this contradicts our daily experience with time and with energy converting systems reacting in time. As a consequence, Equation (4) cannot be applied to justify a time-neutral nature supporting energy conservation only. It expresses an energy-driven evolving nature, which leaves a time track of abandoned information.

Equation (8) was, in subchapter 2.8., also used to show that time neutrality contradicts established experimental knowledge about the function of energy turnover. Information is not conserved between free and entropic energy, but has to change in order to facilitate energy turnover. In turn, the need for information turnover during energy conversion contradicts time neutrality of natural laws, as seen from (8).

It is an interesting discovery, that the frequently used Lagrange-Euler formalism for the description of dynamic mechanisms included the possibility to derive an energy-driven irreversible nature as done here by insisting on the experimentally observed, actually existing time asymmetry in Equation (4). The only prerequisite would have been to accept the reality, that experienced time is indeed asymmetric ((4a) not zero). Then equation precisely (4) tells, that energy is actually driving irreversibility and changes, what every engineer would have understood to be an experimental fact. This did not happen and shows, how strongly rooted the historically grown convention of time-neutrality and time symmetry in natural laws was and still is. It also led to the (here considered erroneous) conviction that the frozen clock-time (the “alias” for measuring real time flow) itself is determining reality. It cannot, since it does not trace the actual changes occurring during energy turnover, but simply acts as an information providing scale, suitable for measuring changes only.

Energy (free, available energy) has a time dependent and time driving component (considered in the total derivative of energy in (4)), which can be identified as its content of information (order), which is being gradually erased and correspondingly decreases during entropy formation. This conclusion is supported by the rearranged Equation (5), which then expresses, that the evolution of the Lagrange function is determined by the decreasing differential least action. This fulfillment of the principle of least action, by energy, which is an experimental fact, equally requires that energy has a dynamic property. Free, available energy generates oriented time, here called action-time, as a flow of action or a flow of information loss (as seen from (7) and (8)). As Equation (5) shows, the principle of least action is specifying the dynamic mechanism through which energetic processes and thus erasure of information are implemented, but with Lagrange function L and Energy E acting as dynamic variables.

3.2. What Would Be Different in a Fundamentally Time-Oriented Nature?

The attempt here, to bring the established paradigm of time neutrality, which could never be supported by direct experimental evidence, into critical discussion, is a mayor challenge, because it is deeply rooted in physics and anchored in much-tested theories. Besides of the arguments and proofs presented here it will be necessary to demonstrate, that a transition from a time-neutral to a fundamentally directed, irreversible nature, brings substantial advantages for general physical understanding in terms of simplicity, logic and meaningfulness.

Such evidence partially already exists as a result of recent investigations, by the author, originally aimed at investigating and questioning the origin and necessity of the rising number of paradoxes and irrational theoretical models in concepts of physics, which were incorporated into “scientific understanding” during the past century (e.g. non-locality, uncertainty, zero-point energy, energy from nothing (Big Bang), expanding empty space, relativistic paradoxes, time as illusion, time-travel, bent empty space, multi-dimensions, multi-universes). The conclusion reached from such an effort was, that the irrational assumptions and paradoxes were ultimately assumed and required in response to the (claimed, here considered incorrect) time-neutral character of fundamental physical laws. If, on the other hand, a dynamic energy is allowed to push time, action time, as underpinned in this publication by deriving the dynamically understood Equations (4), (5) and (8), existing experimental reality supports a quite different irreversible, self-organizing nature and universe [21]-[26]. It is rational, requires less assumptions, is simpler in structure and, due to its entirely logic nature, more convincing. It appears to be, as also the simple derivation of important thermodynamic entropy laws (from (8), subchapter 2.9.) underlines, clearly favored by Ockham’s law of parsimony.

The author is convinced that he has proven that time-neutrality of fundamental laws is not compatible with our long-term experience with energy as well

as information. This has the consequence that important theories basing on time-neutrality (the possibility to displace systems in time homogeneously in positive and negative direction) are either wrong, superfluous, or just applicable as limiting cases. Abandoning time neutrality, on the other hand, means that new theories and concepts describing nature will become possible. In order to rise interest in critically questioning time-neutrality and in looking at consequences, a few examples may show the contours, scientific prospects and consistency of the alternative, of an energy driven, time-determining self-organizing universe, based on the dynamic understanding of energy and time as discussed above:

- Quantum states become dynamic phenomena and have to be understood differently. Particle and wave are not any longer equivalent and simultaneously present in time neutrality. Instead, the spatially extended wave results from the particle, but requires information on matter for the reversion into the particle and to be in balance with it (analogy to concept of Maxwell demon). This information (on matter) is activated in the quantum state and turned out to be the missing information needed to overcome quantum paradoxes [21].
- Matter is self-organized energy. This immediately explains the known proportionality between energy and matter (relativity considerations are not required). A new and different way of looking at the large and complex family of elementary particles is possible (comparison with self-organized, inactive viruses) [22].
- The “information on matter” attributed to dynamic quantum states and present around them seems to fulfill all attributes of gravitation and provides the link between the quantum world and cosmology [23]. Gravitation is information on matter. Satellites are teleguided by this information (gravitation), when following the principle of least action.
- The ongoing turnover of quantum states between particle and wave, via information they contain, explains the always constant remaining light velocity (light particles, including their velocity, are recreated via information in any relative system). The same information on matter explains gravitation itself. A postulated bent space-time, which enforces exactly these two natural phenomena via the General Relativity Theory [27], is not at all needed and manifestations attributed to it may find different explanations [24]. This realization that the Theory of Relativity is not required is the more relevant, since above considerations (subchapters 2.6. and 2.7.) have shown, that clock-time, used in it, is not the real dynamic action time (9) to which energy systems are exposed, but just a frozen technical time scale (10).

Relativity Theory, based on the assumption of time-neutral natural laws and clock-time, is presently generally accepted because claimed to have passed essential experimental trials. Tests, which differentiate between a space-time universe and an energy-driven universe, subject to action time, are unavoi-

ble. They could experimentally concentrate on the distinction between the contradicting gravitation models they propose. It is bent space in the first case, information on matter in the second. Gravitation (which present quantum theory is not able not consider on particle level, but dynamic quantum understanding can [21] [23]) between two neutrons and two spheres of the size of the Earth increases by a factor of 10^{114} (!). Gravitation in the form of information (on matter) could handle changes over so many orders of magnitude, as well as small fluctuations within (e.g. apparently observed in LIGO experiments), not however a bent space, bent over 114 orders of magnitude (!) around a sphere. Apart from the impossibility to imagine such an immensely fine grading of still measurable space bending around a sphere, a bent space would provide analogue signals, which, as experience shows, can practically only be measured within 0,01 % of the maximum signal.

- Present quantum physics does not allow spreading, propagating photons to produce entropy. They can only lose energy when colliding or encountering a gravitation field. In contrast, dynamic quanta can respect the entropy law for spreading radiation [23] [26], which Einstein still compared with the entropy of an expanding gas to propose the photon concept in analogy to gas particles [28]. This means that the presently claimed cosmological redshift of starlight (attributed to an expanding empty (!) space) may in part simply be entropy generation by expanding, propagating radiation with corresponding consequences for a theory on space dynamics and the origin of the universe [23] [26].
- Due to a dynamic energy, entropy generation is a rate limiting process (relation (8) with (7)). This not only, as shown above, explains the second law of thermodynamics, but also allows derivation of maximum entropy generation (within the given restraints) as entropy law for self-organization processes within non-linear irreversible thermodynamics. Evolution of life would follow such an aim (which is presently denied), which is however subject to and controlled by the superposed genetic code [25]. This explains evolution towards higher complexity and intensifying symbiotic coexistence, as well as the vitality and determination of life as a strive for increasing energy (entropy) turnover (with accompanying increasing local build-up of order and structures) [26]. Such a result, indicating an aim in evolution, is in strict conflict with present understanding of biological mechanisms and origin of intensive controversy (e.g. [29]). Evolution towards maximum entropy generation as an inbuilt aim is also applicable to galactic structures such as, for example, black hole-quasar associations [26].
- Information, which has an energy content, and is contained in biological structures, can, in an irreversible world, also self-organize via feedback processes. This leads to consciousness and spirit [26] with the necessary much more complex information structure. These phenomena could not be explained up to now, which has been criticized, by US philosopher Thomas

Nagel, as a serious weakness of the present natural scientific world model [30]. Possible implications of a universe, controlled by information (in form of gravitation) and aiming at evolving spirit, for evolution of humanity is discussed in [26].

At the beginning, it was mentioned that quantum theory links energy and entropy with time via the uncertainty relation [6]. What is the ultimate meaning of this relation between energy and time? Because of a so far assumed fundamental time neutrality of quantum states, and since time entered the Schrödinger equation as clock-time via external perturbation theory, the exact meaning of time-energy uncertainty is still debated in spite of significant efforts undertaken to better understand it [31]. The here presented dynamic interpretation of energy and time provides new viewpoints for discussion. One is that the uncertainty relation in quantum physics has to be interpreted differently, because it reflects a dynamic, not a time-neutral phenomenon [26]. The second is that energy and time are indeed linked because free energy generates time via turnover of action, energy times time, and erasure of information on the way to entropy formation (5) (8). Clock-time of quantum physics, however, is not the real dynamic time. It is just a frozen scale.

3.3. A Way to Better Understand Energy, Nature and the Universe

In his famous “Lectures on Physics” Richard Feynman emphasized that “...in today’s physics we have no knowledge what energy actually is. (...) It is an abstract thing, that does not tell us the mechanisms and reasons for the different formulas (it fulfills)”. A look at formula (3) for energy may, superficially seen, support this impression. The here presented approach can, however, show the way to an appropriate answer. Energy behaves similar to money, which, in an economy, also provides for goods and services and involves information turnover (Equation (8)). Money does not need to be handled and used physically in form of materials such as metal or paper. It equally well works in form of pure information (e.g. via credit cards, crypto-currencies). Energy functions basically also as a product of information and information technology in nature. This can readily be deduced from Equation (8). It is the turnover of information (I_{act}) and the natural law implementing this, which is facilitating the function of useful, free energy (similar to the function of money and information within a financial economy [26]). Since action time (9) itself is related to information, the saying, from Benjamin Franklin, “time is money”, has also a deeper significance. It means that energy turnover is related to time flow, which is actually expressed by relations (4) and (8).

Can the here developed dynamic energy concept now tell the reason for its most important formula, energy conservation? It can! Valuable, free energy works via stored information, countable in bits (8). Exactly this energy for bits ($kT \ln 2$) stored in information appears again as entropic energy (heat) when

erased. Alternatively, information can, during energy conversion, first be transferred to other (valuable) energy carriers, which store part of the information in between, and be erased later.

A concept of nature with an energy-driven time not only explains the second law of thermodynamics and yields the entropy law for irreversible thermodynamics (subchapter 2.9.), but also recognizes information as a key element for understanding general creativity in nature. Information is involved in feedback processes and the build-up of local inorganic and organic order at the expense of entropy generation and, in form of gravitation, in the dynamics of a quite different universe [23] [26]. In it, time does not move forward or backward homogeneously along a given lane or alley as an intricate part of a four-dimensional space-time. Contrary to this, time, as explained here, is the result of an energy-driven information erasure, which we register as a flow of action. It generates, what we experience as proceeding time and only develops in the direction we experience within a classically understood space. It is for this reason that invariance against displacement in time in positive and negative direction, as hitherto assumed, cannot and does not work. Time (clock-time), within a space-time constructed by it, is itself an illusion and gives a misleading impression of natural processes and nature whenever energy turnover is involved and wherever irreversibility cannot be neglected for simplification.

With the concept of a fundamentally irreversible nature based on an energy-driven time-arrow it is not only easily possible to allocate and accommodate many natural phenomena in a consistent scheme, as the above discussion shows. It would, for the first time, also be possible to say what nature actually is [26]: “Nature is the self-realization of energy through time”: Energy self-organizes to matter. Matter self-organizes to inorganic structures and life. Information, provided and active in evolved structures, self-organizes to consciousness and spirit. This appears to be a surprising, but plausible aim for a universe, which is essentially controlled by information.

There is another precise, far reaching new conclusion to be drawn for a fundamentally irreversible nature: With the given explanations for energy (a product of information, like money) and the function of nature (self-realization of energy through time) the universe could not have originated from a chaotic explosion (Big Bang), forced to yield a high entropy, low information product. It must have started from information, which is the essence, the drive of available, free energy, which also generates what we experience as natural reality and, most important, as passing time. This result attributes the origin of the universe to an entirely logic mechanism in itself, which is even understood that way by larger religions (information, as included in words) [26]. The information contained in valuable energy is gradually erased, while creating the large diversity of inorganic and organic structures in the universe and leaving a trace of abandoned, erased information, which we are experiencing as time flow. Without information at the beginning no start and flow of time (action time (9)) would have been

possible either.

It also becomes understandable why it just was time-neutral fundamental physics that conduced to a chaotic, explosive start of the universe: entropy production and energy loss by spreading photons, like in a spreading gas (as still in comparison discussed by Einstein to justify the particle concept of light [28]), could, as a fundamentally irreversible process, not be properly considered (as redshift) in present time neutral quantum physics.

Numerous now well accepted theoretical concepts will have to change to be compatible with a fundamentally irreversible nature while most experimentally relevant present knowledge will stay as tolerable approximations to time neutrality, proximity to equilibrium and absence of feedback conditions.

To find the right concept of time is a key to understanding nature and the universe. Questioning time neutrality and time symmetry appears to show the way to a more intelligent and ultimately better understandable universe.

3.4. Conclusions

The natural philosopher Heraclitus (520-460 BC) did not only observe that “everything changes and nothing stands still”, he also said, that “time is a game played beautifully by children”. Did he mean that time is at the origin of creativity and imagination? Is time part of and generated out of changes, as discussed above? It seems that such an impression of time as a source of diversity has been communicated again and again in literature sources. In the Indian Sanskrit epic Mahabharata from around 200 BC one can read: “time makes all things grow and destroys all”. Such a view survived the time-neutral concepts of scientific progress. The Argentinian writer and philosopher Jorge Luis Borges commented: “Time is the substance I am made of. Time is a river that carries me along, but I am the river”. Indeed, energy turnover in the human body is part of time flow, it is the river mentioned by Borges. Swiss writer-philosopher Ludwig Hohl also considered time as a source of unfolding vitality [32]. As a consequence, he expected that exclusion of such a “creative” time from natural science should yield a one-sided development of knowledge. Present science and technology, in spite of ongoing acceleration of research and progress, have indeed been criticized for not fulfilling essential expectations for socially and environmentally relevant progress. As a consequence, a reorientation was called for by experienced philosophers [33]. The late Japanese physicist-psychologist-philosopher Masanao Toda made in this regard a quite precise scientific comment: “Our intuition screams out that time is something that flows, unlike physical time, which is frozen”.

The here presented work shows that time is not at all an illusion, just a frozen, neutral scale, along which systems move, but indeed the origin of changes and creativity in nature. It is the dynamics and erasure of information as expression of energy turnover, of feedback reactions and of creativity in nature, which are shaping an ever-changing nature and universe. The here given formalism and

analysis of the consequences from such a concept has shown that our scientific understanding and world view would open new perspectives while simultaneously becoming more elegant, more rational, simpler and more future oriented. The easy derivation of thermodynamic laws and a more reasonable understanding of evolution promise important new insights. In the field of practical progress, it may be expected that environmentally benign materials and technologies, which evolution has so successfully applied via irreversible processes, may become more accessible and imitable in the long term. The finding that information plays a fundamental role in nature and that self-organization of information yields consciousness and spirit may also stimulate new intellectual ideas about the origin and destination of the universe. But ahead of that a critical confrontation with highly developed, established concepts and theories basing on “time-neutral” physics is inevitable. This paper has been written to provide physical-theoretical arguments for a serious discussion. An entirely irreversible nature around us may underline the need for such a controversy.

Conflicts of Interest

The author declares no conflicts of interest regarding the publication of this paper.

References

- [1] BBC Presentation and Video (Twitter) by Katie Robertson: 10 February 2020: Are You Experiencing Time Wrong?
- [2] Boltzmann, L. (1872) *Sitzungsberichte der Akademie der Wissenschaften*, **66**, 275-370.
- [3] Morimoto, T. (1963) *Journal of the Physical Society of Japan*, **18**, 328-331.
<https://doi.org/10.1143/JPSJ.18.328>
- [4] Prigogine, I. and Stengers, I. (1997) *The End of Certainty: Time, Chaos, and the New Laws of Nature*. Simon and Schuster, New York.
- [5] Karakostas, V. (1996) *Philosophy of Science*, **63**, 374-400.
<https://doi.org/10.1086/289917>
- [6] Beretta, G.P. (2019) *Entropy*, **21**, 679. <https://doi.org/10.3390/e21070679>
- [7] Noether, E. (1918) *Invariante Variationsprobleme*, Nachrichten der Königlichen Gesellschaft der Wissenschaften zu Göttingen, Mathematisch-Physikalische Klasse, S. 235-257; English Translation.
- [8] Wilkens, M. (2015) Noethers Theorem.
<http://www.quantum.physik.uni-potsdam.de/teaching/ws2015/qm2/Noether.pdf>
- [9] Hägele, P.C. (2004) Was hat die Entropie mit Information zu tun?
https://www.uni-ulm.de/~phaegele/Vorlesung/Grundlagen_II/_information.pdf
- [10] Szilard, L. (1929) *Zeitschrift für Physik*, **53**, 840-856.
<https://doi.org/10.1007/BF01341281>
- [11] Landauer, R. (1961) *IBM Journal of Research and Development*, **5**, 183-191.
<https://doi.org/10.1147/rd.53.0183>
- [12] Reichenbach, H. (1956) *The Direction of Time*. University of California Press, Oakland.
- [13] Withrow, G.J. (1979) *What Is Time?* Thames and Hudson, London.

-
- [14] Withrow, G.J. (1980) *The Natural Philosophy of Time*. Clarendon Press, Oxford.
- [15] Davies, P.C.W. (1974) *The Physics of Time Asymmetry*. Surrey University Press, London.
- [16] Zeh, H.D. (1992) *The Physical Basis of the Direction of Time*. Springer, Berlin.
<https://doi.org/10.1007/978-3-662-02759-2>
- [17] Canales, J. (2016) *Physics and the Philosopher: Einstein, Bergson and the Debate that Changed our Understanding of Time*. Princeton University Press, Princeton.
<https://doi.org/10.2307/j.ctvc7763q>
- [18] Rosenblueth, A., Wiener, N. and Bigelow, J. (1943) *Philosophy of Science*, **10**, 18-24.
<https://doi.org/10.1086/286788>
- [19] Young, Ch. (2020) Block Universe Theory: Is the Passing of Time an Illusion?
<https://interestingengineering.com/block-universe-theory-is-the-passing-of-time-an-illusion>
- [20] Wick, G. (1972) *New Scientist*, **53**, 261-263.
- [21] Tributsch, H. (2016) *Journal of Modern Physics*, **7**, 365-374.
<https://doi.org/10.4236/jmp.2016.74037>
- [22] Tributsch, H. (2018) *Journal of Modern Physics*, **9**, 1361-1380.
<https://doi.org/10.4236/jmp.2018.97082>
- [23] Tributsch, H. (2016) *Journal of Modern Physics*, **7**, 1455-1482.
<http://www.scirp.org/journal/jmp>
<https://doi.org/10.4236/jmp.2016.712133>
- [24] Tributsch, H. (2019) *Journal of Modern Physics*, **10**, 1029-1064.
<https://doi.org/10.4236/jmp.2019.108068>
- [25] Tributsch, H. (2018) *Advances in Anthropology*, **8**, 140-174.
https://file.scirp.org/pdf/AA_2018082716575292.pdf
<https://doi.org/10.4236/aa.2018.83008>
- [26] Tributsch, H. (2020) *Time Arrow as Trace of Energy, Logical Key to a Spiritual Universe*. MyMorawa, Vienna.
<https://www.amazon.de/Time-Arrow-Trace-Energy-Spiritual/dp/3990936263>
- [27] Einstein, A. (1916) *Annalen der Physik*, **49**, 769.
<https://doi.org/10.1002/andp.19163540702>
- [28] Einstein, A. (1905) *Annalen der Physik*, **17**, 132.
<https://doi.org/10.1002/andp.19053220607>
- [29] Gould, S.J. (1992) *Scientific American*, **267**, 118-121.
<https://doi.org/10.1038/scientificamerican0792-118>
- [30] Nagel, T. (2012) *Mind and Cosmos, Why the Materialist Neo-Darwinian Conception of Nature Is Almost Certainly False*. Oxford University Press, Oxford.
<https://doi.org/10.1093/acprof:oso/9780199919758.001.0001>
- [31] Busch, P. (2007) The Time-Energy Uncertainty Relation. In: Muga, G., *et al.*, Eds., *Time in Quantum Mechanics*, Springer, Berlin, 73-105.
<https://arxiv.org/pdf/quant-ph/0105049.pdf>
- [32] Hohl, L. (1984) *Die Notizen*. Suhrkamp, Frankfurt.
- [33] Böhme, G., Van Den Daele, W. and Krohn, W. (1976) *Social Science Information*, **15**, 307-330. <https://doi.org/10.1177/053901847601500205>

Variational Calculations of Energies of the $(2snl) 1,3L^\pi$ and $(2pnl) 1,3L^\pi$ Doubly Excited States in Two-Electron Systems Applying the Screening Constant per Unit Nuclear Charge

Momar Talla Gning¹, Ibrahima Sakho^{1*}, Maurice Faye¹, Malick Sow², Babou Diop², Jean Kouhissoré Badiane³, Diouldé Ba³, Abdourahmane Diallo³

¹Department of Physics Chemistry, UFR Sciences and Technologies, University of Thies, Thies, Senegal

²Department of Physics, Faculty of Sciences and Techniques, University Cheikh Anta Diop of Dakar, Dakar, Senegal

³Department of Physics, UFR Sciences and Technologies, University Assane Seck of Ziguinchor, Ziguinchor, Senegal
Email: *aminafatima_sakho@yahoo.fr

How to cite this paper: Gning, M.T., Sakho, I., Faye, M., Sow, M., Diop, B., Badiane, J.K., Ba, D. and Diallo, A. (2021) Variational Calculations of Energies of the $(2snl) 1,3L^\pi$ and $(2pnl) 1,3L^\pi$ Doubly Excited States in Two-Electron Systems Applying the Screening Constant per Unit Nuclear Charge. *Journal of Modern Physics*, 12, 328-352.

<https://doi.org/10.4236/jmp.2021.123024>

Received: January 5, 2021

Accepted: February 23, 2021

Published: February 26, 2021

Copyright © 2021 by author(s) and Scientific Research Publishing Inc. This work is licensed under the Creative Commons Attribution International License (CC BY 4.0).

<http://creativecommons.org/licenses/by/4.0/>



Open Access

Abstract

In this paper, resonance energies and excitation energies of doubly $2sns 1,3S$, $2snp 1,3P$, $2pnp 1,3D$, $2pnd 1,3P$ and $2pnf 1,3G$ excited states of the helium isoelectronic sequence with $Z \leq 10$ are calculated. Calculations are carried out in the framework of the variational procedure of the formalism of the Screening Constant per Unit Nuclear Charge (SCUNC). New correlated wave function of Hylleraas type is used. Precise resonance and excitation energies are tabulated and good agreement is obtained when a comparison is made with available literature values.

Keywords

Doubly Excited States, Helium Isoelectronic Sequence, Screening Constant per Unit Nuclear Charge (SCUNC), Correlated Wave Function, Resonance Energy, Excitation Energies

1. Introduction

Study of Doubly Excited States (DES) of He-like ions remains an active field of investigation due to their importance in the interpretation of astrophysical data [1] [2]. These states were first observed by Madden and Codling [3] [4] in photoabsorption experiments on helium using synchrotron radiation, and further experimental studies have shown their presence in highly charged ions [5]. As shown in various studies, electron correlations play an important role in under-

standing lines atomic species for the diagnosis of astrophysical and laboratory plasma. In addition, DES of the two-electron systems are the most fundamental systems that autoionize. They have been attracting considerable interest, because they are best suited to theoretical study on the resonance phenomena. The understanding of elementary processes in the collisions of electrons with atoms or ions is very important in plasma physics, laser technology, astrophysics and physics of the upper atmosphere.

Experimentally, many of these doubly excited states have been observed in electronic impact experiments by Oda *et al.*, [6] and Hicks and Comer [7]. In their studies, these authors have worked on the energy spectra of ejected electrons from autoionization states in helium excited by electron impact. Other doubly excited states were observed by ion impact by Rudd [8] and by Borde-nave-Montesquieu *et al.*, [9]. These DES were also studied by examining the spectra of ejected electrons by Gelabart *et al.*, [10] and by Rodbro *et al.*, [11].

From a theoretical point of view, several ab initio methods have been used. The complex rotation method [12] used in studies of Feshbach-type $^{1,3}D$ resonances in two-electron systems, $Z = 2 - 10$, the variational method [13] [14], the density functional theory [15] was used to calculate the nonrelativistic energies and densities of the doubly excited states of the He-isoelectronics series ($Z = 2 - 5$). The formalism of the Feshbach projection operators [16] was applied for the calculations of energy positions and widths of singlet and triplet (even and odd) resonances of the heliumlike ($Z = 2 - 10$) systems lying between the $n = 2$ and $n = 3$ thresholds, the complex rotation method [17] [18] [19]. The truncated diagonalization method used for calculations of widths for doubly excited states of two-electron systems [20]. The discretization technique [21] applied to the calculation of energies and widths of $^{1,3}S$ resonances of the He isoelectronic series, the semi-empirical procedure of the Screening Constant by Unit Nuclear Charge (SCUNC) method [22] [23] [24]. The time-dependent variation perturbation theory (TDVPT) [25] is employed to study the $Nlnl^l L^e$ resonances (with $N = 2, \dots, 5$; $n = N, \dots, 5$; $l = l' = 0, 1, 2$ and $L = l + l'$) for the ions from $Z = 2$ to $Z = 5$ in the helium isoelectronic sequence, complex rotation combined with discrete finite base sets to accurately describe doubly excited states [26].

Recently, Gning *et al.*, [27] complex rotation method to determine the resonance parameters of the $((2s^2)^1S^e, (2s2p)^{1,3}P^o)$ and $((3s^2)^1S^e, (3s3p)^{1,3}P^o)$ states of helium-like ions with $Z \leq 10$ via a Scilab program. The variational method of Hylleraas was used by Dieng *et al.*, [28] to determine the resonance energies of the doubly excited states $nln'l'$ and $nln'l'$ (with $n \leq 3$, $n' \leq 4$ and $l = l'$ or $l \neq l'$) of helium-like ions. Very recently, the resonance parameters of the doubly excited $2sns^{1,3}S^e, 2snp^{1,3}P^o, 2pnp^{1,3}D^e, 3d4d^{1,3}G^e$ states of helium and heliumlike ions are calculated by Sow *et al.*, [29].

In general Most of the theoretical methods mentioned above are based on calculation codes or on tedious and complex mathematical calculation programs and in some cases require very powerful computers. In contrast to these me-

thods, the Screening Constant by Nuclear Unit of Charge (SCUNC) method is a very flexible method and has the advantage of providing very precise resonance energies and excitation energies for very high $n = 10$ of the doubly excited states ($Nlnl', {}^{2S+1}L^{\pi}$) without complex mathematical programs or calculation codes. In addition, in the recent past, the variational procedure of the SCUNC method has been successfully applied to calculations of resonance energies of doubly excited states $nlnl'$ ($n = 2 - 4$) in heliumlike ions by Sakho [30] using a special Hylleraas-type wavefunction. The goal of this present work is to extend this study to doubly excited states $Nlnl'$ (with $l = l'$ or $l \neq l'$) by reporting precise resonance energies and excitation energies up to $n = 10$. In this work, calculations are devoted to the doubly $2sns$ ${}^{1,3}S^e$, $2snp$ ${}^{1,3}P^o$, $2pnp$ ${}^{1,3}D^e$, $2pnd$ ${}^{1,3}F^o$ and $2pnf$ ${}^{1,3}G^e$ excited states of He-like ions up to $Z = 10$ via analytical expressions in contrast with ab initio method requiring computational codes to report accurate resonance data.

Section 2 gives the procedure of the construction of the correlated wavefunctions used along with a brief overview of the establishment of the analytical expressions used in the calculations. Section 3 gives the presentation and the discussion of the results obtained compared to available theoretical and experimental data.

2. Theory

2.1. Hamiltonian and Hylleraas—Type Wavefunctions

The description of the properties of matter at the atomic scale is in principle based on the solution of the time independent Schrödinger equation.

$$\hat{H}\Psi = E\Psi \quad (1)$$

where \hat{H} represents the Hamiltonian operator of the considered system (atom, molecule, solid), Ψ the trial wavefunction and E the associated energy.

The Hamiltonian H of the helium isoelectronic series is given by (in atomic units)

$$H = -\frac{1}{2}\Delta_1 - \frac{1}{2}\Delta_2 - \frac{Z}{r_1} - \frac{Z}{r_2} + \frac{1}{r_{12}} \quad (2)$$

In this equation, Z is the nuclear charge Δ_1 is the Laplacian with reference to the coordinates of the vector radius r_1 which detect the position of the electron 1. Δ_2 Laplacian defines the coordinates of the vector radius r_2 which detect the position of the electron 2 and r_{12} inter-electronic distance.

The exact resolution of Equation (1) is usually far too complicated because of the term $r_{12} = u = |r_1 - r_2|$. It is therefore necessary to implement a rough calculation method using a correlated wavefunction.

In this previous work, Sakho [30] used a special-form Hylleraas correlated wavefunction to calculate the energies of the doubly excited states $nlnl'$ ($n = 2 - 4$) of heliumlike ions. In the present study, we have made modifications to these wavefunctions to extend these calculations to the doubly excited states ($Nlnl'$

$2S+1L^{\pi}$). These wavefunctions are defined as follows:

$$\Psi = \sum_{\nu=0}^{\nu=N-\ell-1} (N^2 r_0^2)^{\nu} \sum_{\nu'=0}^{\nu'=n-\ell'-1} (n^2 r_0^2)^{\nu'} \left[1 + (-1)^S C_0 Z (r_1 - r_2) \right] \times (r_1 + r_2)^j (r_1 - r_2)^k |r_1 - r_2|^m e^{-\alpha(r_1+r_2)} \quad (3)$$

In this expression, N and n are the principal quantum numbers, l and l' are orbital quantum numbers, r_0 is Bohr radius, S is the total spin of atomic system, α and C_0 are the variational parameters to be determined by minimizing the energy, Z is the nuclear charge number, r_1 and r_2 are the coordinates of electrons with respect to the nucleus, j, k, m are Hylleraas parameters satisfying the double condition ($j, k, m \geq 0$) and $j + k + m \leq 3$. The set of the parameters (j, k, m) define the basis states and then give their dimension D . From the theoretical viewpoint, the Hylleraas variational method is based on the Hylleraas and Undheim theorem [31] according to which, a good approximation of the energy eigenvalue $E(\alpha, C_0)$ is obtained when the minima of the function $(dE(\alpha, C_0)/d\alpha dC_0)$ converge with increasing values of the dimension D of the basis states and when the function exhibit a plateau.

Using this theorem, the values of the variational parameters α and C_0 can be determined by the following conditions:

$$\frac{\partial E(\alpha, C_0)}{\partial C_0} = 0 \quad (4)$$

and

$$\frac{\partial E(\alpha, C_0)}{\partial \alpha} = 0 \quad (5)$$

For all calculations, we fixed the value of $j = 0$ and $k = m = 1$ and this choice has allowed us to obtain:

$$\Psi = \sum_{\nu=0}^{\nu=N-\ell-1} (N^2 r_0^2)^{\nu} \sum_{\nu'=0}^{\nu'=n-\ell'-1} (n^2 r_0^2)^{\nu'} \left[1 + (-1)^S C_0 Z (r_1 - r_2) \right] \times (r_1 - r_2) |r_1 - r_2| e^{-\alpha(r_1+r_2)} \quad (6)$$

In the framework of the Ritz' variation principle, the energy $E(\alpha, C_0) = \langle H \rangle(\alpha, C_0)$ is calculated from the relation:

$$E(\alpha, C_0) = \langle H \rangle(\alpha) = \frac{\langle \Psi(\alpha, C_0) | H | \Psi(\alpha, C_0) \rangle}{\langle \Psi(\alpha, C_0) | \Psi(\alpha, C_0) \rangle} \quad (7)$$

In this equation, the correlated wavefunctions are given by (6) and the Hamiltonian H of the helium isoelectronic series is given by (2) in atomic units.

Furthermore, the closure relation represents the fact that $|r_1, r_2\rangle$ are continuous bases in the space of the two-electron space, written as follow:

$$\iint dr_1^3 dr_2^3 |r_1, r_2\rangle \langle r_1, r_2| = 1 \quad (8)$$

Using this relation, according to (7), we obtain:

$$\begin{aligned}
 E(\alpha, C_0) &= \iint d\mathbf{r}_1^3 d\mathbf{r}_2^3 \langle \Psi(\alpha, C_0) | \mathbf{r}_1, \mathbf{r}_2 \rangle \times \langle \mathbf{r}_1, \mathbf{r}_2 | \Psi(\alpha, C_0) \rangle \\
 &= \iint d\mathbf{r}_1^3 d\mathbf{r}_2^3 \langle \Psi(\alpha, C_0) | \mathbf{r}_1, \mathbf{r}_2 \rangle \hat{H} \langle \mathbf{r}_1, \mathbf{r}_2 | \Psi(\alpha, C_0) \rangle
 \end{aligned}
 \tag{9}$$

By developing this expression (9), we find:

$$\begin{aligned}
 E(\alpha, C_0) &= \iint d\mathbf{r}_1^3 d\mathbf{r}_2^3 \Psi(\alpha, C_0) \times \Psi^*(\alpha, C_0) \\
 &= \iint d\mathbf{r}_1^3 d\mathbf{r}_2^3 \Psi(\alpha, C_0) \hat{H} \Psi^*(\alpha, C_0)
 \end{aligned}
 \tag{10}$$

This means:

$$N * E(\alpha, C_0) = \iint d\mathbf{r}_1^3 d\mathbf{r}_2^3 \Psi(\alpha, C_0) \hat{H} \Psi^*(\alpha, C_0)
 \tag{11}$$

With the normalization constant

$$N = \iint d\mathbf{r}_1^3 d\mathbf{r}_2^3 |\Psi(\alpha, C_0)|^2
 \tag{12}$$

To make it easier to integrate Equation (11), we operate the variable changes in elliptic coordinates by:

$$s = r_1 + r_2; \quad t = r_1 - r_2; \quad u = r_{12}
 \tag{13}$$

On the basis of these variable changes, the elementary volume element

$$d\tau = d^3r_1 d^3r_2 = 2\pi^2 (s^2 - t^2) u ds du dt
 \tag{14}$$

Using these elliptical coordinates, Equation (11) is written as follows

$$\begin{aligned}
 NE(\alpha, C_0) &= \int_0^\infty ds \int_0^s du \int_0^u dt \left\{ u(s^2 - t^2) \times \left[\left(\frac{\partial \Psi}{\partial s} \right)^2 + \left(\frac{\partial \Psi}{\partial t} \right)^2 + \left(\frac{\partial \Psi}{\partial u} \right)^2 \right] \right. \\
 &\quad \left. + 2 \left(\frac{\partial \Psi}{\partial u} \right) \times \left[s(u^2 - t^2) \times \frac{\partial \Psi}{\partial s} + t(s^2 - u^2) \times \frac{\partial \Psi}{\partial t} - \Psi^2 \times (4Zsu - s^2 + t^2) \right] \right\}
 \end{aligned}
 \tag{15}$$

With respect to the correlated wave functions given by expression (6), it is expressed as follows

$$\begin{aligned}
 \Psi(s, t, u, \alpha, C_0) &= \sum_{\nu=0}^{\nu=N-\ell-1} (N^2 r_0^2)^\nu \sum_{\nu'=0}^{\nu'=n-\ell'-1} (n^2 r_0^2)^{\nu'} \left[1 + (-1)^S C_0 Z t \right] \times t u \exp(-\alpha s)
 \end{aligned}
 \tag{16}$$

Furthermore, according to (12), the normalization constant is written in elliptic coordinates as:

$$N = \int_0^\infty ds \int_0^s du \int_0^u dt u (s^2 - t^2) \times \Psi^2
 \tag{17}$$

2.2. General Formalism of the SCUNC Method

The Screening Constant by Unit Nuclear Charge (SCUNC) formalism is used in this work to calculate the resonance energies and the excitation energies of the $(2snl)^{1,3}L^\pi$ and $(2pnl)^{1,3}L^\pi$ doubly excited states of the helium-isoelectronic up to $Z = 10$.

In the framework of the Screening Constant by Unit Nuclear Charge (SCUNC) formalism, resonance energies of the $(Nlnl', 2s^{l+1}L^\pi)$ doubly excited states are ex-

pressed in Rydberg (Ry) as below [22] [23] [32]

$$E(N\ell n\ell', {}^{2S+1}L^\pi) = -Z^2 \left(\frac{1}{N^2} + \frac{1}{n^2} \left[1 - \beta(N\ell n\ell', {}^{2S+1}L^\pi, Z) \right]^2 \right) Ry \quad (18)$$

In this equation, the principal quantum numbers N and n , are respectively for the inner and the outer electron of the He-isoelectronic series. In this equation, the β -parameters are screening constant by unit nuclear charge expanded in inverse powers of Z and given by

$$\beta(N\ell n\ell', {}^{2S+1}L^\pi, Z) = \sum_{k=1}^q f_k \left(\frac{1}{Z} \right)^k \quad (19)$$

where $f_k = f_k(N\ell n\ell', {}^{2S+1}L^\pi)$ are screening constants to be evaluated based on variational predictable using a wavefunction.

Furthermore, in the framework of the Screening Constant by Unit Nuclear Charge formalism, the β -screening constant is expressed in terms of the variational α -parameter as follows:

- For the doubly excited states $(2sn\ell) {}^{1,3}L^\pi$

$$\beta(2sn\ell, {}^{1,3}L^\pi, Z, \alpha) = \frac{\alpha}{Z^2} \left(1 + \frac{L-S+1}{2n+8} \right) \quad (20)$$

- For the doubly excited states $(2pn\ell) {}^{1,3}L^\pi$

$$\beta(2pn\ell, {}^{1,3}L^\pi, Z, \alpha) = \frac{\alpha}{Z^2} \left(1 + \frac{L-S}{n+S(S+1)+3} \right) \quad (21)$$

In these expressions, N and n , are respectively the principal quantum numbers for the inner and outer electron, L characterizes the quantum state under consideration (S, P, D, F , etc.), S is the total spin of the atomic system and α is the variational parameter.

2.3. Energy Resonances of the $(2sn\ell) {}^{1,3}L^\pi$ and $(2pn\ell) {}^{1,3}L^\pi$ Doubly Excited States of Helium and Heliumlike Ions of Nuclear Charge $Z \leq 10$

Using equations (20) and (21), the resonance energies of the doubly excited $(2sn\ell) {}^{1,3}L^\pi$ and $(2pn\ell) {}^{1,3}L^\pi$ states of helium and heliumlike ions of nuclear charge $Z \leq 10$ are then expressed as follows in Rydberg (Ry):

- For the doubly excited states $(2sn\ell) {}^{1,3}L^\pi$

$$E(2sn\ell, {}^{1,3}L^\pi, Z) = -Z^2 \left(\frac{1}{N^2} + \frac{1}{n^2} \left[1 - \frac{\alpha}{Z^2} \left(1 + \frac{L-S+1}{2n+8} \right) \right]^2 \right) Ry \quad (22)$$

- For the doubly excited states $(2pn\ell) {}^{1,3}L^\pi$

$$E(2pn\ell, {}^{1,3}L^\pi, Z) = -Z^2 \left(\frac{1}{N^2} + \frac{1}{n^2} \left[1 - \frac{\alpha}{Z^2} \left(1 + \frac{L-S}{n+S(S+1)+3} \right) \right]^2 \right) Ry \quad (23)$$

In these equations, only the parameter α is unknown. Considering the $2p3p$

$^1D^{\circ}$ level of heliumlike ions ($Z = 2 - 10$), we calculated the values of the variational parameters α and C_0 , the results are presented in **Table 1** below.

The Equations (22) and (23) are used to calculate the resonance energies of the $(2snl) \ ^{1,3}L^{\pi}$ and $(2pnl) \ ^{1,3}L^{\pi}$ doubly excited states of helium and heliumlike ions of nuclear charge $Z \leq 10$ without a complex calculation program.

3. Results and Discussions

The results obtained in the present study for the resonance energies and the excitation energies of the doubly excited $2sns \ ^{1,3}S^{\circ}$, $2snp \ ^{1,3}P^{\circ}$, $2pnp \ ^{1,3}D^{\circ}$, $2pnd \ ^{1,3}F^{\circ}$ and $2pnf \ ^{1,3}G^{\circ}$ states with $n = 2 - 10$ of the helium isoelectronic sequence ($Z = 2 - 10$) are presented in **Tables 1-14** where a comparison between our present results and the experimental and theoretical values available in the literature is made.

Table 1 presents the values of the variational parameters α and C_0 $2 \leq Z \leq 10$. These parameters are calculated by determining the expression of $E = f(\alpha, C_0)$ from Equation (15) and wavefunction (16) using conditions (4) and (5). All the calculations are performed using a Maxima computer program.

In **Table 2** and **Table 3**, we have listed resonance energies of the $2sns \ ^{1,3}S^{\circ}$ and $2snp \ ^{1,3}P^{\circ}$ doubly excited states of the helium isoelectronic sequence up to $Z = 10$. In **Table 4**, **Table 5**, **Table 6**, the present results for the resonance energies of the $2pnp \ ^{1,3}D^{\circ}$, $2pnd \ ^{1,3}F^{\circ}$ and $2pnf \ ^{1,3}G^{\circ}$ doubly excited states up to $Z = 10$ are presented.

In **Table 7**, the present resonance energies of doubly $2sns \ ^{1,3}S^{\circ}$ ($n = 3 - 5$) excited states are compared with various calculations. The data of Sow *et al.*, [29] [33] are obtained from variational calculations using wave function of Hylleraas type. Ho [18] [19] and Kar and Ho [34] applied the complex coordinate rotation (CCR) method whereas Sakho [24] used the semi-empirical procedure of the SCUNC method. Lipsky *et al.*, [35] used truncated diagonalization method of Ray and Mukherjee [25] applied the Time-Dependent Variation Perturbation Theory (TDVPT) whereas Inanov and Safronova [36] computed double sums over the complete hydrogen spectrum (CHS) to report their data. Roy *et al.*, [15] used the Density-Functional Theory (DFT) formalism and Macias and Riera [21] applied the discretization method. Comparison shows that the present results are generally in good agreement with all the cited literature data up to $Z = 10$. These agreements point out the validity of the new correlated wave functions used in the present calculations.

Table 1. Values of variational parameters α and C_0 of Helium-like ions ($Z = 2 - 10$).

Z	2	3	4	5	6	7	8	9	10
α	1.2996	2.0074	2.7157	3.4242	4.1327	4.8414	5.5500	6.2587	6.9674
C_0	0.4433	0.3106	0.2630	0.2385	0.2236	0.2135	0.2063	0.2003	0.1966

Table 2. Energy resonances ($-E$) of doubly excited $2sns^{1,3}S^e$ ($n = 3 - 10$) states of He-like systems ($Z = 2 - 10$). The results are expressed in atomic units. 1 a.u. = 2 Ry = 27.211396 eV.

$2sns^1S^e$								
Z	$2s3s^1S^e$	$2s4s^1S^e$	$2s5s^1S^e$	$2s6s^1S^e$	$2s7s^1S^e$	$2s8s^1S^e$	$2s9s^1S^e$	$2s10s^1S^e$
	$-E$							
2	0.59450	0.55363	0.53457	0.52414	0.51782	0.51369	0.51086	0.50882
3	1.41465	1.28879	1.23026	1.19834	1.17903	1.16647	1.15783	1.15164
4	2.59511	2.33601	2.21568	2.15014	2.11052	2.08476	2.06707	2.05440
5	4.13627	3.69550	3.49096	3.37961	3.31235	3.26863	3.23862	3.21712
6	6.03848	5.36746	5.05622	4.88685	4.78458	4.71812	4.67251	4.63985
7	8.30160	7.35181	6.91141	6.67183	6.52719	6.43322	6.36873	6.32257
8	10.92578	9.64864	9.05659	8.73458	8.54020	8.41393	8.32730	8.26528
9	13.91114	12.25801	11.49180	11.07512	10.82364	10.66029	10.54822	10.46801
10	17.25749	15.17981	14.21697	13.69342	13.37747	13.17226	13.03148	12.93073
$2sns^3S^e$								
Z	$2s3s^3S^e$	$2s4s^3S^e$	$2s5s^3S^e$	$2s6s^3S^e$	$2s7s^3S^e$	$2s8s^3S^e$	$2s9s^3S^e$	$2s10s^3S^e$
	$-E$							
2	0.60134	0.55701	0.53649	0.52534	0.51862	0.51426	0.51127	0.50913
3	1.42690	1.29483	1.23370	1.20049	1.18047	1.16748	1.15857	1.15219
4	2.61287	2.34476	2.22066	2.15325	2.11261	2.08622	2.06814	2.05520
5	4.15959	3.70699	3.49750	3.38370	3.31508	3.27055	3.24002	3.21818
6	6.06737	5.38169	5.06432	4.89192	4.78797	4.72050	4.67424	4.64115
7	8.33609	7.36880	6.92108	6.67787	6.53123	6.43605	6.37080	6.32412
8	10.96587	9.66838	9.06783	8.74160	8.54490	8.41723	8.32970	8.26709
9	13.95684	12.28051	11.50461	11.08313	10.82899	10.66405	10.55096	10.47007
10	17.30879	15.20507	14.23134	13.70241	13.38347	13.17648	13.03456	12.93304

Table 3. Energy resonances ($-E$) of doubly excited $2snp\ ^1P^0$ ($n = 2 - 10$) states of He-like systems ($Z = 2 - 10$). The results are expressed in atomic units. 1 a.u. = 2 Ry = 27.211396 eV.

		$2snp\ ^1P^0$						
Z	$2s2p\ ^1P^0$	$2s3p\ ^1P^0$	$2s4p\ ^1P^0$	$2s5p\ ^1P^0$	$2s6p\ ^1P^0$	$2s7p\ ^1P^0$	$2s8p\ ^1P^0$	$2s9p\ ^1P^0$
	$-E$							
2	0.69291	0.58789	0.55036	0.53269	0.52296	0.51703	0.51314	0.51045
3	1.74081	1.40265	1.28286	1.22688	1.19622	1.17762	1.16547	1.15710
4	3.28658	2.57761	2.32737	2.21076	2.14705	2.10846	2.08331	2.06601
5	5.33124	4.11321	3.68413	3.48448	3.37556	3.30964	3.26673	3.23723
6	7.87570	6.00985	5.35334	5.04818	4.88182	4.78122	4.71576	4.67078
7	10.91966	8.26738	7.33495	6.90181	6.66582	6.52318	6.43040	6.36667
8	14.46346	10.88596	9.62901	9.04542	8.72759	8.53553	8.41065	8.32490
9	18.50742	13.86572	12.23563	11.47906	11.06715	10.81832	10.65655	10.54549
10	23.05105	17.20646	15.15467	14.20266	13.68447	13.37149	13.16806	13.02842
		$2snp\ ^3P^0$						
Z	$2s3p\ ^3P^0$	$2s4p\ ^3P^0$	$2s5p\ ^3P^0$	$2s6p\ ^3P^0$	$2s7p\ ^3P^0$	$2s8p\ ^3P^0$	$2s9p\ ^3P^0$	$2s10p\ ^3P^0$
	$-E$							
2	0.59450	0.55363	0.53457	0.52414	0.51782	0.51369	0.51086	0.50882
3	1.41465	1.28879	1.23026	1.19834	1.17903	1.16647	1.15783	1.15164
4	2.59511	2.33601	2.21568	2.15014	2.11052	2.08476	2.06707	2.05440
5	4.13627	3.69550	3.49096	3.37961	3.31235	3.26863	3.23862	3.21712
6	6.03848	5.36746	5.05622	4.88685	4.78458	4.71812	4.67251	4.63985
7	8.30160	7.35181	6.91141	6.67183	6.52719	6.43322	6.36873	6.32257
8	10.92578	9.64864	9.05659	8.73458	8.54020	8.41393	8.32730	8.26528
9	13.91114	12.25801	11.49180	11.07512	10.82364	10.66029	10.54822	10.46801
10	17.25749	15.17981	14.21697	13.69342	13.37747	13.17226	13.03148	12.93073

Table 4. Energy resonances ($-E$) of doubly excited $2pnp\ ^1D^e$ ($n = 3 - 10$) states of He-like systems ($Z = 2 - 10$). The results are expressed in atomic units. 1 a.u. = 27.211396 eV.

$2pnp\ ^1D^e$								
Z	$2p3p\ ^1D^e$	$2p4p\ ^1D^e$	$2p5p\ ^1D^e$	$2p6p\ ^1D^e$	$2p7p\ ^1D^e$	$2p8p\ ^1D^e$	$2p9p\ ^1D^e$	$2p10p\ ^1D^e$
	$-E$							
2	0.57145	0.54242	0.52824	0.52022	0.51521	0.51188	0.50954	0.50783
3	1.37190	1.26812	1.21866	1.19117	1.17429	1.16316	1.15543	1.14985
4	2.53222	2.30568	2.19870	2.13965	2.10359	2.07994	2.06358	2.05179
5	4.05304	3.65541	3.46853	3.36578	3.30321	3.26227	3.23402	3.21369
6	5.93482	5.31758	5.02833	4.86966	4.77323	4.71023	4.66680	4.63558
7	8.17746	7.29211	6.87805	6.65127	6.51362	6.42378	6.36190	6.31747
8	10.78111	9.57909	9.01774	8.71064	8.52440	8.40295	8.31935	8.25935
9	13.74595	12.17862	11.44746	11.04781	10.80562	10.64776	10.53916	10.46124
10	17.07173	15.09056	14.16713	13.66273	13.35722	13.15819	13.02130	12.92313
$2pnp\ ^3D^e$								
Z	$2p3p\ ^3D^e$	$2p4p\ ^3D^e$	$2p5p\ ^3D^e$	$2p6p\ ^3D^e$	$2p7p\ ^3D^e$	$2p8p\ ^3D^e$	$2p9p\ ^3D^e$	$2p10p\ ^3D^e$
	$-E$							
2	0.58952	0.55108	0.53306	0.52318	0.51716	0.51323	0.51051	0.50856
3	1.40563	1.28417	1.22755	1.19661	1.17785	1.16562	1.15721	1.15116
4	2.58196	2.32928	2.21174	2.14761	2.10880	2.08354	2.06616	2.05371
5	4.11895	3.68665	3.48577	3.37629	3.31009	3.26702	3.23742	3.21622
6	6.01698	5.35647	5.04978	4.88274	4.78178	4.71612	4.67103	4.63873
7	8.27591	7.33868	6.90372	6.66691	6.52384	6.43083	6.36697	6.32122
8	10.89589	9.63337	9.04765	8.72886	8.53631	8.41116	8.32524	8.26372
9	13.87705	12.24059	11.48160	11.06860	10.81920	10.65713	10.54588	10.46623
10	17.21919	15.16024	14.20551	13.68609	13.37249	13.16871	13.02886	12.92873

Table 5. Energy resonances ($-E$) of doubly excited $2pnd^{1,3}F^0$ ($n = 3 - 10$) states of He-like systems ($Z = 2 - 10$). The results are expressed in atomic units. 1 a.u. = 27.211396 eV.

$2pnd^1F^0$								
Z	$2p3d^1F^0$	$2p4d^1F^0$	$2p5d^1F^0$	$2p6d^1F^0$	$2p7d^1F^0$	$2p8d^1F^0$	$2p9d^1F^0$	$2p10d^1F^0$
	$-E$							
2	0.55847	0.53593	0.52452	0.51787	0.51364	0.51077	0.50873	0.50722
3	1.34648	1.25562	1.21157	1.18674	1.17133	1.16109	1.15393	1.14871
4	2.49403	2.28702	2.18814	2.13309	2.09923	2.07688	2.06136	2.05012
5	4.00193	3.63052	3.45449	3.35706	3.29742	3.25823	3.23108	3.21148
6	5.87075	5.28644	5.01078	4.85878	4.76601	4.70519	4.66313	4.63284
7	8.10035	7.25468	6.85698	6.63822	6.50496	6.41774	6.35752	6.31418
8	10.69095	9.53537	8.99315	8.69541	8.51431	8.39591	8.31424	8.25552
9	13.64274	12.12860	11.41935	11.03041	10.79408	10.63972	10.53332	10.45687
10	16.95544	15.03424	14.13548	13.64314	13.34424	13.14914	13.01474	12.91822
$2pnd^3F^0$								
Z	$2p3d^3F^0$	$2p4d^3F^0$	$2p5d^3F^0$	$2p6d^3F^0$	$2p7d^3F^0$	$2p8d^3F^0$	$2p9d^3F^0$	$2p10d^3F^0$
	$-E$							
2	0.57844	0.54548	0.52981	0.52111	0.51576	0.51223	0.50978	0.50800
3	1.38513	1.27386	1.22158	1.19282	1.17529	1.16381	1.15587	1.15015
4	2.55185	2.31416	2.20300	2.14208	2.10507	2.08089	2.06422	2.05223
5	4.07913	3.66667	3.47423	3.36899	3.30516	3.26353	3.23486	3.21428
6	5.96741	5.33162	5.03543	4.87366	4.77566	4.71179	4.66785	4.63632
7	8.21656	7.30894	6.88656	6.65606	6.51653	6.42565	6.36316	6.31835
8	10.82674	9.59872	9.02766	8.71622	8.52779	8.40513	8.32082	8.26037
9	13.79811	12.20105	11.45879	11.05418	10.80949	10.65025	10.54084	10.46241
10	17.13043	15.11579	14.17988	13.66989	13.36157	13.16098	13.02319	12.92444

Table 6. Energy resonances ($-E$) of doubly excited $2pnf^{l^3}G^e$ ($n = 4 - 10$) states of He-like systems ($Z = 2 - 10$). The results are expressed in atomic units. 1 a.u. = 27.211396 eV.

		$2pnf^{l^1}G^e$					
Z	$2p4f^{l^1}G^e$	$2p5f^{l^1}G^e$	$2p6f^{l^1}G^e$	$2p7f^{l^1}G^e$	$2p8f^{l^1}G^e$	$2p9f^{l^1}G^e$	$2p10f^{l^1}G^e$
	$-E$						
2	0.53593	0.52452	0.51787	0.51364	0.51077	0.50873	0.50722
3	1.25562	1.21157	1.18674	1.17133	1.16109	1.15393	1.14871
4	2.28702	2.18814	2.13309	2.09923	2.07688	2.06136	2.05012
5	3.63052	3.45449	3.35706	3.29742	3.25823	3.23108	3.21148
6	5.28644	5.01078	4.85878	4.76601	4.70519	4.66313	4.63284
7	7.25468	6.85698	6.63822	6.50496	6.41774	6.35752	6.31418
8	9.53537	8.99315	8.69541	8.51431	8.39591	8.31424	8.25552
9	12.12860	11.41935	11.03041	10.79408	10.63972	10.53332	10.45687
10	15.03424	14.13548	13.64314	13.34424	13.14914	13.01474	12.91822
		$2pnf^{l^3}G^e$					
Z	$2p4f^{l^3}G^e$	$2p5f^{l^3}G^e$	$2p6f^{l^3}G^e$	$2p7f^{l^3}G^e$	$2p8f^{l^3}G^e$	$2p9f^{l^3}G^e$	$2p10f^{l^3}G^e$
	$-E$						
2	0.54020	0.52672	0.51913	0.51442	0.51127	0.50907	0.50746
3	1.26389	1.21579	1.18914	1.17280	1.16204	1.15457	1.14916
4	2.29940	2.19444	2.13665	2.10140	2.07829	2.06230	2.05078
5	3.64705	3.46288	3.36180	3.30031	3.26009	3.23233	3.21236
6	5.30713	5.02128	4.86470	4.76961	4.70751	4.66470	4.63393
7	7.27957	6.86959	6.64532	6.50928	6.42052	6.35939	6.31549
8	9.56445	9.00787	8.70370	8.51934	8.39915	8.31643	8.25705
9	12.16188	11.43618	11.03988	10.79984	10.64342	10.53582	10.45862
10	15.07172	14.15444	13.65380	13.35071	13.15331	13.01755	12.92018

Table 7. Comparison of the present calculations on resonance energies for the doubly $2sns\ 1^3S^e$ ($n = 3 - 5$) excited states of He-like ions up to $Z = 10$ with available literature values. All energies are given in atomic units. $1\text{ a.u.} = 27.211396\text{ eV}$.

States											
$2sns\ 1^3S^e$	Z	2	3	4	5	6	7	8	9	10	
$2s3s\ 1^3S^e$	$-E^p$	0.59450	1.41465	2.59511	4.13627	6.03848	8.30160	10.92578	13.91114	17.25749	
	$-E^q$	0.59924	1.42338	2.59644	4.14121	6.05348	8.32620	10.95973	13.94576	17.30205	
	$-E^r$	0.58993	1.41557	2.60205	4.14950	6.05799	8.32750	10.95820	13.94989	17.30269	
	$-E^s$	0.59031	1.41479	2.60073	4.14793	6.05631	8.32584	10.95651	13.94829	17.30121	
	$-E^t$	0.61164	1.41169	2.59664	4.14303						
	$-E^u$	0.59522	1.40999	2.58534	4.12279						
	$-E^v$						6.05795		10.95814		17.30265
	$-E^w$	0.57698	1.39125	2.56721	4.10436						
	$-E^x$		1.41557	2.60205	4.14950						
	$-E^y$	0.58743	1.41872	2.60771	4.14154	6.06229	8.32902	10.94143	13.93837	17.28455	
$2s4s\ 1^3S^e$	$-E^p$	0.55363	1.28879	2.33601	3.69550	5.36746	7.35181	9.64864	12.25801	15.17981	
	$-E^q$	0.55044	1.28504	2.33922	3.69031	5.32084	7.29306	9.58847	12.19147	15.11308	
	$-E^r$	0.53529	1.26279	2.30279	3.65529	5.32030	7.29780	9.58780	12.18999	15.10499	
	$-E^s$	0.54449	1.27602	2.32017	3.67686	5.34609	7.32782	9.62207	12.22882	15.14806	
	$-E^t$	0.54402	1.23704	2.25736	3.67871						
	$-E^u$	0.56179	1.29209	2.33514	3.69129						
	$-E^v$						5.35476		9.63463		15.16445
	$-E^w$	0.53928	1.27497	2.45622	3.84877	5.49894	7.33583	9.90044	12.77848	15.07605	
$2s5s\ 1^3S^e$	$-E^p$	0.53457	1.23026	2.21568	3.49096	5.05622	6.91141	9.05659	11.49180	14.21697	
	$-E^q$	0.54682	1.23981	2.21956	3.48607						
$2s3s\ 3^3S^e$	$-E^p$	0.60134	1.42690	2.61287	4.15959	6.06737	8.33609	10.96587	13.95684	17.30879	
	$-E^q$	0.58775	1.42352	2.62004	4.17550	6.04756	8.31893	10.99338	14.02878	17.42454	
	$-E^r$	0.60149	1.43840	2.63728	4.19761	6.11922	8.40204	11.04604	14.05119	17.41748	
	$-E^t$	0.55931	1.43934	2.63792	4.19769						
	$-E^s$	0.58559	1.41169	2.59899	4.14739	6.05679	8.32739	10.95899	13.95199	17.30599	
	$-E^u$	0.59355	1.42376	2.61516	4.16756						
	$-E^v$		1.44020	2.63901	4.19894						
	$-E^w$	0.61136	1.44296	2.62278	4.19909	6.14473	8.41859	11.03398	14.06547	17.36901	
$2s4s\ 3^3S^e$	$-E^p$	0.55701	1.29483	2.34476	3.70699	5.38169	7.36880	9.66838	12.28051	15.20507	
	$-E^q$	0.55485	1.26547	2.30884	3.69471	5.39502	7.40835	9.66087	12.25931	15.20525	
	$-E^r$	0.54909	1.28559	2.33479	3.69669	5.37119	7.35809	9.65759	12.26996	15.19419	
	$-E^s$	0.54491	1.27986	2.31108	3.69755	5.34981	7.35529	9.63054	12.29178	15.13992	

$-E^p$: Present work, values calculated from Equation (22); $-E^q$: Sow *et al.* [33]; $-E^r$: Ho [18]; $-E^s$: Sakho [24]; $-E^t$: Lipsky *et al.* [35]; $-E^u$: Ray and Mukherjee [25]; $-E^v$: Kar [34]; $-E^w$: Roy *et al.* [15]; $-E^x$: Ho [19]; $-E^y$: Ivanov and Safronova [36]; $-E^z$: Macias and Riera [21]; $-E^k$: Sow *et al.* [29].

Table 8. Comparison of the present calculations on resonance energies for the doubly $2snp\ ^1\ ^3P^0$ ($n = 2 - 5$) excited states of He-like ions up to $Z = 10$ with available literature values. All energies are given in atomic units. 1 a.u. = 2 Ry = 27.211396 eV.

States										
$2snp\ ^1\ ^3P^0$	Z	2	3	4	5	6	7	8	9	10
	$-E^p$	0.69291	1.74081	3.28658	5.33124	7.87570	10.91966	14.46346	18.50742	23.05105
	$-E^q$	0.69309	1.75735	3.31957	5.38010	7.94042	10.99980	14.55934	18.61867	23.17779
	$-E^b$	0.71367	1.77242	3.33060	5.38965	7.94814	11.00679	14.56522	18.62381	23.18293
	$-E^c$	0.69346	1.75809	3.31993	5.38083	7.94116	11.00054	14.56008	18.60250	23.17852
$2s2p\ ^1P^0$	$-E^{d,e}$	0.69383 ^d	1.75588 ^e							
	$-E^f$	0.69383	1.75515	3.31626	5.37789	7.93895	11.00017	14.56155	18.62308	23.18440
	$-E^g$	0.71362	1.77489	3.36839	5.42760	7.98151	11.09005	14.67334	18.73256	23.26332
	$-E^h$	0.69298	1.75696	3.31809	5.38608	7.94403	10.97484	14.56189	18.57691	23.15271
	$-E^i$	0.69226	1.76471	3.31757	5.37469	7.93602	10.98991	14.56175	18.62290	23.17804
	$-E^p$	0.58789	1.40265	2.57761	4.11321	6.00985	8.26738	10.88596	13.86572	17.20646
$2s3p\ ^1P^0$	$-E^b$	0.58615	1.39611	2.56731	4.09939	5.99271	8.24691	10.86273	13.83905	17.17699
	$-E^f$	0.58615	1.40493	2.58495	4.12621	6.02836	8.29175	10.91638	13.90190	17.24865
	$-E^i$	0.56431	1.35936	2.51307	4.04289	5.91618	8.15979	10.75069	13.71700	17.04579
	$-E^p$	0.55036	1.28286	2.32737	3.68413	5.35334	7.33495	9.62901	12.23563	15.15467
$2s4p\ ^1P^0$	$-E^b$	0.54058	1.26712	2.30565	3.65692	5.32093	7.29731	9.58606	12.18717	15.10103
	$-E^f$	0.54830	1.28255	2.32917	3.68816	5.35989	7.34398	9.64045	12.24928	15.17122
	$-E^p$	0.53269	1.22688	2.21076	3.48448	5.04818	6.90181	9.04542	11.47906	14.20266
$2s5p\ ^1P^0$	$-E^f$	0.53103	1.22596	2.21047	3.48530	5.05009	6.90520	9.04988	11.48453	14.20949
	$-E^p$	0.59450	1.41465	2.59511	4.13627	6.03848	8.30160	10.92578	13.91114	17.25749
	$-E^i$	0.58601	1.40483	2.58477	4.12583	6.02800	8.29129	10.98369	13.90124	17.24789
$2s3p\ ^3P^0$	$-E^k$	0.57942	1.39354	2.57931	4.12121	6.02422	8.28835	10.91359	13.89994	17.24740
	$-E^i$	0.57880	1.39517	2.58219	4.11905	6.02267	8.27916	10.91127	13.83614	17.21117
	$-E^l$	0.58335	1.40295	2.58433	4.12734					
	$-E^p$	0.55363	1.28879	2.33601	3.69550	5.36746	7.35181	9.64864	12.25801	15.17981
$2s4p\ ^3P^0$	$-E^i$	0.54337	1.27326	2.31566	3.67057	5.337978	7.317897	9.610323	12.21526	15.13269
	$-E^l$	0.54220	1.27261	2.31591	3.64826					
	$-E^p$	0.53457	1.23026	2.21568	3.49096	5.05622	6.91141	9.05659	11.49180	14.21697
$2s5p\ ^3P^0$	$-E^i$	0.52473	1.21422	2.19371	3.46321	5.02272	6.87223	9.01175	11.44127	14.16080

$-E^p$: Present work, values calculated from Equation (22); $-E^q$: Ho [17]; $-E^b$: Ivanov and Safronova [36]; $-E^c$: Drake and Dalgarno [2]; $-E^d$: Experimental data, Diehl *et al.* [37]; $-E^e$: Experimental data, Kossmann *et al.* [40]; $-E^f$: Sakho *et al.* [22]; $-E^g$: Biaye *et al.* [38] [39]; $-E^h$: Gning *et al.* [27]; $-E^i$: Sow *et al.* [29]; $-E^j$: Sakho *et al.* [23]; $-E^k$: Ho [18]; $-E^l$: Lipsky *et al.* [35].

Table 9. Comparison of the present calculations on resonance energies for the doubly $2pnp\ ^1\ ^3D^e$ ($n = 3 - 5$) excited states of He-like ions up to $Z = 10$ with available literature values. All energies are given in atomic units. 1 a.u. = 2 Ry = 27.211396 eV.

States										
$2pnp\ ^1\ ^3D^e$	Z	2	3	4	5	6	7	8	9	10
	$-E^p$	0.57145	1.37190	2.53222	4.05304	5.93482	8.17746	10.78111	13.74595	17.07173
	$-E^q$	0.57940	1.39115	2.54216	4.03186	5.91564	8.15486	10.74894	13.69746	17.02625
	$-E^b$	0.56907	1.37390	2.53992	4.06708	5.95537	8.20478	10.81531	13.78694	17.11970
$2p3p\ ^1D^e$	$-E^c$	0.56504	1.36527	2.52749	4.05099					
	$-E^d$	0.58390	1.38020	2.53724	4.05599					
	$-E^e$		1.34617	2.54029	4.06777	5.87173	8.10114	10.69138	13.64254	16.95466
	$-E^f$	0.55612	1.34413	2.49002	3.99582					
	$-E^i$	0.56859	1.37868	2.54641	4.06276	6.00418	8.20771	10.84569	13.81923	17.09193
$2p4p\ ^1D^e$	$-E^p$	0.54242	1.26812	2.30568	3.65541	5.31758	7.29211	9.57909	12.17862	15.09056
	$-E^q$	0.55938	1.27684	2.32878	3.64061	5.29086	7.26753	9.55347	12.17767	15.05129
	$-E^b$	0.53645	1.26032	2.29672	3.64562	5.30703	7.28095	9.56736	12.16627	15.07769
	$-E^d$	0.55730	1.27980	2.31544	3.66419					
	$-E^i$	0.53811	1.26503	2.30731	3.64021	5.29988	7.28815	9.59002	12.14703	15.04906
$2p5p\ ^1D^e$	$-E^p$	0.52824	1.21866	2.21174	3.46853	5.02833	6.87805	9.01774	11.44746	14.16713
	$-E^d$	0.54482	1.23381	2.21046	3.47687					
	$-E^e$	0.52222								
	$-E^h$	0.52242								
$2p3p\ ^3D^e$	$-E^p$	0.58952	1.40563	2.58196	4.11895	6.01698	8.27591	10.89589	13.87705	17.21919
	$-E^q$	0.58080	1.40543	2.58479	4.13099	6.03511	8.30190	10.92526	13.91198	17.25727
	$-E^b$	0.58337	1.40353	2.58541	4.12864	6.03309	8.29874	10.92553	13.91345	17.26251
	$-E^c$	0.58498	1.40743	2.59117	4.13589					
	$-E^e$	0.58378	1.40557	2.58834	4.13214	6.03699	8.30293	10.92996	13.91808	17.26731
	$-E^f$	0.58319	1.40401	2.58599	4.12923					
	$-E^i$	0.58546	1.40511	2.58809	4.13378	6.03163	8.29953	10.93380	13.92114	17.26719
$2p4p\ ^3D^e$	$-E^p$	0.55108	1.28417	2.32928	3.68665	5.35647	7.33868	9.63337	12.24059	15.16024
	$-E^q$	0.53275	1.27584	2.30842	3.64892	5.30830	7.28858	9.57982	12.17055	15.10668
	$-E^b$	0.54075	1.27067	2.31355	3.66911	5.33726	7.31797	9.61119	12.21708	15.13522
	$-E^i$	0.54805	1.28091	2.29456	3.65863	5.34968	7.32021	9.61492	12.21952	15.33671

$-E^p$: Present work, values calculated from Equation (23); $-E^q$: Sow *et al.* [33]; $-E^b$: Sakho [22]; $-E^c$: Roy *et al.* [15]; $-E^d$: Ray and Mukherjee [25]; $-E^e$: Ho and Bathia [12]; $-E^f$: Lipsky *et al.* [35]; $-E^g$: Bhatia [41]; $-E^h$: Herrick and Sinanoglu [42]; $-E^i$: Sow *et al.* [29].

Table 8 shows a comparison of the present SCUNC results of resonance energies of the doubly $2snp\ 1,3P^0$ ($n = 2 - 5$) excited states of He-like systems up to $Z = 10$ with the results of Ho [17] who used the complex rotation method, Ivanov and Safronova [36], the results of Drake and Dalgarno [2] from the $1/Z$ expansion perturbation theory, the values of Sakho *et al.*, [22] [23] obtained from the semi-empirical procedure of the SCUNC formalism. Comparison is also done with the experimental data of Diehl *et al.*, [37], the theoretical results of Lipsky *et al.*, [35], Gning *et al.*, [27], Sow *et al.*, [29], Biaye *et al.*, [38] [39] who performed their calculations in the framework of a variational calculations using wave function of Hylleraas type, and with the experimental data of Kossmann *et al.*, [40]. In general, very good agreement is obtained between the present calculations and those of the above-mentioned works for all the states studied for $Z = 2 - 10$. As underlined above, the present good agreements between theory and experiments demonstrate the validity of the new correlated wave functions constructed in this work.

Table 10. Comparison of the present calculations on resonance energies for the doubly $2pnd\ 1,3P^0$ ($n = 3 - 5$) excited states of He-like ions up to $Z = 5$ with available literature values. All energies are given in atomic units. 1 a.u. = 27.211396 eV.

States					
$2pnd\ 1,3P^0$	Z	2	3	4	5
	$-E^a$	0.55847	1.34648	2.49403	4.00193
$2p3d\ 1P^0$	$-E^a$	0.54764	1.32705	2.47020	3.97508
	$-E^b$	0.55795	1.34415	2.48636	
	$-E^a$	0.53593	1.25562	2.28702	3.63052
$2p4d\ 1P^0$	$-E^a$	0.53377	1.25268	2.28421	3.62815
	$-E^b$	0.53209	1.24800	2.27389	3.61152
	$-E^a$	0.52452	1.21157	2.18814	3.45449
$2p5d\ 1P^0$	$-E^a$	0.52607	1.21304	2.19005	3.45691
	$-E^a$	0.57844	1.38513	2.55185	4.07913
$2p3d\ 3P^0$	$-E^a$	0.56977	1.38243	2.55741	4.09360
	$-E^b$	0.56587	1.37371	2.54341	
	$-E^a$	0.54548	1.27386	2.31416	3.66667
$2p4d\ 3P^0$	$-E^a$	0.54222	1.27095	2.31236	3.66617
	$-E^b$	0.53567	1.26072	2.29819	3.64827
	$-E^a$	0.52981	1.22158	2.20300	3.47423
$2p5d\ 3P^0$	$-E^a$	0.52954	1.22108	2.20263	3.47402

$-E^a$: Present work, values calculated from Equation (23); $-E^b$: Roy *et al.* [15]; $-E^c$: Lipsky *et al.* [35].

Table 11. Comparison of the present calculations on the variational calculation of the excitation energies of the doubly excited states $2sns\ ^1,^3S^e$ ($n = 3 - 4$) of He-like systems with some theoretical results available in the literature consulted for $Z = 2 - 5$. All the results are expressed in atomic units: 1 a.u. = 27.211396 eV.

States	Z	2	3	4	5
$2s3s\ ^1S^e$	E^p	2.3092	5.8653	11.0605	17.8947
	E^q	2.3138			
	E^b	2.3139			
	E^c	2.3194			
	E^d	2.3130			
	E^e	2.3267	5.8887	11.0884	17.9266
	E^f	2.3085		11.0721	17.9131
	E^g		5.8643		
	E^h		5.8642	11.0533	17.8812
	E^i		5.8682		
	E^j		5.8649		
	E^k				11.0535
$2s4s\ ^1S^e$	E^p	2.3501	5.9911	11.3196	18.3355
	E^f	2.3419			
	E^l	2.3592	6.0039	11.3354	18.3541
	E^m	2.3684	6.0171	11.3528	18.3757
$2s3s\ ^3S^e$	E^p	2.3024	5.8530	11.0427	17.8714
	E^q	2.3011			
	E^c	2.3102	5.8562	11.0404	17.8634
	E^g			11.0193	17.8379
	E^h		5.8397	11.0166	17.8320
	E^i	2.3016	5.8406		
$2s4s\ ^3S^e$	E^j	2.3022			
	E^p	2.3467	5.9851	11.3108	18.3239
	E^l	2.3546	5.9943	11.3208	18.3343
	E^m	2.3625	6.0064	11.3373	18.3343

E^p : Present work; E^q : Burgers *et al.* [44]; E^b : Oza [33]; E^c : Koyama *et al.* [46]; E^l : Experimental value of Hicks and Comer [7]; E^f : Roy *et al.* [15]; E^i : Ray and Mukherjee [25]; E^g : Lipsky *et al.* [35]; E^h : Macias and Riera [21]; E^j : Conneely and Lipsky [20]; E^k : Bhatia [41]; E^e : Ho [18]; E^d : Sakho [24]; E^m : Ivanov and Safronova [36].

Table 12. Comparison of the present calculations on the variational calculation of the excitation energies of the doubly excited states $2snp^{1,3}P^0$ ($n = 3 - 5$) of He-like systems with some theoretical results available in the literature consulted for $Z = 2 - 5$. All the results are expressed in atomic units: 1 a.u. = 27.211396 eV.

States	Z	2	3	4	5
$2s2p^1P^0$	E^p	2.2108	5.5391	10.3689	16.6997
	E^u	2.2097		10.3394	16.6529
	E^b		5.5249		
	E^c		5.5238		
$2s3p^1P^0$	E^p	2.3158	5.8773	11.0779	17.9178
	E^u	2.3174		11.0707	17.9046
	E^b		5.8751		
$2s4p^1P^0$	E^p	2.3534	5.9971	11.3282	18.3468
	E^u	2.3553		11.3265	18.3427
	E^b		5.9975		
$2s5p^1P^0$	E^p	2.3710	6.0530	11.4448	18.5465
	E^u	2.3725		11.4452	18.5455
	E^b		6.0541		
$2s3p^3P^0$	E^p	2.3092	5.8653	11.0605	17.8947
	E^u	2.3178	5.8751	11.0708	17.9052
	E^d		5.8735	11.0663	17.8977
	E^c			11.0729	17.9083
$2s4p^3P^0$	E^p	2.3501	5.9911	11.3196	18.3355
	E^u	2.3604		11.3399	18.3605
	E^d		6.0048		
$2s5p^3P^0$	E^p	2.3692	6.0497	11.4399	18.5400
	E^u	2.3788	6.0658	11.4619	18.5678
	E^d		6.0625		

E^p : Present work; E^u : Sakho [23]; E^b : Roy *et al.* [15]; E^c : Koyama *et al.* [46]; E^d : Kar and Ho [34]; E^e : Lipsky *et al.* [35].

Table 13. Comparison of the present calculations on the variational calculation of the excitation energies of the doubly excited states $2pnp^{1,3}D^e$ ($n = 3 - 4$) of He-like systems with some theoretical results available in the literature consulted for $Z = 2 - 5$. All the results are expressed in atomic units: 1 a.u. = 27.211396 eV.

States	Z	2	3	4	5
$2p3p^1D^e$	E^p	2.3323	5.9080	11.1233	17.9779
	E^q	2.3387		11.1281	17.9800
	E^b	2.3345			
	E^c	2.3350			
	E^d	2.3318	5.9105	11.12764	17.9834
	E^e		5.9058	11.1153	17.9632
	E^f		5.9016		
	E^g		5.9080		
	E^h		5.9060	11.11564	17.9639
	E^i		5.9116		
$2p4p^1D^e$	E^p	2.3613	6.0118	11.3499	18.3756
	E^d	2.3692	6.0234	11.3645	18.3929
	E^b	2.3673	6.0196	11.3588	18.3854
$2p3p^3D^e$	E^p	2.3142	5.8743	11.0736	17.9120
	E^q	2.3187	5.8725	11.0644	17.8951
	E^b	2.3199			
	E^d			11.0792	17.9142
	E^c		5.8743	11.0672	
	E^e		5.8747		
	E^g		5.8752		
	E^h			11.0702	17.9023
	E^i		5.8759		
	E^k	2.3200			
$2p4p^3D^e$	E^p	2.3526	5.9957	11.3263	18.3443
	E^d	2.3641	6.0116	11.3461	18.3679
	E^b	2.3629	6.0092	11.3420	18.3619

E^p : Present work; E^q : Roy *et al.* [15]; E^b : Lindroth [26]; E^c : Oza [45]; E^d : Ivanov and Safronova [36]; E^e : Ho and Bhatia [12]; E^f : Bhatia [41]; E^g : Macias *et al.* [48]; E^h : Sakho [24]; E^i : Conneely and Lipsky [20]; E^j : Ray and Mukherjee [25]; E^k : Bhatia and Temkin [49]; E^l : Lipsky *et al.* [35].

Table 14. Comparison of the present calculations on the variational calculation of the excitation energies of the doubly excited states $2pnd^{1,3}F^0$ ($n = 3 - 5$) of He-like systems with some theoretical results available in the literature consulted for $Z = 2 - 5$. All the results are expressed in atomic units: 1 a.u. = 27.211396 eV.

States	Z	2	3	4	5	
$2p3d^1F^0$	E^p	2.3453	5.9334	11.1615	18.0290	
	E^r	2.3561	5.9529	11.1854	18.0559	
	E^b	2.3454				
	E^c	2.3458				
	E^d			5.9338	11.1692	18.0433
	E^e			5.9161	11.1483	18.0205
$2p4d^1F^0$	E^p	2.3678	6.0243	11.3685	18.4005	
	E^r	2.3700	6.0272	11.3714	18.4028	
	E^c	2.3716				
	E^e	2.3489	6.0071	11.3536	18.3882	
	E^d		6.0319	11.3817	18.4195	
$2p5d^1F^0$	E^p	2.3792	6.0683	11.4674	18.5765	
	E^r	2.3777	6.0669	11.4655	18.5741	
	E^c	2.3833				
	E^d		6.0761	11.4800	18.5943	
	E^e	2.3600	6.0495	11.4526	18.5628	
$2p3d^3F^0$	E^p	2.3253	5.8948	11.1037	17.9518	
	E^r	2.3340	5.8975	11.0982	17.9374	
	E^b	2.3375				
	E^c	2.3379				
	E^d		5.9067	11.1138	17.9611	
$2p4d^3F^0$	E^p	2.3582	6.0061	11.3414	18.3643	
	E^r	2.3615	6.0090	11.3432	18.3648	
	E^c	2.3681				
	E^d		6.0197	11.3590	18.3873	
$2p5d^3F^0$	E^p	2.3739	6.0583	11.4526	18.5567	
	E^r	2.3742	6.0588	11.4529	18.5570	
	E^c	2.3815				
	E^d		6.0701	11.4692	18.5800	

E^p : Present work; E^r : Roy *et al.* [15]; E^b : Lindroth [26]; E^c : Conneely and Lipsky [20]; E^d : Lipsky *et al.* [36]; E^e : Ray *et al.* [25].

Table 9 compares the results for resonance energies of the doubly $2p3p^{1,3}D^e$, $2p4p^{1,3}D^e$ and $2p5p^{1,3}D^e$ excited states with the theoretical results of Sow *et al.*, [29] [33], Ho and Bathia [12] using the complex rotation method, Sakho [24], Lipsky *et al.*, [35], Roy *et al.*, [15], Ray and Mukherjee [25], Bhatia [41] who employed the Feshbach projection Operator (FPO) formalism, Herrick and Sinanoglu [42]. In general comparison show satisfactory agreement between the calculations.

Table 10 lists the present resonance energies of the doubly $2pnd^{1,3}P^0$ ($n = 3 - 5$) excited states. For these levels, literature data are very scarce. Comparisons show a good agreement between the present calculations and the theoretical results of Roy *et al.*, [15] and of Lipsky *et al.*, [35]. For the $2pnf^{1,3}G^e$ doubly excited states, no literature data were found for comparison. The SCUNC data quoted may be good reference for these doubly excited states.

In **Table 11**, the present SCUNC results for excitation energies of the doubly $2sns^{1,3}G^e$ excited states with $n = 2 - 5$ and $Z = 2 - 5$ of He-like systems are listed. The excitation energies are evaluated with respect to the ground state of Frankowski and Pekeris [43]. Comparisons are made with the results from the CCR results [19] and of Burgers *et al.*, [44], the values of the variational algebraic (VA) method of Oza [45], the values of Koyama *et al.*, [46] obtained from the the hyperspherical coordinate approaches, the experimental data of Hicks and Comer [7], the DFT results of Roy *et al.*, [15], the TDVPT results of Ray and Mukherjee [25], the TDM data of Lipsky *et al.*, [35] and of Macias and Riera [21], the diagonalization values of Conneely and Lipsky [20], the FPO values of Bhatia [47], the CCR calculations of Ho [18], the SCUNC method data of Sakho [24], the CHS results of Ivanov and Safronova [36]. Comparisons indicate that the current SCUNC calculations agree very well with all the literature data. This demonstrates again the validity of the present SCUNC variational procedure.

Table 12 shows the present excitation energies of the doubly $2snp^{1,3}P^0$ excited states ($n = 2 - 5$) of He-like systems. Good agreement is obtained when comparing the SCUNC results to the results of Sakho [23], Roy *et al.*, [15], Koyama *et al.*, [46], Kar and Ho [34], Lipsky *et al.*, [35].

Table 13 presents the SCUNC values for excitation energies of the doubly $2pnp^{1,3}D^e$ ($n = 4 - 5$) of helium and helium-like ions of nuclear charge $Z \leq 5$. Comparison is done with the DFT data of Roy *et al.*, [15], the CCR results of Lindroth [26], the VA calculations of Oza [45], the CHS results of Ivanov and Safronova [36], the CCR results of Ho and Bathia [12] and of Bhatia [41], the discretization calculations of Macias *et al.*, [48], the semi-empirical SCUNC data of Sakho [24], the TDM values of Conneely and Lipsky [20] and of Lipsky *et al.*, [35], the TDVPT data of Ray and Mukherjee [25], to the results of Bhatia and Temkin [49] and the TDM. Overall, good agreement is obtained.

In **Table 14**, we have listed our results on the calculation of the excitation energies of the doubly excited $2pnd^{1,3}P^0$ ($n = 2 - 5$) states of He-like systems with $Z \leq 5$. The SCUNC calculations are seen to agree well with the results of Roy *et*

al., [15], Lindroth [26], Conneely and Lipsky, Lipsky *et al.*, [35] and of Ray *et al.*, [25].

Overall, the good agreements between our present calculations and the various experimental and theoretical literature results justify the possibility to use the variational procedure of the Screening Constant by Unit Nuclear Charge formalism to calculate precise resonance energies of doubly ($Nlnl', {}^{2S+1}L^\pi$) excited states of two electrons systems. It should be mentioned that the present results are obtained from analytical formulae without any code of calculations or a super-powerful computer. In this work, it has been demonstrated that the variational procedure of the Screening Constant by Unit Nuclear Charge (SCUNC) method can be used to compute precise resonance energies and excitation energies of doubly ($Nlnl', {}^{2S+1}L^\pi$) excited states of He-like systems. The new results obtained for $2pnl^{1,3}G^\pi$ doubly excited states may be benchmarked data for theorists focusing their study on the DES of He-like systems. It should be underlined that, until this date the variational procedure of the SCUNC formalism has not been applied to atomic systems containing more than two electrons such as lithium isoelectronic sequence. The good agreement obtained in this paper opens the way for applying the variational procedure of the SCUNC formalism to investigate the properties of complex atomic systems. Study is in such direction.

4. Conclusion

In this work, resonance energies and excitation energies of the doubly $2sns {}^{1,3}S^\pi$, $2snp {}^{1,3}P^\pi$, $2pnp {}^{1,3}D^\pi$, $2pnd {}^{1,3}F^\pi$ and $2pnf^{1,3}G^\pi$ excited states of He-like systems are reported up to $Z = 10$. Calculations are made in the framework of the variational procedure of the Screening Constant by Unit Nuclear Charge (SCUNC) formalism. New correlated wavefunction of Hylleraas-type adapted to the correct description of electron-electron correlation phenomena in the ($Nlnl', {}^{2S+1}L^\pi$) doubly excited states of two-electron systems are constructed. Overall, good agreement is obtained with various theoretical and experimental literature data. The adequacy of the present theory in the treatment of the properties of two-electron systems demonstrates the possibilities to extend the variational procedure of the SCUNC formalism to investigate the properties of complex atomic systems beginning by the lithium isoelectronic sequence.

Conflicts of Interest

The authors declare no conflicts of interest regarding the publication of this paper.

References

- [1] Doscheek, G.A., Meekins, P., Kerptin, R.W., Chubb, T.A. and Friedman, H. (1971) *The Astrophysical Journal*, **164**, 165. <https://doi.org/10.1086/150827>
- [2] Drake, G.W.F. and Dalgarno, A. (1971) *Proceedings of the Royal Society of London A*, **320**, 549-560. <https://doi.org/10.1098/rspa.1971.0009>
- [3] Madden, R.P. and Codling, K. (1963) *Physical Review Letters*, **10**, 516.

- <https://doi.org/10.1103/PhysRevLett.10.516>
- [4] Madden, R.P. and Codling, K. (1965) *Astrophysical Journal*, **141**, 364. <https://doi.org/10.1086/148132>
- [5] Hansen, J.E., et al. (1991) *Zeitschrift für Physik D*, **21**, 587. https://doi.org/10.1007/978-3-322-84218-3_3
- [6] Oda, N., Nishimura, F. and Tashira, S. (1970) *Physical Review Letters*, **24**, 42. <https://doi.org/10.1103/PhysRevLett.24.42>
- [7] Hicks, P.J. and Comer, J. (1975) *Journal of Physics B: Atomic and Molecular Physics*, **8**, 1866. <https://doi.org/10.1088/0022-3700/8/11/022>
- [8] Rudd, M.E. (1965) *Physical Review Letters*, **15**, 580. <https://doi.org/10.1103/PhysRevLett.15.580>
- [9] Bordenave-Montesquieu, A., Gleizes, A., Rodiere, M. and Benoit-Cattin, P. (1973) *Journal of Physics B: Atomic and Molecular Physics*, **6**, 1997. <https://doi.org/10.1088/0022-3700/6/10/016>
- [10] Gelebart, F., Tweed, R.J. and Peresse, J. (1976) *Journal of Physics B: Atomic and Molecular Physics*, **9**, 1739. <https://doi.org/10.1088/0022-3700/9/10/018>
- [11] Rodbro, M., Bruch, R. and Bisgaard, P. (1979) *Journal of Physics B: Atomic and Molecular Physics*, **12**, 2413. <https://doi.org/10.1088/0022-3700/12/15/009>
- [12] Ho, Y.K. and Bhatia, A.K. (1991) *Physical Review A*, **44**, 2895. <https://doi.org/10.1103/PhysRevA.44.2895>
- [13] Hylleraas, E.A. (1928) *Zeitschrift für Physik*, **48**, 469-494. <https://doi.org/10.1007/BF01340013>
- [14] Hylleraas, E.A. (1929) *Zeitschrift für Physik*, **54**, 347-366. <https://doi.org/10.1007/BF01375457>
- [15] Roy, K.A., Singh, R. and Deb, M.B. (1997) *Journal of Physics B: Atomic, Molecular and Optical Physics*, **30**, 4763. <https://doi.org/10.1088/0953-4075/30/21/014>
- [16] Bachau, H., Martin, F., Riera, A. and Yanez, M. (1991) *Atomic Data Nuclear Data Tables*, **48**, 167-212. [https://doi.org/10.1016/0092-640X\(91\)90006-P](https://doi.org/10.1016/0092-640X(91)90006-P)
- [17] Ho, Y.K. (1980) *Physics Letters. A*, **79**, 44. [https://doi.org/10.1016/0375-9601\(80\)90313-8](https://doi.org/10.1016/0375-9601(80)90313-8)
- [18] Ho, Y.K. (1981) *Physical Review A*, **23**, 2137. <https://doi.org/10.1103/PhysRevA.23.2137>
- [19] Ho, Y.K. (1986) *Physical Review A*, **34**, 4402. <https://doi.org/10.1103/PhysRevA.34.4402>
- [20] Conneely, M.J. and Lipsky, L. (1978) *Journal of Physics B: Atomic and Molecular Physics*, **24**, 4135. <https://doi.org/10.1088/0022-3700/11/24/008>
- [21] Macias, A. and Riera, A. (1986) *Physics Letters A*, **119**, 28-32. [https://doi.org/10.1016/0375-9601\(86\)90639-0](https://doi.org/10.1016/0375-9601(86)90639-0)
- [22] Sakho, I., Ndao, A.S., Biaye, M. and Wagué, A. (2008) *European Physical Journal D*, **47**, 37-44. <https://doi.org/10.1140/epjd/e2008-00018-2>
- [23] Sakho, I., Ndao, A.S., Biaye, M. and Wagué, A. (2008) *Physica Scripta*, **77**, Article ID: 055303. <https://doi.org/10.1088/0031-8949/77/05/055303>
- [24] Sakho, I. (2011) *European Physical Journal D*, **61**, 267-283. <https://doi.org/10.1140/epjd/e2010-10294-8>
- [25] Ray, D. and Mukherjee, P.K. (1991) *Journal of Physics B: Atomic, Molecular and Optical Physics*, **24**, 1241. <https://doi.org/10.1088/0953-4075/24/6/013>

- [26] Lindroth, E. (1994) *Physical Review A*, **49**, 4473.
<https://doi.org/10.1103/PhysRevA.49.4473>
- [27] Gning, et al. (2015) *Radiation Physics and Chemistry*, **106**, 1-6.
- [28] Dieng, M., Biaye, M., Gning, Y. and Wagué, A. (2013) *Chinese Journal of Physics*, **51**, 674-691. <http://PSROC.phys.ntu.edu.tw/cjp>
- [29] Sow, B., Diouf, A., Gning, Y., Diop, B., Sow, M. and Wague, A. (2018) *International Journal of Physics*, **6**, 174-180.
- [30] Sakho, I. (2011) *Journal of Atomic and Molecular Sciences*, **2**, 20-42.
<https://doi.org/10.4208/jams.062910.072810a>
- [31] Hylleraas, E.A. and Undheim, B. (1930) *Zeitschrift für Physik*, **65**, 759-772.
<https://doi.org/10.1007/BF01397263>
- [32] Sakho, I. (2018) The Screening Constant by Unit Nuclear Charge Method. Description & Application to the Photoionization of Atomic Systems. ISTE Science Publishing Ltd., London and John Wiley & Sons, Inc., Hoboken.
<https://doi.org/10.1002/9781119476948>
- [33] Sow, B., et al. (2016) *American Journal of Modern Physics*, **5**, 146-153.
- [34] Kar, S. and Ho., Y.K. (2009) *Journal of Physics B: Atomic, Molecular and Optical Physics*, **42**, Article ID: 044007. <https://doi.org/10.1088/0953-4075/42/4/044007>
- [35] Lipsky, L., Anania, R. and Conneely, M.J. (1977) *Atomic Data Nuclear Data Tables*, **20**, 127-141. [https://doi.org/10.1016/0092-640X\(77\)90042-0](https://doi.org/10.1016/0092-640X(77)90042-0)
- [36] Ivanov, A.I. and Safronova, I.U. (1993) *Optics and Spectroscopy*, **75**, 516.
- [37] Diehl, S., Cubaynes, D., Bizau, J.-P., Wuilleumier, F.J., Kenedy, E.T., Mosnier, J.-P. and Morgan, T.J. (1999) *Journal of Physics B: Atomic, Molecular and Optical Physics*, **32**, 4193. <https://doi.org/10.1088/0953-4075/32/17/305>
- [38] Biaye, M., Konté, A., Ndao, A.S., Faye, N.A.S. and Wagué, A. (2005) *Physica Scripta*, **71**, 39. <https://doi.org/10.1088/0031-8949/71/1/006>
- [39] Biaye, M., Konté, A., Ndao, A.S. and Wagué, A. (2005) *Physica Scripta*, **72**, 373.
<https://doi.org/10.1238/Physica.Regular.072a00373>
- [40] Kossmann, H., Krassig, B. and Schmidt, V. (1988) *Journal of Physics B: Atomic, Molecular and Optical Physics*, **21**, 1489.
<https://doi.org/10.1088/0953-4075/21/9/009>
- [41] Bhatia, A.K. (1972) *Physical Review A*, **6**, 120.
<https://doi.org/10.1103/PhysRevA.6.120>
- [42] Herrick, D.R. and Sinanoglu, O. (1975) *Physical Review A*, **11**, 97.
<https://doi.org/10.1103/PhysRevA.11.97>
- [43] Frankowski, F. and Pekeris, L.C. (1966) *Physical Review*, **146**, 46.
<https://doi.org/10.1103/PhysRev.146.46>
- [44] Burgers, A., Wintgen, D. and Rest, J.M. (1995) *Journal of Physics B: Atomic, Molecular and Optical Physics*, **28**, 3163.
<https://doi.org/10.1088/0953-4075/28/15/010>
- [45] Oza, D.H. (1986) *Physical Review A*, **33**, 824.
<https://doi.org/10.1103/PhysRevA.33.824>
- [46] Koyama, N., Fukuda, H., Motoyama, T. and Matsuzawa, M. (1986) *Journal of Physics B: Atomic and Molecular Physics*, **19**, L331.
<https://doi.org/10.1088/0022-3700/19/10/001>
- [47] Bhatia, A.K. (1977) *Physical Review A*, **15**, 1315.
<https://doi.org/10.1103/PhysRevA.15.1315>

- [48] Macias, A., Martin F., Riera, A. and Yanez, M. (1987) *Physical Review A*, **36**, 4187.
<https://doi.org/10.1103/PhysRevA.36.4187>
- [49] Bhatia, A.K. and Temkin, A. (1975) *Physical Review A*, **11**, 2018.
<https://doi.org/10.1103/PhysRevA.11.2018>

Possibility of Geometrical Interpretation of Quantum Mechanics and Geometrical Meaning of “Hidden Variables”

O. A. Olkhov

N. N. Semenov Federal Research Center Institute of Chemical Physics Russian Academy of Sciences, Moscow, Russia
Email: oleg.olkhov@rambler.ru

How to cite this paper: Olkhov, O.A. (2021) Possibility of Geometrical Interpretation of Quantum Mechanics and Geometrical Meaning of “Hidden Variables”. *Journal of Modern Physics*, 12, 353-360.
<https://doi.org/10.4236/jmp.2021.123025>

Received: January 5, 2021

Accepted: February 23, 2021

Published: February 26, 2021

Copyright © 2021 by author(s) and Scientific Research Publishing Inc.

This work is licensed under the Creative Commons Attribution International License (CC BY 4.0).

<http://creativecommons.org/licenses/by/4.0/>



Open Access

Abstract

Interpretation of wave function for free particle is suggested as a description of microscopic distortion of the space-time geometry, namely, as some closed topological 4-manifold. Such geometrical object looks in three-dimensional Euclidean space as its topological defect having stochastic and wave-corpuscular properties of quantum particle. All possible deformations (homeomorphisms) of closed topological manifold play the role of “hidden variables”, responsible for statistical character of the theory.

Keywords

Quantum Mechanics, Geometrical Interpretation of Quantum Mechanics, “Hidden Variables”

1. Introduction

This investigation started long ago as an attempt to extend Einstein’s idea of the geometrization of the theory of gravity to a possible geometrization of quantum theory. In the Einstein’s general theory of relativity, gravitation is considered as a result of macroscopic distortion of the space-time geometry [1]; in this work, quantum particles are considered as a microscopic distortion of the space-time geometry. Suggested geometrization of quantum mechanics means new interpretation of its existing mathematical formalism commonly referred to as “Copenhagen interpretation”. This new interpretation gives possibility to explain known strange features of above mathematical formalism (statistical description, wave-corpuscular dualism) with the help of notions from everyday life (physical model). Attempts to find such explanation started just after the creation of quantum mechanics and this problem is still considered by many physicists as

actual. For example, V. Ginsburg considered interpretation of quantum mechanics as the one of three great problems of modern physics (as the problem of appearance of life and the problem of irreversibility of time) [1]. The problem of interpretation of quantum mechanics was investigated for many years by t'Hooft [2] (here is a detailed list of references on the problem). But why any interpretation is needed for mathematical formalism if it is in a good agreement with experiment? One of reasons is the fact that new physical models open new opportunities for development of theories. For example, many attempts (Einstein Weyl, Calutza and others) have been made for this reason to find geometrical interpretation of classical electrodynamics, although it is in a very good agreement with experiment [3] [4]. In addition, the quantum theory cannot be considered as the final one. Another, more concrete, reason—the contradiction between Bohr and Einstein regarding the completeness of quantum mechanics which did not resolved until now [5] [6]. In contrast to Bohr, Einstein thought that the quantum mechanics is not a complete theory because it says nothing about physical reality, responsible for statistical character of the theory (so called “hidden variables” [2] [7] [8]), and the answer to this question is, may be, the main result of this work. As for physical models, author knows two interpretations of quantum mechanics where mathematical formalism of quantum mechanics is not questioned. One is the Everett's “Many Universes Interpretation”, where statistical character of quantum theory is explained by existence of infinite number of Universes, corresponding to various realizations of reality [9]. This interpretation has its supporters in spite of exotic character and serious criticism [10]. Another interpretation is the t'Hooft “The Cellular Automaton Interpretation of Quantum Mechanics”, where a very special set of mutually orthogonal states in Hilbert space is considered [2]. This approach is now under development. Among the works where the apparatus of quantum physics is undergoing serious changes we can mention the string theory (see, e.g. [11]) and Santini's investigations [12]. The possibility is shown in this work to interpret the quantum mechanical wave function for free particle as a description of microscopic distortion of the space-time geometry. Some characteristics of this geometrical object play the role of “hidden variables” responsible for stochastic behavior of quantum particle, and these characteristics are the physical reality that exists before measurement. Other characteristics explain wave-corpuseular properties of the particle. It may be said that quantum mechanics within suggested interpretation satisfies the completeness criterion formulated by Einstein. Preliminary results see [13] [14] [15] [16] [17].

2. Quantum Particle as the Microscopic Distortion of the Space-Time Geometry

Let's consider the free neutral particle with mass m and spin 0. It will be shown that wave function of such particle can be interpreted as a mathematical description of some geometrical object. This scalar wave function is the solution of the

Klein-Fock-Gordon equation, and it has the form [18] [19]

$$\Psi = \text{const} \cdot \exp\left(-\frac{i}{\hbar}(Et - \mathbf{p}\mathbf{r})\right). \quad (1)$$

This function describes within existing interpretation the particle's state with definite energy E and definite momentum \mathbf{p} . The particle's position before measurements is unknown—it may be observed in any point with equal probability. This fact reflects statistical character of quantum mechanics—unusual property within classical representations. Another unusual property—wave-corpuseular dualism of quantum particles that is defined by phase of the wave function and by wave length and frequency, connecting with the particle's energy and momentum by known relations [18] [19]

$$\lambda_i = \frac{\hbar}{p_i}, \omega = \frac{E}{\hbar}, i = x, y, z. \quad (2)$$

Substituting (2) in (1), we have

$$\Psi = \text{const} \cdot \exp(-i\omega t + i\mathbf{k}\mathbf{r}), k_i = 2\pi\lambda_i \quad (3)$$

This type of functions (plane wave) is often used in classical physics (for example, for description of plane running sound wave). Within existing interpretation of quantum mechanics the origin of periodical dependence of wave function is not discussing.

Let us rewrite the function (1) not with space coordinates x, y, z and, separately with time coordinate t , but with only space coordinates x^1, x^2, x^3, x^4 of the specific space—the space of events of the special theory of relativity—four dimensional pseudo Euclidean space of index 1 (the Minkowski space [20]). Time, multiplied by light velocity, plays in this space the role of fourth space coordinate ($ct = x^4$). Using in (1) instead of E the relativistic 4-momentum $p_4 = E/c$, the wave function can be written in symmetric form as

$$\Psi = \text{const} \cdot \exp(-ix^\mu p_\mu). \quad (4)$$

Here and later relativistic units are used where $\hbar = c = 1$. Summation over repeating indexes is suggested in (4) with signature $(+---)$. In relativistic case [18] [19]

$$p_1^2 - p_2^2 - p_3^2 - p_4^2 = m^2 \quad (5)$$

where m —the particle's mass. Let's write down (4) in such a way that it contains only values with dimensionality of length

$$\Psi = \text{const} \cdot \exp(-2\pi ix^\mu \lambda_\mu^{-1}), \quad (6)$$

where

$$\lambda_1^{-2} - \lambda_2^{-2} - \lambda_3^{-2} - \lambda_4^{-2} = \lambda_m^{-2}, \lambda_\mu = 2\pi p_\mu^{-1}, \lambda_m = 2\pi m^{-1}. \quad (7)$$

In contrast to (1, 3) function (6) does not look as a plane wave—it represents periodical function of four space coordinates in the Minkowsri space.

Function (6) may be considered as a function realizing representation of the

group whose elements are discrete translations along four coordinates axes in the Minkowski space. Indeed, function (6) goes into itself at translations

$$x^\mu \rightarrow x^\mu + n_\mu \lambda_\mu, \quad (8)$$

where n_μ —integers ($\mu = 1, 2, 3, 4$). This group is isomorphic to the group \mathbb{Z}^4 , whose elements are products of integers n_μ . In turn, the group \mathbb{Z}^4 is isomorphic to the fundamental group of closed 4-manifold that is homeomorphic to the four dimensional torus T^4 [21] [22]. Now we may formulate the main hypothesis: quantum particle, described by the wave function (6), can be considered as a closed space-time manifold that is homeomorphic to the four dimensional torus imbedded into five dimensional pseudo Euclidean space of index 1. Relation (7) imposes a metric restriction on the acceptable under deformations path lengths λ_i ($i = 1, 2, 3, 4$). Thus, the relation (7) defines also the geometrical interpretation of the particle's mass and 4-momentum. It will be shown in the next Section that such geometrical object looks in three dimensional Euclidean space as moving topological defect of this space having stochastic and wave-corpuscular properties of quantum particle.

Representation of particle as a closed manifold means that this particle before measurement may be considered as a “mixture” of its all possible geometrical representations (homeomorphisms), and only interaction with device fixes one of them. This means that wave function describes not an individual particle, but statistical ensemble of all its possible geometrical representations, and this explains statistical character of quantum mechanics. Thus, ensemble of all possible homeomorphisms plays the role of “hidden variables,” responsible for stochastic behavior of particles.

3. Quantum Particle as a Topological Defect of Euclidean Space

Let's proceed to decoding of the representation of quantum particle as a closed 4-manifold, that is let's show how such object looks from the point of view of the observer in Euclidean space. But the important notice should be made before going to this problem. The geometry of four dimensional closed manifolds is now under development: the full recognition algorithm is not now known even for three dimensional closed manifolds [22]. Therefore the only way to establish what the representation of quantum particle as a closed 4-manifold means from the point of view of the observer in Euclidean space is to use low dimensional analogies. Having this in mind let's consider closed manifold homeomorphic to the two dimensional torus embedded into three dimensional pseudo Euclidean space of index 1. To obtain concrete result only one of infinite number of possible homeomorphisms of this manifold will be considered, namely usual two dimensional torus $T^2 = S^1 \times S^1$, where S^1 —a circle. Such torus may be considered in three dimensional Euclidean space as a surface obtained by rotation of a circle around vertical axis lying in the plain of this circle (**Figure 1(a)**). In pseudo Euclidean three dimensional space this circle is located in pseudo Euclidean plane

and it looks on Euclidean plane of **Figure 1(b)** as an isosceles hyperbola [23]. That is two dimensional torus, representing particle, looks in three dimensional Euclidean space as a hyperboloid (**Figure 1(b)**). Within considered low dimensional analogy physical space-time (space of events) is a two dimensional pseudo Euclidean space, and the particle's positions in different moments of time in the Euclidean (one dimensional) space are defined by points of intersection with this space of the projections of the hyperboloid's temporary cross-sections. These cross-sections look as expanding circles in two-dimensional Euclidean plane XY (**Figure 2(a)**). These circles can be considered as moving topological defect of one dimensional physical space. It is the fact that intersection point belongs to topological defect that distinguishes this point at **Figure 2(a)** from neighboring points of one dimensional Euclidean space, turning it into a physical "material point".

The particle's positions in Euclidean (one dimensional) space are defined by points of its intersection with the circle, corresponding to the only one of the torus possible homeomorphisms. Accounting for all possible homeomorphisms leads, obviously, to "blurring" of this circle and so leads to transformation of the one intersection point in finite region of Euclidean space (this region is indicated at **Figure 2(b)** by a bold line segment on X-axis). This region has at every moment of time a finite size because the range of all possible homeomorphisms is limited by metric condition (7) that restrict the maximum possible dimensions of closed manifold. As a result, the observer in Euclidean space will detect the

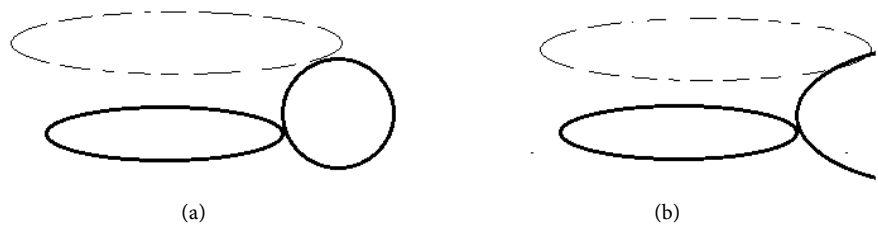


Figure 1. Two-dimensional torus embedded into three-dimensional Euclidean and pseudo Euclidean spaces.

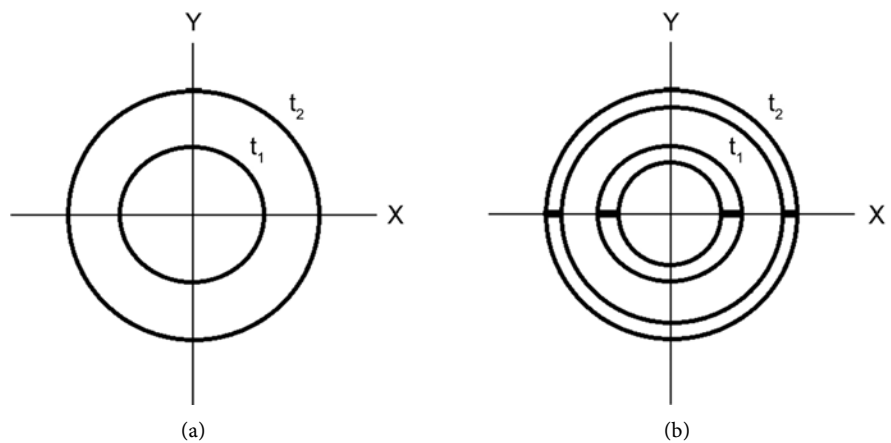


Figure 2. Topological defect of one dimensional Euclidean space (X-axis).

particle with equal probability in one of points of above mentioned region. This means that wave function describes not a position of separate particle but the ensemble of its possible positions, and this explains statistical character of quantum mechanics. It is obvious that all possible homeomorphisms of the closed manifold, representing this particle, play the role of “hidden variables”, responsible for the particle’s stochastic behavior: each homeomorphism corresponds to the one particle’s possible position in Euclidean space. The points of the intersection region have different velocities. This means that the intersection region at **Figure 2(b)** are moving expanding, and finally it will fill all Euclidean (one dimensional) space. In result the probability to observe the particle in any point of space will be the same, as it should be according to laws of quantum mechanics for free particle, described by wave function (1).

The fact that the particle can be represented in physical Euclidean space as a part of topological defect allows to explain the particle’s wave properties. It is sufficient for this to suppose that the defect’s position in the external five dimensional Euclidean space relative to the three dimensional space changes according to periodical law described by wave function (1) (a rigorous proof of this assumption is not possible within the framework of low dimensional analogy). It can be said that the phase of the defect’s periodical movement is an additional degree of freedom on which the effect of the particle on the device depends. The particle’s corpuscular properties (4-momentum) are defined through parameters of above periodical movement of defect by relations

$$p_{\mu} = 2\pi\lambda^{-1}. \quad (9)$$

These relations are identical to the definition (2) of the particle’s wave length through its momentum within existing interpretation [19], but now they have the “reverse” meaning of definition of momentum through the wave length, as it should be in the consistent theory where less general concepts (classical momentum) are defined through more fundamental ones (wave length of the defect’s periodical movement).

4. Conclusion

The wave function plays a dual role within suggested interpretation. First, it is a function, realizing the representation of the fundamental group for a closed 4-manifold, representing a free particle. Second, this function describes periodical movement of topological defect in the external space, and intersection of this defect with physical space defines the possible particle’s positions. These properties of the wave function make it possible to explain the stochastic behavior of the particle and its wave-corpuscular dualism. The role of “hidden variables”, responsible for the particle’s stochastic behavior, is played by all possible homeomorphisms of the closed 4-manifold, representing the particle. Notice in conclusion that relation (7) defines geometrical interpretation of the particle’s mass as a characteristic of some fundamental length λ_m . Geometrical interpretation of elementary electrical charge and the particle’s spin and possibility of

application of geometrical approach to the quantum field theory is now under consideration. After that, the advantages of the proposed approach will become clear.

Conflicts of Interest

The author declares no conflicts of interest regarding the publication of this paper.

References

- [1] Ginzburg, V.L. (1999) *Uspekhi Fizicheskikh Nauk (Physics-Uspekhi)*, **169**, 419.
- [2] T'Hooft, G. (2005) arXiv 14.05.1548.
- [3] Vladimirov, Y.S. (2005) *Geometrophysics*. Binom, Moscow. (In Russian)
- [4] Vizgin, V.P. (1985) *Unified Field Theory in the First Third of the Twentieth Century*. Nauka, Moscow. (In Russian)
- [5] Einstein, A., Podolsky, B. and Rosen, N (1935) *Physical Review*, **47**, 777.
- [6] Bohr, N. (1935) *Physical Review*, **48**, 696. <https://doi.org/10.1103/PhysRev.48.696>
- [7] Von Neumann, J. (1932) *Mathematical Foundations of Quantum Mechanics* (German Edition 1932). Princeton University Press, Princeton.
- [8] Bell, J.S. (1964) *Physics*, **1**, 195. <https://doi.org/10.1103/PhysicsPhysiqueFizika.1.195>
- [9] Everett, H. (1957) *Reviews of Modern Physics*, **29**, 454. <https://doi.org/10.1103/RevModPhys.29.454>
- [10] Mensky, M.B. (2007) *Uspekhi Fizicheskikh Nauk (Physics-Uspekhi)*, **177**, 415.
- [11] Btcker, K., Becker, M. and Schwarz, J.H. (2007) *String Theory and M-Theory: A Modern Introduction*. Cambridge University Press, Cambridge.
- [12] Santini, R.M. (2019) *Ratio Mathematica*, **37**, 5.
- [13] Olkhov, O.A. (2007) *Journal of Physics. Conference Series*, **67**, Article ID: 012037. <https://doi.org/10.1088/1742-6596/67/1/012037>
- [14] Olkhov O.A (2002) arXiv 0802.2269.
- [15] Olkhov, O.A. (2008) *AIP Conferences Proceedings*, **962**, 316. <http://arXiv.org/pdf/0801.3746>
- [16] Olkhov, O.A. (2014) *Russian Journal of Physical Chemistry B*, **8**, 30. <https://doi.org/10.1134/S199079311401014X>
- [17] Olkhov, O.A. (2020) Geometrical Interpretation of Quantum Mechanics. *International Teleconference on Einstein's Argument That Quantum Mechanics Is Not a Complete Theory*, Miami, 1-5 September 2020, Section 5. <http://www.world-lecture-series.org/level-X11-epr-teleconference-2020>
- [18] Bjorken, J.D. and Drell, S.D. (1968) *Relativistic Quantum Mechanics*. Vol. 1, McGraw-Hill Book Company, New York, Ch. 9.
- [19] Berestetskii, B.N., Lifshits, E.M. and Pitaevskii, L.P. (2001) *Quantum Electrodynamics*. Pergamon Press, Oxford.
- [20] Pauli, W. (1958) *Theory of Relativity*. Pergamon Press, Oxford, Ch. 2.
- [21] Dubrovin, B.A., Fomenko, A.T. and Novikov, S.P. (1985) *Modern Geometry—Methods and Applications*. Vol. 2, Springer, Berlin. <https://doi.org/10.1007/978-1-4612-1100-6>

- [22] Fomenko, A.T. (1998) Visual Geometry and Topology. Moscow University Press, Moscow, Ch. 1, §1.1, Ch. 2, §5.1. (In Russian)
- [23] Rashevski, P.K. (1967) Riemannian geometry and Tensor Analysis. Nauka, Moscow, §§44, 62. (In Russian)

Video-Based Face Recognition with New Classifiers

Soniya Singhal¹, Madasu Hanmandlu², Shantaram Vasikarla³

¹Electrical Engineering Department, Indian Institute of Technology, New Delhi, India

²CSE Department, MVSR Engg. Cllege, Nadergul, Hyderabad, India

³Computer Science Department, California State University, Northridge, CA, USA

Email: soniyatech90@gmail.com, mhmandlu@gmail.com, shantaram@computer.org

How to cite this paper: Singhal, S., Hanmandlu, M. and Vasikarla, S. (2021) Video-Based Face Recognition with New Classifiers. *Journal of Modern Physics*, 12, 361-379.

<https://doi.org/10.4236/jmp.2021.123026>

Received: January 14, 2021

Accepted: February 23, 2021

Published: February 26, 2021

Copyright © 2021 by author(s) and Scientific Research Publishing Inc.

This work is licensed under the Creative Commons Attribution International License (CC BY 4.0).

<http://creativecommons.org/licenses/by/4.0/>



Open Access

Abstract

An exhaustive study has been conducted on face videos from YouTube video dataset for real time face recognition using the features from deep learning architectures and also the information set features. Our objective is to cash in on a plethora of deep learning architectures and information set features. The deep learning architectures dig in features from several layers of convolution and max-pooling layers though a placement of these layers is architecture dependent. On the other hand, the information set features depend on the entropy function for the generation of features. A comparative study of deep learning and information set features is made using the well-known classifiers in addition to developing Constrained Hanman Transform (CHT) and Weighted Hanman Transform (WHT) classifiers. It is demonstrated that information set features and deep learning features have comparable performance. However, sigmoid-based information set features using the new classifiers are found to outperform MobileNet features.

Keywords

Face Recognition on Videos, Information Sets, Constrained Hanman Transform Classifier, Weighted Hanman Transform Classifier, Video Face Dataset, MobileNet, Vgg-16, Inception Net, ResNet

1. Introduction

Face recognition from videos is still a challenging problem. One source of videos is CCT cameras installed wherever the thefts and criminal activities are expected. We can see the use of these cameras for surveillance and security at places like airports, hospitals, banks, streets, homes, offices etc. With the increased terrorist

attacks, concern about public safety has become paramount importance world-wide. Earlier the passport photo used to be the only identity for travelers, but now secret cameras at airports keep a strict vigil on their activities as well. They record real time videos during the immigration checks. Their applications are furthered in detecting the poses of people, tracking the objects and activities.

Face recognition has been in vogue for the user verification and authentication, public safety, attendance management and counting of people. But real time detection and recognition of a face are very difficult as they have to be faster without compromising on accuracy. Tracking the presence of an authorized human is an added overhead to prevent his/her access.

There are two approaches based on 1) image-based and 2) video-based. The first approach has been researched from multiple perspectives, not limited to performance, computational constraints, and image acquisition under both the constrained and unconstrained environments including occlusions. On the other hand, the second approach has not been explored to that extent desirable and it is still an active research field due to an additional challenge posed by videos. Motivated to counter this challenge, we have made an attempt to investigate both the information set features and deep learning neural network features in this work. Moreover, depending on an application, video based face recognition can be performed using either image-to-video or video-to-video. The image-to-video methods are suited to applications involving an identification of a person. Here the presence of a person in videos is determined based on still image dataset. On the other hand, video-to-video matching is mainly used to find all the occurrences of a subject within a collection of video data. Here both the system input and the database are in the form of videos and video-to-video matching is more challenging than image-to-video matching. Typical solutions to this problem involve multiple stages like extracting features from the input videos and then matching with the target video features. In this work, we are concerned with the real time face recognition involving image-to-video methods.

There are multiple factors in the way of performing real time face recognition. Pose and location of a person in a video vary widely. Moreover, the varying expressions, illumination, background, occlusions affect the processing after the acquisition of the video. Every frame of a face video may witness a significant change in the form of pose, expression and illumination. Considering all the frames will make a face recognition system slow because of computational complexity. Therefore, only a few frames at a certain frame rate have to be selected to reduce the training time in the recognition system.

Zheng *et al.* [1] have proposed an automatic system for the unconstrained video-based face recognition. First of all, faces are localized in videos using two Deep Convolutional Neural Networks (DCNN) detectors. The regions of bounding boxes earmarked from the earlier step are then grouped based on face association and tracking methods. Faces are then recognized by the face matcher using an unsupervised subspace learning approach and a subspace-to-subspace

similarity metric.

Deep learning networks have been favored by researchers in the field of image processing as they are well suited for the extraction of features from images of all sorts and classifying the same by the inbuilt classifiers like softmax in the very networks. Face recognition, emotion recognition, optical character recognition, detection of diseases from medical images are some of the applications where deep learning networks have become a natural choice. They outperform the classical methods for the pattern recognition and classification problems by extents. Because of their wide usage, several deep learning networks have emerged starting with convolutional neural networks (CNN) having different architectures like Alex Net, LeNet, Vgg-16 to Region-CNN (RCNN), MobileNet, ResNet etc.

A survey on face recognition using deep learning is made in [2] on two aspects: data and algorithms. For algorithms, network architectures are surveyed. Also, they have categorized loss functions into Euclidean-distance based, angular or cosine-margin based, softmax and its variations. For data, some commonly used datasets are surveyed. As mentioned in [2] that technical challenge with matching faces cross ages, poses and styles still remains. Deep learning has improved continuously over the past few years and now it even assists humans in face verification. But the applications requiring high accuracy at a very low alarm rate like financial identity verification are still difficult even with massive training data.

We will discuss some of the deep learning neural networks later on in connection with our application. They are not without drawbacks as can be noticed. Training these models is cumbersome as they need huge dataset to train from scratch; but with transfer learning the need for huge training data can be reduced. As there are many deep learning architectures in the literature the choice and suitability of particular architecture to an application are fraught with difficulties. The unavailability of big public databases hampers the effective use of deep learning neural networks. To mitigate this problem, data augmentation from the available samples is employed during training. Traditional methods seek image synthesis for augmentation that includes but not limited to cropping, rotating, flipping, random sampling or adding noise in images and these operations involve transformations that do not affect the category. In real life scenario, the augmentation may not be necessitated but cannot altogether be ruled out.

Close on the heels of real life scenario, Inoue [3] has suggested an augmentation technique that takes the average of two randomly selected images from a training set. If two labeled images are chosen, then the label of the first is considered for the generated one. This method of sample pairing leads to reduction in error rate over the traditional approaches. But the selection of images has a significant impact on the accuracy. Surprisingly, if images belong to the same class, improvement is poorer. There is no valid reason for this anomaly therefore choosing sample pairs is a difficult task. Generative Adversarial Nets (GAN) [4] can generate new images similar in all aspects to the training images. They com-

prise two networks, namely, generator and discriminator that compete with each other in performance. The generator tries to make similar input images while the discriminator estimates the probability of whether a sample is taken from the original network and not from the generated network. The learning aim of generator is to increase the probability of discriminator making a mistake. It is interesting to train GANs if the number of training set images is small. Also, GAN requires the choice of a good equilibrium which is not ensured thus leading to unstable training.

We are more interested in the transfer learning approaches for Deep Neural Networks (DNNs) as they save time to build a model not from scratch. Moreover, this sort of learning helps solve other's problem. DNN's can deal with small training datasets. Lin *et al.* [5] have proposed a transferred deep feature fusion framework that utilizes two Deep Convolution Neural Networks (DCNNs) for feature extraction and identification of the unknown (test) face from the known (training) faces. The architectures used are ResNet-50 and GoogLeNet-BN and these are trained on different databases to get more generalized feature representation. For training, data augmentation is adopted by flipping, cropping and resizing images. The fusion occurs at two stages, one at the features level and another at the similarity scores level. In the first fusion stage, the features extracted from the output layers of the networks are fused together. Then template based on one vs. the rest—SVM is trained on these features. A template is a collection of all frames of a video and the images of a focused subject are used as a single representation for the matching task. Finally, One Shot Similarity (OSS) is applied to identify the input. OSS of two vectors say p and q , is measured by considering p as a positive set and all other samples that don't belong to either of these two vectors as a negative set and then classification is performed. Similarly, it's done for q and then the average of these is taken. In the second fusion stage, multiple matching scores obtained for each template-pair are fused into a single score.

Most of the research works on DCNNs [1] [2] [4] [5] have some common problems. They require larger dataset, memory and computation time. As we are all aware bigger the dataset the better is the model and so the need arises for data augmentation. Though this helps reduce the problem of overfitting but is computationally expensive and also increases the training time. Sample pairing type augmentations [3] have a disadvantage that they make a little sense from the humanistic perspective. It is very difficult to interpret why the performance boost takes place by mixing images. One reason could be that the increase in the data size facilitates robust representation of the low-level characteristics. For Generative Adversarial Networks (GANs) in [4], getting high-resolution output is still challenging. Increasing the output size of the images produced by the generator is likely to cause training instability and non-convergence. Moreover, fine tuning of these networks is also challenging. Another drawback is that they do not encode the position and orientation of the objects.

The present work involving real time face recognition using videos is in continuation of our earlier work on face recognition [6] where we have addressed the real time face recognition problems such as pose and illumination variations using the information set features that arise out of the representation of the possibilistic certainty using Mamta-Hanman entropy function. To see the relative merits of information set features vis-a-vis deep learning-based features, we are motivated to investigate the effectiveness of DCNNs on videos by overriding their requirement for large databases with smaller databases. As there are many candidates to choose from different deep learning neural architectures, some experimental study will be conducted. We are also bent upon developing two classifiers, viz., Constrained Hanman transform (CHT) classifier and Weighted Hanman transform (WHT) classifier in this work.

The rest of the paper is organized as follows: Section 2 presents the extraction of features. Section 3 contains the proposed classifier and algorithm. DNNs used are discussed in Section 4. The details of the databases are given in Section 5. Section 6 discusses the results of experiments on two video databases. The conclusions are given in Section 7.

2. The Concept of Information Set

The concept of information set was introduced by Hanmandlu in a guest editorial [7] so as to extend the scope of a fuzzy set by empowering the membership function involved in it as an agent through the proposition of an information theoretic entropy function christened as Hanman-Anirban entropy function [8]. This is more general in the sense that it can represent both probabilistic uncertainty and the possibilistic certainty unlike Shannon, Renyi, Tsallis and Pal and Pal entropy functions that represent only the probabilistic uncertainty considered as a measure of disorder called information. The offshoot of Hanman-Anirban is called Mamta-Hanman entropy function [9], defined as

$$H = \frac{1}{n^2} \sum \sum p_{ij}^\alpha e^{-(cp_{ij}^\gamma + d)^\beta} \quad (1)$$

where c , d , α , β and γ are the constant parameters and p_{ij} is the probability. For simplicity we take $\gamma = 1$ in Equation (1) that represents the probabilistic uncertainty. In this paper, we are concerned with the possibilistic certainty in the gray levels of a sub-image which is proved to be better than the probabilistic uncertainty. We term a sub-image as the information source and the gray levels as the information source values to prepare the ground to represent the possibilistic certainty as will be clear shortly. To this end, we replace the probability p_{ij} with the information source values I_{ij} in Equation (1) leading to:

$$H = \frac{1}{n^2} \sum \sum I_{ij}^\alpha e^{-(cI_{ij}^\gamma + d)^\beta} \quad (2)$$

We now choose the parameters of the exponential gain function such that it takes the form of a membership function whose role is to fit an appropriate pos-

sibility distribution for the information source values.

Selecting $\gamma = 1$, $c = \frac{1}{I_{\max}}$, $d = 1 - \frac{I_{\text{avg}}}{I_{\max}}$ in Equation (2) leads to

$$H = \frac{1}{n^2} \sum \sum I_{ij}^\alpha e^{-(1-\mu_{ij})^\beta} = \frac{1}{n^2} \sum \sum I_{ij}^\alpha e^{-\bar{\mu}_{ij}^\beta} \quad (3)$$

where $0 < \alpha < 2$ and the membership function is $\mu_{ij} = \frac{|I_{ij} - I_{\text{avg}}|}{I_{\max}}$. Taking the first order approximation in the exponential gain function in Equation (3) leads to,

$$H = \frac{1}{n^2} \sum \sum I_{ij}^\alpha (1 - \bar{\mu}_{ij}^\beta) = \frac{1}{n^2} \sum \sum I_{ij}^\alpha \mu_{ij}^\beta \quad (4)$$

As we have modeled the distribution of I_{ij} to get μ_{ij} , Equation (4) gives the possibilistic certainty; but if we replace μ_{ij} with its complement then it gives the possibilistic uncertainty.

2.1. Dilemma between Certainty and Uncertainty

It is time to understand the difference between the two. We have been making a concerted effort over the years through the aegis of information set theory to clear up this dilemma. As probabilities express a random phenomenon, the classical entropy functions give a measure of disorder or uncertainty in a system. In some situations probabilities act as possibilities. For instance, the occurrences of minerals in sea water are random, but their effect on the taste of the water is not random but fuzzy as we can easily associate a concept like bitterness to it because the variation in bitterness leads to a fuzzy set. The degree of bitterness is described by a membership function which gives a certainty value. But the bitterness depends on the amounts of minerals dissolved in the water.

The variation in any information source (attribute) values gives rise to a distribution. If this distribution can be modelled by a mathematical function using the statistics of the distribution termed as the possibilistic entropy function, then we get the extent of certainty of the attribute to a specified concept or class. Otherwise the distribution is random; hence it can only be represented by a mathematical function without using the statistics of the distribution termed as the probabilistic entropy function in which case we get the extent of uncertainty involved in relating the variable to the concept/class. The difference between the two is whether or not the distribution of a variable can be modelled using its statistics. This is termed as certainty/uncertainty principle.

The advantage of using statistical parameters in the modelling of a distribution of information source values by a mathematical function bestows us the facility to change the parameters thereby changing the function. If the information source values have the corresponding degrees of association provided by a mathematical function to a concept or class then both the information source values and the degrees of association together represent the certainty whether or

not the mathematical function involves the statistical of parameters of the distribution of the information source values. We will be using this simple concept while designing the classifiers. We now define the information set concept that is the backbone of the information set theory.

2.2. Definition of Information Set

The set of information values $\{I_{ij}^\alpha \mu_{ij}^\beta\}$ is called the information set such that each information value is a product of the information value and the corresponding membership function value. The values of α and β need to be selected appropriately.

An in depth of study on information set theory can be found from [10] [11] [12]. The adaptive forms of Mamta-Hanman and Hanman-Anirban entropy functions are presented in [6] and [12] respectively, which will give more teeth to be able to derive Hanman transform from them as shown later.

2.3. Operations on Information Sets

Let H1 and H2 be two information sets. The operations of union, Intersection and complement are given as under.

- 1) *Union*: It is the t-norm of $H1_{ij}$ and $H2_{ij}$ that are the corresponding information values of two information sets.
- 2) *Intersection*: It is the t-conorm or S-norm of $H1_{ij}$ and $H2_{ij}$.
- 3) *Complement Information*: If the membership function is complement we get complement information $\{I_{ij}^\alpha \bar{\mu}_{ij}^\beta\}$.
- 4) *Thresholding*: Unlike cut-sets, the information sets are subjected to thresholding for the choice of information content.
- 5) *Functions*: Information set allows generation of modified features by applying different functions on the basic information values.

2.4. Functional Information Set Features

To derive these features, the unit of information is taken as either the information value, $I_{ij}^\alpha \mu_{ij}^\beta$ or the complement information value, $I_{ij}^\alpha \bar{\mu}_{ij}^\beta$ and then an appropriate function is applied on this unit information. The formulation of such features is now discussed.

2.4.1. Energy (EN) Feature

Energy feature is derived from Equation (4) by taking $\beta = 2$ in $\bar{\mu}_{ij}^\beta$ for the k^{th} window denoted by E_k as:

$$E_k = \frac{1}{n^2} \sum_{i=1}^n \sum_{j=1}^n I_{ij}^\alpha \bar{\mu}_{ij}^2 \quad (5)$$

2.4.2. Sigmoid (SG) Feature

Applying the sigmoid function on the unit of information leads to the following sigmoid feature (SG) denoted by S_k :

$$S_k = \frac{1}{n^2} \sum_{i=1}^n \sum_{j=1}^n \frac{I_{avg}}{1 + e^{-I_{ij}^\alpha \mu_{ij}^\beta}} \quad (6)$$

2.4.3. Effective Information (EI) Feature

As the above μ_{ij}^β is not found suitable, we have chosen an exponential membership function $\mu_{ij} = e^{-\left(\frac{|I_{ij} - I_{ref}|}{f_h^2}\right)}$ which is obtained from the exponential gain function $e^{-(cI_{ij}^\gamma + d)^\beta}$ of (2) on substituting $\gamma = 1$, $c = \frac{1}{f_h^2}$, $d = -\frac{I_{ref}}{f_h^2}$. The use of centroidal approach on the information values $I_{ij}^\alpha \mu_{ij}^\beta$ gives the effective information (EI) denoted by I_k as follows:

$$I_k = \frac{\sum_i \sum_j I_{ij}^\alpha \mu_{ij}^\beta}{\sum_i \sum_j \mu_{ij}^\beta} \quad (7)$$

where I_{ref} can be taken as I_{max} and the fuzzifier is given by:

$$f_h^2 = \frac{\sum_i \sum_j (I_{ij} - I_{ref})^4}{\sum_i \sum_j (I_{ij} - I_{ref})^2}$$

2.4.4. Possibilistic Renyi Entropy (RE) Feature

Renyi entropy function is based on probabilities; so it cannot be used as feature as we are dealing with the attribute (information source) values. But its possibilistic form is derived by Bhatia and Hanmandlu in [13] by making it adaptive. We will first consider the Renyi entropy (RE) function with the probability replaced by the information source value. Denoting RE by R_k for k^{th} window, it is expressed as

$$R_k = \frac{1}{n^2} \frac{1}{1 - \alpha} \left\{ \log \left(\sum_{i=1}^n \sum_{j=1}^n I_{ij}^\alpha \right) \right\} \quad (8)$$

Since $\left(\sum_{i=1}^n \sum_{j=1}^n I_{ij}\right) \neq 1$, unlike the sum of the probabilities equals 1 we have normalized the r.h.s. of (8) by dividing with the number of the information source values I_{ij} to get what we call the approximate normalized possibilistic Renyi entropy function. We have fixed $\alpha = 2$ obtained by experimentation as discussed in Section 6 on results; so RE feature is computed from

$$R_k = \frac{1}{n^2} \left\{ \log_e \left(\sum_{i=1}^n \sum_{j=1}^n I_{ij}^2 \right) \right\}.$$

We will now derive adaptive Renyi entropy (ARE) function by assuming α to be a variable.

Then one term of (8) becomes:

$$R_{A,ij} = \frac{\alpha}{1 - \alpha} \left\{ \log_e I_{ij} \right\} \quad (9)$$

Assuming $\frac{1}{1 - \alpha} = \mu_{ij}$ makes $\frac{\alpha}{1 - \alpha} = -\bar{\mu}_{ij}$, the complementary membership function of I_{ij} . In view of this (9) becomes

$$R_{A,ij} = -\bar{\mu}_{ij} \left\{ \log_e I_{ij} \right\} \quad (10)$$

where $\mu_{ij} = \frac{|I_{ij} - I_{avg}|}{I_{max}}$.

Summing the above for $i = 1, \dots, n$ and $j = 1, \dots, n$ we get ARE as:

$$R_{Ak} = -\frac{1}{n^2} \sum_{i=1}^n \sum_{j=1}^n \bar{\mu}_{ij} \log_e I_{ij} \quad (11)$$

2.5. Derivation of Hanman Classifier

A classifier works on the training feature vectors and a testing feature for the classification we denote a feature vector by $\{x_i\}$. We will now derive Hanman transform that is a higher level information set. To derive this, we invoke the adaptive Mamta-Hanman entropy function [6], defined as

$$H = \frac{1}{n} \sum x_i^\alpha e^{-(c(\cdot)x_i^\gamma + d(\cdot))^\beta} \quad (12)$$

where the parameters $c(\cdot)$ and $d(\cdot)$ are variables and x_i^α denotes the feature vector. Setting the parameter $c(\cdot)$ to μ_i and $d(\cdot)$ to zero in Equation (10) yields us the most general Hanman Transform, given by

$$H = \frac{1}{n} \sum x_i^\alpha e^{-(\mu_i x_i^\gamma)^\beta} \quad (13)$$

To simplify the above, the three parameters: α , γ and β are set to unity resulting in the basic Hanman transform:

$$H = \frac{1}{n} \sum x_i e^{-(\mu_i x_i)} \quad (14)$$

The above requires the generation of feature vector x_i and its membership function. However, it would be more effective if we compute the error vector between the training feature vector and the test feature vector. The development of classifier based on this transform will be discussed now.

2.6. Properties of Information Sets and Hanman Transform

To give an insight into the Information set theory, it is essential to enlist some important properties some of which are common to both information sets and Hanman transform and some specific to either of the two. These are discussed in the following:

1) Both information values and Hanman transform values are natural variables. The electro-chemical pulse from dendrite is either magnified or inhibited by the synapse before reaching a neuron. This is equivalent to changing an attribute by its membership value as in a basic information value. Evaluation of an attribute based on the information on it gives the Hanman transform value and the function of this transform is similar to the higher level activity of neurons in the human brain.

2) The summation of information values gives us an estimate of the output.

This useful result helps us simplify the Takagi-Sugeno-Kang (TSK) fuzzy rule.

Proof: Consider a TSK fuzzy rule

If x_1 is A_1 and x_2 is A_2 and x_n is A_n then $y = a_0 + a_1x_1 + a_2x_2 + \dots + a_nx_n$

If the fuzzy sets A_1, \dots, A_n are replaced with the information values, then we can write $y = \mu_1x_1 + \mu_2x_2 + \dots + \mu_nx_n$. This output is a sum of information values with $a_0 = 0$.

3) From 2), we can deduce that $y = w_1\mu_1x_1 + w_2\mu_2x_2 + \dots + w_n\mu_nx_n$ for the situation when A_1, \dots, A_n have different sizes.

4) Transfer learning is possible through Hanman transform

$H = \frac{1}{n} \sum x_i e^{-(\mu_i(y)x_i)}$ where the membership $\mu_i(y)$ is derived from another attribute y .

5) If μ_1 and μ_2 are treated as two agents then $\{x(\mu_1 - \mu_2)\}$ is the divergent information set and the Hanman transform divergent set is simply the corresponding Hanman transform $\{x \exp(-x(\mu_1 - \mu_2))\}$.

6) Both basic information value and Hanman transform can be used in the learning of parameters in an optimization problem [14] [15] using $H_a = a_i f(a_i)$ and $H_a = \frac{1}{n} \sum a_i e^{-a_i f(a_i)}$ respectively. Here a_i is the parameter set to be learned and $f(a_i)$ is the output of the objective function.

7) Hanman transform can be used to evaluate the membership function value as $\mu_i(\text{new}) = \mu_i(\text{old}) e^{-x_i \mu_i(\text{old})}$ which is recursive. If we have a correction term, say $v_i(\text{old})$ necessitated due to inappropriate membership function model, then we can have a non-linear state space model from this recursive relation represented as: $\mu_i(k+1) = \mu_i(k) e^{-x_i \mu_i(k)} + v_i(k)$, where k denotes the k^{th} instant. The model parameters of this model can be easily learned using competitive-cooperative learning models (cclms) which also use the output-based Hanman transform [15] as mentioned in 6).

3. Design of Classifier Based on Hanman Transform

Unlike in many classifiers there is no training phase in the design of this classifier but only the testing phase because the need for the unknown parameters is eliminated completely by assuming suitable parameters in the Hanman transform. Separating training phase from testing phase would entail the computation of parameters which we have avoided by having only the testing phase. This approach is amply suitable for the case of availability of only a few training samples.

Here, we compute the error vectors between the training feature vectors and test feature vector and then taking two error vectors at a time we compute all the possible t-normed error vectors. From these normed error vectors, we select the one with the least entropy value thus eliminating all other normed error vectors. This acts as a support vector for the class.

Proof: As we are extracting information set value/feature from each window/sub-image and sum of these values over all windows or the entire image gives the

certainty because $H = \frac{1}{n} \sum x_i \mu_i$ which in the case of unsupervised learning provides an estimate of the output whereas $\bar{H} = \frac{1}{n} \sum x_i (1 - \mu_i)$ gives uncertainty or disorder which we are not considering here. Subtraction of information values of the training image and test image leads to one error vector $\{e_i\}$. As we have several training images and one test image, subtraction of their information value gives several error vectors or a set of error vectors. The t-norm of any two error vectors yields the minimum of these vectors called t-normed error vector denoted by $\{\tilde{e}_i\}$. Let us compute the certainty value of this t-normed error vector as $E = \frac{1}{n} \sum \tilde{e}_i \tilde{\mu}_i(\tilde{e}_i)$, where the t-normed error vector $\{\tilde{e}_i\}$ is converted into membership function vector, $\{\tilde{\mu}_i(\tilde{e}_i)\}$ called M-error vector. If we select the t-normed error vector with the least certainty value out of all possible t-normed error vectors of a user, it means all other t-normed errors have more certainty than the one we have selected and thus it serves as the limit of tolerance which is akin to the support vector of SVM for a class/user. The information set theory offers us an easy way to determine the limit of tolerance as against lengthy computation required to compute the support vectors in support vector machine (SVM). In the proposed approach we will be using Hanman transform to compute the least certainty valued t-normed error vector for the high level representation of certainty as follows: $E_T = \frac{1}{n} \sum \tilde{e}_i \exp\{-\tilde{e}_i \tilde{\mu}_i(\tilde{e}_i)\}$. Here we have used the exponential membership function $\tilde{\mu}_i(\tilde{e}_i)$ of \tilde{e}_i without using the statistical parameters. But their product gives the certainty of t-normed error vector belonging to a class.

We will now present two classifiers based on Hanman transform (HT). The first classifier is called Constrained HT (CHT) for which an objective function J_M is formed using M-vector. The user with the least value of the product, $(E_T J_M)$ is identified with the unknown user or test sample. The second classifier is called Weight HT (WHT) for which we form a weight vector using the values of M-vector and these weights are used in the Hanman transform to get the least value of $E_{WT} = \frac{1}{n} \sum w_i \tilde{e}_i \exp\{-\tilde{e}_i \tilde{\mu}_i(\tilde{e}_i)\}$ that gives the identity of the unknown user.

Before presenting the algorithm, let the length of feature vector be n , the number of training samples be s for each class, the number of test samples be n and the number of classes be C . It may be noted that we have used a different notation in the algorithms from the above for the convenience of representation.

3.1. Algorithm-1 of Constrained Hanman Transform (CHT) Classifier

1) Compute the error vector between the m^{th} training feature vector of I^{th} user x_{mj}^I and the test feature vector t_j as given by

$$e_{mj}^I = |x_{mj}^I - t_j| \quad (15)$$

where $m = 1, 2, \dots, s$ and $j = 1, 2, \dots, n$.

2) Compute the Frank t-normed error vector for I^h user on a pair (m, h) of the error vectors using

$$E_{mh}^l(j) = T(e_{mj}^l, e_{hj}^l); m \neq h \quad (16)$$

where $T(x, y) = \log_p \left(1 + \frac{(p^x - 1)(p^y - 1)}{p - 1} \right)$ and p is set to 2.

3) Compute the exponential membership function of t-normed error vector from:

$$M_{mh}^l(j) = e^{-E_{mh}^l(j)} \quad (17)$$

4) Compute the weight W_l using

$$W_l = \left(1 - \min_{m,h} J_{mh}^l \right)^2 \quad (18)$$

where J_{mh}^l is the average of the membership function values of I^h user given by:

$$J_{mh}^l = \frac{\sum_{q=1}^n M_{mh}^l(q)}{n}; m \neq h$$

This average must be closer to 1; hence called the unity constraint.

5) Evaluate $H_{mh}(l), h = 1, 2, \dots, s$ using Hanman Transform in Equation (14) as

$$H_{mh}(l) = \sum_{q=1}^n E_{mh}^l(q) e^{-E_{mh}^l(q) M_{mh}^l(q)} \quad (19)$$

for $m \neq h$ and $m, h = 1, 2, \dots, s$ and $l = 1, 2, \dots, C$

And compute K_l from:

$$K_l = \min_{m,h} H_{mh}(l) \quad (20)$$

where l stands for I^h user.

6) Repeat Steps 1 - 4 for all users ($l = 1, 2, \dots, C$) and if $l = \arg \min_l \{ (K_l, W_l) \}$, then the test user gets identified with I^h user.

3.2. Algorithm-2 of Weighted Hanman Transform (WHT) Classifier

In this algorithm, Steps 1 - 3 of the above algorithm are the same as the above.

1) Compute the weight

$$w^l(q) = \left[1 - M_{mh}^l(q) \right]^2 \quad (21)$$

2) Evaluate $H_{mh}(l), h = 1, 2, \dots, s$ using the Weighted Hanman Transform, expressed as

$$H_{mh}(l) = \sum_{q=1}^n w^l(q) E_{mh}^l(q) e^{-E_{mh}^l(q) M_{mh}^l(q)} \quad (22)$$

for $m \neq h$ and $m, h = 1, 2, \dots, s$ and $l = 1, 2, \dots, C$

3) Repeat Steps 1 - 5 for all users and then find $H(l) = \min H_{mh}(l)$ for each user.

4) The I^h user for which $H(I)$ is minimum gives the identity of the user.

3.3. Steps for Classification

The steps to be followed for the classification are:

- 1) For every image, take $n \times n$, compute a find feature vector by selecting one of the features derived in Section 2.4.
- 2) Divide the entire feature set into the training and testing sets.
- 3) For every test image, apply any classifier.
- 4) Compute the accuracy.

4. Description of Deep Learning Neural Architectures

Various deep learning networks have emerged in the past and are still emerging because of growing interest in researchers to try them for different industrial applications. They are a popular choice for the solution of image processing problems. A few such networks used in this paper are briefly described.

4.1. Vgg-16

VGG-16 is a dense CNN introduced in 2014 by Visual Geometry Group from Oxford [16]. It was developed for ImageNet Large Scale Visual Recognition Challenge (ILSVR). It contains 16 convolution layers with only 3×3 convolutions and multiple filters stacked over each other. Two Fully-Connected (FC) layers with 4096 nodes and one FC with 1000 nodes are followed by a softmax classifier at the top. The average of RGB values is subtracted from images at the pre-processing stage. It has been used as one of the most prominent baseline CNN architectures in object detection and recognition problems. However, it has 138 million parameters that pose a challenge to train it from scratch. It has achieved top-5 accuracy of 90.1% on ImageNet dataset. But its memory consumption and computational cost are high.

4.2. InceptionV3

InceptionV3 was introduced in [17]. This architecture contains multiple kernel sizes (5×5 , 3×3 , 1×1) to capture information at varied scales. To reduce dimensionality, 1×1 convolutions are applied before going for larger kernels. InceptionV3 is a 42 layers-deep network. It is made up of symmetric and asymmetric building blocks, including convolutions, average pooling, max pooling, concatenations, dropouts, and fully connected layers. Average pooling layer is applied after the last convolution layer which reduces the number of parameters drastically as compared to those of FC layer. This network is reported to have 5.6% top-5 error on ILSVR 2012 for classification.

4.3. ResNet-50

Kaiming He *et al.* [18] have introduced Residual Neural Network (ResNet) in the year 2015. A network with a residual block is the one where a layer feeds into its

next layer followed by another layer a few hops ahead. This is also known as skip connection and it helps overcome the degradation problem of deeper networks. It is observed that deeper networks get saturated as training proceeds and the parameters are not properly learned. These residuals skip the training of few layers thereby increasing the performance. The identity shortcuts are directly used when the input and output are of the same dimension. Each ResNet block is either two layers or three layers deep. ResNet-50 is 50 layers-deep architecture and each block has three convolution layers with the corresponding output sizes are $[56 \times 56, 28 \times 28, 14 \times 14, 7 \times 7]$. The three layers involve 1×1 , 3×3 and 1×1 convolutions where 1×1 layers are responsible for reducing and then increasing dimensions and 3×3 layers for smaller input/output dimensions. It is followed by fully connected softmax. As mentioned in [18] this network achieves 3.57% on ImageNet dataset.

4.4. MobileNet

MobileNet [19] is a light-weight CNN built by Google to overcome the high memory and resource consumption problems with embedded devices. These can perform classification, detection, embeddings and segmentation like other CNNs on devices like phones which have very limited memory. The reason why MobileNet is computationally light is mainly because it uses depth-wise separable convolutions unlike other networks. Depth-wise separable convolution consists of two layers; the depth-wise convolution and the point-wise convolution. In the depth-wise convolution, one filter per input channel is used while in the normal convolution, one filter is used for all the input channels simultaneously and its computational cost is directly proportional to the spatial dimension of the feature maps and also to the number of the input and output channels while for a MobileNet it is proportional to the spatial dimension of the feature maps and the number of output channels. Thus, the cost of the computation is reduced effectively. The output of this depth-wise convolution is linearly combined using 1×1 filter in the point-wise convolution. MobileNet is usually not as accurate as other larger and resource intensive networks but it is much faster. This accuracy and resource trade-off can be further tuned by two hyper-parameters in MobileNet: width multiplier and resolution multiplier. The width multiplier is used to thin the network, while the resolution multiplier changes the input dimensions of the image thereby reducing the internal representation at every layer.

5. Databases

We have used two video databases: YouTube Faces (YTF) in [20] and UPNA Head Pose (UPNA) in [21] as these are publicly available.

5.1. YTF

This database contains 1595 subjects with varying poses, expressions, occlusions

and illuminations. The number of videos varies from 1 to 6 for all subjects. We have considered the first video of each subject. Frames (referred as images further) are extracted from videos at a rate such that the smallest set has 48 frames while the longest video contains 6070 frames. We have a total of 292,192 frames for all subjects. But we have considered only 200 subjects with 50 frames per subject. Out of 200 subjects, some have lesser than 50 frames, so a total of 9986 frames is used in all experiments.

5.2. UPNA

This database was created mainly for tracking of heads and the estimation of poses. There are 10 subjects with 12 videos in each subject, 6 males and 4 females. Each video is 10 s long and contains 300 frames. In each subject, 6 videos are with guided-movement sequences and remaining 6 videos are with free-movement sequences. In the guided sequences, the user follows a specific movement, *i.e.* translation in three spatial axes and rotations comprising roll, yaw and pitch. In the free sequences, the user moves his/her head at free will while making translations and rotations along the three spatial axes. The ranges of movement are large, translations going up to more than 200 mm in any axis from the starting point, and rotations ranging up to 30°. For experimental purpose, we have considered only one video of each subject making free movements. Out of 6 such videos per subject, one is randomly chosen. The number of frames extracted from each video is 50 to avoid time complexity. A rate of extraction was set such that 50 frames are obtained from over the entire length of each video and are not the continuous frames.

6. Results of Experimentation

The experiments are carried out on Intel core i7 processor with 2.70 GHz and 8 GB of RAM. The recognition accuracy is computed based on the correct classification of the test frames. The results are obtained by following the steps given in Section 3.3.

The performance of the information set features extracted in Section 2.4 is shown in **Table 1** using different classifiers. The value of α is selected as 2.0 experimentally as the power of the information source (input) values. The algorithm is tested at different window sizes and the best results are obtained with features extracted from window of 35. Here a few, *i.e.* 10% of images are considered per person for training to reduce the computational cost. Out of 9986 images in YTF, only 989 are used for training and the remaining for the test while for UPNA out of total 500 images, 50 are used for training and 450 for testing.

Table 1 also gives the results of face recognition by Hanman Transform (HT) classifier, Constrained Hanman Transform (CHT) classifier and Weighted Hanman Transform (WHT) classifier. For some feature types, HT and CHT are giving the same results. But two feature types SG and RE show good performance on the classifiers compared. Comparative results are obtained with sigmoid (SG)

Table 1. Recognition accuracy in (%) of the features with different classifiers.

YTF						
Feature	HT	CHT	WHT	LR	SVM	KNN
EN	82.22	88.80	96	94.30	95.41	95.23
SG	99.23	95.71	97.78	97.70	98.18	98.11
EI	85.01	74.34	30.56	96.74	97.77	97.65
RE	99.07	96.63	99.56	97.30	98.09	97.99
ARE	98.93	94.55	98.89	97.03	97.73	97.54
UPNA						
Feature	HT	CHT	WHT	LR	SVM	KNN
EN	97.56	100	97.56	98	97.55	94.44
SG	100	100	100	100	100	96.44
EI	60.67	99.78	60.67	93.56	91.78	91.78
RE	100	92.67	100	100	89.11	87.56
ARE	94	78	95.56	99.11	60.22	95.78

features on YTF using HT and SVM with recognition accuracies of 99.23% and 98.18% respectively but the highest accuracy of 99.56% is obtained with WHT on RE features. The SG and RE features also give consistent results on UPNA with the classifiers used. The information set features outperform the deep learning (CNN) architectures' features on YTF but both information set features and CNN architectures' features demonstrate a comparable performance on UPNA. The computation required with information set features is much less than those of CNN architectures.

We have tried to cut down the computation cost by considering only 10% of the data as training set and the remaining as the testing test. To validate our approach on YTF, we have compared the results of CNNs on only 200 subjects. To reduce the computation time, we have considered 50 (few subjects have lower than 50 images) frames per subject randomly chosen.

Similarly, for UPNA there are 10 subjects with 50 frames each. 10% of data is used in training and remaining in testing.

The input tensor size is taken as 224×224 . The input sizes, kernels, degrees and parameter values are experimented to get the best results shown in **Table 2**. On the classifier front Support Vector Machine (SVM) with the polynomial kernel of degree 2 is found to be the best. Another classifier called K-Nearest Neighbors (KNN) is tried for different values of K but $K = 1$ gives the best results.

Table 2. Recognition accuracy with various CNN architectures.

YTF			
CNN Architecture	LR	SVM	KNN = 1
InceptionV3	98.08	98.18	98.16
ResNet-50	52.02	52.70	92.19
Vgg-16	98.75	98.74	98.74
MobileNet	98.84	98.73	98.73
UPNA			
CNN Architecture	LR	SVM	KNN = 1
InceptionV3	98.89	97.33	98.22
ResNet-50	9.11	9.11	84.89
Vgg-16	100	100	96.67
MobileNet	100	100	89.11

As far as computational speed is concerned Vgg-16 is the slowest and MobileNet is the fastest due to their architectures. Coming to the effectiveness of features barring ResNet-50, the features from other architectures display consistent performance on both YTF and UPNA with LR, SVM and KNN classifiers. The highest score of 98.84% shown highlighted is obtained with LR on YTF. Both Vgg-16 and MobileNet have outperformed InceptionV3 and ResNet-50. Note that while extracting features using deep learning and information set-based methods, the input images are not subjected to any kind of pose and illumination correction.

As can be noticed from the above the main problem with the information set features is the choice of window size/sub-image and feature type whereas the problems with deep learning architectures include: Choice of architecture, Number of convolution and max pooling layers, activation function, and the number of filters to be used. The problems associated with the extraction of information set features can be easily fixed and the computational burden is also less; hence these features are more preferable.

7. Conclusions

An attempt has been made to make a comparative study between the deep learning features and information set features using several well-known classifiers on face videos. This study is necessitated to wean away from the blind following of deep learning methods and the related architectures for the solutions to all kinds of problems. There is a problem of choice in the ordering of the convolution and max-pooling layers in these architectures. It has been found that consideration of a large number of layers need not be accompanied with

commensurate performance. Of all the deep learning architectures, MobileNet is found to be the best followed by Vgg-16.

An alternate approach that deals with information set-based features is mainly concerned with certainty or uncertainty in the attribute or information source values, which is found using entropy functions. They provide a lot of flexibility in the generation of different types of features. In this paper, a few information set-based features have been derived followed by the formulation of Constrained Hanman Transform (CHT) and Weighted Hanman Transform (WHT) classifiers. Two information set features called Sigmoid and Renyi entropy fare extremely well on all classifiers in two datasets YTF and UPNA whereas InceptionV3, Vgg-16 and MobileNet fare extremely well on LR, SVM and KNN.

The main contributions of the paper include: 1) Promulgation of logical operations on information sets and their properties 2) Derivation of Hanman transform-based classifiers and 3) Application of both deep learning and information set based features for the video-based face recognition.

The overall performance of deep learning methods appears somewhat inferior to that of information set features with HT-based classifiers that are computationally very fast. The information set theory offers flexibility in feature extraction and classifier construction.

Our future work is concerned with extending the theory to differential entropy functions.

Conflicts of Interest

The authors declare no conflicts of interest regarding the publication of this paper.

References

- [1] Zhengm J., Ranjanm R., Chenm C., Chenm J., Castillo, C.D. and Chellappa, R. (2020) *IEEE Transactions on Biometrics, Behavior, and Identity Science*, **2**, 194-209. <https://doi.org/10.1109/TBIOM.2020.2973504>
- [2] Wang, M. and Deng, W. (2018) Deep Face Recognition: A Survey. <https://doi.org/10.1016/j.neucom.2020.10.081>
- [3] Inoue, H. (2018) Data Augmentation by Pairing Samples for Images Classification. <https://arxiv.org/abs/1801.02929>
- [4] Goodfellow, I.J., Pouget-Abadie, J., Mirza, M, *et al.* (2014) Generative Adversarial Nets. *Proceedings of the 27th International Conference on Neural Information Processing Systems*, Volume 2, 2672-2680. <https://dl.acm.org/doi/10.5555/2969033.2969125>
- [5] Xiong, L., Karlekar, J., Zhao, J., Feng, J., Pranata, S. amd Shen, S. (2017) A Good Practice towards Top Performance of Face Recognition: Transferred Deep Feature Fusion. <https://arxiv.org/abs/1704.00438>
- [6] Hanmandlu, M. and Singhal, S. (2017) *Applied Soft Computing*, **53**, 396-406. <https://doi.org/10.1016/j.asoc.2017.01.014>
- [7] Hanmandlu, M. (2011) *Defence Science Journal*, **61**, 405-407. <https://doi.org/10.14429/dsj.61.1192>

-
- [8] Hanmandlu, M. and Das, A. (2011) *Defence Science Journal*, **61**, 415-430. <https://doi.org/10.14429/dsj.61.1177>
- [9] Mamta and Hanmandlu, M. (2014) *Engineering Applications of Artificial Intelligence*, **36**, 269-286. <https://doi.org/10.1016/j.engappai.2014.06.028>
- [10] Sayeed, F. and Hanmandlu, M. (2017) *Knowledge and Information Systems*, **52**, 485-507. <https://doi.org/10.1007/s10115-016-1017-x>
- [11] Agarwal, M. and Hanmandlu, M. (2016) *IEEE Transactions on Fuzzy Systems*, **24**, 1-15. <https://doi.org/10.1109/TFUZZ.2015.2417593>
- [12] Hanmandlu, M., Bansal, M. and Vasikarla, S. (2020) *Journal of Modern Physics*, **11**, 122-144. <https://doi.org/10.4236/jmp.2020.111008>
- [13] Bhatia, A. and Hanmandlu, M. (2018) *Journal of Modern Physics*, **9**, 112-129. <https://doi.org/10.4236/jmp.2018.92008>
- [14] Grover, J. and Hanmandlu, M. (2018) *Applied Intelligence*, **48**, 3394-3410. <https://doi.org/10.1007/s10489-018-1154-x>
- [15] Grover, J. and Hanmandlu, M. (2020) *Applied Intelligence*. <https://doi.org/10.1007/s10489-020-01881-3>
- [16] Simonyan, K. and Zisserman, A. (2015) Very Deep Convolutional Networks for Large-Scale Image Recognition. <https://arxiv.org/abs/1409.1556v6>
- [17] Szegedy, C., Vanhoucke, V., Ioffe, S., Shlens, J. and Wojna, Z. (2016) Rethinking the Inception Architecture for Computer Vision. 2016 *IEEE Conference on Computer Vision and Pattern Recognition (CVPR)*, Las Vegas, 27-30 June 2016, 2818-2826. <https://doi.org/10.1109/CVPR.2016.308>
- [18] He, K.M., Zhang, X.Y., Ren, S.Q. and Sun, J. (2016) Deep Residual Learning for Image Recognition. *IEEE Conference on Computer Vision and Pattern Recognition (CVPR)*, Las Vegas, 27-30 June 2016, 770-778. <https://doi.org/10.1109/CVPR.2016.90>
- [19] Howard, A.G., et al. (2017) MobileNets: Efficient Convolutional Neural Networks for Mobile Vision Applications. <https://arxiv.org/abs/1704.04861>
- [20] Wolf, L., Hassner, T. and Maoz, I. (2011) Face Recognition in Unconstrained Videos with Matched Background Similarity. *IEEE Conference on Computer Vision and Pattern Recognition (CVPR)*, Colorado Springs, 20-25 June 2011, 529-534. <https://doi.org/10.1109/CVPR.2011.5995566>
- [21] Ariz, M., Bengoechea, J.J., Villanueva, A. and Cabeza, R. (2016) *Computer Vision and Image Understanding*, **148**, 201-210. <https://doi.org/10.1016/j.cviu.2015.04.009>

Flavour and Colour of Quarks in Spin Topological Space

Shaoxu Ren

Institute of Physical Science and Engineering Tongji University, Shanghai, China

Email: shaoxu-ren@hotmail.com

How to cite this paper: Ren, S.X. (2021) Flavour and Colour of Quarks in Spin Topological Space. *Journal of Modern Physics*, 12, 380-389.
<https://doi.org/10.4236/jmp.2021.123027>

Received: January 14, 2021

Accepted: February 23, 2021

Published: February 26, 2021

Copyright © 2021 by author(s) and Scientific Research Publishing Inc. This work is licensed under the Creative Commons Attribution International License (CC BY 4.0).

<http://creativecommons.org/licenses/by/4.0/>



Open Access

Abstract

An assumption that *all* the six flavour quarks are attributed to be the components of *a same, a common* isospin multiplets space named **STS** is proposed. Base on **Pauli Exclusion Principle**, every quark is assigned to different flavour marks in STS. Every flavour quark possesses *its own colour spectral line array* specially appointed. The collection of colour spectral line arrays of the six flavour quarks constructs together the **CSDF**, Colour Spectrum Diagram of Flavour, further baryons and mesons could be constructed from **CSDF**. STS, Spin Topological Space is a math frame with infinite dimensional matrix representation for spin angular momentum. Flavours is an isospin angular momentum coupling phenomena of the three-colour-quarks.

Keywords

Pauli Exclusion Principle, **STS**, Spin Topological Space, **STC**, Spin Topological Coordinate, Colour Spectral Line Array, **CSDF**, Colour Spectrum Diagram of Flavour

1. Introduction

In isotopic spin space of **Standard Model**, **SM**, Gell-Mann M [1] and Zweig G [2], the isospin quantum number I and the third component I_3 , for flavour quarks u, d are $1/2, +1/2$ and $1/2, -1/2$ respectively, for flavour quarks s, c, b, t are $0, 0$. $u (I_3 = +1/2)$ and $d (I_3 = -1/2)$ quarks are assigned to an isodoublet with $I = 1/2$, the dimension of matrix representation of the isodoublet is equal to $2 \times 1/2 + 1 = 2$. This matrix representation is an analogy with ordinary angular momentum $\vec{\sigma}/2$, $\vec{\sigma}$ is Pauli matrix. And the remaining four flavour quarks $s (I_3 = 0)$, $c (I_3 = 0)$, $b (I_3 = 0)$, $t (I_3 = 0)$ are assigned to four isosinglets with $I = 0$, respectively, the dimension of matrix representation of each isosinglet is equal to $2 \times 0 + 1 = 1$. Further, there is an isodoublet and there are

four isosinglets in isospin scheme for flavour quarks [3].

It is a curious question, what will happen? if the above six flavour quarks are all put into a *common* multiplet, that is, if these flavours are treated equally in one isotopic spin space. According to **Pauli Exclusion Principle, PEP**, each of those values of $I_3(q_i)$ of six flavour quarks should not be the same each other. Following the unified math symmetry picture, all eigenvalues of $I_3(q_i)$ of flavour q_i quark are proposed to be half-integers, to be $+5/2, +3/2, +1/2, -1/2, -3/2, -5/2$. $q_i = q_t, q_c, q_u, q_d, q_s, q_b, i = t, c, u, d, s, b$ respectively are shown in **Table 1**.

Table 1. Flavours quarks from **SM** to **STS**.

Flavour	I	$I_3(q_i)$	matrix	PEP	I	$I_3(q_i)$	matrix
Quark	SM			\Rightarrow	STS		infinite dimension
t	0	$I_3(t)=0$	1 dimension		1/2	$I_3(t)=+5/2^\diamond$	infinite dimension
c	0	$I_3(c)=0$	1 dimension		1/2	$I_3(c)=+3/2^\diamond$	infinite dimension
u	1/2	$I_3(u)=+1/2$	2 dimension		1/2	$I_3(u)=+1/2$	infinite dimension
d	1/2	$I_3(d)=-1/2$	2 dimension		1/2	$I_3(d)=-1/2$	infinite dimension
s	0	$I_3(s)=0$	1 dimension		1/2	$I_3(s)=-3/2^\diamond$	infinite dimension
b	0	$I_3(b)=0$	1 dimension		1/2	$I_3(b)=-5/2^\diamond$	infinite dimension

In **Table 1**, the right side is more graceful and elegant than the left side, but how can we obtain *those* third component eigenvalues $I_3(q_i)$ of *isospin* 1/2 particles, that labelled by mark \diamond , which are greater than $+1/2$ or less than $-1/2$ in **Table 1**? Next, we resort to **Spin Topological Space** ([4] [5] [6] [7]), abbreviation **STS**, that can help us to construct what we want to get the right side in **Table 1**.

2. STS, Spin Topological Space

Spin angular momentum $\vec{\pi}$ of a spin particle in STS math frame, is labelled by two subscripts j, k (if in real region):

$$\vec{\pi}_{j,k} = (\pi_{1;j,k}, \pi_{2;j,k}, \pi_{3;j,k}) \quad (1)$$

$\vec{\pi}_{j,k}$ satisfy angular momentum commutation rule (2)

$$\vec{\pi}_{j,k} \times \vec{\pi}_{j,k} = i\vec{\pi}_{j,k} \quad (2)$$

$$\pi_{1;j,k} = \frac{1}{2}(\pi_j^+ + \pi_k^-) \quad (3.1)$$

$$\pi_{2;j,k} = \frac{1}{2i}(\pi_j^+ - \pi_k^-) \quad (3.2)$$

$$\pi_{3;j,k} = \frac{1}{2}(\pi_j^+ \pi_k^- - \pi_k^- \pi_j^+) \quad (3.3)$$

$j, k \in \text{STS}$. $\pi_{1;j,k}$ and $\pi_{2;j,k}$ are two infinite dimensional Non-Hermitian Matrices. $\pi_{3;j,k}$ is an infinite dimensional Hermitian Matrix [4] [7]. Using the three components of $\vec{\pi}_{j,k}$, we get the expressions for the eigenvalue of Casimir Operator $\pi_{j,k}^2$ and the eigenvalue of the third component $\pi_{3;j,k}$ of $\vec{\pi}_{j,k}$ below

$$\pi_{j,k}^2 = \pi_{1;j,k}^2 + \pi_{2;j,k}^2 + \pi_{3;j,k}^2 = \frac{1}{4} \left\{ (j-k)^2 - 1 \right\} I_0 \tag{4}$$

$$\pi_{3;j,k} = \pi_0(0) + \frac{1}{2} (j+k+1) I_0 \tag{5}$$

$$\pi_0(0) = \text{diag} \{ \dots, 5, 4, 3, 2, 1, 0, -1, -2, -3, -4, -5, \dots \} \tag{6}$$

$$I_0 = \text{diag} \{ \dots, 1, 1, 1, 1, 1, 1, 1, 1, 1, 1, \dots \} \tag{7}$$

formulas (4), (5) show $\pi_{j,k}^2$ and $\pi_{3;j,k}$ are diagonal infinite dimensional matrices. Here $\pi_0(0)$ is the vacuum background spin angular momentum of $\pi_{3;j,k}$. If in case of no confusion, it is convenient to instead of (5) to use (9) to deal with I_3 , then obtain following expressions

$$\pi_{j,k}^2 = \frac{1}{4} (S_{j,k}^2 - 1) \tag{8}$$

$$\pi_{3;j,k} = \frac{1}{2} (A_{j,k} + 1) \tag{9}$$

$$S_{j,k} = j - k, \quad A_{j,k} = j + k \tag{10}$$

$$(j, k) = \left(\frac{1}{2} (A_{j,k} + S_{j,k}), \frac{1}{2} (A_{j,k} - S_{j,k}) \right) \tag{11}$$

Call (j, k) , **STC**, Spin Topological Coordinate of spin particle in STS.

Addition of $\vec{\pi}_{j,k}$ and $\vec{\pi}_{r,s}$, $\vec{\Pi}_{j,k;r,s}$ is given below

$$\vec{\pi}_{j,k} \times \vec{\pi}_{j,k} = i\vec{\pi}_{j,k}, \quad \vec{\pi}_{r,s} \times \vec{\pi}_{r,s} = i\vec{\pi}_{r,s} \tag{12}$$

$$\vec{\Pi}_{j,k;r,s} \times \vec{\Pi}_{j,k;r,s} = i\vec{\Pi}_{j,k;r,s} \tag{13}$$

$$\vec{\Pi}_{j,k;r,s} = \frac{1}{2} (\vec{\pi}_{j,k} + \vec{\pi}_{r,s}) \tag{14}$$

$$\Pi_{j,k;r,s}^2 = \frac{1}{16} \left((S_{j,k} + S_{r,s})^2 - 4 \right) = \frac{1}{4} \left((S_{j,k}/2 + S_{r,s}/2)^2 - 1 \right) \tag{15}$$

$$\Pi_{3;j,k;r,s} = \frac{1}{2} (\pi_{3;j,k} + \pi_{3;r,s}) \tag{16}$$

$\Pi_{j,k;r,s}^2$ and $\Pi_{3;j,k;r,s}$ are Casimir operator and the third component of spin particle $\vec{\Pi}_{j,k;r,s}$ in STS.

3. Flavour Quarks in STS

Now we continue **Table 1** quark model in STS, in *flavour isotopic space*, $\vec{\pi}$ is replaced by $\vec{I}(q_i)$, then obtain Casimir Operator $I^2(q_i)$ (18) and the third component eigenvalues $I_3(q_i)$ (19) of flavour q_i quarks (*fermion* $I(q_i) = \frac{1}{2}$ (17)). Details are shown in **Table 2**.

Table 2. Flavour quantum number of quarks in STS (isospin $I = \hbar/2$).

$I_{3;j,k}(q_i)$	$= \frac{1}{2}(A_{j,k}(q_i)+1)$	$A_{j,k}(q_i)$	$S_{j,k}(q_i)$	$(j,k)_{q_i}$
$I_{3;+3,+1}(t) = +5/2^*$	$\frac{1}{2}(+4+1)$	$A_{+3,+1}(t) = +4$	$S_{+3,+1}(t) = +2$	$(+3,+1)_t$
$I_{3;+2,0}(c) = +3/2^*$	$\frac{1}{2}(+2+1)$	$A_{+2,0}(c) = +2$	$S_{+2,0}(c) = +2$	$(+2,0)_c$
$I_{3;+1,-1}(u) = +1/2$	$\frac{1}{2}(0+1)$	$A_{+1,-1}(u) = 0$	$S_{+1,-1}(u) = +2$	$(+1,-1)_u$
$I_{3;0,-2}(d) = -1/2$	$\frac{1}{2}(-2+1)$	$A_{0,-2}(d) = -2$	$S_{0,-2}(d) = +2$	$(0,-2)_d$
$I_{3;-1,-3}(s) = -3/2^*$	$\frac{1}{2}(-4+1)$	$A_{-1,-3}(s) = -4$	$S_{-1,-3}(s) = +2$	$(-1,-3)_s$
$I_{3;-2,-4}(b) = -5/2^*$	$\frac{1}{2}(-6+1)$	$A_{-2,-4}(b) = -6$	$S_{-2,-4}(b) = +2$	$(-2,-4)_b$

Note: $A_{j,k}(q_i)$ is named as *flavour quantum number* of quarks, which are even numbers.

$$I(q_i) = \frac{1}{2} \tag{17}$$

$$I_{j,k}^2(q_i) = \text{diag} \left\{ \dots, \frac{+3}{4}, \frac{+3}{4}, \frac{+3}{4}, \frac{+3}{4}, \frac{+3}{4}, \frac{+3}{4}, \frac{+3}{4}, \dots \right\} \tag{18}$$

$$I_{3;j,k}(q_i) = \text{diag} \left\{ \dots, \frac{+7}{2} \blacklozenge, \frac{+5}{2} \blacklozenge, \frac{+3}{2} \blacklozenge, \frac{+1}{2}, \frac{-1}{2}, \frac{-3}{2} \blacklozenge, \frac{-5}{2} \blacklozenge, \dots \right\}, i = t, c, u, d, s, b \tag{19}$$

4. Colour Quarks in STS

Now **Suppose** that except *flavour quantum number* marked $A_{j,k}(q_i)$ in STS (Table 2), quark could even possess *colour quantum number array* that called as **Colour Spectral Line Array** labelled by q_{RGB} (20), which is an array comprised of *three colour quantum numbers*, marked q_{R} , q_{G} and q_{B} , they are third-fractions.

$$q_{\text{RGB}} \equiv (q_{\text{R}}, q_{\text{G}}, q_{\text{B}}) \equiv (A(q_{\text{R}}), A(q_{\text{G}}), A(q_{\text{B}})) \tag{20}$$

Different flavour quark possesses its own colour spectral line array, for example, array $u_{\text{RGB}} \equiv (u_{\text{R}}, u_{\text{G}}, u_{\text{B}}) = \left(\frac{+2}{3}, \frac{+5}{3}, \frac{+11}{3} \right)$ is the colour spectral line array of flavour u quark, and array $d_{\text{RGB}} \equiv (d_{\text{R}}, d_{\text{G}}, d_{\text{B}}) = \left(\frac{-16}{3}, \frac{-13}{3}, \frac{-7}{3} \right)$ is colour spectral line array of flavour d quark. Flavour $A_{j,k}(q_i)$ and colour q_{RGB} are the identities of quark particles.

Definition CSDF, Colour Spectrum Diagram of Flavour is composed of six (or more) colour spectral line arrays of flavour quarks, somewhat similar to the Gene diagram of chromosomes. Explicit scheme of **CSDF** is given below.

CSDF, Colour Spectrum Diagram of Flavour

	$t, \frac{+5}{2}$	$c, \frac{+3}{2}$	$u, \frac{+1}{2}$	$d, \frac{-1}{2}$	$s, \frac{-3}{2}$	$b, \frac{-5}{2}$
Quark	$I_3(t_R, t_G, t_B)$	$I_3(c_R, c_G, c_B)$	$I_3(u_R, u_G, u_B)$	$I_3(d_R, d_G, d_B)$	$I_3(s_R, s_G, s_B)$	$I_3(b_R, b_G, b_B)$
$I_3(q_{RGB})$	$(\frac{+41}{6}, \frac{+44}{6}, \frac{+50}{6})$	$(\frac{+23}{6}, \frac{+26}{6}, \frac{+32}{6})$	$(\frac{+5}{6}, \frac{+8}{6}, \frac{+14}{6})$	$(\frac{-13}{6}, \frac{-10}{6}, \frac{-4}{6})$	$(\frac{-31}{6}, \frac{-28}{6}, \frac{-22}{6})$	$(\frac{-49}{6}, \frac{-46}{6}, \frac{-40}{6})$
	$\bar{t}, \frac{-5}{2}$	$\bar{c}, \frac{-3}{2}$	$\bar{u}, \frac{-1}{2}$	$\bar{d}, \frac{+1}{2}$	$\bar{s}, \frac{+3}{2}$	$\bar{b}, \frac{+5}{2}$
Anti-Quark	$I_3(\bar{t}_R, \bar{t}_G, \bar{t}_B)$	$I_3(\bar{c}_R, \bar{c}_G, \bar{c}_B)$	$I_3(\bar{u}_R, \bar{u}_G, \bar{u}_B)$	$I_3(\bar{d}_R, \bar{d}_G, \bar{d}_B)$	$I_3(\bar{s}_R, \bar{s}_G, \bar{s}_B)$	$I_3(\bar{b}_R, \bar{b}_G, \bar{b}_B)$
$I_3(\bar{q}_{RGB})$	$(\frac{-41}{6}, \frac{-44}{6}, \frac{-50}{6})$	$(\frac{-23}{6}, \frac{-26}{6}, \frac{-32}{6})$	$(\frac{-5}{6}, \frac{-8}{6}, \frac{-14}{6})$	$(\frac{+13}{6}, \frac{+10}{6}, \frac{+4}{6})$	$(\frac{+31}{6}, \frac{+28}{6}, \frac{+22}{6})$	$(\frac{+49}{6}, \frac{+46}{6}, \frac{+40}{6})$
	$\nearrow \uparrow \searrow$					
	$\begin{matrix} & & \\ & & \\ & & \end{matrix}$	$\begin{matrix} & & \\ & & \\ & & \end{matrix}$	$\begin{matrix} & & \\ & & \\ & & \end{matrix}$	$\begin{matrix} & & \\ & & \\ & & \end{matrix}$	$\begin{matrix} & & \\ & & \\ & & \end{matrix}$	$\begin{matrix} & & \\ & & \\ & & \end{matrix}$
	$\swarrow \downarrow \nwarrow$					
	$t, +4$	$c, +2$	$u, 0$	$d, -2$	$s, -4$	$b, -6$
Quark	(t_R, t_G, t_B)	(c_R, c_G, c_B)	(u_R, u_G, u_B)	(d_R, d_G, d_B)	(s_R, s_G, s_B)	(b_R, b_G, b_B)
q_{RGB}	$(\frac{+38}{3}, \frac{+41}{3}, \frac{+47}{3})$	$(\frac{+20}{3}, \frac{+23}{3}, \frac{+29}{3})$	$(\frac{+2}{3}, \frac{+5}{3}, \frac{+11}{3})$	$(\frac{-16}{3}, \frac{-13}{3}, \frac{-7}{3})$	$(\frac{-34}{3}, \frac{-31}{3}, \frac{-25}{3})$	$(\frac{-52}{3}, \frac{-49}{3}, \frac{-43}{3})$
	$\bar{t}, -6$	$\bar{c}, -4$	$\bar{u}, -2$	$\bar{d}, 0$	$\bar{s}, +2$	$\bar{b}, +4$
Anti-Quark	$(\bar{t}_R, \bar{t}_G, \bar{t}_B)$	$(\bar{c}_R, \bar{c}_G, \bar{c}_B)$	$(\bar{u}_R, \bar{u}_G, \bar{u}_B)$	$(\bar{d}_R, \bar{d}_G, \bar{d}_B)$	$(\bar{s}_R, \bar{s}_G, \bar{s}_B)$	$(\bar{b}_R, \bar{b}_G, \bar{b}_B)$
\bar{q}_{RGB}	$(\frac{-44}{3}, \frac{-47}{6}, \frac{-53}{6})$	$(\frac{-26}{3}, \frac{-29}{3}, \frac{-35}{3})$	$(\frac{-8}{3}, \frac{-11}{3}, \frac{-17}{3})$	$(\frac{+10}{3}, \frac{+7}{3}, \frac{+1}{3})$	$(\frac{+28}{3}, \frac{+25}{3}, \frac{+19}{3})$	$(\frac{+46}{3}, \frac{+43}{3}, \frac{+37}{3})$

5. Hypothesis

Flavours are coupling phenomena of isospin angular momenta of three-colour-quarks.

To track the idea, we make use of **CSDF**, and of angular momentum formulae (21) and (22) of three spin particles below. Further obtain **STC array** of flavour quarks in **Table 3**. In other words, obtain the relationships **STC array**,

$(j, k)_{q_i} = ((j, k)_{q_R}, (j, k)_{q_G}, (j, k)_{q_B})$ between flavour quantum number, $A_{j,k}(q_i)$ and Colour Spectral Line Array $q_{RGB} = (q_R, q_G, q_B)$.

$$I^2(3q) = \frac{1}{36} \left((S(q_R) + S(q_G) + S(q_B))^2 - 9 \right) = \frac{3}{4} \tag{21}$$

$$I_3(3q) = \frac{1}{3} (I_3(q_R) + I_3(q_G) + I_3(q_B)) = \frac{1}{2} \left(\frac{A(3q)}{3} + 1 \right) \tag{22.1}$$

$$I_3(q) = \overline{I_3(3q)} = \frac{1}{3} I_3(3q) \tag{22.2}$$

Table 3. STC array of colour quantum numbers of flavour quarks.

$(j, k)_{q_i}$	$(j, k)_i$	$(j, k)_c$	$(j, k)_u$	$(j, k)_d$	$(j, k)_s$	$(j, k)_b$
	$(j, k)_{r_i}$	$(j, k)_{c_i}$	$(j, k)_{u_i}$	$(j, k)_{d_i}$	$(j, k)_{s_i}$	$(j, k)_{b_i}$
$(j, k)_{q_{r_i}}$	$\left(\frac{+44}{6}, \frac{+32}{6}\right)_{r_i}$	$\left(\frac{+26}{6}, \frac{+14}{6}\right)_{c_i}$	$\left(\frac{+8}{6}, \frac{-4}{6}\right)_{u_i}$	$\left(\frac{-10}{6}, \frac{-22}{6}\right)_{d_i}$	$\left(\frac{-28}{6}, \frac{-40}{6}\right)_{s_i}$	$\left(\frac{-46}{6}, \frac{-58}{6}\right)_{b_i}$
	$(j, k)_{i_g}$	$(j, k)_{u_g}$	$(j, k)_{c_g}$	$(j, k)_{d_g}$	$(j, k)_{s_g}$	$(j, k)_{b_g}$
$(j, k)_{q_{i_g}}$	$\left(\frac{+47}{6}, \frac{+35}{6}\right)_{i_g}$	$\left(\frac{+29}{6}, \frac{+17}{6}\right)_{c_g}$	$\left(\frac{+11}{6}, \frac{-1}{6}\right)_{u_g}$	$\left(\frac{-7}{6}, \frac{-19}{6}\right)_{d_g}$	$\left(\frac{-25}{6}, \frac{-37}{6}\right)_{s_g}$	$\left(\frac{-43}{6}, \frac{-55}{6}\right)_{b_g}$
	$(j, k)_{u_b}$	$(j, k)_{c_b}$	$(j, k)_{d_b}$	$(j, k)_{s_b}$	$(j, k)_{r_b}$	$(j, k)_{b_b}$
$(j, k)_{q_{u_b}}$	$\left(\frac{+53}{6}, \frac{+41}{6}\right)_{u_b}$	$\left(\frac{+35}{6}, \frac{+23}{6}\right)_{c_b}$	$\left(\frac{+17}{6}, \frac{+5}{6}\right)_{d_b}$	$\left(\frac{-1}{6}, \frac{-13}{6}\right)_{s_b}$	$\left(\frac{-19}{6}, \frac{-31}{6}\right)_{r_b}$	$\left(\frac{-37}{6}, \frac{-49}{6}\right)_{b_b}$

6. Baryons and Mesons in STS

Due to baryons all are “white colour” particles, which are made of colourful quarks. To help with **CSDF**, picking up three colour quantum numbers: $q_R^1 \subseteq q_{RGB}^1$, $q_G^2 \subseteq q_{RGB}^2$ and $q_B^3 \subseteq q_{RGB}^3$, respectively from any three quarks q^1 , q^2 and q^3 (q^1 , q^2 and q^3 can be any flavour), then various visible baryons could be produced. In this way, for example, baryon decuplet is constituted as shown in **Table 4**.

According to SM, the “colourless phenomena” of all mesons could be satisfied by blending with a quark with colour and antiquark with anti-colour, that is to say, $q_R \bar{q}_{\bar{R}}$, or $q_G \bar{q}_{\bar{G}}$, or $q_B \bar{q}_{\bar{B}}$. Contrary to SM, in STS a meson is similar to a baryon, a meson also is a three-body system that comprises a quark (colour), an antiquark (anti-colour) and a gluon (white). This gluon plays the role of mediator to fasten quark and antiquark together in a meson.

Colour spectral line array of meson is symbolized with $q_i \bar{q}_j g_k = (q_i, \bar{q}_j, g_k)$. The mentioned above is the case of $i = j$, $k = 0$. The discussion about $i \neq j$, $k \neq 0$ will be given later.

In what follows base on **CSDF**, we list the weight diagram **Table 5** of meson octet. Here g_0 is the gluon basic state with $I_3^2(g_0) = 0\hbar$, $A(g_0) = -1$.

7. $\vec{A}(q) \cdot \vec{A}(q)$ Interaction in STS

This paragraph suggests some ideas, similar to spin-spin $\vec{S}_i \cdot \vec{S}_j$ interaction in spin space [3], to discuss $\vec{A}(q) \cdot \vec{A}(q)$ Interaction in STS. **Table 4** shows that baryons, like quarks (**CSDF**), are marked by *colour spectral line arrays* too, but a slight different from quarks. Actually, there are two kinds of colour spectral line arrays: right-hand colour quantum numbers (*r-h*) (23.1) and left-hand colour quantum numbers (*l-h*) (23.2) for a given baryon, which made of quark q^1 , q^2 and q^3 . Each baryon exists in one of three possible states, labelled with cases: I, II and III in case (23.1) and case (23.2) respectively. The results in **Table 4** are the case of I of (*r-h*) only shown below.

Table 4. Weight diagram for baryon decuplet with $S = +4$ in STS.

$I_3(\Delta^-) = \frac{-3}{2}, -4$ (d_R, d_G, d_B) $\left(\frac{-16}{3}, \frac{-13}{3}, \frac{-7}{3}\right)$	$I_3(\Delta^0) = \frac{-1}{2}, -2$ (u_R, d_G, d_B) $\left(\frac{+2}{3}, \frac{-13}{3}, \frac{-7}{3}\right)$	$I_3(\Delta^+) = \frac{+1}{2}, 0$ (u_R, d_G, u_B) $\left(\frac{+2}{3}, \frac{-13}{3}, \frac{+11}{3}\right)$	$I_3(\Delta^{++}) = \frac{+3}{2}, +2$ (u_R, u_G, u_B) $\left(\frac{+2}{3}, \frac{+5}{3}, \frac{+11}{3}\right)$
$I_3(\Sigma^-) = \frac{-5}{2}, -6$ (d_R, s_G, d_B) $\left(\frac{-16}{3}, \frac{-31}{3}, \frac{-7}{3}\right)$	$I_3(\Sigma^0) = \frac{-3}{2}, -4$ (u_R, s_G, u_B) $\left(\frac{+2}{3}, \frac{-31}{3}, \frac{-7}{3}\right)$	$I_3(\Sigma^+) = \frac{-1}{2}, -2$ (u_R, s_G, u_B) $\left(\frac{+2}{3}, \frac{-31}{3}, \frac{+11}{3}\right)$	
	$I_3(\Xi^-) = \frac{-7}{2}, -8$ (d_R, s_G, s_B) $\left(\frac{-16}{3}, \frac{-31}{3}, \frac{-25}{3}\right)$	$I_3(\Xi^0) = \frac{-5}{2}, -6$ (u_R, s_G, s_B) $\left(\frac{+2}{3}, \frac{-31}{3}, \frac{-25}{3}\right)$	
	$I_3(\Omega^-) = \frac{-9}{2}, -10$ (s_R, s_G, s_B) $\left(\frac{-34}{3}, \frac{-31}{3}, \frac{-25}{3}\right)$		

Note: in **Table 4**, the value I_3 of every baryon all is half integer, contrary to those what the I_3 might take both half integer and integer (include zero) in case of $J^P = 3/2^+$ in SM.

Table 5. Weight diagram for meson octet with $S = +1$ in STS.

$I_3(k^0) = +1, A(k^0) = +1$ (d_R, \bar{s}_R, g_0) $\left(\frac{-16}{3}, \frac{+28}{3}, \frac{-3}{3}\right)$	$I_3(k^+) = +2, A(k^+) = +3$ (u_R, \bar{s}_R, g_0) $\left(\frac{+2}{3}, \frac{+28}{3}, \frac{-3}{3}\right)$	
$I_3(\pi^-) = -1, A(\pi^-) = -3$ (d_R, \bar{u}_R, g_0) $\left(\frac{-16}{3}, \frac{-8}{3}, \frac{-3}{3}\right)$	$I_3(\pi^0, \eta) = 0, A(\pi^0, \eta) = -1$ (u_R, \bar{u}_R, g_0) $\left(\frac{+2}{3}, \frac{-8}{3}, \frac{-3}{3}\right)$ (d_R, \bar{d}_R, g_0) $\left(\frac{-16}{3}, \frac{+10}{3}, \frac{-3}{3}\right)$	$I_3(\pi^+) = +1, A(\pi^+) = +1$ (u_R, \bar{d}_R, g_0) $\left(\frac{+2}{3}, \frac{+10}{3}, \frac{-3}{3}\right)$
$I_3(k^-) = -2, A(k^-) = -5$ (s_R, \bar{u}_R, g_0) $\left(\frac{-34}{3}, \frac{-8}{3}, \frac{-3}{3}\right)$	$I_3(\bar{k}^0) = -1, A(\bar{k}^0) = -3$ (s_R, \bar{d}_R, g_0) $\left(\frac{-34}{3}, \frac{+10}{3}, \frac{-3}{3}\right)$	
octet mesons		

Note: in **Table 5**, the value I_3 of every meson all is integer, contrary to those what the I_3 might take both half integer and integer in case of $J^P = 0^-$ in SM.

There is an amusing equality (23) below among q^1, q^2 and q^3 that is obtained from $q_{\text{RGB}} \equiv (q_{\text{R}}, q_{\text{G}}, q_{\text{B}})$

$$\text{IV}(r-h). q^1 + q^2 + q^3 \equiv \text{I. } q_{\text{R}}^1 + q_{\text{G}}^2 + q_{\text{B}}^3 = \text{II. } q_{\text{R}}^2 + q_{\text{G}}^3 + q_{\text{B}}^1 = \text{III. } q_{\text{R}}^3 + q_{\text{G}}^1 + q_{\text{B}}^2, \tag{23.1}$$

$$A = \frac{1}{3}(q^1 + q^2 + q^3)$$

$$\text{IV}(l-h). q^2 + q^1 + q^3 \equiv \text{I. } q_{\text{R}}^2 + q_{\text{G}}^1 + q_{\text{B}}^3 = \text{II. } q_{\text{R}}^3 + q_{\text{G}}^2 + q_{\text{B}}^1 = \text{III. } q_{\text{R}}^1 + q_{\text{G}}^3 + q_{\text{B}}^2, \tag{23.2}$$

$$A = \frac{1}{3}(q^2 + q^1 + q^3)$$

example of p^+

$$\text{IV}(r-h). u^1 + d^2 + u^3 \equiv \text{I. } u_{\text{R}} + d_{\text{G}} + u_{\text{B}} = \text{II. } d_{\text{R}} + u_{\text{G}} + u_{\text{B}} = \text{III. } u_{\text{R}} + u_{\text{G}} + d_{\text{B}}, \tag{24.1}$$

$$A = \frac{1}{3}(u^1 + d^2 + u^3) = \frac{0}{3} = 0$$

$$= \frac{+2}{3} + \frac{-13}{3} + \frac{+11}{3} = \frac{-16}{3} + \frac{+5}{3} + \frac{+11}{3} = \frac{+2}{3} + \frac{+5}{3} + \frac{-7}{3}, \tag{24.2}$$

example of n^0

$$\text{IV}(r-h). u^1 + d^2 + d^3 \equiv \text{I. } u_{\text{R}} + d_{\text{G}} + d_{\text{B}} = \text{II. } d_{\text{R}} + d_{\text{G}} + u_{\text{B}} = \text{III. } d_{\text{R}} + u_{\text{G}} + d_{\text{B}}, \tag{25.1}$$

$$A = \frac{1}{3}(u^1 + d^2 + d^3) = \frac{-18}{3} = -6$$

$$= \frac{+2}{3} + \frac{-13}{3} + \frac{-7}{3} = \frac{-16}{3} + \frac{-13}{3} + \frac{+11}{3} = \frac{-16}{3} + \frac{+5}{3} + \frac{-7}{3}, \tag{25.2}$$

If array q_{RGB} is defined as a vector (26)

$$q_{\text{RGB}} \equiv (q_{\text{R}}, q_{\text{G}}, q_{\text{B}}) = \vec{A}(q_i) \tag{26}$$

Then the next two tables are constructed from **CSDF**, which may offer some heuristic search for classification of particle mass.

Table 6. Mass Values Comparison between Prediction and Experiment for proton and neutron [3].

	$\text{I}^2 + \text{II}^2 + \text{III}^2$	Prediction	Experiment
$A^2(p^+) = \vec{A}(p^+) \cdot \vec{A}(p^+)$	$\text{I}^2 \propto (+2)^2 + (-13)^2 + (+11)^2 = 294$		
	$\text{II}^2 \propto (-16)^2 + (+5)^2 + (+11)^2 = 402$	774	774 + 1098 = 1872 ↔ 938 + 940 = 1878
	$\text{III}^2 \propto (+2)^2 + (+5)^2 + (-7)^2 = 78$	1872/2 = 936	1878/2 = 939
$A^2(n^0) = \vec{A}(n^0) \cdot \vec{A}(n^0)$	$\text{I}^2 \propto (+2)^2 + (-13)^2 + (-7)^2 = 222$	774/936 = 0.827	938/939 = 0.999
	$\text{II}^2 \propto (-16)^2 + (-13)^2 + (+11)^2 = 546$	1098	1098/936 = 1.173 ↔ 940/939 = 1.001
	$\text{III}^2 \propto (-16)^2 + (+5)^2 + (-7)^2 = 330$	0.827 + 1.173 = 2	0.999 + 1.001 = 2

Table 7. Comparison between $A^2(q)/A^2(u)$ and $M(q)/M(u)$ of three generations of quarks (ref: diagram **CSDF**).

$A^2(q) = q_R q_R + q_G q_G + q_B q_B$	$A^2(q)/A^2(u)$	$\text{Mev}/c^2(q) \Rightarrow M(q)/M(u)$	q
$A^2(t) \propto (+38)^2 + (+41)^2 + (+47)^2 = 5334$	$\Rightarrow 5334/150 = 35.56$	$173 \times 10^3 \Rightarrow 7521.7$	t
$A^2(c) \propto (+20)^2 + (+23)^2 + (+29)^2 = 1770$	$\Rightarrow 1770/150 = 11.8$	$1.275 \times 10^3 \Rightarrow 554.3$	c
$A^2(u) \propto (+2)^2 + (+5)^2 + (+11)^2 = 150$	$\Rightarrow 150/150 = 1$	$2.3 \times 10^0 \Rightarrow 1$	u
$A^2(d) \propto (-16)^2 + (-13)^2 + (-7)^2 = 474$	$\Rightarrow 474/150 = 3.16$	$4.8 \times 10^0 \Rightarrow 2.1$	d
$A^2(s) \propto (-34)^2 + (-31)^2 + (-25)^2 = 2742$	$\Rightarrow 2742/150 = 18.28$	$95.0 \times 10^0 \Rightarrow 41.3$	s
$A^2(b) \propto (-52)^2 + (-49)^2 + (-43)^2 = 6954$	$\Rightarrow 6954/150 = 46.36$	$4.18 \times 10^3 \Rightarrow 1817.4$	b

In **Table 6** and **Table 7**, $A^2(p^+)$, $A^2(n^0)$ and $A^2(q)$ are the scalar products of $\vec{A}(q_i)$ (26). The masses of particles (both proton, neutron and quarks) are supposed to be proportional to the scalar products from their corresponding **CSDF**.

8. Conclusions

In this paper we have pointed links between flavour quarks and colour quarks in math frame STS, Spin Topological Space: the flavour viewed as a number, named as *flavour quantum number* $A_{j,k}(q_i)$ and the colour viewed as an array, named as *colour spectral line array* q_{RGB} consist of *three colour quantum numbers* q_R , q_G and q_B or $A(q_R)$, $A(q_G)$ and $A(q_B)$. The former is even number, the latter are third-fractions. When one thinks $I_3(q_R)$, $I_3(q_G)$ and $I_3(q_B)$ as three distinct angular momentums respectively, using momentum addition of three-body, one can construct a variety of baryons.

In contrast to SM, mesons only are made of quark and antiquark, it becomes more complex, as now gluon joins into meson mechanism. In account of what happened in *colour spectral line array* $q_i \bar{q}_j g_k$ when $i \neq j$, $k \neq 0$, many efforts are needed, after all, so much is not fully understood.

Perhaps **CSDF**, Colour Spectrum Diagram of Flavour is an essential conception for us to realize what flavour and colour of quarks are.

Acknowledgements

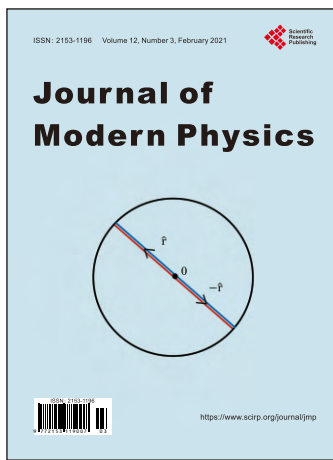
The author thanks my intimate friend, Xin Mao, for valuable discussions and encouragements, and grateful to Jia Guan who helpfully supportes this paper Latex version.

Conflicts of Interest

The author declares no conflicts of interest regarding the publication of this paper.

References

- [1] Gell-Mann, M. (1964) *Physics Letters*, **8**, 214-215.
[https://doi.org/10.1016/S0031-9163\(64\)92001-3](https://doi.org/10.1016/S0031-9163(64)92001-3)
- [2] Zweig, G. (1964) An SU(3) Model for Strong Interaction Symmetry and Its Breaking Version 2. CERN-TH-412. Version 1 Is CERN Preprint 8182/TH.401.
- [3] Martin, B.R. and Shaw, G. (2017) *Particle Physics*. 4th Edition, John Wiley & Sons, Ltd., The Atrium, Southern Gate, Chichester, West Sussex, PO19 8SQ, Kingdom.
- [4] Ren, S.X. (2011) *The Third Kind of Particle*. Shanghai Electronic Publishing Limited, Shanghai.
- [5] Ren, S.X. (2012) *The Third Kind of Particle*. Modern Culture Publishing House, Hong Kong.
- [6] Ren, S.X. (2015) *Interaction of the Origins of Spin Angular Momentum*. China Science Literature Publishing House, Hong Kong.
- [7] Ren, S.X. (2017) 642 WE-Heraeus-Seminar, Non-Hermitian Hamiltonians in Physics: Theory and Experiment. Physikzentrum Bad Honnef Germany.



Call for Papers

Journal of Modern Physics

ISSN: 2153-1196 (Print) ISSN: 2153-120X (Online)
<https://www.scirp.org/journal/jmp>

Journal of Modern Physics (JMP) is an international journal dedicated to the latest advancement of modern physics. The goal of this journal is to provide a platform for scientists and academicians all over the world to promote, share, and discuss various new issues and developments in different areas of modern physics.

Editor-in-Chief

Prof. Yang-Hui He

City University, UK

Subject Coverage

Journal of Modern Physics publishes original papers including but not limited to the following fields:

Biophysics and Medical Physics
Complex Systems Physics
Computational Physics
Condensed Matter Physics
Cosmology and Early Universe
Earth and Planetary Sciences
General Relativity
High Energy Astrophysics
High Energy/Accelerator Physics
Instrumentation and Measurement
Interdisciplinary Physics
Materials Sciences and Technology
Mathematical Physics
Mechanical Response of Solids and Structures

New Materials: Micro and Nano-Mechanics and Homogeneization
Non-Equilibrium Thermodynamics and Statistical Mechanics
Nuclear Science and Engineering
Optics
Physics of Nanostructures
Plasma Physics
Quantum Mechanical Developments
Quantum Theory
Relativistic Astrophysics
String Theory
Superconducting Physics
Theoretical High Energy Physics
Thermology

We are also interested in: 1) Short Reports—2-5 page papers where an author can either present an idea with theoretical background but has not yet completed the research needed for a complete paper or preliminary data; 2) Book Reviews—Comments and critiques.

Notes for Intending Authors

Submitted papers should not have been previously published nor be currently under consideration for publication elsewhere. Paper submission will be handled electronically through the website. All papers are refereed through a peer review process. For more details about the submissions, please access the website.

Website and E-Mail

<https://www.scirp.org/journal/jmp>

E-mail: jmp@scirp.org

What is SCIRP?

Scientific Research Publishing (SCIRP) is one of the largest Open Access journal publishers. It is currently publishing more than 200 open access, online, peer-reviewed journals covering a wide range of academic disciplines. SCIRP serves the worldwide academic communities and contributes to the progress and application of science with its publication.

What is Open Access?

All original research papers published by SCIRP are made freely and permanently accessible online immediately upon publication. To be able to provide open access journals, SCIRP defrays operation costs from authors and subscription charges only for its printed version. Open access publishing allows an immediate, worldwide, barrier-free, open access to the full text of research papers, which is in the best interests of the scientific community.

- High visibility for maximum global exposure with open access publishing model
- Rigorous peer review of research papers
- Prompt faster publication with less cost
- Guaranteed targeted, multidisciplinary audience



**Scientific
Research
Publishing**

**Website: <https://www.scirp.org>
Subscription: sub@scirp.org
Advertisement: service@scirp.org**